U.S. DEPARTMENT OF COMMERCE
National Technical Information Service
PB-284 100

Project Da Vinci II Data Analysis and Interpretation

U.S. Research Triangle Inst, Research Triangle Park, N C

Prepared for

Environmental Protection Agency, Research Triangle Park, N C Office of Air Quality Planning and Standards

Jun 78

PB 284 100

United States
Environmental Protection
Agency

Office of Air Quality
Planning and Standards
Research Triangle Park NC 27711

EPA-450/3-78-028
June 1978

Air

EPA

Project Da Vinci II: Data Analysis and Interpretation

REPRODUCED BY
NATIONAL TECHNICAL
INFORMATION SERVICE
U. S. DEPARTMENT OF COMMERCE
SPRINGFIELD, VA. 22161

244

TECHNICAL REPORT DATA

(Please read Instructions on the reverse before completing)

1. REPORT NO. EPA-450/3-78-028	2.	3. RECIPIENT'S ACCESSION NO. PB284100
4. TITLE AND SUBTITLE Project Da Vinci II: Data Analysis and Interpretation		5. REPORT DATE June, 1978
		6. PERFORMING ORGANIZATION CODE
7. AUTHOR(S) C. E. Decker, J. E. Sickles, II, W. D. Bach, F. M. Vukovich, and J. J. B. Worth		8. PERFORMING ORGANIZATION REPORT NO.
9. PERFORMING ORGANIZATION NAME AND ADDRESS Research Triangle Institute Research Triangle Park, N.C. 27709		10. PROGRAM ELEMENT NO.
		11. CONTRACT/GRANT NO. 68-02-2568
12. SPONSORING AGENCY NAME AND ADDRESS U. S. Environmental Protection Agency Office of Air Quality Planning and Standards Monitoring and Data Analysis Division Research Triangle Park, N.C. 27711		13. TYPE OF REPORT AND PERIOD COVERED Final
		14. SPONSORING AGENCY CODE
15. SUPPLEMENTARY NOTES		

16. ABSTRACT

Air quality data observed aboard a manned balloon is reported and analyzed, together with concurrent data from the St. Louis RAMS monitoring network, and from a mobile van which was driven beneath the track of the balloon. The study was conducted on June 8-9, 1976, near and downwind of St. Louis, Missouri, during a period of atmospheric stagnation. During daylight hours, ozone levels measured aboard the balloon and at ground level were similar. At night, ozone trapped aloft by a nocturnal inversion remains stable, whereas ozone observed at ground level decays rapidly. Transport of ozone aloft overnight, for distances of at least 180 km, is documented. With the weak synoptic flow conditions prevailing on June 8, a daytime heat island effect is documented. Maximum ozone concentrations were observed at a location where this complex flow field converges.

17. KEY WORDS AND DOCUMENT ANALYSIS

a. DESCRIPTORS	b. IDENTIFIERS/OPEN ENDED TERMS	c. COSATI Field/Group
Ozone Photochemical Air Pollutants Primary and Secondary Pollutants Long-Range Transport Atmospheric Stagnations Balloon-Borne Measurements Vertical Pollutant Profiles	Atmospheric Ozone Levels Ozone Formation and Transport	Atmospheric Photochemistry Air Pollution

18. DISTRIBUTION STATEMENT Release Unlimited	19. SECURITY CLASS *(This Report)* Unclassified	21. NO. OF PAGES 244
	20. SECURITY CLASS *(This page)* Unclassified	22. PRICE PCA11 / MF A01

EPA-450/3-78-028

Project Da Vinci II: Data Analysis and Interpretation

by

C.E. Decker, J.E. Sickles, II, W.D. Bach,
F.M. Vukovich, and J.J.B. Worth

Research Triangle Institute
Research Triangle Park, N.C. 27709

Contract No. 68-02-2568

EPA Project Officer: Dr. Edwin L. Meyer

Prepared for

U.S. ENVIRONMENTAL PROTECTION AGENCY
Office of Air and Waste Management
Office of Air Quality Planning and Standards
Research Triangle Park, North Carolina 27711

June 1978

This report is issued by the Environmental Protection Agency to report technical data of interest to a limited number of readers. Copies are available free of charge to Federal employees, current contractors and grantees, and nonprofit organizations - in limited quantities - from the Library Services Office (MD-35), U.S. Environmental Protection Agency, Research Triangle Park, North Carolina 27711; or, for a fee, from the National Technical Information Service, 5285 Port Royal Road, Springfield, Virginia 22161.

This report was furnished to the Environmental Protection Agency by Research Triangle Institute, Research Triangle Park, N.C. 27709, in fulfillment of Contract No. 68-02-2568. The contents of this report are reproduced herein as received from Research Triangle Institute. The opinions, findings, and conclusions expressed are those of the author and not necessarily those of the Environmental Protection Agency. Mention of company or product names is not to be considered as an endorsement by the Environmental Protection Agency.

Publication No. EPA-450/3-78-028

CONTENTS

Page

Figures vi

Tables x

Acknowledgments xi

1.0 EXECUTIVE SUMMARY 1

1.1 Introduction and Objectives 1

1.2 Data Analysis 2

1.3 Principal Findings 2

1.4 Conclusions 5

2.0 INTRODUCTION 7

2.1 Background 7

2.2 Research Objectives 8

2.3 Report Organization 8

3.0 PROJECT DA VINCI II FIELD EXPERIMENT 9

3.1 Air Quality Measurements 10

3.1.1 Da Vinci II Measurements 10

3.1.2 Supporting Aircraft Measurements 11

3.1.3 Acoustic Sounder Measurement 13

3.1.4 RTI-EML Measurements 13

3.1.4.1 Ground Level Measurements 13

3.1.4.2 RTI Balloon-Borne Measurements 14

3.1.5 State Agency Measurements 16

3.1.6 RAMS Network Measurements 16

3.1.7 Emissions Inventory Data 18

3.2 Flight Description 20

3.3 Meteorological Conditions for the Period Encompassing Flight Day 25

3.4 Quality Control Program 27

3.5 Analysis Approach 28

4.0 ATMOSPHERIC CHEMISTRY ANALYSIS FOR DA VINCI II 31

4.1 Objectives of Analysis 31

4.2 Approach 31

4.3 Results and Discussion 31

4.3.1 Emissions Inventory 31

Page

4.3.2 Air Contaminant Considerations for the Period Encompassing Flight Day 37

4.3.3 Air Quality at the Launch Site 42

4.3.4 Air Contaminant Behavior at Ground Level During the Flight 43

4.3.4.1 Air Quality at RAMS Stations 43

4.3.4.2 Air Quality at the RTI-EML 58

4.3.5 Air Contaminant Behavior Aloft During the Flight 62

4.3.5.1 NOAA Aircraft 62

4.3.5.2 Acoustic Sounder 70

4.3.5.3 Temperature, Relative Humidity, and Condensation Nuclei on Da Vinci II 70

4.3.5.4 Ozone and Sulfur Dioxide on Da Vinci II 75

4.3.5.5 Hydrocarbons on Da Vinci II 82

4.3.6 Air Quality Aloft and at the Ground 90

4.3.6.1 Sulfur Dioxide 90

4.3.6.2 Ozone 92

4.3.7 Considerations for Future Programs 97

4.4 Findings 98

5.0 MESOMETEOROLOGICAL AND AIR POLLUTION STUDY RELATIVE TO DA VINCI II 101

5.1 Introduction 101

5.2 Data Sources 102

5.3 Surface Temperature Distribution 102

5.4 Surface Wind Distribution 108

5.5 Temperature and Wind Profiles 113

5.6 Simulation Results 118

5.7 Surface Ozone Distribution 129

5.8 Da Vinci II and RTI-EML Ozone Data 133

5.9 Aircraft Ozone Profiles 138

5.10 Summary and Conclusions 139

6.0 METEOROLOGICAL ANALYSIS FOR DA VINCI II 145

6.1 Plume Identification 145

6.1.1 Introduction 145

6.1.2 Data Sources 146

6.1.3 Method of Computation 146

Page
6.1.4 Results 150
6.1.4.1 Wind Shear 150
6.1.4.2 Low Altitude Plume 153
6.1.4.3 The Plume at Altitude 154
6.1.5 Interpretation 154
6.1.6 Conclusions 157
6.2 Cross Section Analyses 158
6.2.1 Introduction 158
6.2.2 Analysis Approach 159
6.2.2.1 Analysis of Winds Aloft 159
6.2.2.2 Rawinsonde Analyses 162
6.2.2.3 Acoustic Sounder 165
6.2.3 Conclusions 167
6.3 Modeling Atmospheric Chemistry and Physics 168
6.3.1 Need for Modeling 168
6.3.2 Results of Model Application 169
7.0 PRINCIPAL FINDINGS AND CONCLUSIONS 171
7.1 Principal Findings 171
7.2 Conclusions 173
8.0 REFERENCES 175

APPENDIXES

Appendix A. Evaluation of Sample Collection Containers for Hydrocarbon Sampling 177
Appendix B. Evaluation of Laboratory and Quality Control Practices for Hydrocarbon Sampling and Analysis (Da Vinci II Participants) 207
Appendix C. RTI Quality Control Program Relative to Da Vinci II for Hydrocarbon Sampling 213
Appendix D. Objective Analysis Technique 219
Appendix E. Planetary Boundary Layer Model 223

LIST OF FIGURES

Figure		Page
1	Da Vinci II balloon and gondola	9
2	Photograph of gondola and scientific equipment	10
3	RTI Environmental Monitoring Laboratory onsite at Arrowhead Airport	14
4	Track of Da Vinci II and route of RTI-EML during first 12 h of flight	17
5	Flight track of Da Vinci II and ground track of the RTI-EML from launch at Arrowhead Airport to touchdown in Indiana	21
6	RTI-EML located adjacent to gondola for post-flight calibration of Da Vinci II analyzers	22
7	Da Vinci II altitude data, 8 and 9 June 1976	24
8	RAMS meteorological parameters for 6-9 June 1976	27
9	Ozone distribution in the northeastern quadrant of the United States based on daily maximum hourly concentrations	39
10	Mean profiles for RAMS network on 6-9 June 1976	40
11	Hourly average ozone concentration prior to launch at Arrowhead Airport 1-8 June 1976	43
12	Mean pollutant concentrations at urban, suburban, and nonurban sites in St. Louis on 8 June 1976	46
13	Air temperature at urban, suburban, and nonurban sites in St. Louis on 8 June 1976	48
14	Temperature gradient through the first 30 m (100 ft) at urban and nonurban sites in St. Louis on 8 June 1976	48
15	Carbon monoxide concentration relative to downtown St. Louis along west to east and south to north directions on 8 June 1976	49
16	Nitrogen oxides concentration relative to downtown St. Louis along west to east and south to north directions on 8 June 1976	50
17	Ozone concentration relative to downtown St. Louis along west to east and south to north directions on 8 June 1976	51
18	Nonmethane hydrocarbon concentration at the time of maximum THC concentration relative to downtown St. Louis along west to east and south to north directions on 8 June 1976	52
19	Hourly ozone isopleths (computer-generated) for St. Louis RAPS area on 8 June 1976	55

Figure Page

20 Ground-level ozone concentrations measured by RTI-EML and nearest RAMS Station during flight of Da Vinci II 60

21 Unadjusted ozone profiles as measured in St. Louis on 8 June 1976 during vertical flights of the NOAA aircraft that started at 0915 and 1148 CST 64

22 B_{scat} profiles as measured in St. Louis on 8 June 1976 during vertical flights of the NOAA aircraft that started at 0915 and 1148 CST 65

23 Relative humidity profiles as measured in St. Louis on 8 June 1976 during vertical flights of the NOAA aircraft that started at 0915 and 1148 CST 66

24 Nitrogen dioxide profiles as measured in St. Louis on 8 June 1976 during vertical flights of the NOAA aircraft that started at 0915 and 1148 CST 67

25 Adjusted ozone profiles as measured in St. Louis on 8 June 1976 during vertical flights of the NOAA aircraft that started at 0915 and 1148 CST 68

26 ANL acoustic sounder data along the flight track of Da Vinci II, 8 and 9 June 1976 72

27 Air temperature on Da Vinci II, 8 and 9 June 1976 73

28 Relative humidity on Da Vinci II, 8 and 9 June 1976 74

29 Condensation nuclei on Da Vinci II, 8 and 9 June 1976 75

30 Ozone on Da Vinci II as measured by Sandia Laboratories and ASL, 8 and 9 June 1976 77

31 Ozone on Da Vinci II as measured by ASL and represented by connected dots, 8 and 9 June 1976 78

32 Sulfur dioxide on Da Vinci II as measured by Sandia Laboratories and represented by connected dots, 8 and 9 June 1976 79

33 Pollutant concentrations as determined by RTI from grab samples collected on Da Vinci II, 8 and 9 June 1976 84

34 Hourly average sulfur dioxide aloft and at ground level, 8 and 9 June 1976 92

35 Hourly average ozone aloft and at ground level, 8 and 9 June 1976 94

36 Ozone upwind and downwind of Indianapolis at an altitude of 457 m (1,500 ft) above ground on 9 June 1976 as measured on the ICFAR aircraft 96

37 The area of immediate interest around St. Louis showing the locations of the RAPS stations and the two upper air sounding stations 103

Figure		Page
38	The ground track of the Da Vinci II gondola and the track of the RTI-EML from lift-off at Arrowhead Airport through 2000 CST	104
39	The hourly temperature difference between the St. Louis center city and the rural/suburban area some 15 mi away	105
40	Spatial distribution of the St. Louis urban heat island [°C] at 0500, 0900, and 1400 CST on 8 June	107
41	Spatial distribution of the St. Louis urban heat island [°C] at 1800 and 2000 CST on 8 June	109
42	Interpolated surface wind field [m/s] at 0500, 0900, 1000, and 1400 CST on 8 June	110
43	Interpolated surface wind field [m/s] at 1500, 1800, and 2000 CST on 8 June	111
44	Diurnal variability of the potential temperature [°K] profile on 8 June over the St. Louis center city (station 141) and over the rural area southwest of St. Louis (station 142)	114
45	Diurnal variability of the wind speed [m/s] and wind direction profiles over the St. Louis center city on 8 June	116
46	Diurnal variability of the wind speed [m/s] and wind direction profiles over the rural area southwest of St. Louis on 8 June	117
47	Horizontal flow and horizontal distribution of the vertical velocity along with a vertical cross section of the vertical velocity profile are shown	119
48	Horizontal distribution of the potential temperature [°K] perturbation and vertical cross section of the potential temperature field constructed along the section line are shown	121
49	Simulated horizontal flow and horizontal distribution of the vertical velocity along with a vertical cross section of the vertical velocity profile are shown	122
50	Horizontal distribution of the potential temperature perturbation; vertical cross section of the potential temperature field; and the horizontal distribution of the potential temperature perturbation are shown	123
51	Simulated horizontal flow and horizontal distribution of the vertical velocity along with a vertical cross section of the vertical velocity profile are shown	125
52	Horizontal distribution of the potential temperature perturbation and vertical cross section of the potential temperature field are shown	126

Figure Page

53 Simulated horizontal flow and horizontal distribution of the vertical velocity with a cross section of the vertical velocity profile are shown 127

54 Horizontal distribution of the potential temperature perturbation and vertical cross section of the potential temperature field are shown 128

55 Simulated horizontal flow and horizontal distribution of the vertical velocity along with a vertical cross section of the vertical velocity profile are shown 130

56 Horizontal distribution of the potential temperature perturbation and vertical cross section of the potential temperature field are shown 131

57 Surface ozone distribution in the study area at 0500, 0900, and 1300 CST on 8 June 132

58 Surface ozone distribution in the study area at 1600, 1900, and 2100 CST on 8 June 134

59 Variation of altitude with time for the flight of Da Vinci II 135

60 Hourly average ozone concentrations measured along the Da Vinci II flight track 137

61 Vertical ozone profiles flown by a NOAA aircraft in the vicinity of the Da Vinci II gondola on the morning of 8 June 1976 140

62 Pilot balloon launch sites 148

63 Typical analysis of air leaving St. Louis during Da Vinci II flight 148

64 Dispersion of air, initially, over St. Louis at indicated altitudes (km) and times, resulting from wind shear 151

65 Movement of air at 50 m from St. Louis between 0800 and 2000 CST, 8 June 1976 and for 18 h of transport 152

66 Motion of air initially over St. Louis at the indicated altitudes and times and near the Da Vinci II altitude 155

67 Horizontal wind vectors aloft along Da Vinci II track, from pilot balloon observations 161

68 Cross section of potential temperature along Da Vinci II path (from rawinsonde data) 164

69 Cross section of wind speed along Da Vinci II path (from rawinsonde data) 166

70 Vertical profiles of u, v, θ, and c at indicated times from PBL model simulation of 8 June 170

LIST OF TABLES

Table — Page

1 Identification of selected data collected on Da Vinci II 12

2 RTI-EML air quality instrumentation and calibration procedures 15

3 RAMS instrumentation 19

4 Counties for which emissions inventory data were retrieved 20

5 Major altitude excursions of Da Vinci II 25

6 Major SO_2 point sources along the flight track of Da Vinci II 32

7 Major NO_x point sources along the flight track of Da Vinci II 33

8 Major HC point sources along the flight track of Da Vinci II 34

9 Major CO point sources along the flight track of Da Vinci II 35

10 Emissions summaries for counties along the flight track of Da Vinci II 37

11 Summary of air quality parameters at Arrowhead Airport for the 16-day period 44

12 Nocturnal increases in ozone concentration at the surface during the flight of Da Vinci II 62

13 Mean HC concentrations at Da Vinci II and at selected RAMS stations 86

14 Mean hydrocarbon concentrations and excursions from the mean on Da Vinci II 88

15 Pilot balloon observations 147

16 Winds at 650 m MSL from RAMS pilot balloon stations 158

17 Rawinsonde data used in analyses 163

ACKNOWLEDGMENTS

This project was conducted by Research Triangle Institute (RTI), Research Triangle Park, North Carolina, under Contract 68-02-2568 for the United States Environmental Protection Agency (EPA). The support of this agency is gratefully acknowledged as is the advice and guidance of the Project Officer, Mr. E. L. Meyer, Jr., and other staff members of the Office of Air Quality Planning and Standards.

Work on this project was performed by staff members of the Systems and Measurements Division and the Energy, Engineering, and Environmental Sciences Division of RTI, under the direction of Mr. J. J. B. Worth, Group III Vice President. Mr. Worth was Laboratory Supervisor for the project. Mr. C. E. Decker served as Project Leader and was responsible for the coordination of the program. Staff members of RTI who contributed to the preparation of this report are recognized and listed in alphabetical order: Dr. W. D. Bach, Mr. C. E. Decker, Mr. R. B. Denyszyn, Dr. J. E. Sickles II, Dr. F. M. Vukovich, Dr. D. E. Wagoner, and Mr. J. J. B. Worth. Special recognition is given to Dr. L. A. Ripperton for technical guidance and advice in the interpretation of the data.

Special recognition is given to Dr. B. Zak of Sandia Laboratories who directed the Da Vinci II project and contributed valuable information for use in this report.

1.0 EXECUTIVE SUMMARY

1.1 Introduction and Objectives

During 8-9 June 1976, Research Triangle Institute (RTI) under sponsorship of the U.S. Environmental Protection Agency (EPA) participated in Project Da Vinci II, an Energy Research and Development (ERDA) experiment. Project Da Vinci II was a manned, balloon-borne scientific experiment conducted by Sandia Laboratories for ERDA in the St. Louis, Missouri, area to study the behavior of air pollutants in the lower atmosphere. The primary emphasis of the experiment was focused upon the chemical and meteorological processes by which gaseous effluents from urban areas are reacted or transformed while being transported away from an urban area. Measurements of sulfur dioxide, sulfates, ozone, ozone precursors, and meteorological parameters were made to determine changes in their relative concentrations in space and time as the balloon drifted with the wind.

The underlying concept of the Da Vinci II balloon flight takes advantage of a quasi-Lagrangian frame of reference for an instrumented platform to monitor atmospheric processes within a moving air parcel. In this study, both chemical and meteorological processes could be monitored continuously as they were occurring. This approach afforded the opportunity to follow the transport of various pollutants and examine their behavior during transport. In addition, pollutant behavior could be investigated under varying meteorological conditions, such as occur in the daytime mixed layer or within the layer bounded by the subsidence inversion and the radiation inversion at night.

Da Vinci II was launched from Arrowhead Airport, 24 km west of St. Louis, Missouri, on 8 June 1976, at 0756 CST. The craft carried a four-person crew and a payload of scientific equipment designed to quantify selected chemical and meteorological parameters associated with the atmosphere. Supporting data were also collected by an aircraft, the RTI Environmental Monitoring Laboratory (RTI-EML), and at ground stations. Da Vinci II landed at 0805 CST on 9 June 1976, in southwest Indiana after having traveled some 340 km in a 24-h period. A report of the Da Vinci II field program is presented in EPA Report No. 450/3-77-009.[1]

The objective of this study was to consolidate, analyze, and interpret selected data collected during the flight of Da Vinci II in order to expand the present understanding of the transport of air pollution from urban to nonurban areas, with primary emphasis on the transport of ozone. Emphasis was also focused on relating emissions upwind, within, and downwind of the urban area to observed levels of primary and secondary pollutants upwind, within, and downwind of the urban area. An additional consideration was the interpretation of the data so that EPA could further develop and apply methodologies for evaluating the effectiveness of existing or proposed control strategies for meeting ambient air quality standards.

1.2 Data Analysis

The analyses of both the chemical and the atmospheric processes for Da Vinci II consider data taken from two frameworks. Ground station chemical and meteorological and upper air data were taken from a Eulerian system (i.e., the observer is fixed in space and observes changes as the medium moves past), while Da Vinci II measurements (aboard the balloon) were taken in a nearly Lagrangian system (i.e., the observer is moving (approximately) with the medium and measures the changes that occur from processes within the moving volume). Meteorological characteristics of the balloon environment are related to the chemical and oxidant concentrations measured aboard the Da Vinci II balloon and to measurements from other platforms--aircraft, the RTI-EML, and ground stations.

Information was assembled from many sources to provide a comprehensive description of the atmospheric and pollutant behavior during the study period both aloft and at ground level. Aircraft data, when available, were used to supplement information from the balloon to describe processes that were occurring aloft. Data from the Regional Air Monitoring Study (RAMS) network, the RTI-EML, and Indiana, Illinois, and Kentucky State pollution monitoring stations were employed to describe pollutant behavior at the ground. Emissions inventory data were also examined to locate major pollutant sources within the study area.

Independent analyses of the data were performed to provide chemical and meteorological interpretations for Da Vinci II. These analyses are documented in detail in the body of the report.

1.3 Principal Findings

Selected data collected by various participants during the flight of Da Vinci II were consolidated, summarized, and segmented into general subject areas for analysis and interpretation. These subject areas include atmospheric chemistry and meteorological analyses. Data were analyzed and interpreted according to the objectives for each analysis and have been incorporated to combine both a chemical and meteorological interpretation of results. Principal findings from these studies are summarized below.

1. Conditions of high ozone concentrations persisted aloft for the study period. These conditions were widespread and extended for several hundred kilometers. Air containing high concentrations of ozone, approximately 0.11 ppm, was being transported into the study area on the flight day.
2. Da Vinci II was launched into air that had an immediate fetch over a nonurban area, although the total experiment was conducted within a stagnant, polluted, high-pressure system. Air parcel trajectories suggest that Da Vinci II was launched into air that 72 h earlier had been in eastern Kentucky and the Ohio Valley.
3. Da Vinci II did not travel in the heart of the St. Louis urban plume as defined by ozone concentrations. Examination of the hydrocarbon concentrations sampled on Da Vinci II suggests that the flight occurred in air characteristic of suburban-to-nonurban areas.
4. The ozone concentration at the flight level (700 m) of Da Vinci II was greater than 0.08 ppm when Da Vinci II reached that altitude. Since it reached that level prior to 1030 CST when deep convective mixing was experienced in the urban boundary layer, a major portion of the upper level ozone concentration must have come from sources other than St. Louis on the morning of 8 June.
5. During the morning, ground-level ozone concentrations were less than concentrations aloft. The observed increase of ozone concentrations aloft, therefore, could not have resulted from upward mixing of ozone from the ground, but was probably due to tropospheric photochemical synthesis.
6. Vertical profiles show substantial ozone concentrations aloft between 762 and 1,981 m (2,500-6,500 ft) on the morning of 8 June with a sharp decline in ozone concentration above 2,133 m (7,000 ft). Mean ozone concentrations between 2,133 and 2,743 m (7,000-9,000 ft) were less than those measured between 762 and 1,981 m (2,500-6,500 ft) by a factor of 2.4. These observations suggest that stratospheric intrusion was not responsible for the elevated ozone concentrations that existed aloft on 8 June.
7. The impact of anthropogenic emissions on ambient concentrations within the urban area is variable and depends strongly on the time of day. Ground-level CO and NO_x were diluted by factors of 5 to 7 between the morning and afternoon. This behavior probably reflects the significant increase in the mixed volume that occurs with the dissipation of the surface-based radiation inversion and the establishment of well mixed conditions.
8. As vertically well mixed conditions were established between 0500 and 1100 CST, both downward mixing and photochemical synthesis contributed to the observed increase in ground level ozone concentration. This ground level increase exceeded that aloft by a factor of approximately two.

9. Between 1100 and 1700 CST on flight day, a near zero ozone concentration gradient existed from the ground into the mixed layer. This is based, to a large extent, on the close comparison of ozone concentrations determined on Da Vinci II with those beneath Da Vinci II at ground level.

10. After well-mixed conditions were established and until the nocturnal inversion began to form, the increases in ozone concentrations aloft and at ground level were approximately equal and probably resulted from photochemical synthesis.

11. The airflow in the immediate vicinity of St. Louis on 8 June was governed by the synoptic scale flow and an intense circulation produced by the urban heat island. Da Vinci II responded to both of these scales of motion.

12. A major air pollution plume (defined by the ozone distribution) was found at the surface. The maximum ozone concentration in this plume was immediately downstream (within 5 km) of the center of downtown St. Louis between 1000 and 1500 CST. Simulation results (meteorological model) suggest that if a plume existed in the upper portions of the boundary layer, it would have moved in a different direction than the surface plume.

13. Between 1000 and 1500 CST, the maximum ozone concentration in the major air pollution plume at the surface (as defined by ozone distribution) was found in a region where there was a zone of horizontal convergence in the wind field associated with the urban heat island circulation.

14. After 1500 CST, the maximum ozone concentration in the air pollution plume (as defined by the ozone distribution) moved farther downstream (greater than 15 km) when the heat island circulation and its accompanying convergence zone was dissipating.

15. Within the layer that had been well mixed during the daytime, stratification, which occurred at night with the establishment of the nocturnal radiation inversion, resulted in the formation of two regimes of ozone concentrations. Ozone concentrations within the radiation inversion were much reduced compared to levels above it. This is presumably due to destruction by surface deposition and reaction with ozone-destructive agents emitted into and trapped within the inversion.

16. Ozone data obtained aboard Da Vinci II were used to calculate a nighttime ozone half-life of 116 h. Examination of available hydrocarbon precursor data obtained aboard Da Vinci II suggests that concentrations of ozone destructive and other HC species aloft were low during the flight. The dark phase half-life of ozone under the conditions of presumed low levels of precursors is sufficient to allow transport of ozone from an urban area overnight to another area without significant diminishment due to decay.

17. Penetration through the nocturnal radiation inversion resulted in the mixing of high levels of ozone to the ground and precursors from the ground to aloft. This was suggested by the sharp nighttime ozone peaks and the associated declines of NO_x and CO observed at

selected ground stations. This phenomenon occurred frequently in May and June and was observed at ground stations covering an area of several hundred kilometers. It may also provide mechanisms for increasing nighttime ozone destruction aloft and for enhancing early morning ozone synthesis by distributing ozone precursors aloft above the inversion before sunrise.

18. The balloon may have entered an air parcel that was enriched in hydrocarbons after 2100 CST on 8 June and traveled within this parcel for the remainder of the flight.

19. Sharp, short-term reductions in ozone concentrations occurred aloft during the nighttime portion of the flight and were coincident with increases in SO_2 concentration. Both SO_2 and NO_x are emitted by power plants. Although NO_x was not measured in this study, the observed ozone behavior is probably the result of destruction by reaction with NO_x.

20. The influence of ozone precursors emitted in the urban area was manifested at ground level by ozone concentration enhancement over nonurban concentrations. The magnitude of this enhancement was 0.06 to 0.11 ppm. Both the buildup and movement of the region of enhanced ozone were documented, although detailed definition of the extent and magnitude were severely hampered by the lack of a comprehensive supporting aircraft measurement program.

21. High ozone concentrations measured aloft aboard Da Vinci II on the morning of 9 June in Southwestern Indiana are attributed to long distance transport of ozone. High ozone at the surface is influenced by synthesis and mixing downward of the ozone aloft in the morning. After a well-mixed layer is established, changes resulting from mixing are minimized. Further increases in ozone concentration at the surface can be attributed to synthesis.

22. The use of a Lagrangian system to document ozone transport and address atmospheric chemistry problems has been shown to be feasible. Interpretation of these data are severely limited, however, unless supporting data that define vertical and horizontal pollutant distributions are also available.

1.4 Conclusions

The conclusions listed below are derived from the analysis of the Da Vinci II data relative to the objectives of this project.

1. The synoptic wind flow pattern as modified locally by the urban heat island circulation prevented Da Vinci II from passing over the St. Louis urban area and taking up a position in the urban plume.

2. During the nocturnal phase of the flight, changes in ozone concentrations observed aboard Da Vinci II could not be directly attributed to the downtown St. Louis urban plume.

3. General meteorological conditions--a subsidence inversion aloft and a strong radiative inversion based at the ground--were nearly ideal for long-distance transport aloft of ozone at night, while keeping ozone separated from ground level emissions and destruction and limiting vertical mixing.

4. The dark-phase stability of ozone above the nocturnal surface-based radiation inversion suggests that transport of ozone can occur aloft over long distances at night without significant diminishment. It is possible for the ozone to be transported overnight several hundred kilometers and be mixed to the ground on the next day with a significant impact on ground-level air quality.

5. The occurrence of high ozone concentrations aloft on the morning of 9 June, in a rural area in southwestern Indiana, is attributed to long-distance transport of ozone.

6. Balloon-borne experiments are a feasible approach for addressing atmospheric chemistry problems, provided supporting data from ground stations, a ground-level chase vehicle, and an instrumented aircraft are available to complement the interpretation. The omission of any one of these measurement platforms severely limits the interpretation effort.

2.0 INTRODUCTION

2.1 Background

Previous studies of nonurban ozone concentrations have led to the conclusion that nonurban ozone is significantly affected by long-distance transport of ozone.[2,3] These studies have suggested that the unique precursor, synthesis, destruction, and transport conditions within a high-pressure system are conducive to the transport of ozone in large concentrations for long distances. At night, the radiative temperature inversion develops, stabilizes the air, and inhibits vertical transfer processes. The inversion effectively insulates the ozone aloft from destruction by contact with the surface or by reaction with ozone-destructive agents (NO, NO_2) that may be emitted near the ground. Overnight, the air is transported farther downwind and diffused horizontally. After sunrise, heat is gradually added to the surface layers, while concurrently ozone is being generated by photosynthesis in the precursor-rich air. When enough heat has been added to eliminate the "inverted" temperature structure, vertical mixing is no longer inhibited and ozone-rich air from aloft may be brought to ground.

Understanding the role of urban ozone and its interactions with rural air quality background levels through transport, diffusion, and chemical reactions is important for strategy decisions relating to regional air quality control. One of the specific questions yet to be answered is, "How do urban ozone and associated precursors affect the observed high levels of rural oxidant?" The basic strategy question is whether urban hydrocarbon control will reduce oxidant concentrations equally in the city and in the downwind rural areas.

To examine the question of urban transport, it is necessary to trace or move with an air parcel from a highly urban area into a "relatively clean" rural environment. An opportunity for such a definitive field experiment existed during June 1976 in association with a scheduled Energy Research and Development Administration (ERDA) experiment, Project Da Vinci II.

Project Da Vinci II was a manned, balloon-borne scientific experiment conducted by ERDA Sandia Laboratories in early June in St. Louis, Missouri, to study the behavior of air pollutants in the lower atmosphere. The primary emphasis of the experiment was focused upon the chemical and meteorological processes by which gaseous effluents from urban areas are reacted or transformed while being transported away from an urban area. Measurements of sulfur dioxide, sulfates, ozone, ozone precursors, and meteorological parameters were made to determine changes in their relative concentrations or values in space and time as the balloon drifted nearly with the wind. The Da Vinci II field program is described in EPA Report No. 450/3-77-009.[1]

The balloon-borne measurement program offered these distinct advantages:

1. Air quality measurements could be made in a quasi-Lagrangian frame of reference (i.e., within a moving air parcel).
2. The results of chemical processes occurring in an urban air parcel could be continuously monitored over the time interval of transport.
3. Continuous airborne sampling could be conducted within a layer of air bounded aloft by the subsidence inversion and below by the ground-based radiation inversion.
4. This experiment provides the needed data to document uniquely the contribution of a single city's effluvia to the background pollution levels within a given air parcel.

2.2 Research Objective

The objective of this study was to consolidate, analyze, and interpret selected data collected during the flight of Da Vinci II in order to expand the present understanding of the transport of air pollution from urban to nonurban areas. Emphasis was focused on relating emissions upwind, within, and downwind of an urban area to observed levels of primary and secondary pollutants upwind, within, and downwind of the urban area. An additional consideration was the interpretation of the data, so that EPA could further develop and apply methodologies for evaluating the effectiveness of existing or proposed control strategies for meeting ambient air quality standards.

2.3 Report Organization

This report includes four major sections that describe the field experiment and present an in-depth analysis and interpretation of the Da Vinci II data. Section 3.0 contains a general description of the Da Vinci II field experiment and includes mobile and airborne measurements, flight description and meteorological considerations during the flight, quality control program, and the analysis approach. In section 4.0, atmospheric chemistry analyses are described and results are discussed. In section 5.0, an in-depth evaluation of the mesometeorological conditions during the flight and the effect of the heat island circulation on Da Vinci II are addressed. Meteorological analyses, such as plume identification, cross section analysis, and modeling of atmospheric chemistry and physics are described in section 6.0.

3.0 PROJECT DA VINCI II FIELD EXPERIMENT

The Da Vinci II system was assembled under the direction of Sandia Laboratories and consists of a double-decked gondola approximately 3 m square; a 22-m suspension harness that connects the gondola with the balloon; data-receiving systems for the chase vehicles; and navigational and life support equipment for a crew of four. The gondola and balloon system was designed to permit several days of flight for a crew of four with approximately 909 kg of scientific and power supply equipment on board.

The balloon is constructed of 2-mil, double layer, polyethylene (figure 1) and has a nominal volume of about 186,000 ft^3. It has a diameter of about 22 m, a gore length of 36 m, and 49 load-bearing tapes of 450 kg test. Helium was used as the lifting gas. Two valves at the balloon apex are operated on separate electrical systems to vent helium as needed to assist in

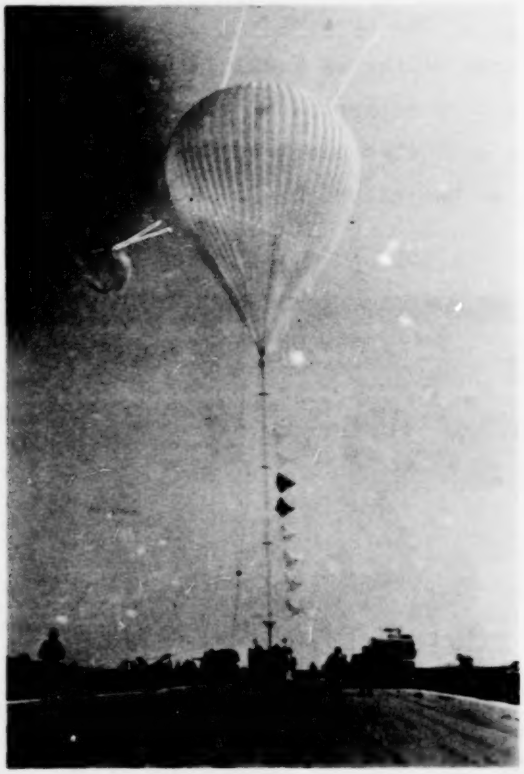

Figure 1. Da Vinci II balloon and gondola.

controlling the altitude of the balloon. Figure 1 is a picture of the inflated balloon and gondola prior to launch.

The gondola was constructed by the Grumman Aircraft Corporation and is 3 m square and double-tiered. It is especially designed to protect crew and equipment in event of rough landing and yet to be used again. The lower deck has about 1 m of head room and is used for batteries, supplies, ballast, life support equipment, and crew sleeping quarters. The upper deck is fiberglass and is used for flight operations and for conducting the scientific experiments. The bottom of the gondola is equipped with a layer of impact material or "crush pads" about 0.5 m thick to provide shock absorption in landings. Scientific equipment is located throughout the flight train. A closeup photograph of the gondola and supporting scientific instrumentation is shown in figure 2.

3.1 Air Quality Measurements

3.1.1 Da Vinci II Measurements

During the course of the Da Vinci II experiment, both air quality and meteorological data were collected at many locations by various organizations. These included data collected aloft on the balloon and by supporting aircraft; and data collected at the ground by the RTI-EML chase vehicle, Argonne National

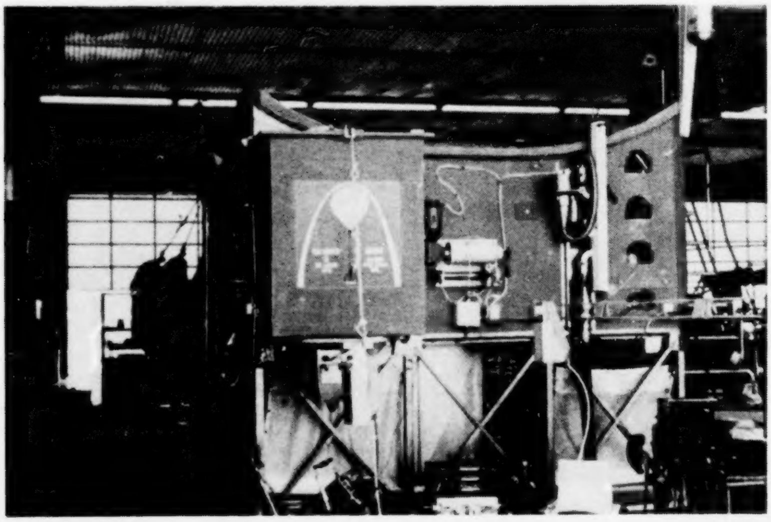

Figure 2. Photograph of gondola and scientific equipment.

Laboratory (ANL) acoustic sounders, selected State agencies, and the Regional Air Monitoring System (RAMS) network.

The types of data that were collected on the balloon are identified and described in table 1. Sandia Laboratories provided altitude data and concentration data for ozone, sulfur dioxide, carbon monoxide, methane, hydrogen, and neon. The last four species were determined by analysis from grab samples. Altitude data are 1-min averages obtained from an encoding altimeter. Ozone and SO_2 concentration data are also 1-min averages. The O_3 and SO_2 instruments were operated only during selected intervals over the flight in an effort to conserve electrical power. The Dasibi ozone monitor and the TECO pulsed fluorescence sulfur dioxide monitor were calibrated by RTI both before and after the flight. Personnel from the National Oceanic and Atmospheric Agency (NOAA) aboard Da Vinci II collected temperature, relative humidity, and condensation nuclei data manually during the flight. Temperature and relative humidity were measured with a sling psychrometer. Condensation nuclei were determined with a manually operated Gardner instrument.

Grab samples were collected in light-shielded Tedlar® bags for subsequent determination of selected hydrocarbons and halocarbons by the Research Triangle Institute. Grab samples were also collected in evacuated stainless steel cans for analysis by Washington State University. Samples were collected sequentially; this prevented the simultaneous collection of samples of the same air parcel.

The U.S. Army Atmospheric Sciences Laboratory (ASL) flew instruments aboard Da Vinci II for determining temperature, relative humidity, and ozone. Ozone was determined continuously by the solid-phase chemiluminescent instrument located on the balloon. Data from this device were recorded at 2-s intervals. The solid-phase instrument was calibrated against the Dasibi.

3.1.2 Supporting Aircraft Measurements

Two vertical flights were conducted within 2 km of the balloon on 8 June by a NOAA aircraft. The first vertical was flown from 0915 to 0933 CST and the second was flown from 1148 to 1211 CST. During these flights O_3, NO, NO_2, NO_x, Bscat, and relative humidity were measured. Both O_3 and NO_x were determined by Monitor Labs instruments. Cross calibrations were not conducted, thus preventing a comparison with other instruments employed in the Da Vinci II experiment.

Table 1. Identification of selected data collected on Da Vinci II

Participant	Parameter	Comment
Sandia Laboratories	Altitude	Encoding Altimeter
	Ozone	Dasibi Instrument
	Sulfur Dioxide	Thermo-Electron (TECO) Pulsed Fluorescent Instrument
	CO, CH_4, H_2, Ne	Grab samples collected in evacuated stainless steel cans for detailed GC analysis by NCAR at Boulder, CO.
National Oceanic and Atmospheric Agency (NOAA)	Temperature	Thermometer (Dry Bulb)
	Relative Humidity	Sling Psychrometer
	Condensation Nuclei	Gardner Small Particle Detector, Type CN
Research Triangle Institute (RTI)	CO, CH_4, C_2H_2, C_2H_4+C_2H_6, C_3H_6, C_3H_8, i-C_4H_{10}, n-C_4H_{10}, 1-C_4H_8, T-2-C_4H_8, iC_5H_{10}, F-11, F-12	Grab samples collected in light-shielded Tedlar® bags for detailed GC analysis at Research Triangle Park, NC.
Washington State University (WSU)	C_2H_2, C_2H_4, C_2H_6, N_2O, $CC\ell_4$, $CH_3CC\ell_3$, F-11, F-12	Grab samples collected in evacuated stainless steel cans for detailed GC analysis at Pullman, WA.
U.S. Army Atmospheric Sciences Laboratory (ASL)	Ozone Temperature Relative Humidity	Solid-phase chemiluminescent instrument; data recorded every 2 s over complete flight.

Between 1500 and 1743 CST on the afternoon of 9 June after the balloon had landed, two regional-scale horizontal flights were conducted by the Indianapolis Center for Advanced Research (ICFAR). Ozone was measured at 458 m (1,500 ft) above ground level (AGL) and 671 m (2,200 ft) AGL over a distance extending from 225 km northeast to 290 km southwest of Indianapolis. Cross calibrations were not conducted with other instruments employed in the Da Vinci II experiment. Both the NOAA and ICFAR data were used as reported by the respective investigators.

3.1.3 Acoustic Sounder Measurement

Sequential acoustic soundings of the lower atmosphere were conducted by Argonne National Laboratory (ANL). Two mobile acoustic sounders were employed at ground level to measure the thermal structure of the planetary boundary layer. These devices were employed in a "leap frog" fashion to follow the track of the balloon.

3.1.4 RTI-EML Measurements

3.1.4.1 Ground Level Measurements

Continuous ozone, nitrogen oxide (NO, NO_x), and sulfur dioxide measurements and continual (i.e., once every 5 min) measurements for THC, CH_4, and CO were made aboard the RTI-EML for a 16-day period prior to the launch of Da Vinci II and during the actual flight. During that period, the RTI-EML was parked at Arrowhead Airport, located approximately 24 km west of St. Louis. Sample air was aspirated through a Teflon®-glass manifold system from a height of 10 m. Figure 3 shows the RTI-EML onsite at Arrowhead Airport prior to the launch of Da Vinci II. During the in-transit measurement period, sample air was provided to the instruments through a Teflon®-glass manifold. Its inlet was located approximately 3.5 m from the ground and extended 1 m in front of the RTI-EML. Theoretical calculations and extensive road tests were conducted to insure that effects due to aerodynamic characteristics of the RTI-EML and vehicular exhausts on the ambient air sample were minimized. A minimum flow of 0.1 m^3/min was maintained through the manifold at all times. To demonstrate the feasibility of making mobile air quality measurements using this system, drive-by comparisons were conducted on the RTI campus using a stationary ozone monitor (i.e., ground station) and multiple passes of the RTI-EML. Ozone measurements were selected for comparison purposes. Results of multiple

Figure 3. RTI Environmental Monitoring Laboratory onsite at Arrowhead Airport.

comparisons showed agreement, in the mean, between stationary and mobile ozone measurements to within 0.003 ppm.

Instrumentation and calibration procedures used to obtain ambient air measurements prior to the flight and during the flight for the above-mentioned pollutants are summarized in table 2. Appropriate quality control procedures and a sufficient number of instrument calibrations were performed to obtain high quality data. Quality control procedures included verifying calibration procedures, standards, and operating procedures; performing dynamic calibrations and checks; maintaining adequate records to describe instrument performance; and thorough training of the instrument technicians.

3.1.4.2 RTI Balloon-Borne Measurements

Instrumentation and equipment were installed on board the Da Vinci gondola by RTI for the collection of time-integrated samples in Tedlar® bags at hourly intervals for subsequent selected hydrocarbon and halocarbon analyses at RTI.

The detailed hydrocarbon analyses were performed using a modified Perkins-Elmer Model 900 gas chromatograph coupled to a Hewlett-Packard Model 2100A computer. The following ten hydrocarbons were selected for routine analysis:

Table 2. RTI-EML air quality instrumentation and calibration procedures

Pollutant*	Instrument	Measurement Principle	Minimum Detectable Concentration	Mode	Calibration Procedure
O_3	Bendix 8002	Chemiluminescence	1 ppb	Continuous	Gas Phase Titration
NO	Bendix 8101B	Chemiluminescence	5 ppb	Continuous	NBS SRM (NO in N_2); Gas Phase Titration (NO_x)
NO_x	Bendix 8101B	Chemiluminescence	5 ppb	Continuous	NBS SRM (NO in N_2); Gas Phase Titration (NO_x)
SO_2	Teco 43	Pulsed Fluorescence	2 ppb	Continuous	NBS Permeation Tube
THC CH_4 CO	Beckman 6800	Flame Ionization	20 ppb	Cyclic, 5 minutes	CH_4 and CO in Certified Aluminum Cylinders

*O_3--ozone.
NO--nitric oxide.
NO_x--oxides of nitrogen.
SO_2--sulfur dioxide.
THC--total hydrocarbons.
CH_4--methane.
CO--carbon monoxide.
N_2--nitrogen.

ethylene/ethane
acetylene
propane
propylene
isobutane
n-butane
1-butene
trans-2-butene
isopentane
cyclopentane

Separation of the C_2-C_5 hydrocarbons was made on a 1.8-m x 0.15-cm i.d. Durapak n-octane (100-120 mesh) column that was operated at 23° C. The sum of the above 10 nonmethane hydrocarbons was computed for each grab sample collected on board the Da Vinci II system and is hereafter referred to as Σ NMHC. Methane and carbon monoxide concentrations were measured on each grab sample using a Beckman 6800 Air Quality Chromatograph.

Freon® 11 and Freon® 12 analyses were performed on grab samples collected during flight using a Perkins-Elmer Model 3920 gas chromatograph with electron-capture detector. These compounds were separated on a 2-m glass column packed with Chromosorb W-H.P. and coated with 10 percent DC-200. A quality control program was conducted by RTI in conjunction with hydrocarbon sampling and analysis and is described in appendix C.

3.1.5 State Agency Measurements

Hourly average ozone data were acquired for the period 6-10 June from 35 air monitoring sites operated by various State air pollution control agencies. The data were collected at nine Kentucky stations, six Indiana stations, and twenty Illinois stations.

3.1.6 RAMS Network Measurements

The U.S. Environmental Protection Agency has sponsored a multiyear air pollution measurement program in St. Louis, Missouri. This program is known as the Regional Air Pollution Study or RAPS. A network comprised of 25 ground stations was established to provide selected air quality and meteorological data for the St. Louis area on a continual basis. This network is known as the Regional Air Monitoring System (RAMS).

RAMS stations are located on concentric circles having radii of 4, 9, 20, and 40 km from a center in downtown St. Louis. The stations are numbered from 101 to 125 with the station numbers generally increasing with distance from the downtown area. The locations of stations 101 through 121 are shown in figure 4. The remaining four stations, the most remote in the network, are located just off the map; station 122 is located north, 123 is east, 124 is south, and 125 is west.

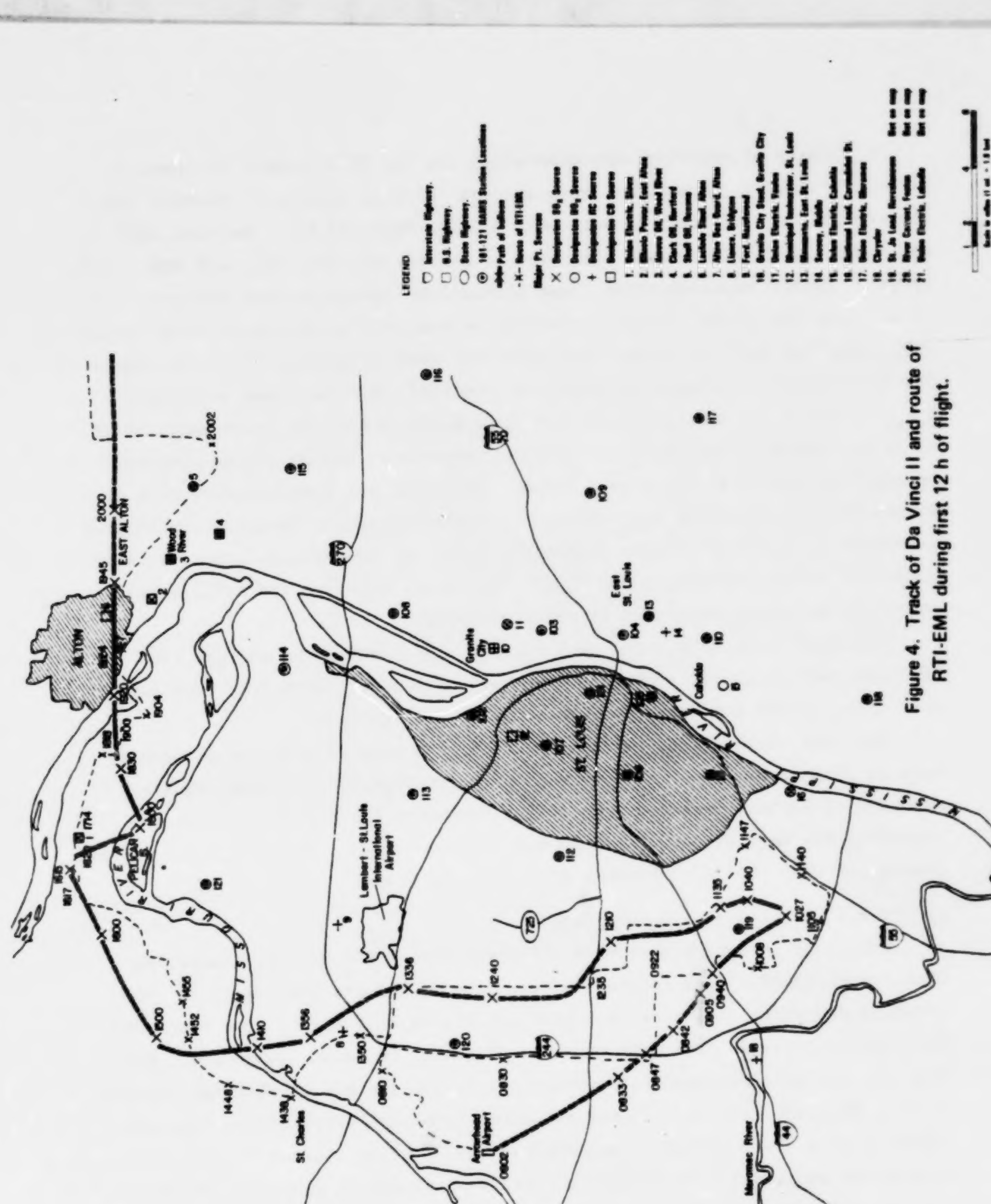
LEGEND
ALTON
EAST ALTON
Wood River
St Charles
Lambert - St Louis International Airport
Arrowhead Airport
Granite City
ST. LOUIS
East St. Louis
Cahokia
Meramec River
Labadie
270
244
44
55
40
725

Figure 4. Track of Da Vinci II and route of RTI-EML during first 12 h of flight.

A summary of selected instrumentation for the RAMS network is shown in table 3. With few exceptions, each station is fully equipped. Monitor Labs instruments were employed to determine O_3, NO, NO_2, and NO_x. Beckman 6800 environmental chromatographs were used to monitor CO, THC, CH_4, and NMHC. Two types of sulfur monitors using flame photometric detection were employed. In 13 stations the Tracor sulfur chromatograph was used to determine total sulfur (TS), SO_2, and H_2S; the Meloy instrument was used to monitor TS in the remaining 12 stations. Integrating nephelometers (MRI) were employed to measure B_{scat}. Wind speed and wind direction were monitored by MRI instruments at 10 or 30 m, depending on the site. Ambient temperature was monitored with MRI temperature probes at 5 m at all sites. Dew point was determined by EG & G thermoelectric dew point hygrometers. At selected sites, vertical temperature gradients of up to ±5° C were determined using MRI temperature probes located on towers at altitudes of 5 and 30 m. Barometric pressure and total solar radiation were also monitored at selected sites.

Validated RAMS data for June 5 through 9 were retrieved on tape from the EPA data bank as hourly averages. The data were then transferred from tape to disc files by RTI for subsequent examination and analysis.

The time designations employed by RAMS have been adopted for all hourly data in this study. Hour designations progress from 0000 to 2300 and are reported in Central Standard Time (CST). Averages for a particular hour represent the mean of data taken during that hour, i.e., the 0700 value is the average of data collected between 0700 and 0759 CST.

3.1.7 Emissions Inventory Data

Emissions inventory data were retrieved from EPA's National Emissions Data System (NEDS). The retrievals were made in May and June of 1977. The counties for which data were requested are listed in table 4. Two types of data were retrieved: raw data reports and county emissions summaries. Raw data reports were employed to identify and locate the major pollution sources of SO_x, NO_x, THC, and CO. County emissions summaries describe the contributions of area sources such as automobiles and of point sources to the total countywide emissions. It should be noted that different practices of reporting and updating records by regulatory agencies introduce uncertainties into these data. For this reason, officials with various State and local agencies having jurisdiction within the study area were interviewed to obtain current

Table 3. RAMS instrumentation

Measured Quantity	Instrument Model	Units	Station No.																								
			101	102	103	104	105	106	107	108	109	110	111	112	113	114	115	116	117	118	119	120	121	122	123	124	125
O_3	Monitor Labs 8410A	ppm	X	X	X	X	X	X	X	X	X	X	X	X	X	X	X	X	X	X	X	X	X	X	X	X	X
$NO-NO_x$	Monitor Labs 8440	ppm	X	X	X	X	X	X	X	X	X	X	X	X	X	X	X	X	X	X	X	X	X	X	X	X	X
$CO-CH_4-THC$	Beckman 6800	ppmC	X	X	X	X	X	X	X	X	X	X	X	X	X	X	X	X	X	X	X	X	X	X	X	X	X
$TS-SO_2-H_2S$	Tracor 270HA	ppm	X		X	X	X	X		X					X	X	X	X				X	X	X			
TS	Meloy SA 185	ppm		X					X		X	X	X	X					X	X	X				X	X	X
Light Scattering Coefficient, B_{scat}	MRI 1561	m^{-1}	X	X	X	X	X	X	X	X	X	X	X	X	X	X	X	X	X	X	X	X	X	X	X	X	X
Wind Speed	MRI 1022 S	$m\ s^{-1}$	X	X	X	X	X	X	X	X	X	X	X	X	X	X	X	X	X	X	X	X	X	X	X	X	X
Wind Direction	MRI 1022 D	Degrees	X	X	X	X	X	X	X	X	X	X	X	X	X	X	X	X	X	X	X	X	X	X	X	X	X
Temperature	MRI 840-2	°C	X	X	X	X	X	X	X	X	X	X	X	X	X	X	X	X	X	X	X	X	X	X	X	X	X
Dew Point	Cambridge 880	°C	X	X	X	X	X	X	X	X	X	X	X	X	X	X	X	X	X	X	X	X	X	X	X	X	X
Temp. Gradient	MRI 840-1 & 2	°C	X	X		X	X	X	X		X		X	X	X									X	X		
Barometric Pressure	MRI 751	in Hg	X								X			X										X	X	X	X
Total Solar Radiation ($\lambda>295$)	Eppley Pyranometer	$cal\ cm^{-2}\ min^{-1}$			X	X				X						X				X				X			

Table 4. Counties for which emissions inventory data were retrieved

Missouri

Lincoln*
Warren*
Franklin*
St. Charles*
St. Louis*
Jefferson*

Illinois

Jersey*
Macoupin*
Madison*
St. Clair*
Monroe*
Montgomery
Bond
Clinton
Washington
Shelby
Fayette
Marion
Jefferson
Effingham
Clay
Wayne
Cumberland
Jasper
Richland
Edwards
White
Clark
Crawford
Lawrence
Wabash

Indiana

Sullivan
Knox
Gibson
Posey

*Counties included in the greater St. Louis area.

information on major sources. In addition, the detailed emissions inventory established in support of RAPS was used to supplement NEDS data. The RAPS emissions inventory can resolve emissions data within the study area to time increments as fine as 1 h. The RAPS data bank was incomplete at the time of the current study and validated data were not available. Preliminary retrievals of annual emissions rates were therefore used in the present study; the counties for which RAPS emissions inventories were used are noted in table 4.

3.2 Flight Description

On 8 June 1976, at 0756 CST, the Da Vinci II system was launched from Arrowhead Airport, 24 km west of St. Louis, Missouri. During the next 24 h Da Vinci II drifted south, then turned north, and finally east across the southern Illinois plains before landing in a wheatfield in southwestern Indiana (see figure 4). Figure 4 shows the flight track of Da Vinci II for the first 12 h in and about the St. Louis area, the RTI-EML ground track, and

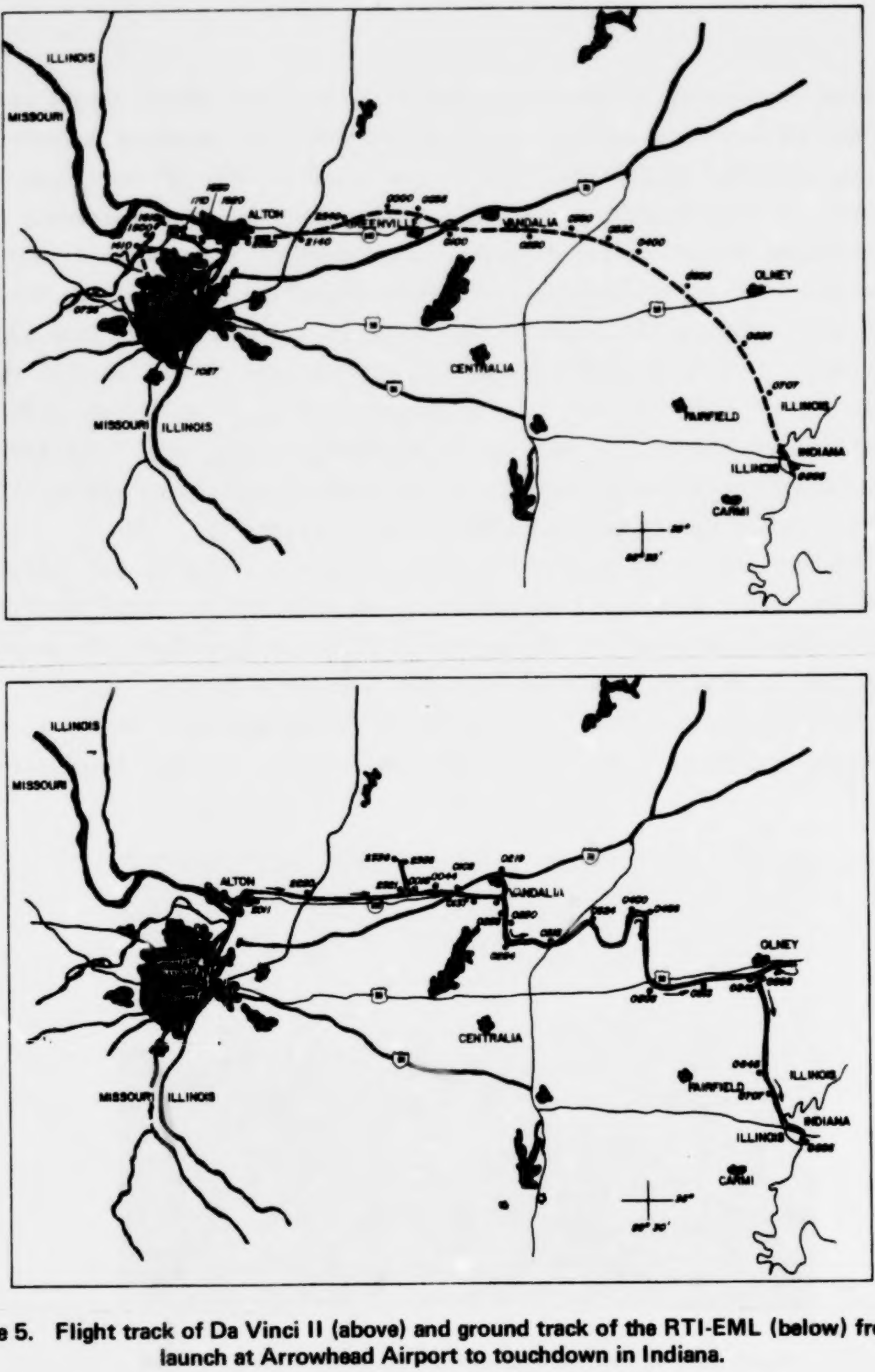
ILLINOIS
MISSOURI
1610
1710
ALTON
2140
GREENVILLE
VANDALIA
0400
OLNEY
CENTRALIA
1027
0707
FAIRFIELD
ILLINOIS
INDIANA
CARMI
MISSOURI
ILLINOIS
ILLINOIS
MISSOURI
ALTON
2011
0219
VANDALIA
0400
OLNEY
CENTRALIA
FAIRFIELD
ILLINOIS
INDIANA
CARMI
MISSOURI
ILLINOIS
88° 30'

Figure 5. Flight track of Da Vinci II (above) and ground track of the RTI-EML (below) from launch at Arrowhead Airport to touchdown in Indiana.

major pollution sources in the area. Figure 5 shows the entire flight track of Da Vinci II and the ground track of the RTI-EML from launch at Arrowhead Airport to touchdown in Indiana. The flight ended at 0805 CST on 9 June 1976.

During the 24-h flight, the RTI-EML was used to obtain measurements of ozone, nitrogen oxides, sulfur dioxides, total hydrocarbons, methane, and carbon monoxide at ground level approximately along and underneath Da Vinci II's track (see figure 5). With the exception of a 2-h period of time early in the morning (≈0300 to 0500 CST) on 9 June 1976, the RTI-EML was in visual and radio contact with Da Vinci II. At the conclusion of the flight (0805 CST, 9 June 1976), the RTI-EML was within 0.8 km of the landing site. The RTI-EML was then brought adjacent to Da Vinci II for postcalibration of the Dasibi ozone monitor that was flown aboard the balloon (figure 6).

Da Vinci II spent the first 12 h of the flight drifting in the vicinity of St. Louis. (See figure 4.) After launch at 0756 CST, Da Vinci II drifted to the southeast crossing U.S. Highway 40 at 0830 and Interstate 244 at 0838 CST. At 0940 it crossed I-44 passing within 5 km of a Chrysler assembly plant. At approximately 1027 CST Da Vinci II turned and began moving to the northwest recrossing I-44 at 1140 and U.S. 40 at 1215. It then moved directly

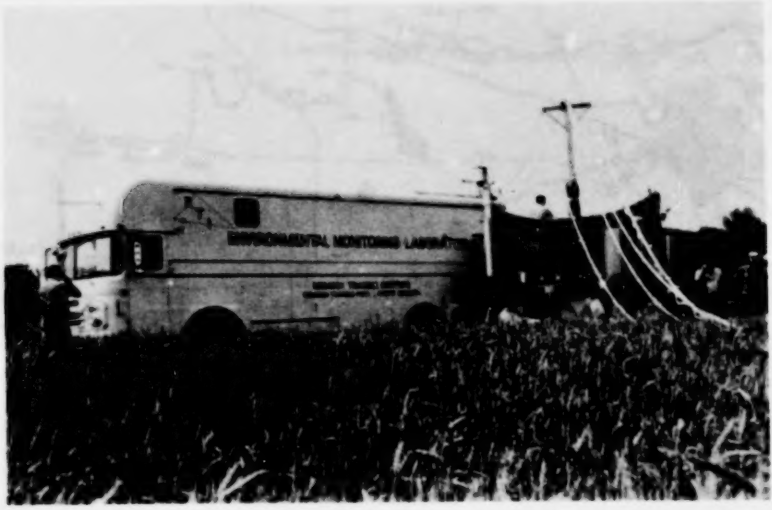

Figure 6. RTI-EML located adjacent to gondola for post-flight calibration of Da Vinci II analyzers.

north for the next hour and 20 minutes. Moving to the northwest during the period between 1336 and 1356 CST, Da Vinci II passed over I-70 and I-270. This location is within 4 km of Lambert Field (St. Louis International Airport) and a Ford assembly plant. The direction shifted to slightly east of north and Da Vinci II crossed the Missouri River for the first time at 1410 CST. At 1500 the direction began to shift more toward the east. The airspeed was reduced significantly, and from 1615 to 1830 CST the craft covered only about 6 km. During this period Da Vinci II passed within about 3 km of the Union Electric Sioux Power Plant and crossed the Missouri River and Pelican Island. At 1830 the airspeed increased with the craft moving directly to the east. Da Vinci II crossed the Mississippi River at 1910 and had passed over the southeastern tip of Alton, Illinois, by 1945 CST. This location is within 1 km of the Illinois Power Wood River Power Plant in East Alton. Between 1945 and 2015 CST it traveled 3 to 5 km north of a heavily industrialized area. Three major oil refineries are located in Wood River and Roxana. Drifting to the east, Da Vinci II moved outside the St. Louis study area at approximately 2140 CST when it crossed I-55 near Hamel at the intersection with Illinois 140.

The entire flight track of Da Vinci II from launch to touchdown is illustrated in figure 5. The portion of the flight track traveled by Da Vinci II after it left the greater St. Louis area until touchdown is referred to as the "downwind flight track." Da Vinci II moved eastward from St. Louis on the evening of 8 June crossing I-55 at 2140 CST, and passed 8 km north of Greenville and 14 km south of Coffeen at just after midnight. An 870-MW coal-fired power plant located at Coffeen was the only major point source in close proximity to the downwind flight track. Da Vinci II crossed I-70 near the intersection with Illinois 140 at 0100 on 9 June. The craft continued its eastward path and passed 10 km to the south of Vandalia at 0200. Between 0300 and 0330 CST it crossed I-57, and its direction began to shift toward the southeast. From this point until touchdown Da Vinci II was passing over oil fields. During the interval between 0505 and 0635 CST, the flight track crossed U.S. 50 and moved toward the south. Da Vinci II maintained this direction as it drifted over the Wabash River into Indiana, crossed I-64, and touched down in a wheat field. The craft landed at 0805 CST on the morning of 9 June after having flown approximately 340 km in 24 h.

The altitude-time profile presented in figure 7 shows the vertical move-

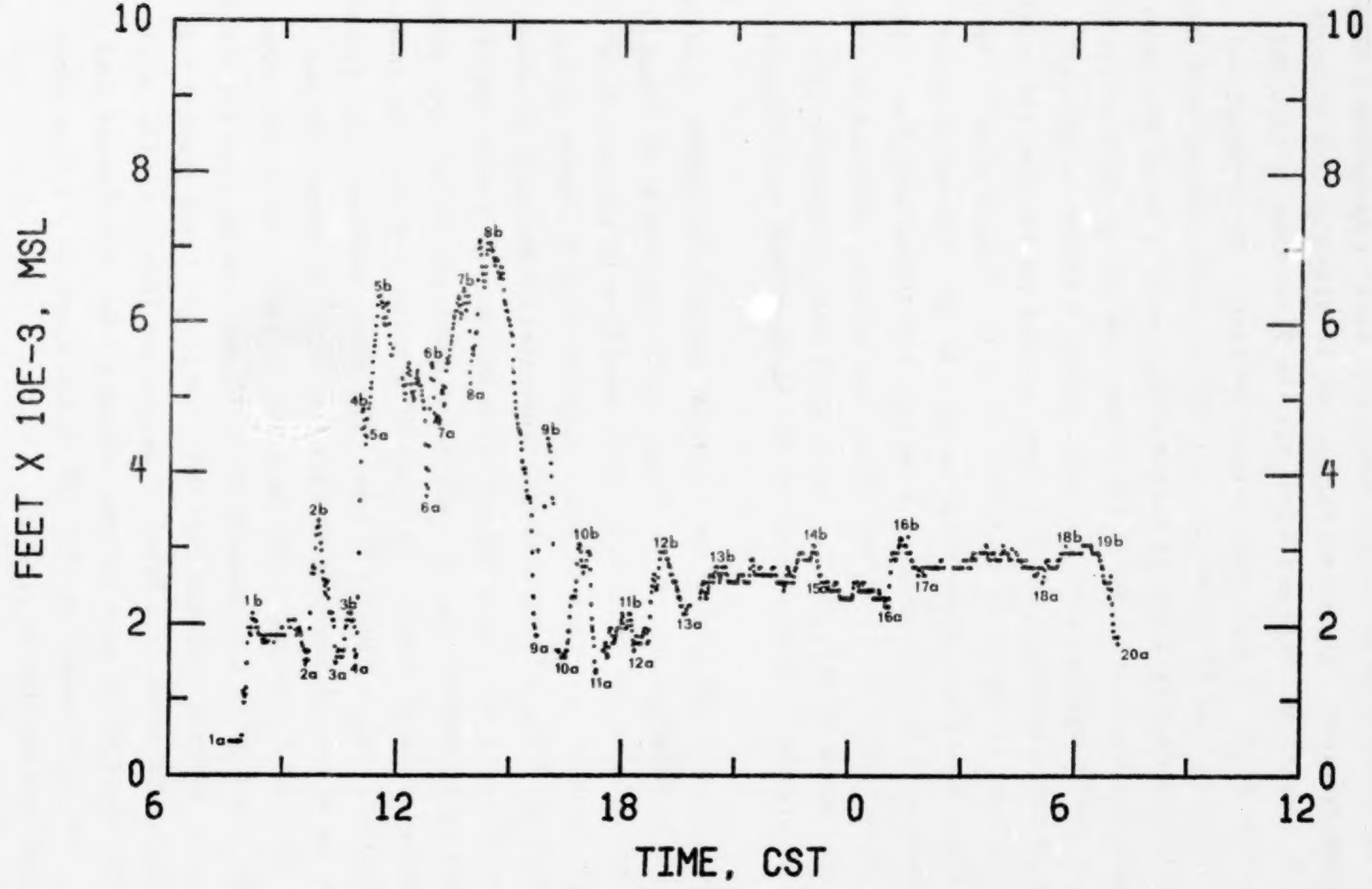

Figure 7. Da Vinci II altitude data, 8 and 9 June 1976.
(See table 5 for key to numbered altitude excursions.)

Table 5. Major altitude excursions of Da Vinci II

No.	Time CST	Minimum altitude feet, MSL	No.	Time CST	Maximum altitude feet, MSL
1a	0756	450	1b	0813	2150
2a	0937	1483	2b	0956	3350
3a	1025	1473	3b	1047	2150
4a	1056	1550	4b	1105	4850
5a	1110	4370	5b	1130	6350
6a	1247	3677	6b	1254	5450
7a	1306	4650	7b	1343	6450
8a	1355	5177	8b	1409	7093
9a	1543	1850	9b	1603	4350
10a	1625	1550	10b	1651	3050
11a	1719	1350	11b	1741	1950
12a	1820	1650	12b	1901	2950
13a	1941	2150	13b	2009	2550
14	-	-	14b	2304	3050
15a	2318	2550	-	-	-
16a	0100	2250	16b	0123	3150
17a	0151	2650	-	-	-
18a	0509	2550	18b	0538	2950
19	-	-	19b	0637	2950
20a	0710	1763	-	-	-

ment of Da Vinci II during the flight. The numbered altitude excursions are identified in table 5. Shortly after launch, Da Vinci II achieved an altitude of approximately 579 m (1,900 ft) MSL and maintained this altitude until it began to experience thermal turbulence. The craft descended to 452 m (1,483 ft) at 0937 CST, rose to 1,021 m (3,350 ft) at 0956 CST and descended to 449 m (1,473 ft) at 1025 CST.

It was at this time that the balloon turned from a southeastward to a northwestward horizontal direction. The balloon continued to experience vertical perturbations, was allowed to rise at 1056 CST to conserve helium, and at 1130 CST achieved an altitude of 1,935 m (6,350 ft). Most of the northward leg of the flight track was traversed at altitudes between 1,219 m and 2,133 m (4,000 and 7,000 ft). Shortly after crossing the Missouri River during the interval from 1425 to 1543 CST, the craft experienced a sharp descent from 2,149 m (7,050 ft) to 564 m (1,850 ft). As the balloon was moving slowly eastward across the Missouri and Mississippi Rivers, four less severe altitude excursions occurred at 1603, 1651, 1741, and 1901 CST. From 1941 until the final descent for landing at 0637 on 9 June, altitude was relatively stable between 655 m and 930 m (2,150 and 3,050 ft).

3.3 Meteorological Conditions for the Period Encompassing Flight Day

The general meteorological conditions were examined for 6-9 June 1976. This 4-day period encompasses the flight day. The conditions that were examined include synoptic-scale air mass behavior, wind speed, wind direction, insolation, and temperature. These factors exert a significant influence on the extent to which pollutants may interact in the atmosphere. Physical factors determine the extent of both vertical mixing and horizontal transport. Atmospheric mixing dictates the extent to which pollutants such as hydrocarbons and nitrogen oxides accumulate and therefore determines their ambient concentration levels. Insolation and temperature are influential in determining the progression of photochemical reactions such as those that result in the formation of ozone.

The study area came under the influence of a high pressure system during the first week of June. This system followed an unusual track moving southwestward from Ontario on 2 June toward the mid-Mississippi Valley where it stagnated and gave rise to high levels of air pollution. As the center of the high pressure system moved to the south on 3-6 June, winds from the east brought polluted air into the midwest. As the system continued to move to the south, return flow caused a shift in wind direction. By the morning of 8 June, the surface winds had shifted 180° and were from the west. The air mass then began to progress slowly to the east. By 12 June, this system had been pushed off the east coast by another air mass.

Mean profiles of selected meteorological parameters monitored in St. Louis by RAMS describe hourly behavior of these parameters averaged across the RAMS network. These profiles are presented in figure 8 for the 4-day period, 6-9 June.

The 0700 CST surface weather maps prepared by the National Weather Service were examined for 6-9 June. A large high pressure system was centered over Wisconsin on 6 June and covered most of the midwestern and eastern States. By 7 June the high pressure system was centered over the St. Louis area and remained there for the flight day, 8 June. The system began to weaken on 9 June, although it continued to dominate the weather map. The behavior of

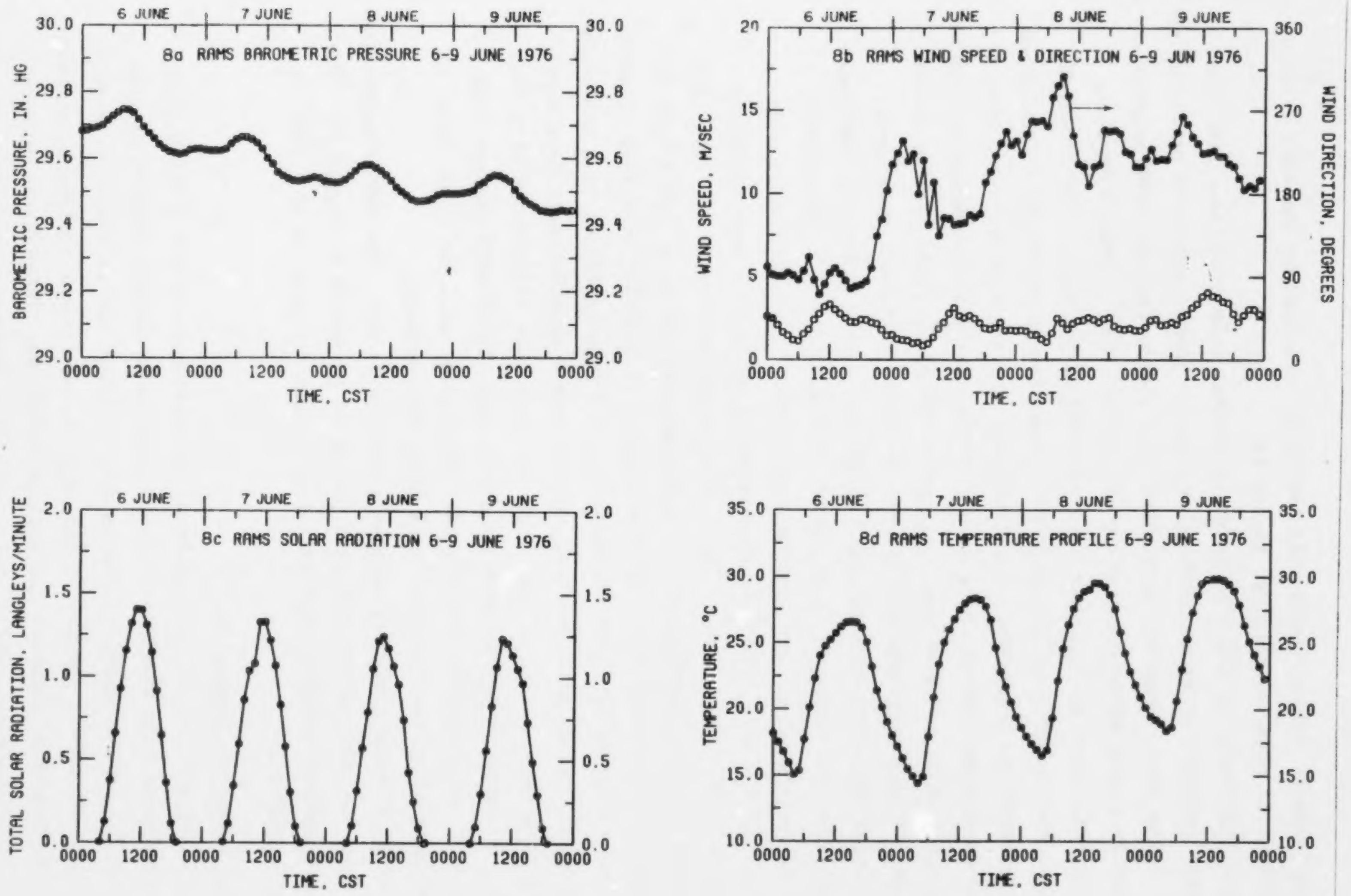

Figure 8. RAMS meteorological parameters for 6-9 June 1976.

the high pressure system during this period is reflected by the RAMS network mean barometric pressure profile, figure 8a.

Near the center of the high pressure system, calm conditions and clear skies were recorded at many reporting stations. These conditions prevailed in the St. Louis area. Mean hourly surface wind speeds from the RAMS network as indicated in figure 8b were generally less than 3 $m\ s^{-1}$. Mean RAMS solar radiation data shown in figure 8c also indicate clear skies. The stagnant conditions associated with this type of weather system allow the accumulation of both primary and secondary air pollutants. The regional scale problem of elevated summertime ambient ozone levels is associated with atmospheric conditions of this type. In addition, calm winds and clear skies provide favorable conditions for the development of strong nocturnal radiation inversions.

Although the winds were generally light and disorganized, the RAMS mean wind direction profile shown in figure 8b indicates distinct directional changes in surface winds over the 6-9 June period. On 6 June winds were generally from the east; however, they began to shift to a more southerly component shortly after sundown. On 7 June, winds were basically from the south, shifting from southwesterly to southeasterly and back. On flight day, mean winds were from the west: for the first 5 or 6 h they were from slightly south of west; during the 0700 CST hour they had begun shifting to a northwesterly component; before noon they had shifted from a northwesterly to a more southerly component; by sunset the winds had once more shifted and were from the west. Although it may be somewhat fortuitous, these RAMS surface wind patterns were qualitatively reflected by the daytime movement of Da Vinci II. On the morning of 9 June the winds were from the southwest.

A slight warming trend was evident from 6 to 9 June. The mean temperature profile from the RAMS network for this period is presented in figure 8d. The maximum and minimum ambient temperatures on flight day were 30.2° C (86° F) and 13.8° C (57° F).

3.4 Quality Control Program

To achieve and maintain a high level of confidence in air quality data, it is essential to have a well-designed, operational quality control program. Quality control for air quality measurements on board the Da Vinci II gondola and RTI-EML included (1) the use of reference or equivalent analyzers, whenever possible, reference or accepted calibration techniques, NBS-SRMs as primary standards for calibration, and standard operation, maintenance, and calibration procedures; (2) reference of calibration systems and personnel to systems and standards maintained by the Quality Assurance Branch, Environmental Monitoring and Support Laboratory, Environmental Protection Agency, Research Triangle Park, North Carolina; (3) performance of dynamic calibration of air quality analyzers prior to and after the flight of Da Vinci II; (4) maintenance of adequate records that describe instrument performance; (5) design and checkout of intake manifold of RTI-EML for mobile sampling; and (6) system comparison (RTI-EML) to stationary monitor (i.e., drive-by comparison) to assess comparability of mobile measurements to ground station measurements. In addition, logs and records were maintained during the flight that documented the position of the RTI-EML relative to the Da Vinci II gondola, identified times when the RTI-EML was stationary and generator exhaust might influence ambient measurements, and described the Da Vinci II flight and RTI-EML tracks. Data were examined and validated immediately after the flight using accepted techniques. Primary standards used for calibration purposes were verified prior to and immediately after the Da Vinci II flight.

3.5 Analysis Approach

The atmosphere is the active medium where all chemical processes occur. The investigation of the role of the atmospheric processes upon the air chemical processes, as revealed through measurements, is an essential part of the total analysis effort. If the atmosphere were purely passive, laboratory models would be sufficient to explain the measurements.

The analyses of both the chemical and the atmospheric processes for Da Vinci II consider data taken from two frameworks. Ground station chemical and meteorological and upper air data were taken from a Eulerian system; i.e., the observer is fixed in space and observes changes as the medium moves past, while Da Vinci II measurements (aboard the balloon) were taken in a nearly Lagrangian system; i.e., the observer is moving (approximately) with the medium and measures the changes that occur from processes within the flow. Meteorological characteristics of the balloon environment are related to the chemical and oxidant concentrations measured aboard Da Vinci II and to measurements from other platforms--aircraft, RTI-EML, and ground stations.

Information was assembled from many sources to provide a comprehensive description of the atmospheric and pollutant behavior during the study period both aloft and at ground level. Aircraft data, when available, were used to supplement information from the balloon to describe processes that were occurring aloft. Data from the Regional Air Monitoring Study (RAMS) network, the RTI-EML, and Indiana, Illinois, and Kentucky State pollution monitoring stations were employed to describe pollutant behavior at the ground. Emissions inventory data were also examined to locate major pollutant sources within the study area.

Independent analyses of the data were performed to provide chemical and meteorological interpretations for Da Vinci II. These analyses are discussed in the following sections.

4.0 ATMOSPHERIC CHEMISTRY ANALYSIS FOR DA VINCI II

4.1 Objectives of Analysis

The purpose of this analysis of Da Vinci II data was to examine the atmospheric chemistry processes that occurred and to investigate relationships between primary and secondary air pollutants upwind, within, and downwind of a city. The behavior of ozone and its precursors was a major concern. Specific objectives were to describe and examine the following:

1. The levels of ozone and ozone precursors that occurred upwind of the urban area;
2. The impact of urban sources of ozone precursors on the ambient concentrations of both ozone and its precursors;
3. The impact of precursor and ozone transport on urban ozone concentration levels;
4. The transformations of ozone and precursors during transport;
5. Differences between daytime and nighttime pollutant behavior;
6. The scale or extent of urban transport; and
7. The feasibility of balloon-borne experiments for obtaining the data needed to address these points.

4.2 Approach

Information from many sources was assembled to provide a comprehensive description of the atmospheric and pollutant behavior during the study period both aloft and at ground level. Aircraft data, where available, were used to supplement information from Da Vinci II to describe the processes that were occurring aloft. Data from the RAMS network and the RTI-EML were employed to describe pollutant behavior at the ground. Emissions inventory data were also examined to locate major pollutant sources within the study area.

4.3 Results and Discussion

4.3.1 Emissions Inventory

Before an assessment of atmospheric pollutant behavior was conducted, the major sources in the study area were identified. Major point sources of SO_2, NO_x, HC, and CO were ranked and are listed in tables 6-9. In these tables the sources within the St. Louis area covered by the first 12 h of the flight are segregated from the sources within the area covered by the last 12 h of the flight (downwind flight track). The positions of the major point sources and highways are located along the flight track of Da Vinci II as illustrated in figure 4.

Table 6. Major SO_2 point sources along the flight track of Da Vinci II

Rank[a]	Source	County	State	Source Type	Emission Rate, Tons Per Year NEDS	 RAPS[b]
Greater St. Louis Area						
1	Union Electric, Labadie	Franklin	Mo.	Electric Generation	274,200	263,608
2	Union Electric, Meramec	St. Louis	Mo.	Electric Generation	104,740	187,440
3	Illinois Power, East Alton	Madison	Ill.	Electric Generation	93,580[c]	47,590
4	Union Electric, Sioux	St. Charles	Mo.	Electric Generation	88,900	275,824
5	St. Jo Lead	Jefferson	Mo.	Industrial Process	87,900	29,030
6	Union Electric, Venice	Madison	Ill.	Electric Generation	33,530[c]	11,380
7	Shell Oil, Roxana	Madison	Ill.	Petroleum Refining	30,357[c]	1,140
8	River Cement, Festus	Jefferson	Mo.	Industrial Process	19,900	12,950
9	Alton Box Board, Alton	Madison	Ill.	Industrial Process	13,060[c]	10,280
10	Amoco Oil, Wood River	Madison	Ill.	Petroleum Refining	12,812[c]	14,980
11	Monsanto, East St. Louis	St. Clair	Ill.	Industrial Process	11,840[c]	2,450
12	National Lead, Carondolet St.	St. Louis	Mo.	Industrial Process	7,390	6,470
13	Clark Oil, Hartford	Madison	Ill.	Petroleum Refining	4,950	18,500
Downwind Flight Track						
1	Central Illinois Public Service, Coffeen	Montgomery	Ill.	Electric Generation	82,200	---- [d]
2	I & M, Sullivan	Sullivan	Ind.	Electric Generation	62,200	---- [d]
3	Indiana Public Service, Gibson	Gibson	Ind.	Electric Generation	33,200	---- [d]
4	Central Illinois Public Service, Hutsonville	Crawford	Ill.	Electric Generation	15,760	---- [d]

---

[a] Ranked in decreasing order based on information retrieved from the National Emissions Data System (NEDS).

[b] Unvalidated emissions data from RAPS Emissions Inventory.

[c] On June 7, 1977, Ray Beckett of the Illinois EPA reported the following SO_2 emissions rates (TPY) for selected sources; Illinois Power, East Alton-18115; Union Electric, Venice-10,110; Shell Oil, Roxana-52,500; Alton Box Board, Alton-4580; Amoco Oil, Wood River-9050; Monsanto, East St. Louis-6860; Clark Oil-3150; and Central Illinois Public Service, Coffeen-232,800.

[d] Blanks designate that the data were not available.

Table 7. Major NO_x point sources along the flight track of Da Vinci II

Greater St. Louis Area					Emission Rate, Tons Per Year	
Rank[a]	Source	County	State	Source Type	NEDS	RAPS[b]
1	Union Electric, Meramec	St. Louis	Mo.	Electric Generation	32,080	52,620
2	Union Electric, Labadie	Franklin	Mo.	Electric Generation	31,370	71,730
3	Illinois Power, East Alton	Madison	Ill.	Electric Generation	22,220	9,740
4	Union Electric, Sioux	St. Charles	Mo.	Electric Generation	14,060	131,640
5	Shell Oil, Roxana	Madison	Ill.	Petroleum Refining	10,480	---- [c]
6	Union Electric, Venice	Madison	Ill.	Electric Generation	9,340	7,520
7	Amoco Oil, Wood River	Madison	Ill.	Petroleum Refining	3,525	3,400
8	Alton Box Board, Alton	Madison	Ill.	Industrial Process	2,010	1,660
9	Monsanto, East St. Louis	St. Clair	Ill.	Industrial Process	1,620	---- [c]
10	Clark Oil, Hartford	Madison	Ill.	Petroleum Refining	1,400	970
11	River Cement, Festus	Jefferson	Mo.	Industrial Process	1,340	1,410
12	Union Electric, Cahokia	St. Clair	Ill.	Electric Generation	1,300	---- [c]
13	National Lead, Carondolet St.	St. Louis	Mo.	Industrial Process	1,040	3,820
Downwind Flight Track						
1	Central Illinois Public Service, Coffeen	Montgomery	Ill.	Electric Generation	30,570	---- [c]
2	I & M, Sullivan	Sullivan	Ind.	Electric Generation	24,200	---- [c]
3	Indiana Public Service, Gibson	Gibson	Ind.	Electric Generation	9,260	---- [c]
4	Central Illinois Public Service, Hutsonville	Crawford	Ill.	Electric Generation	3,730	---- [c]

---

[a] Ranked in decreasing order based on information retrieved from the National Emissions Data System (NEDS).

[b] Unvalidated emissions data from RAPS Emissions Inventory.

[c] Blanks designate that the data were not available.

Table 8. Major HC point sources along the flight track of Da Vinci II

Rank[a]	Source	County	State	Source Type	Emission Rate, Tons Per Year NEDS	Emission Rate, Tons Per Year RAPS[b]
Greater St. Louis Area						
1	Clark Oil, Hartford	Madison	Ill.	Petroleum Refining	25,310	770
2	Shell Oil, Roxana	Madison	Ill.	Petroleum Refining	11,870	----[c]
3	Amoco Oil, Wood River	Madison	Ill.	Petroleum Refining	6,870	150
4	Chrysler	St. Louis	Mo.	Industrial Manufacturing	3,740	3,860
5	Ford, Hazelwood	St. Louis	Mo.	Industrial Manufacturing	3,720	809
6	Monsanto, East St. Louis	St. Clair	Ill.	Industrial Process	2,140	----[c]
7	Granite City Steel	Madison	Ill.	Industrial Process	1,570	----[c]
8	Socony Mobile	St. Clair	Ill.	Petroleum Refining	1,340	----[c]
9	Lianco	St. Louis	Mo.	Industrial Process	1,120	----[c]
Downwind Flight Track						
1	Indiana Farm Bureau	Posey	Ind.	Petroleum Refining	3,860	----[c]
2	Essex Int. Inc.	Knox	Ind.	Industrial Process	2,260	----[c]

[a] Ranked in decreasing order based on information retrieved from the National Emissions Data System (NEDS).

[b] Unvalidated emissions data from RAPS Emissions Inventory.

[c] Blanks designate that the data were not available.

Table 9. Major CO point sources along the flight track of Da Vinci II

Rank[a]	Source	County	State	Source Type	Emission Rate, Tons Per Year NEDS	 RAPS[b]
Greater St. Louis Area						
1	Amoco Oil, Wood River	Madison	Ill.	Petroleum Refining	83,400	70
2	Clark Oil, Hartford	Madison	Ill.	Petroleum Refining	57,600	44,060
3	Laclede Steel, Alton	Madison	Ill.	Industrial Process	6,860	---- [c]
4	Granite City Steel	Madison	Ill.	Industrial Process	1,750	---- [c]
5	Monsanto, East St. Louis	St. Clair	Ill.	Industrial Process	1,100	---- [c]
6	Union Electric, Meramec	St. Louis	Mo.	Electric Generation	1,060	530
7	Illinois Power, East Alton	Madison	Ill.	Electric Generation	1,050	500
8	Union Electric, Sioux	St. Charles	Mo.	Electric Generation	780	2,390
9	Municipal Incinerator	St. Louis	Mo.	Solid Waste Disposel	---- [c]	2,880
Downwind Flight Track						
1	Indiana Farm Bureau	Posey	Ind.	Petroleum Refining	11,600	---- [c]

[a] Ranked in decreasing order based on information retrieved from the National Emissions Data System (NEDS).

[b] Unvalidated emissions data from RAPS Emissions Inventory.

[c] Blanks designate that the data were not available.

Within the St. Louis area, electric power plants and petroleum refineries are the major point sources of SO_2 and NO_x (see tables 6 and 7). Petroleum refineries and automobile assembly plants (surface coating) are the major point sources of HC (see table 8). Petroleum refineries are the primary point sources of CO (see table 9).

The electric power plant at Coffeen, Illinois, is the major point source associated with the downwind flight track. Da Vinci II was in close proximity to this source at midnight when it passed to within 14 km of Coffeen. Da Vinci II passed over the eastern edge of Gibson County just prior to its landing in Posey County, Indiana. Although a power plant is located in Gibson County and a petroleum refinery is in Posey County, the effects of these sources were probably not monitored on Da Vinci II because the instruments were shut down in preparation for landing prior to passage over this area.

Total emissions are summarized in table 10 for the greater St. Louis and downwind areas. Point sources such as those listed in table 6 are the major sources of SO_2, contributing 98 and 96 percent of the totals for the two study areas.

Automobiles are the major sources of HC and CO, comprising 60 and 77 percent of the totals for the St. Louis area. Although it is not reflected in table 10, the petrochemical industry in Madison County, Illinois (Wood River), is the dominant source of HC and CO, comprising 67 and 62 percent of Madison County's HC and CO emissions. Automobiles are the major HC and CO sources in the downwind flight track area and contribute 73 and 88 percent of the total.

In the two study areas, power plant NO_x emissions exceed vehicular emissions by 65 to 110 percent. Power plants contribute 52 percent of the NO_x emissions in the St. Louis area and 61 percent downwind. In contrast, vehicular sources contribute only 31 and 28 percent in these areas.

The point of release of air pollutants is important in determining air quality within a study area. This may be particularly significant at night when a radiation inversion traps emissions near the ground and insulates the ground from pollutants released through stacks into the air above the radiation inversion.

Various ratios of pollutants may be calculated for the two regimes based on emissions data. The SO_2/NO_x mass ratio calculated across all power plants is 4.5. This corresponds to a molar concentration ratio of 3.3. The HC/NO_x and CO/NO_x mass ratios calculated from St. Louis area vehicular emissions are

Table 10. Emissions summaries for counties along the flight track of Da Vinci II

Tons Per Year Of Emissions

Greater St. Louis Area[a]	HC	NO_x	CO	SO_2
Total	192,209	232,056	771,857	823,084
Point	65,125 (34)[b]	140,266 (60)	156,839 (20)	802,588 (98)
Power Plant	992 (<1)	120,691 (52)	3,496 (<1)	662,970 (81)
Area	127,084 (66)	91,790 (40)	615,018 (80)	20,496 (2)
Auto	114,921 (60)	72,325 (31)	592,075 (77)	5,593 (<1)
Downwind Flight Track[c]				
Total	65,582	115,971	304,581	238,647
Point	9,058 (14)	78,258 (67)	13,499 (4)	228,359 (96)
Power Plant	594 (<1)	70,815 (61)	1,573 (<1)	203,602 (85)
Area	56,524 (86)	37,713 (33)	291,082 (96)	10,288 (4)
Auto	47,790 (73)	32,349 (28)	267,272 (88)	1,457 (<1)

[a] The following counties were included: Lincoln, Warren, Franklin, St. Charles, St. Louis, and Jefferson (Missouri); Jersey, Macoupin, Madison, St. Clair, and Monroe (Illinois).

[b] Numbers enclosed with parentheses represent the contribution to the total in percent.

[c] The following counties were included: Montgomery, Bond, Clinton, Washington, Shelby, Fayette, Marion, Jefferson, Effingham, Clay, Wayne, Cumberland, Jasper, Richland, Edwards, White, Clark, Crawford, Lawrence, and Wabash (Illinois); Sullivan, Knox, Gibson, and Posey (Indiana).

1.6 and 8.2. These values correspond to molar ratios of 4.3 and 13.4. The overall HC/NO_x and CO/NO_x mass ratios based on emissions from all sources in the St. Louis area are 0.8 and 3.3. The discrepancies between these overall ratios and those for vehicular sources is contributed primarily by NO_x emissions from power plants.

4.3.2 Air Contaminant Considerations for the Period Encompassing Flight Day

Air parcel trajectories performed by Bujnoch of the Institute of Storm

Research suggest that Da Vinci II was launched into relatively dirty air that had been in eastern Kentucky and the Ohio Valley 72 h earlier. This is generally consistent with the southwestward movement of the high pressure system noted in section 3.3.

Maps of ozone distribution for the northeastern quadrant of the United States are presented in figure 9 through the courtesy of Wolff.[4] These diagrams are based on daily maximum ozone concentrations recorded at approximately 81 locations within the area. On 6 June high ozone and high pressure dominated much of the midwest. Regions of high ozone emanating from St. Louis and other areas were evident on 7 and 8 June. As the high pressure system began to weaken in St. Louis on 9 June, the region of high ozone moved to the east covering a portion of middle Ohio and much of the east coast. Thus, for the period from 6 to 9 June, much of the country east of the Mississippi River was experiencing high levels of ozone.

A polluted condition also developed in the St. Louis area during this time period. Mean profiles of selected chemical parameters monitored by the RAMS network are presented in figure 10. These illustrations depict hourly pollutant behavior averaged across the RAMS network for this 4-day period. A deterioration of air quality is illustrated in the O_3 and B_{scat} profiles shown in figures 10a and b. The daily maximum O_3 levels increased from 6 June through 8 June but were reduced on 9 June. Ozone levels exceeded 0.08 ppm on each day. In general, B_{scat} also increased during the period. Nonmethane hydrocarbon and NO_x profiles presented in figures 10c and d also show a slight tendency toward increased levels from 6 through 8 June with a small reduction on 9 June. Nitrogen oxide levels ranged between 0.005 and 0.11 ppm. Nonmethane hydrocarbon concentrations ranged between 0.00 and 1.00 ppmC and also exceeded 0.24 ppmC on each day.

The CO profile shown in figure 10e behaves similarly to the NMHC and NO_x profiles. In addition, maximum NMHC, NO_x, and CO concentrations occurred at night. Frequently, two peaks occurred--the first shortly before midnight and the second in the early morning hours. Absolute maximum NMHC and NO_x levels may occur before midnight rather than in the early morning between 0600 and 0900 CST. In the absence of mixing, CO, NO_x, THC, and CH_4, having ground-based sources, are expected to accumulate beneath the nocturnal radiation inversion. An injection of cleaner air such as that from aloft would be manifest on a concentration profile as a negative inflection surrounded by two

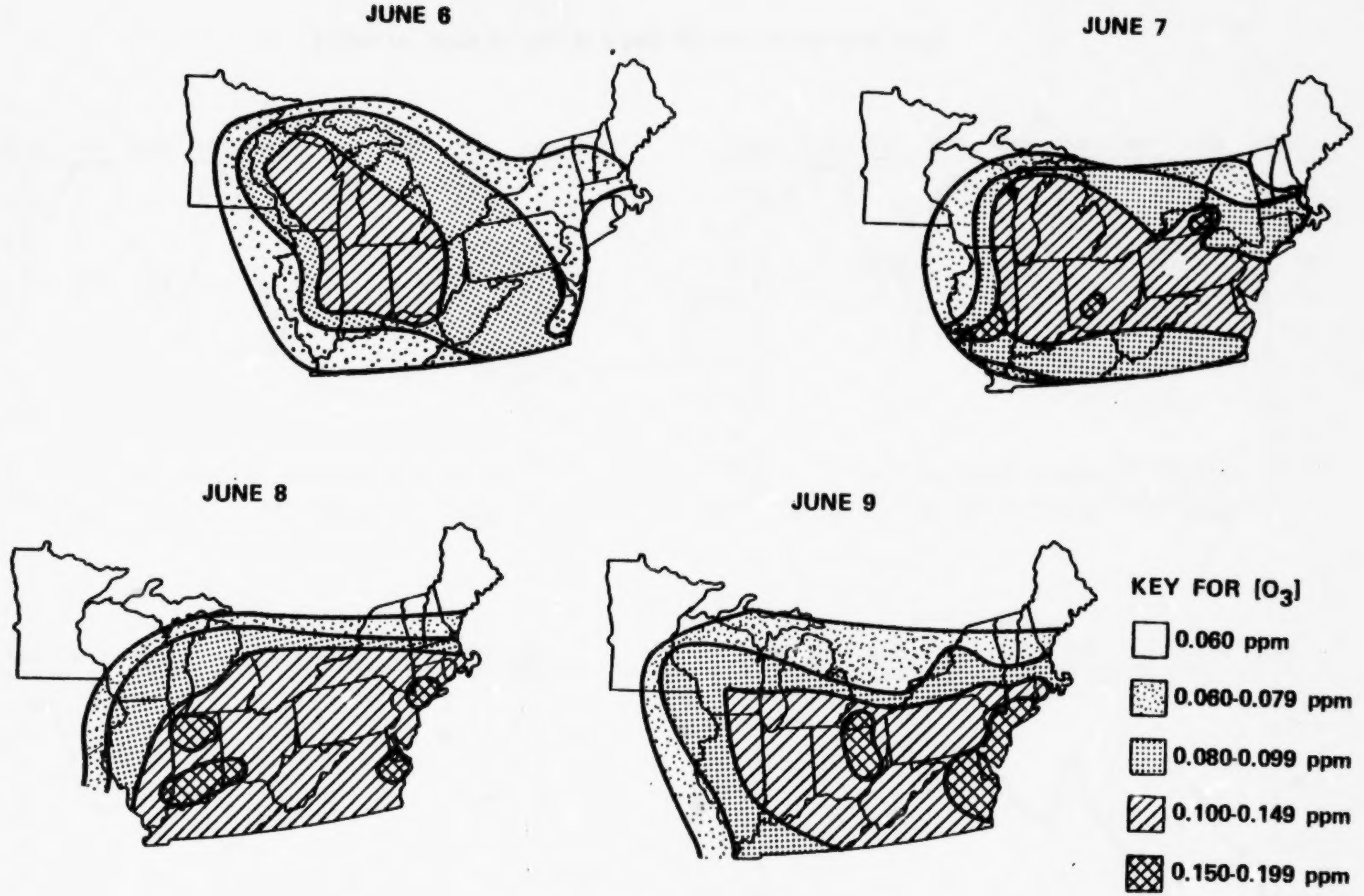
JUNE 6
JUNE 7
JUNE 8
JUNE 9
KEY FOR [O3]
0.060 ppm
0.060-0.079 ppm
0.080-0.099 ppm
0.100-0.149 ppm
0.150-0.199 ppm

Figure 9. Ozone distribution in the northeastern quadrant of the United States based on daily maximum hourly concentrations (courtesy of G. T. Wolff, Interstate Sanitation Commission).

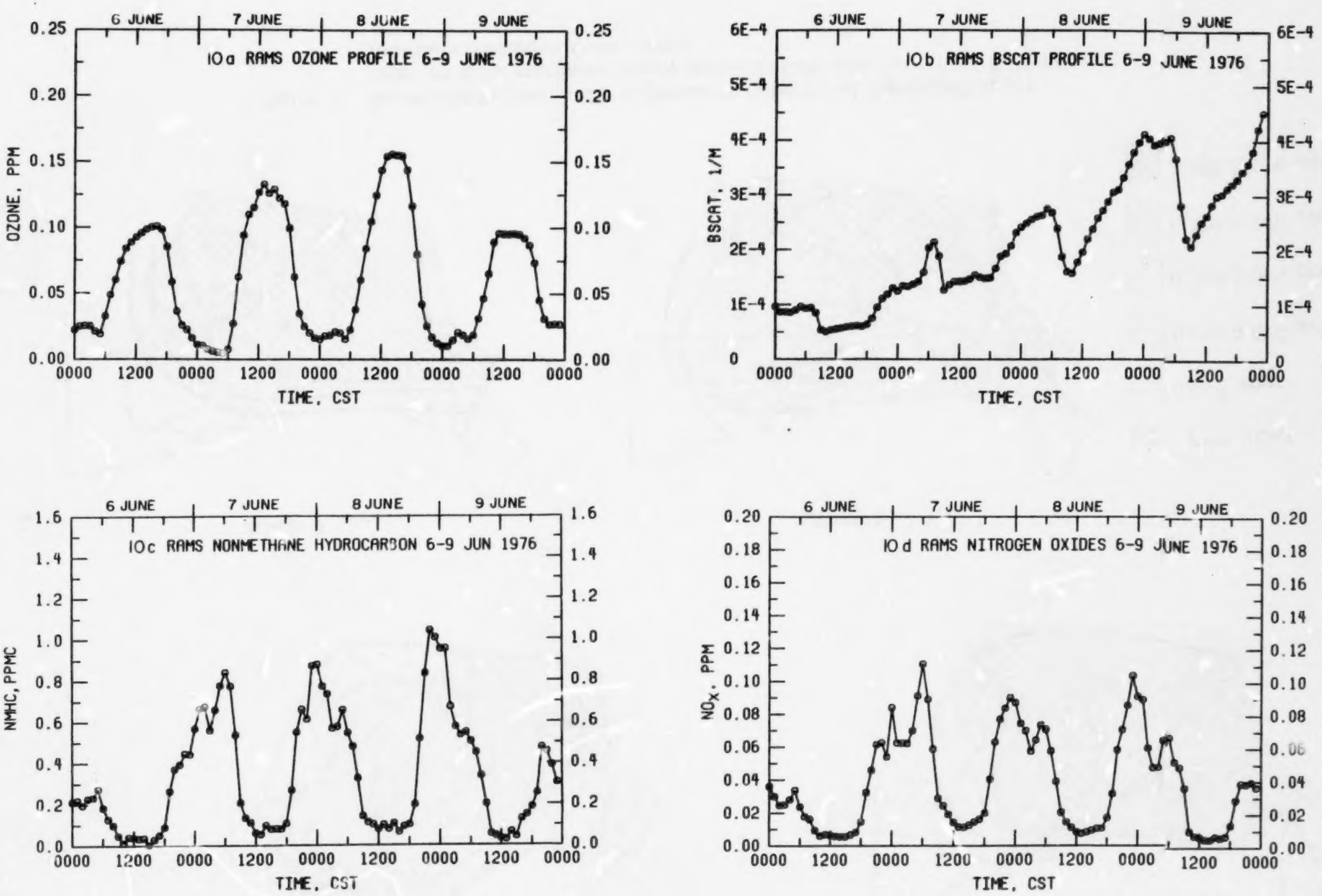

Figure 10. Mean profiles for RAMS network on 6-9 June 1976.

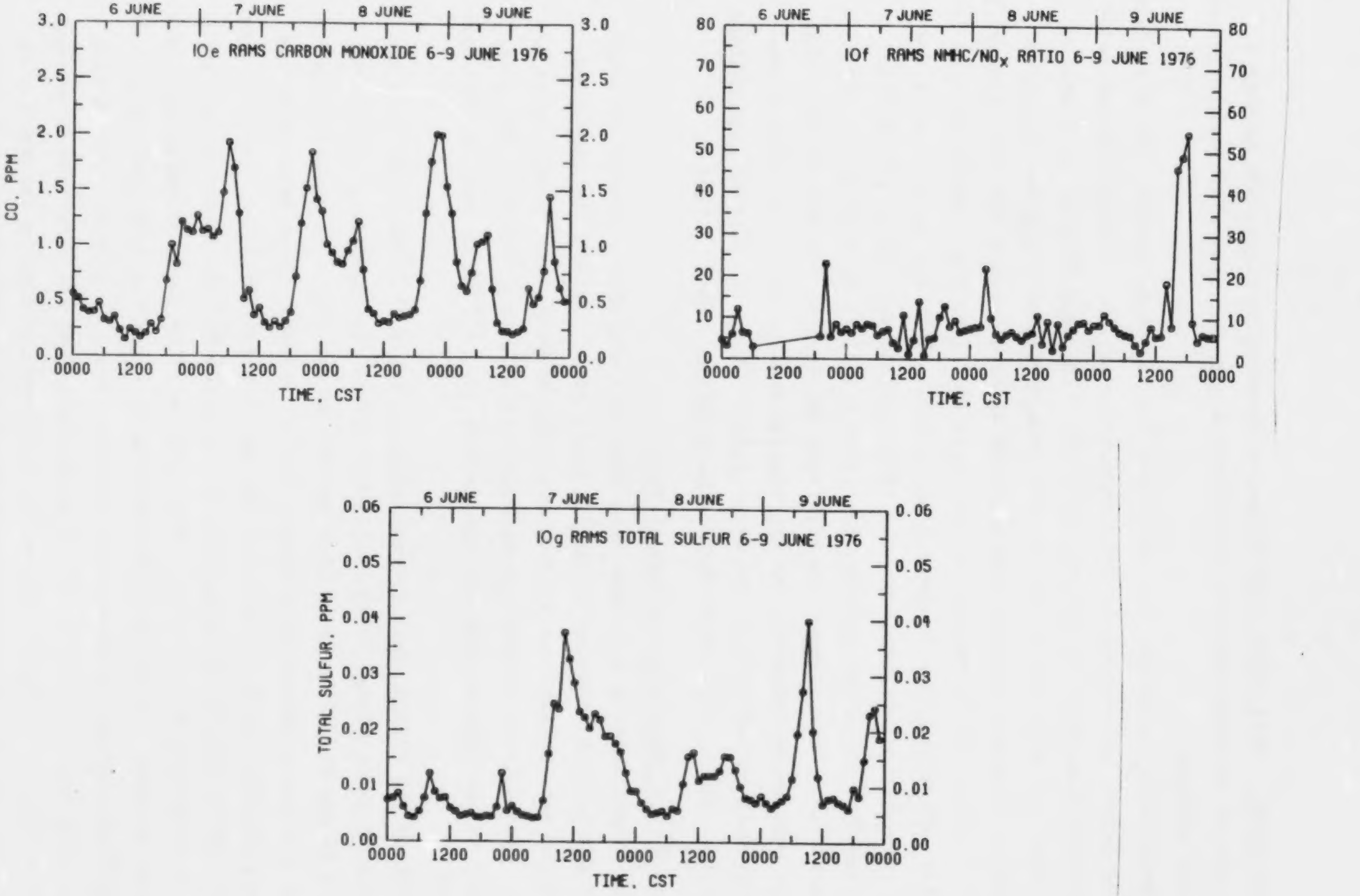

Figure 10. (con.)

positive peaks. This "dual peak" behavior observed in figure 10c through e may be due to increased vertical turbulence mixing air from aloft to the ground at around midnight.

The NMHC/NO_x ratio (R) was calculated for the study period. The R profile shown in figure 10f exhibits a 4-day mean value of 7.5. Automobiles are major ground-based sources of HC and NO_x emissions. The mean R value is 75 percent higher than the value calculated earlier from vehicular emissions estimates.

Sulfur dioxide concentrations measured as total sulfur (TS) were generally below 0.03 ppm. The TS profile is displayed in figure 10g. Sulfur dioxide is primarily emitted aloft from power plant stacks. This may contribute to the erratic behavior of the profile. The RAMS stations located at ground level were frequently insulated from any SO_2-laden air aloft by a nocturnal radiation inversion. This insured low nighttime SO_2 levels. During the day, when vertical mixing was enhanced, the opportunity existed for power plant plumes to become distributed through the mixed layer. Thus, as observed, the daytime ground-level SO_2 profile could exceed the nighttime concentration.

4.3.3 Air Quality at the Launch Site

The hourly network mean data from RAMS have provided a general description of air quality behavior in the St. Louis area. The RTI-EML collected air quality data at the launch site, Arrowhead Airport, for 16 days prior to launch. This site is located approximately 24 km west of downtown St. Louis, 7 km west of the nearest RAMS station, number 120, and 18 km east of RAMS station 125.

Much of the RTI-EML data is summarized in table 11. The ozone data are particularly interesting. Over the 16-day period (384 h), ozone levels exceeded 0.08 ppm for 59 hours or 15.5 percent of the time. Ozone levels exceeding 0.08 ppm occurred daily from 1 June to launch. These high-ozone conditions prevailed for 8, 3, 5, 1, 3, 10, and 11 h for the first 7 days of June.

The hourly average ozone profile at Arrowhead for the period 1 June until launch is presented in figure 11. This profile is in good agreement with data from RAMS stations 120 and 125. In addition to exceeding 0.08 ppm, ozone levels exhibited elevated minimum concentrations from 2 to 4 June. During this period, winds were from the west and north indicating air flow from rural and suburban areas. On 6 and 7 June, winds were from the east to the south with flow from St. Louis. Ozone concentrations that exceeded 0.08 ppm prevailed for 10 h on 6 June and 11 hours on 7 June during the day, and near-zero mini-

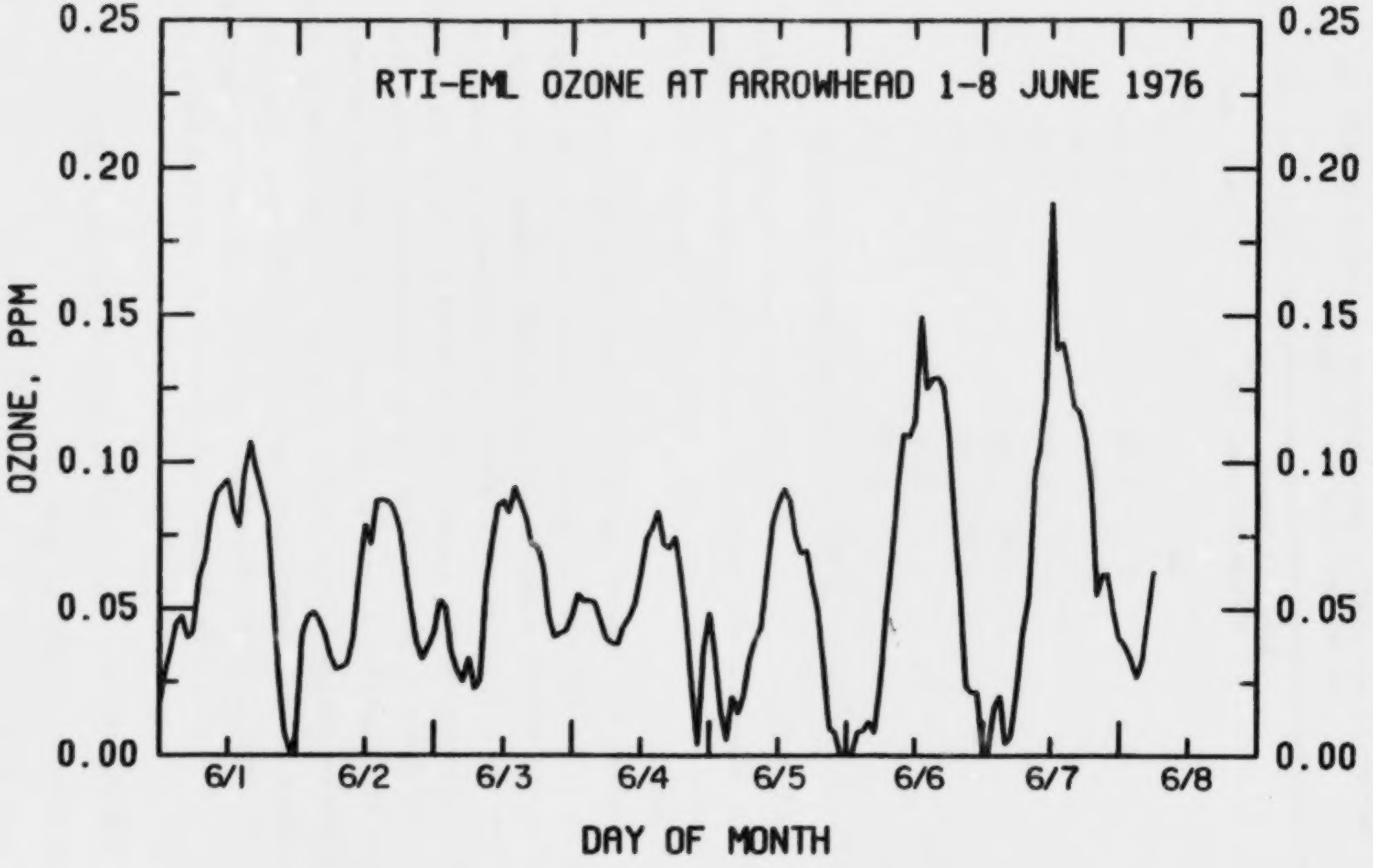

Figure 11. Hourly average ozone concentration prior to launch at Arrowhead Airport, 1-8 June 1976.

Table 11. Summary of air quality parameters at Arrowhead Airport for the 16-day period prior to launch

Parameter	Range of Hourly Average Concentrations, ppm	Mean, ppm
O_3	0* - 0.149	0.050
NO	0 - 0.057	0.004
NO_x	0 - 0.106	0.016
SO_2	0 - 0.084	0.020
THC	1.43 - 4.16	1.825
CH_4	1.37 - 3.44	1.694
NMHC	0 - 0.58	0.132
CO	0.15 - 1.880	0.535

*A reported zero corresponds to the MDC for the instrument employed.

mum values occurred at night. On the afternoon of 7 June, the winds shifted to a more westerly component, and increased minimum nighttime ozone levels were measured at Arrowhead and RAMS station 125. Winds were from the west on the morning of the launch.

Urban and nonurban environments exhibit characteristically different diurnal ozone profiles. The amplitude is greater at urban sites than at nonurban sites. Urban stations exhibit elevated maximum and low minimum ozone concentrations. The near-zero nighttime ozone minima are attributed to scavenging by anthropogenic ozone-destructive agents such as NO and HC, which are emitted by automobiles. The 6 and 7 June profiles typify this behavior. Ozone profiles at nonurban sites exhibit a reduced amplitude, reduced daytime maxima, and increased nighttime minima. These increased minima presumably result from a relative deficiency of ozone-destructive agents in nonurban air. The 2 to 4 June profiles are typical of this behavior. Westerly winds and the elevated nighttime ozone minimum on 7 June suggest that Da Vinci II was launched into air that was coming from nonurban environs.

4.3.4 Air Contaminant Behavior at Ground Level During The Flight

4.3.4.1 Air Quality at RAMS Stations

4.3.4.1.1 Mean Profiles

Mean profiles of selected parameters averaged across the RAMS network for the 4-day period, 6-9 June, were presented earlier in figures 8 and 10. Although attention can be focused on flight day, 8 June, these illustrations provide resolution of temporal behavior only.

To achieve spatial resolution, RAMS stations were stratified into three groups according to distance from the central urban area (CUA). Stations 101 through 113 comprise the "inner" group and are located in the St. Louis urban area. Stations 114 through 121 make up the "middle" group and are largely suburban sites. Stations 122 through 125 comprise the "outer" group and represent nonurban sites. A profile for each group of stations was then drawn on the same figure, and figures were drawn for selected parameters. Such illustrations allow an assessment of both temporal and spatial behavior of selected parameters within the RAPS area.

Figure 12a illustrates the characteristic shapes of urban and nonurban ozone profiles discussed earlier. The nonurban ozone profile has a reduced amplitude, with a higher minimum and a lower maximum than the urban profile. The morning increase and afternoon decline of the nonurban profile are the slowest of the three profiles. Although the suburban ozone maximum occurred 3 h after the urban maximum, both concentrations were of similar magnitude. The suburban ozone minima fall in between those for the urban and nonurban sites.

The profiles of CO, CH_4, NMHC, and NO_x in figures 12b through 12e are similar in shape. The profiles are characteristic of pollutants monitored at the ground that are emitted by ground-based sources. These pollutants accumulate beneath nocturnal radiation inversions both in the early morning and the late evening to concentrations roughly proportional to the magnitude of their emission rates. As daytime solar heating occurs and enhances mixing through a much larger volume, the concentration of these species declines to lower levels. Although the relative rank ordering of the three profiles is generally maintained throughout the day, the profiles seem to approach a common level during the well-mixed portion of the day.

Profiles of the $NMHC/NO_x$ ratio, R, presented in figure 12f, are more erratic than previous species' profiles. The variation increases with distance from the CUA. This behavior may be associated both with instrument variability as ambient hydrocarbon concentrations approach the noise range of the instrument's performance and with real concentrations in areas somewhat removed from high emissions density areas. The urban stations are in the closest proximity

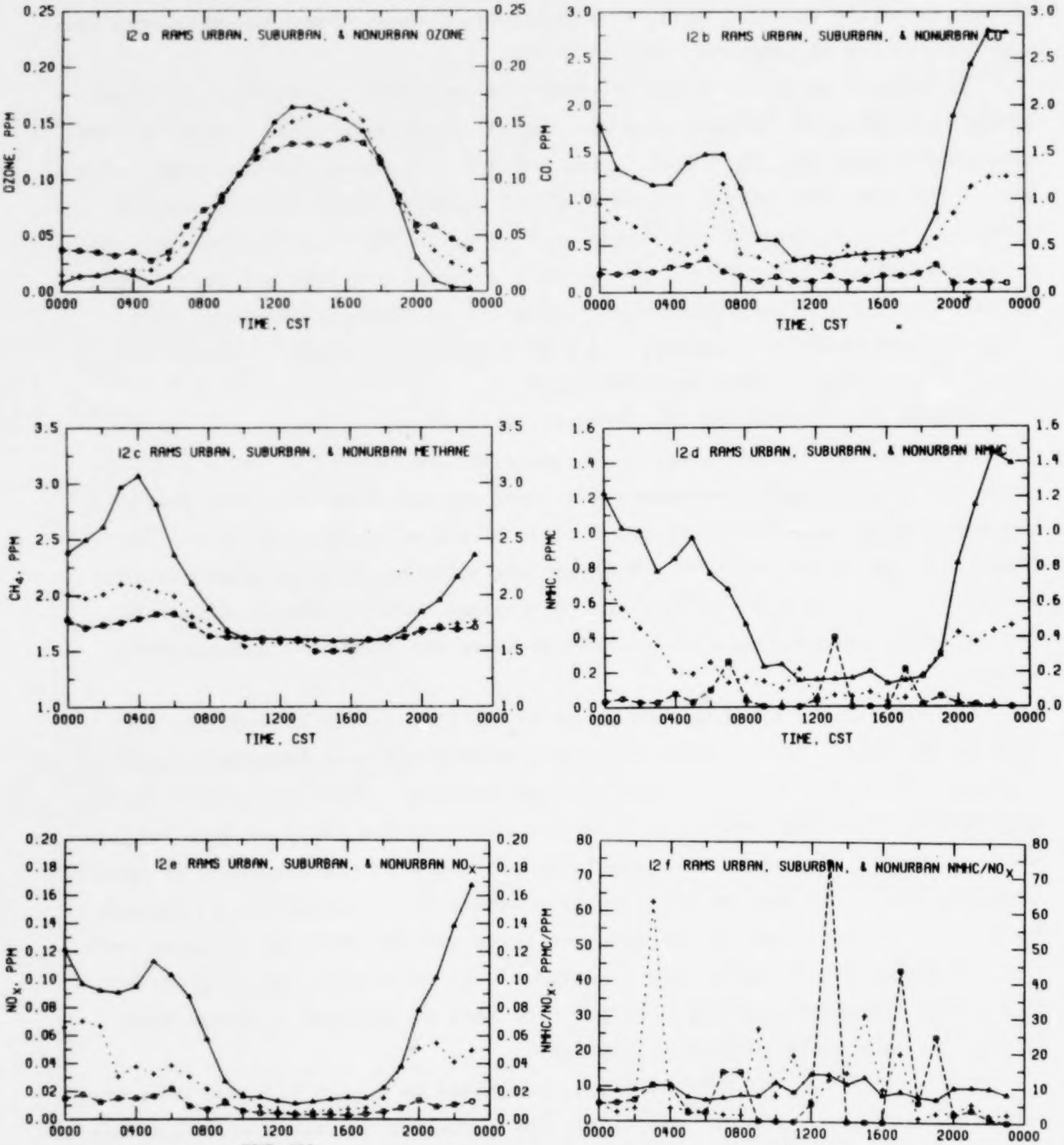

Figure 12. Mean pollutant concentrations at urban (Δ), suburban (+), and nonurban (o) sites in St. Louis on 8 June 1976. RAMS stations 101-113 comprise the urban group. Stations 114-121 make up the suburban category and stations 122-125 constitute the nonurban group.

to sources of HC and NO_x and exhibit the least variability. The R profiles are less variable under stable nighttime conditions than during the well-mixed daytime period. Nighttime urban R values are also slightly higher than those at suburban and nonurban stations although no trend is apparent for the daytime period.

Profiles of two other parameters, temperature and temperature gradient, reveal interesting behavior. The temperature profiles shown in figure 13 illustrate the existence of an urban heat island. At night, urban air was the warmest, and both urban and suburban air temperature were much greater than that at nonurban sites. During the day the temperature differences across these three groups of stations were much reduced.

The temperature gradient profiles in figure 14 are useful in resolving the timing of the establishment and breakup of the nocturnal radiation inversion. Such inversions usually begin to break up in the urban areas prior to nonurban areas. Likewise, they are established in nonurban areas prior to urban areas. On the morning of 8 June the inversion began to break up during the 0600 CST hour. Mixing had occurred through the first 30 m (100 ft) at the urban sites a full hour before it occurred at the nonurban stations. At the 1800 CST hour in the afternoon, the inversion began to reform at the nonurban sites. A 1-h delay occurred between the onset at the nonurban and urban stations. Thus, during the day, well-mixed conditions prevailed through the lowest 30 m (100 ft) for approximately 2 h longer at urban sites than at nonurban sites.

4.3.4.1.2 Concentration-Distance Plots

To gain another perspective on the spatial and temporal distribution of atmospheric contaminants within the RAPS area, concentration data have been plotted with respect to distance from station 101 in both the west-to-east and south-to-north directions. Maximum, 0500-0700 CST mean*, and 1100-1500 CST mean concentration data are presented for CO, NO_x, and O_3 in figures 15, 16, and 17. In addition, NMHC data are presented at the time of the maximum THC concentrations in figure 18. The figures clearly indicate that anthropogenic emissions are concentrated in the heart of the urban area.

The substantial difference between the maximum and the 0500-0700 CST mean concentration data for CO and NO_x indicate that these compounds do not always

---

*Note that the mean of the 0500, 0600, and 0700 CST hourly average concentrations encompasses the period between 6 and 9 a.m., local time.

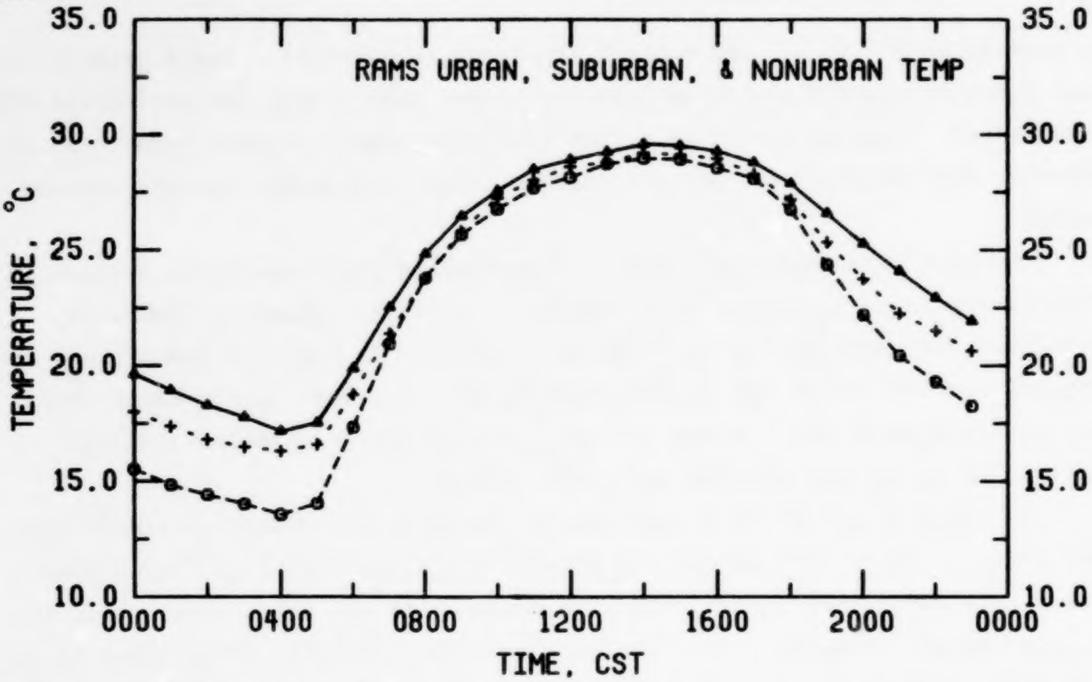

Figure 13. Air temperature at urban (Δ), suburban (+), and nonurban (o) sites in St. Louis on 8 June 1976. RAMS stations 101-113 comprise the urban group. Stations 114-121 make up the suburban category, and stations 122-125 constitute the nonurban group.

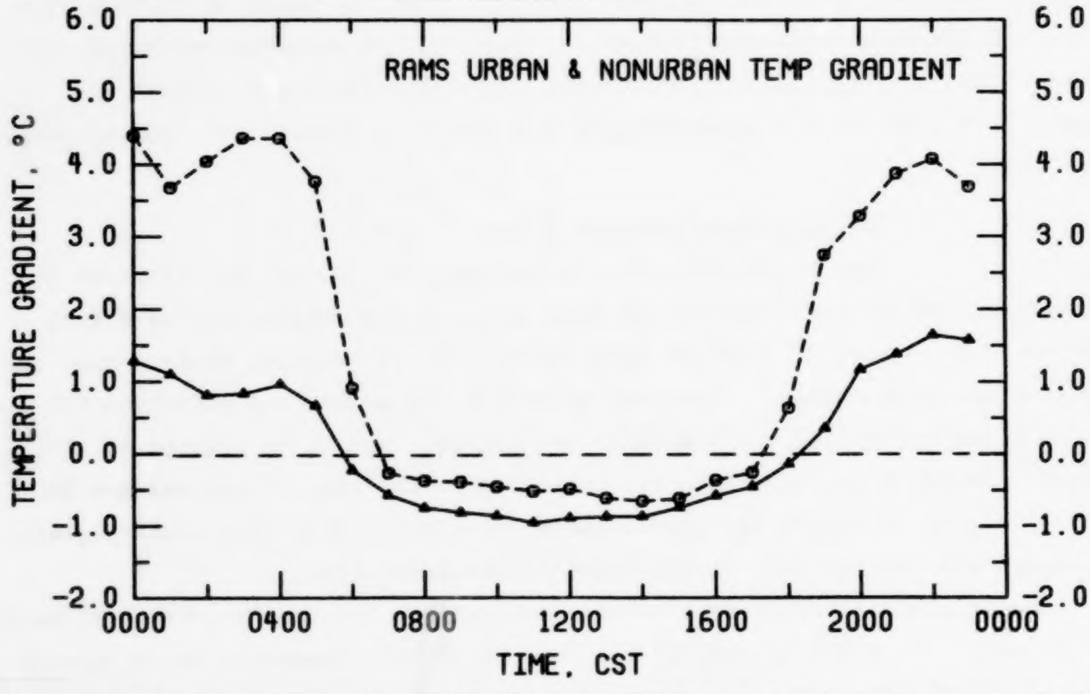

Figure 14. Temperature gradient through the first 30 m (100 ft) at urban (Δ) and nonurban (o) sites in St. Louis on 8 June 1976. RAMS stations 101-113 comprise the urban group and stations 122-125 make up the nonurban category. The gradient is the temperature at 30 m (100 ft) minus the temperature at 5 m (15 ft).

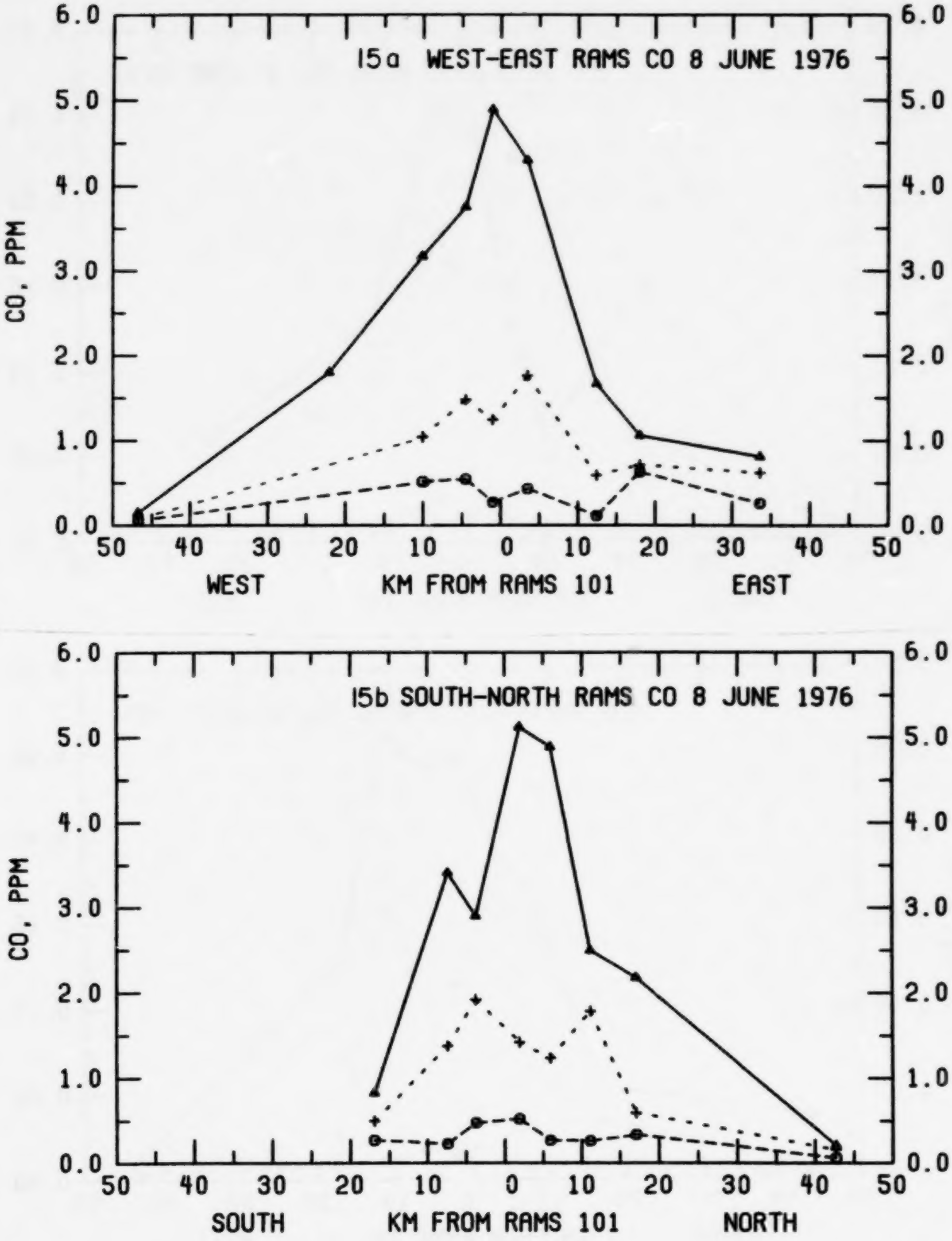

Figure 15. Carbon monoxide concentration relative to downtown St. Louis along west to east and south to north directions on 8 June 1976: (Δ) maximum hourly concentration; (+) 0500-0700 CST mean concentration; and (o) 1100-1500 CST mean concentration.

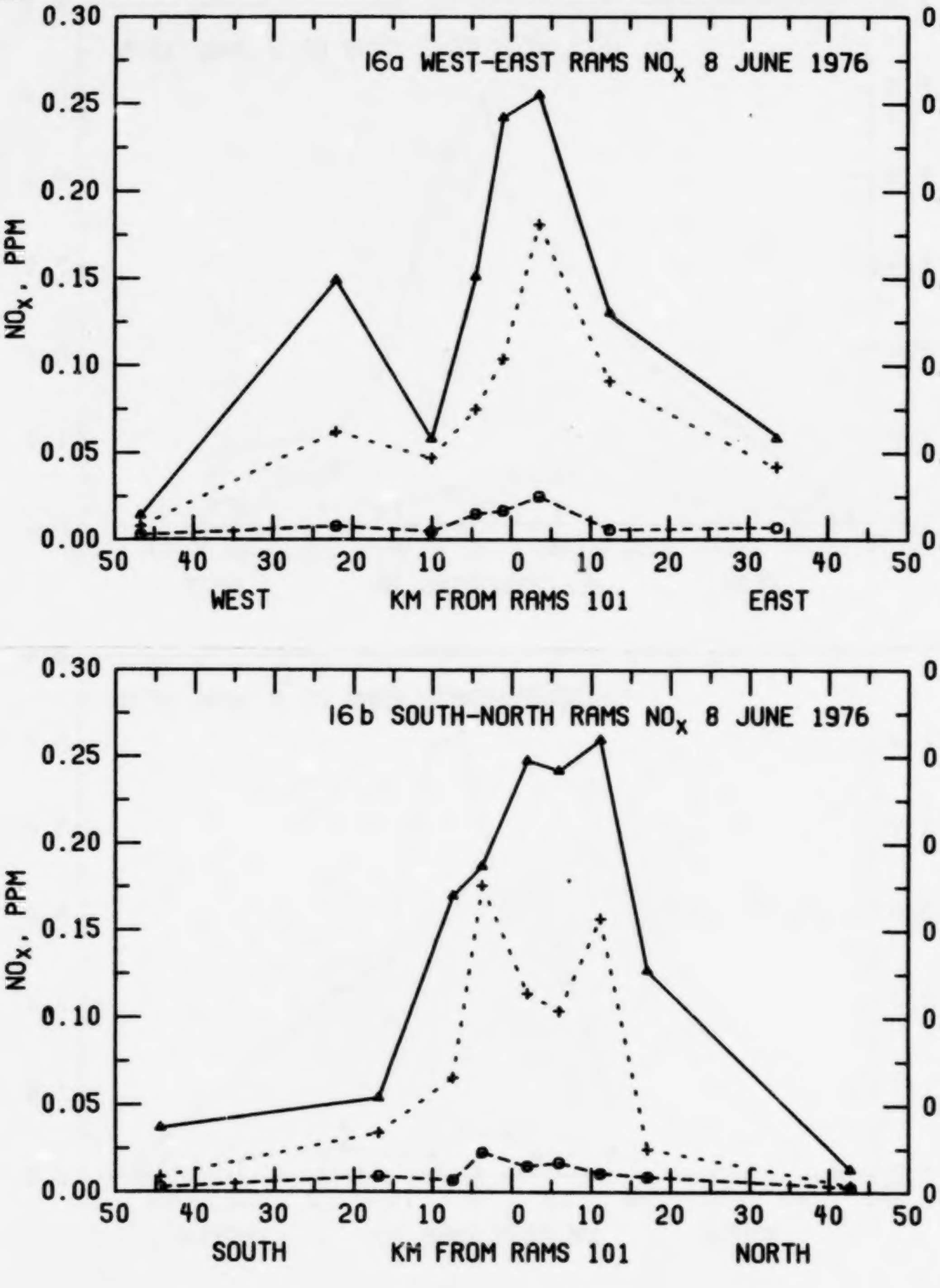

Figure 16. Nitrogen oxides concentration relative to downtown St. Louis along west to east and south to north directions on 8 June 1976: (Δ) maximum hourly concentration; (+) 0500-0700 CST mean concentration; and (o) 1100-1500 CST mean concentration.

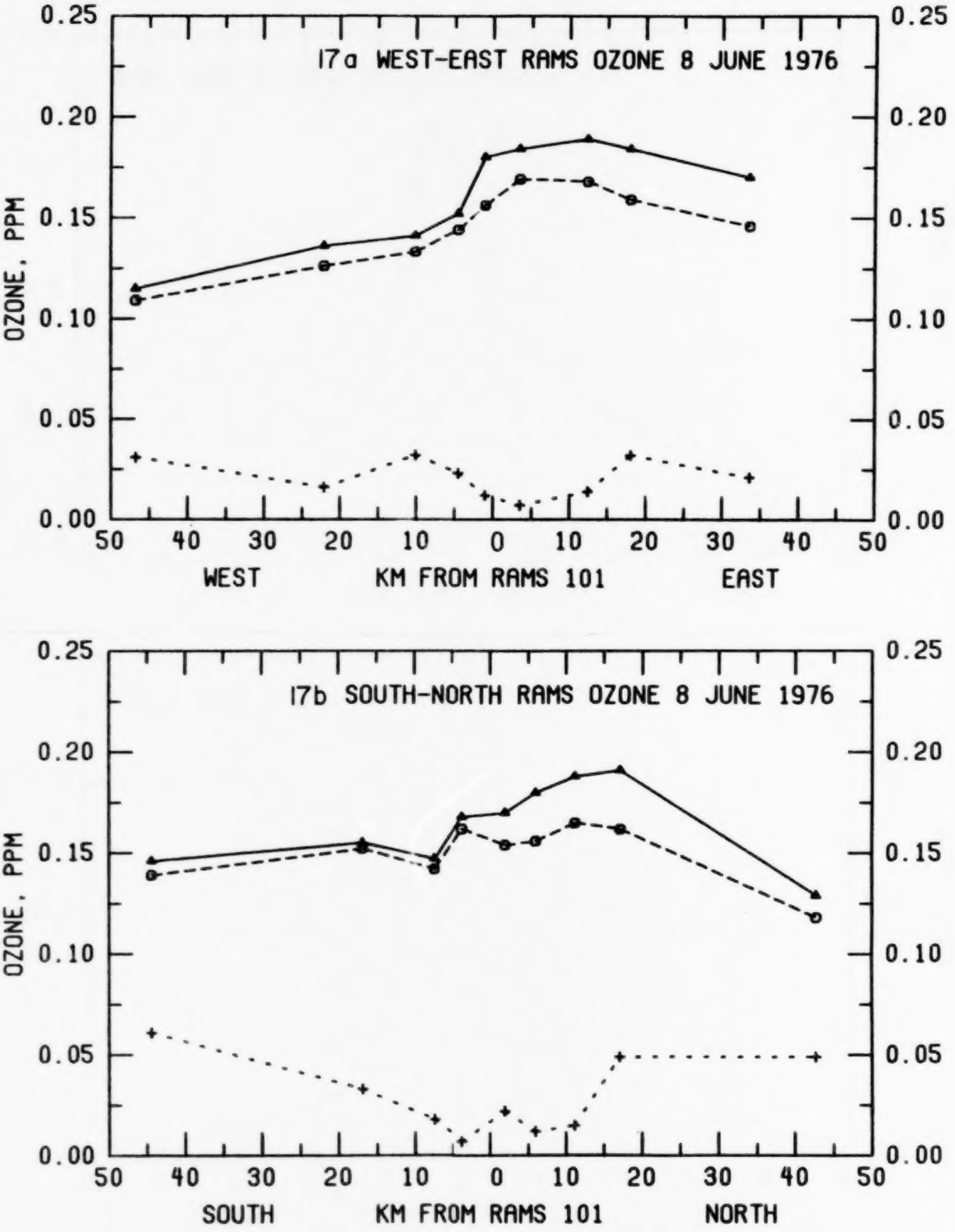

Figure 17. Ozone concentration relative to downtown St. Louis along west to east and south to north directions on 8 June 1976: (Δ) maximum hourly concentration; (+) 0500-0700 CST mean concentration; and (o) 1100-1500 CST mean concentration.

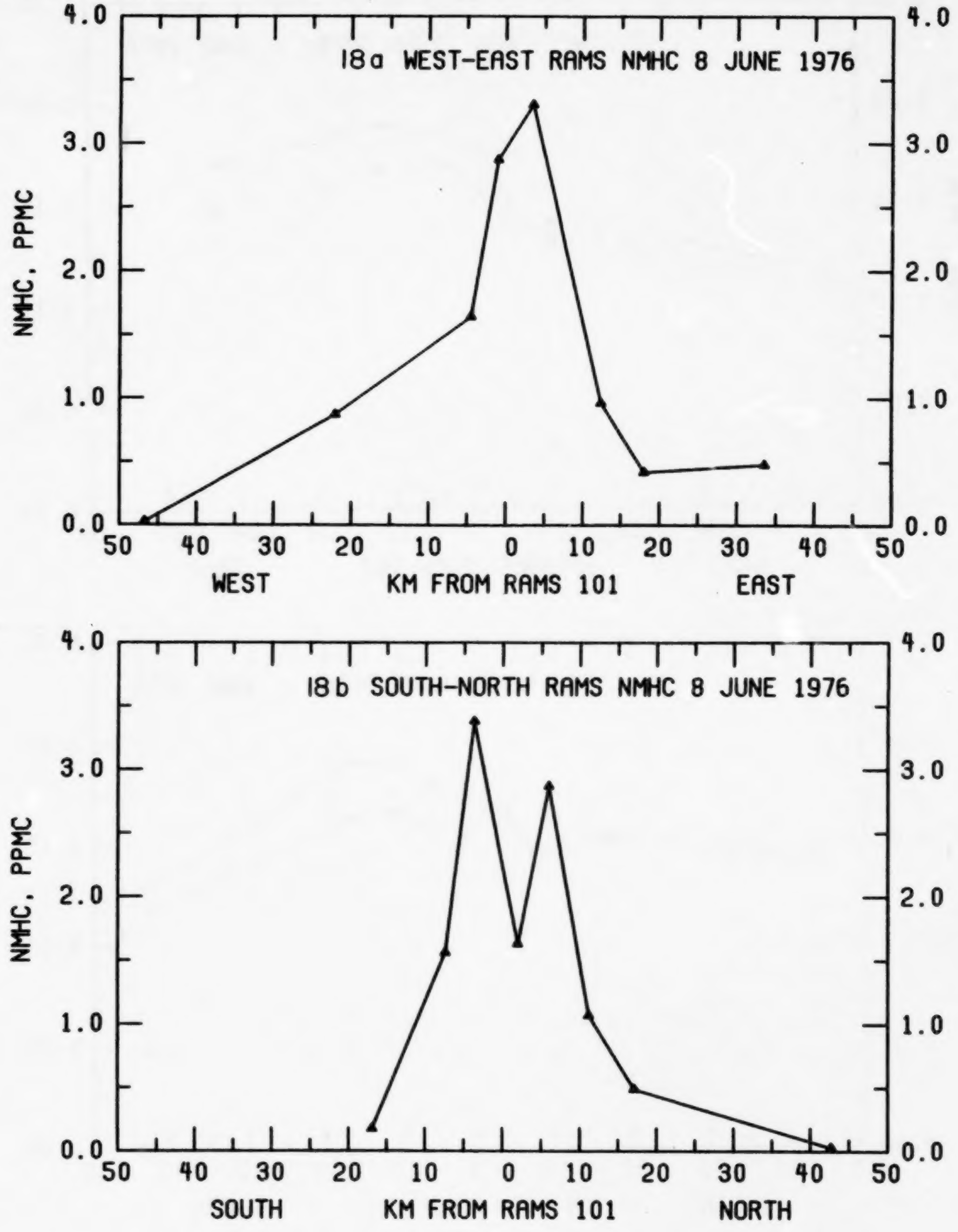

Figure 18. Nonmethane hydrocarbon concentration at the time of maximum THC concentration relative to downtown St. Louis along west to east and south to north directions on 8 June 1976.

achieve their daily maximum between 6 and 9 a.m. local time. As noted earlier, maxima for CO and NO_x occur in the evening.

The 0500-0700 CST mean CO and NO_x data exceed the corresponding 1100-1500 CST data. This difference may be attributed to temporal variation of both emission rates and atmospheric stability. Early morning automotive emissions accumulate in a relatively stable layer of air. Between 1100 and 1500 CST, vehicular emission rates are reduced and atmospheric mixing dilutes these emissions through a large volume. The mean ratio of the 0500-0700 CST CO data to those for the 1100-1500 CST period is 5.1 ± 2.4 for the inner RAMS sites. The corresponding value for NO_x is 9.0 ± 4.2. This suggests that mixing reduced early morning anthropogenic ozone precursor concentrations in the urban area by factors of 5 to 9. In spite of this dilution effect, the 1100-1500 CST data continue to show slightly elevated CO and NO_x levels in the urban area in comparison to the less urban areas.

The behavior of the secondary pollutant, ozone, shown in figure 17 is quite different from that of CO or NO_x. As noted in previous discussions, early-morning ozone levels are reduced in the urban area by reaction with ozone-destructive agents such as NO_x and HC, which accumulate in the relatively stable air.

Figure 17 also provides additional insight toward defining the location of the area affected most strongly by species that act as ozone percursors or ozone-destructive agents. The location of sharp inflections in both the morning and afternoon ozone levels near the center of the city correspond to the sharp increases in the early morning NO_x concentrations.

The close agreement of the maximum and the 1100-1500 CST O_3 data results from the fact that maxima were observed between the 1100 and 1500 CST hours at 18 of 22 RAMS stations.

The significant difference in absolute magnitude between the 0500-0700 CST and 1100-1500 CST ozone data reflects several factors. Beneath the nocturnal inversion, ozone levels are reduced to the early morning levels by destructive processes. Between the 1100 and 1500 CST hours, synthesis and mixing contribute significantly to the observed increase in ozone levels.

As shown earlier, elevated ozone levels prevailed on a regional scale from St. Louis to the east coast on 8 June. Ozone levels during the well-mixed part of the day, therefore, reflect the effects of synthesis superimposed on the existing high-ozone air that had been mixed to the ground. The relative contribution of synthesis increases with increased precursor input. The difference between urban and nonurban ozone maxima may be considered to be a lower limit estimate of the net contribution of urban precursors to ozone behavior. Based on the data in figure 17, a net increase of 0.060 ± 0.015 ppm of O_3 was associated with urban precursors.

On 8 June, winds were from the west. A more realistic estimate of the urban influence on ozone behavior may be the difference between the 1100-1500 CST mean ozone level at the westmost site, station 125, and the maximum ozone level observed within the network. This difference corresponds to 0.112 ppm. Thus on 8 June, a net increase of between 0.06 and 0.11 ppm of ozone was associated with precursors released in the St. Louis urban area.

4.3.4.1.3 Ozone Isopleths

Ozone isopleths, computer-drawn constant concentration lines (see appendix D), have been prepared for selected hours of 8 June. These isopleths, shown in figure 19, have been superimposed on maps of the RAPS area. Each illustration provides hourly resolution of the ground-level spatial distribution of ozone within the RAPS area. The hourly flight track of Da Vinci II is also shown on isopleths for the hours between the time of launch (the 0800 CST hour) and the time when Da Vinci II passed out of the RAPS area (the 2000 CST hour). The following observations have been drawn from these figures.

1. Before dawn (0436 CST), O_3 concentrations were generally low (<0.01 ppm) at points in the downtown area and eastward, whereas higher levels (0.02-0.06 ppm) existed outside the city. This presumably reflects a relatively high level of O_3 in the air mass over this region with the reduced urban levels due to anthropogenic O_3-destructive agents (NO and HC) emitted locally within the city and extending eastward by westerly winds.
2. The above situation prevailed from the 0000 to 0600 CST hours. From the 0600 to 0700 CST hour a noticeable increase (~0.01 ppm) occurred within the study area.
3. By the 0800 CST hour, several O_3 regimes existed in the study area: areas of elevated O_3 were separated by areas of reduced O_3 content. Ozone concentrations both outside and within the city were greater than 0.06 ppm. These regions were separated by areas of reduced O_3 content (0.04 to 0.06 ppm). Ozone levels in the less-urban outlying areas had increased by approximately 0.01 ppm over the 0700 value, whereas ozone levels in the CUA had increased by 0.02 to 0.04 ppm. The increase in ozone concentration is due to mixing from aloft and photochemical synthesis. The greater increase in the CUA is presumably due to the earlier breakup of the nocturnal radiation inversion with downwind mixing of O_3-rich air and generation by increased levels of ozone precursors (HC and NO_x).

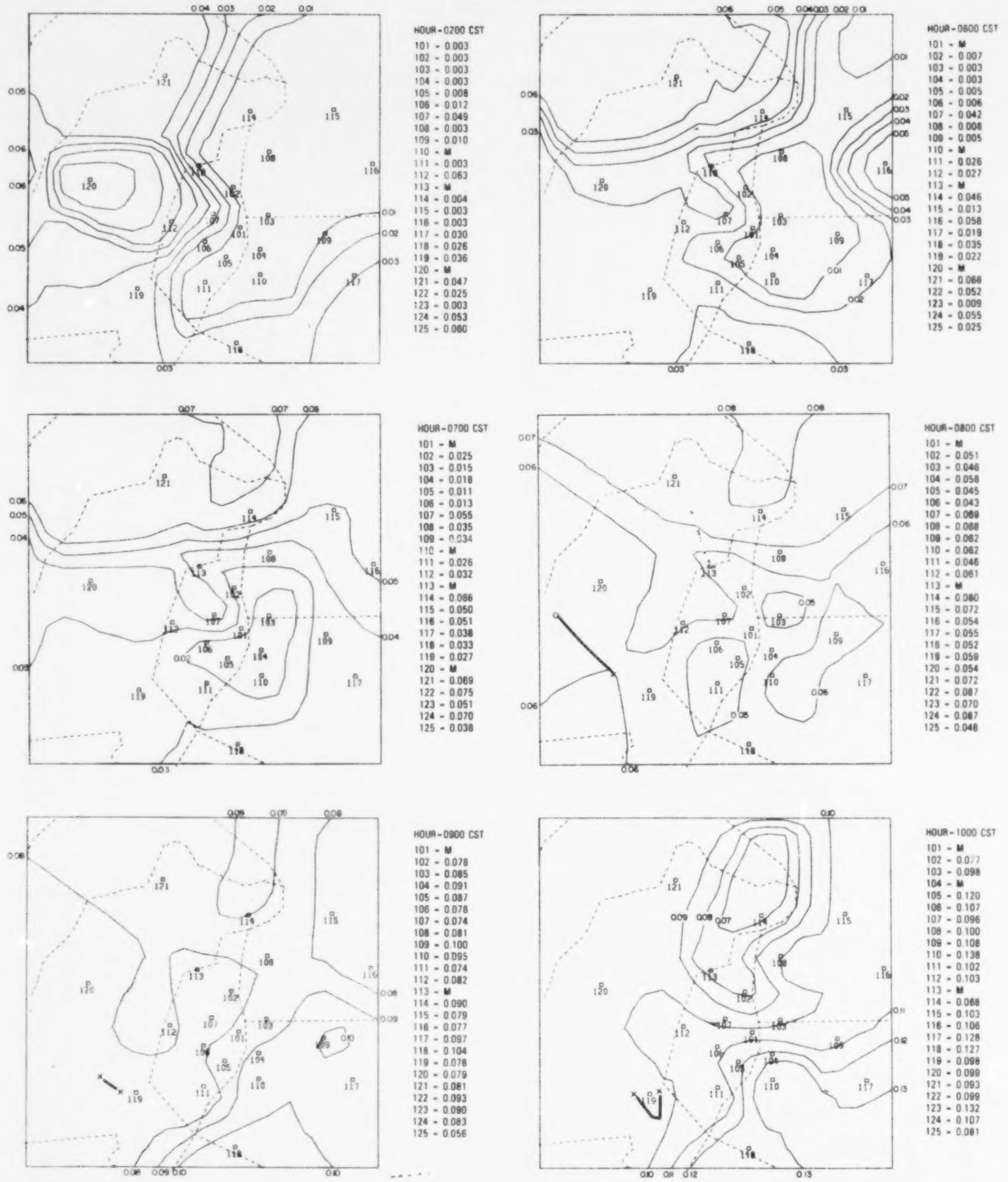
HOUR-0200 CST
101 - 0.003
102 - 0.003
103 - 0.003
104 - 0.003
105 - 0.008
106 - 0.012
107 - 0.049
108 - 0.003
109 - 0.010
110 - M
111 - 0.003
112 - 0.063
113 - M
114 - 0.004
115 - 0.003
116 - 0.003
117 - 0.030
118 - 0.026
119 - 0.036
120 - M
121 - 0.047
122 - 0.025
123 - 0.003
124 - 0.053
125 - 0.080
HOUR-0600 CST
101 - M
102 - 0.007
103 - 0.003
104 - 0.003
105 - 0.005
106 - 0.006
107 - 0.042
108 - 0.008
109 - 0.005
110 - M
111 - 0.026
112 - 0.027
113 - M
114 - 0.046
115 - 0.013
116 - 0.058
117 - 0.019
118 - 0.035
119 - 0.022
120 - M
121 - 0.068
122 - 0.052
123 - 0.009
124 - 0.055
125 - 0.025
HOUR-0700 CST
101 - M
102 - 0.025
103 - 0.015
104 - 0.018
105 - 0.011
106 - 0.013
107 - 0.055
108 - 0.035
109 - 0.034
110 - M
111 - 0.026
112 - 0.032
113 - M
114 - 0.066
115 - 0.050
116 - 0.051
117 - 0.038
118 - 0.033
119 - 0.027
120 - M
121 - 0.069
122 - 0.075
123 - 0.051
124 - 0.070
125 - 0.038
HOUR-0800 CST
101 - M
102 - 0.051
103 - 0.046
104 - 0.058
105 - 0.045
106 - 0.043
107 - 0.069
108 - 0.068
109 - 0.062
110 - 0.062
111 - 0.046
112 - 0.061
113 - M
114 - 0.080
115 - 0.072
116 - 0.054
117 - 0.055
118 - 0.052
119 - 0.059
120 - 0.054
121 - 0.072
122 - 0.087
123 - 0.070
124 - 0.087
125 - 0.048
HOUR-0900 CST
101 - M
102 - 0.078
103 - 0.085
104 - 0.091
105 - 0.087
106 - 0.078
107 - 0.074
108 - 0.081
109 - 0.100
110 - 0.095
111 - 0.074
112 - 0.082
113 - M
114 - 0.090
115 - 0.079
116 - 0.077
117 - 0.097
118 - 0.104
119 - 0.078
120 - 0.079
121 - 0.081
122 - 0.093
123 - 0.090
124 - 0.083
125 - 0.056
HOUR-1000 CST
101 - M
102 - 0.077
103 - 0.098
104 - M
105 - 0.120
106 - 0.107
107 - 0.096
108 - 0.100
109 - 0.108
110 - 0.138
111 - 0.102
112 - 0.103
113 - M
114 - 0.068
115 - 0.103
116 - 0.106
117 - 0.128
118 - 0.127
119 - 0.098
120 - 0.099
121 - 0.093
122 - 0.099
123 - 0.132
124 - 0.107
125 - 0.081

Figure 19. Hourly ozone isopleths (computer-generated) for St. Louis RAPS area on 8 June 1976. Ozone concentrations (ppm) are listed for each RAMS site; missing data are indicated by M; dashed lines represent county boundaries; heavy line indicates position of Da Vinci II during indicated hour.

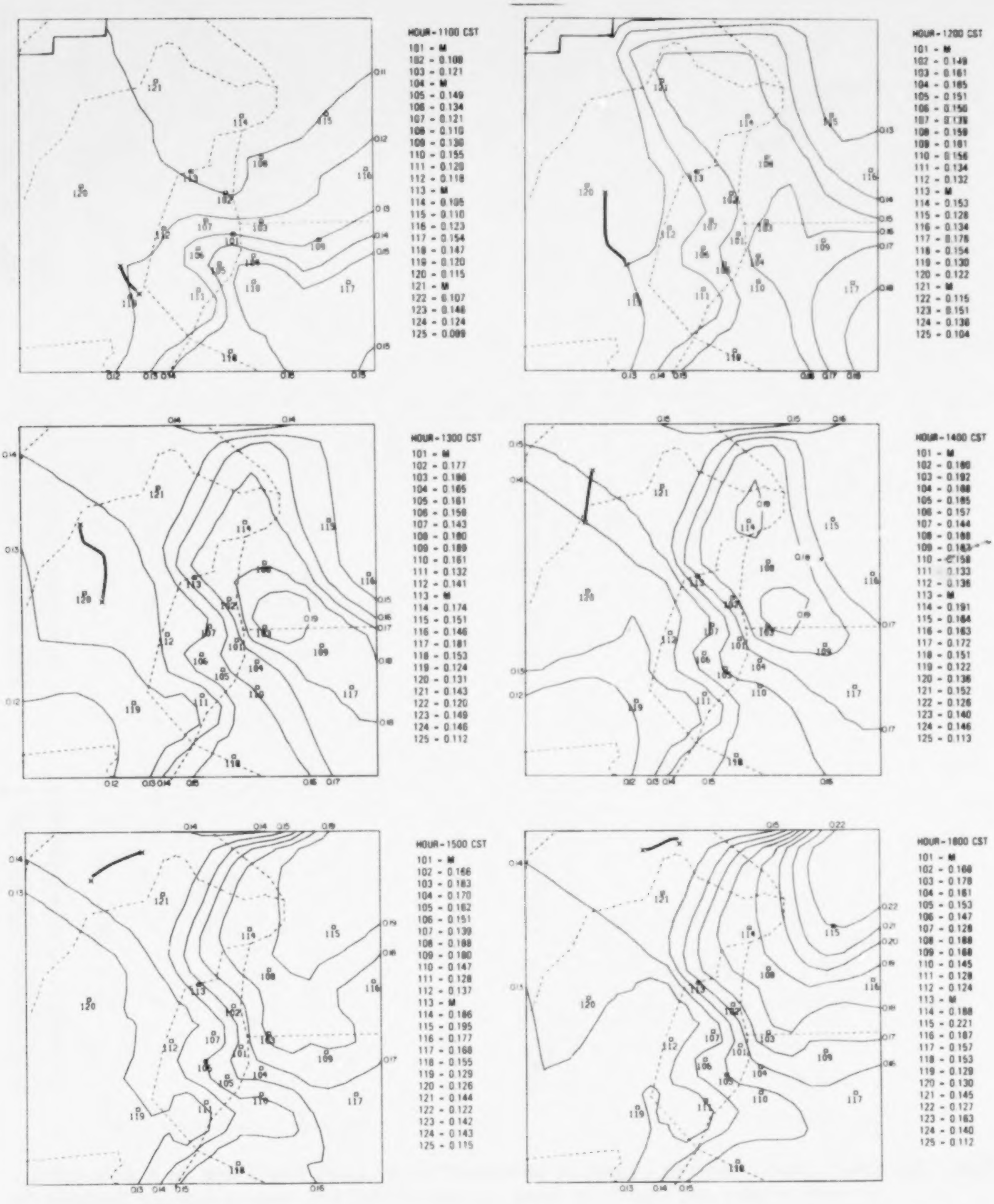

HOUR-1100 CST
101 - M
102 - 0.100
103 - 0.121
104 - M
105 - 0.149
106 - 0.134
107 - 0.121
108 - 0.110
109 - 0.130
110 - 0.155
111 - 0.120
112 - 0.118
113 - M
114 - 0.105
115 - 0.110
116 - 0.123
117 - 0.154
118 - 0.147
119 - 0.120
120 - 0.115
121 - M
122 - 0.107
123 - 0.148
124 - 0.124
125 - 0.099

HOUR-1200 CST
101 - M
102 - 0.149
103 - 0.161
104 - 0.185
105 - 0.151
106 - 0.150
107 - 0.178
108 - 0.158
109 - 0.161
110 - 0.156
111 - 0.134
112 - 0.132
113 - M
114 - 0.153
115 - 0.128
116 - 0.134
117 - 0.178
118 - 0.154
119 - 0.130
120 - 0.122
121 - M
122 - 0.115
123 - 0.151
124 - 0.138
125 - 0.104

HOUR-1300 CST
101 - M
102 - 0.177
103 - 0.186
104 - 0.165
105 - 0.161
106 - 0.158
107 - 0.143
108 - 0.180
109 - 0.189
110 - 0.161
111 - 0.132
112 - 0.141
113 - M
114 - 0.174
115 - 0.151
116 - 0.146
117 - 0.181
118 - 0.153
119 - 0.124
120 - 0.131
121 - 0.143
122 - 0.120
123 - 0.149
124 - 0.146
125 - 0.112

HOUR-1400 CST
101 - M
102 - 0.180
103 - 0.182
104 - 0.188
105 - 0.185
106 - 0.157
107 - 0.144
108 - 0.188
109 - 0.183
110 - 0.158
111 - 0.133
112 - 0.136
113 - M
114 - 0.191
115 - 0.184
116 - 0.163
117 - 0.172
118 - 0.151
119 - 0.122
120 - 0.136
121 - 0.152
122 - 0.126
123 - 0.140
124 - 0.146
125 - 0.113

HOUR-1500 CST
101 - M
102 - 0.166
103 - 0.183
104 - 0.170
105 - 0.162
106 - 0.151
107 - 0.139
108 - 0.188
109 - 0.180
110 - 0.147
111 - 0.128
112 - 0.137
113 - M
114 - 0.186
115 - 0.195
116 - 0.177
117 - 0.168
118 - 0.155
119 - 0.129
120 - 0.126
121 - 0.144
122 - 0.122
123 - 0.142
124 - 0.143
125 - 0.115

HOUR-1600 CST
101 - M
102 - 0.168
103 - 0.178
104 - 0.161
105 - 0.153
106 - 0.147
107 - 0.128
108 - 0.188
109 - 0.168
110 - 0.145
111 - 0.128
112 - 0.124
113 - M
114 - 0.188
115 - 0.221
116 - 0.187
117 - 0.157
118 - 0.153
119 - 0.129
120 - 0.130
121 - 0.145
122 - 0.127
123 - 0.163
124 - 0.140
125 - 0.112

Figure 19. (con.)

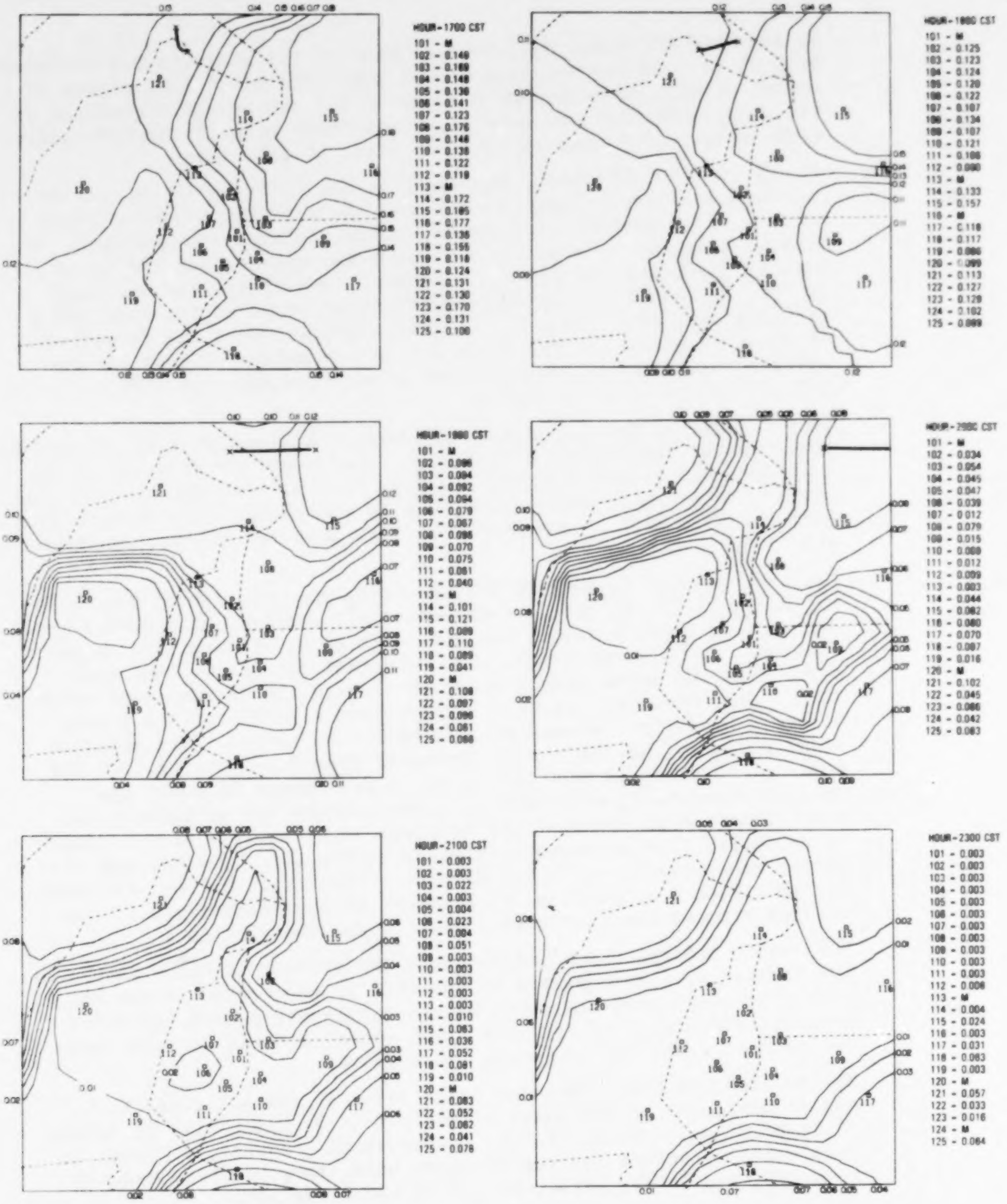
HOUR-1700 CST
101 - M
102 - 0.149
103 - 0.189
104 - 0.148
105 - 0.130
106 - 0.141
107 - 0.123
108 - 0.176
109 - 0.144
110 - 0.138
111 - 0.122
112 - 0.119
113 - M
114 - 0.172
115 - 0.195
116 - 0.177
117 - 0.136
118 - 0.156
119 - 0.110
120 - 0.124
121 - 0.131
122 - 0.130
123 - 0.170
124 - 0.131
125 - 0.100
HOUR-1800 CST
101 - M
102 - 0.125
103 - 0.123
104 - 0.124
105 - 0.120
106 - 0.122
107 - 0.107
108 - 0.134
109 - 0.107
110 - 0.121
111 - 0.106
112 - 0.080
113 - M
114 - 0.133
115 - 0.157
116 - M
117 - C.118
118 - 0.117
119 - 0.086
120 - 0.089
121 - 0.113
122 - 0.127
123 - 0.129
124 - 0.102
125 - 0.089
HOUR-1900 CST
101 - M
102 - 0.086
103 - 0.084
104 - 0.092
105 - 0.084
106 - 0.079
107 - 0.067
108 - 0.096
109 - 0.070
110 - 0.075
111 - 0.061
112 - 0.040
113 - M
114 - 0.101
115 - 0.121
116 - 0.089
117 - 0.110
118 - 0.089
119 - 0.041
120 - M
121 - 0.108
122 - 0.087
123 - 0.086
124 - 0.061
125 - 0.088
HOUR-2000 CST
101 - M
102 - 0.034
103 - 0.054
104 - 0.045
105 - 0.047
106 - 0.039
107 - 0.012
108 - 0.079
109 - 0.015
110 - 0.009
111 - 0.012
112 - 0.009
113 - 0.003
114 - 0.044
115 - 0.082
116 - 0.080
117 - 0.070
118 - 0.007
119 - 0.016
120 - M
121 - 0.102
122 - 0.045
123 - 0.086
124 - 0.042
125 - 0.003
HOUR-2100 CST
101 - 0.003
102 - 0.003
103 - 0.022
104 - 0.003
105 - 0.004
106 - 0.023
107 - 0.004
108 - 0.051
109 - 0.003
110 - 0.003
111 - 0.003
112 - 0.003
113 - 0.003
114 - 0.010
115 - 0.063
116 - 0.036
117 - 0.052
118 - 0.081
119 - 0.010
120 - M
121 - 0.083
122 - 0.052
123 - 0.082
124 - 0.041
125 - 0.078
HOUR-2300 CST
101 - 0.003
102 - 0.003
103 - 0.003
104 - 0.003
105 - 0.003
106 - 0.003
107 - 0.003
108 - 0.003
109 - 0.003
110 - 0.003
111 - 0.003
112 - 0.006
113 - M
114 - 0.004
115 - 0.024
116 - 0.003
117 - 0.031
118 - 0.083
119 - 0.003
120 - M
121 - 0.057
122 - 0.033
123 - 0.016
124 - M
125 - 0.064

Figure 19. (con.)

4. By the 0900 CST hour, O_3 levels at many of the stations had increased by 0.01 to 0.02 ppm and exceed 0.08 ppm. The first indications of a pocket of high ozone became evident in the southeastern quadrant of the study area; this is generally consistent with the northwesterly winds that existed during and just prior to this time.

5. During the 1000 CST hour, O_3 levels at the outlying (N, W, and S) stations were approximately 0.09 ppm, and a distinct area of high ozone (0.11-0.14 ppm) was evident in the southeastern quadrant. An area of slightly reduced ozone content was apparent in the north central quadrant. In general, higher O_3 concentrations occurred in the CUA, and lower O_3 concentrations occurred at the less urban outlying stations. This is the first indication of the formation of an urban plume for St. Louis and is a complete reversal of the urban-nonurban ozone gradient that existed between the 0000 and 0700 CST hours.

6. By the 1200 CST hour, the mean O_3 level at the outlying (N, W, and S) stations was approximately 0.12 ppm. The area of high ozone (0.16-0.18 ppm) had extended to the northern part of the southeastern quadrant; this movement was probably due to the change in wind direction from northwesterly to southwesterly that occurred between the 0900 and 1100 CST hours.

7. For the next 5 h (1300-1700 CST) the mean ozone levels at the outlying stations (N, W, and S) remained nearly constant at 0.12-0.13 ppm. During this time, however, the area of high O_3 behaved in a dynamic fashion. The area of highest O_3 concentration, the O_3 "hot spot," moved from the southeastern quadrant through the northeastern quadrant. This movement was to a large extent a result of the southwesterly winds that prevailed over this time period. The absolute level of O_3 in the "hot spot" increased from 0.178 at the 1200 CST hour to 0.221 at the 1600 CST hour: a net change of 0.043 ppm. This increase in O_3 over time in comparison to the relatively constant behavior at the outlying stations is probably a direct result of synthesis from precursors released in the CUA. The maximum observed concentration of O_3 (0.22 ppm) occurred at the 1600 CST hour. For this hour a substantial O_3 gradient of approximately 0.11 ppm existed between the westernmost station and the "hot spot."

8. Both ozone buildup and plume movement are evident in these isopleths. The limited area encompassed by the RAPS in comparison to the scale of air movement that can occur over a single-day period prevented detailed definition of both the areal extent and the maximum ozone concentration for the St. Louis urban plume.

9. By the 1800 CST hour, the mean ozone level at the outlying (N, W, and S) stations had decreased slightly to 0.11 ppm. High O_3 levels (0.13-0.15 ppm) remained in the northeastern quadrant, although in comparison to values for the previous hour, they had been reduced to a large extent by transport out of the study area.

10. Three O_3 regimes had been established by 1900 CST. At outlying stations (N, W, and S), O_3 levels were between 0.08 and 0.10 ppm. The remnants of the St. Louis plume were evident in the northeastern quadrant (0.11-0.12 ppm O_3). These two areas, however, were separated by an area of reduced O_3 concentration (0.04-0.08

ppm) in the CUA. Compounds that act as precursors in sunlight also act as O_3-destructive agents in the dark. The observed reduction of O_3 in the CUA is presumably due to reaction with anthropogenic NO_x and HC emissions under conditions of reduced light intensity.

11. The three O_3 regimes persisted in the study area for the next 2 h. The areal extent of the low-O_3 air increased. The concentration of O_3 in the CUA had dropped to less than 0.005 ppm by the 2100 CST hour in comparison to values of 0.04 to 0.08 ppm at the outlying stations.
12. By the 2300 CST hour, reduced O_3 levels (~0.005 ppm) were prevalent over most of the study area. Somewhat higher levels (0.02 to 0.06 ppm) occurred at the outlying stations, and the predawn situation had been reestablished.

4.3.4.2 Air Quality at the RTI-EML

Hourly average ozone data collected by the RTI-EML are presented in figure 20. In addition, ground-level ozone concentrations for the track of Da Vinci II were interpolated from hourly RAMS isopleths, such as figure 19, and are also presented in figure 20. The overall agreement between these two profiles is good. The 1100-1500 CST mean ozone concentration from the RTI-EML of 0.123 ± 0.005 ppm compares closely with the 0.134 ± 0.012 ppm from interpolated RAMS data.

The agreement is better between the 0800 and 1700 CST hours than for other times. The flight track of Da Vinci II for the major portion of the day was on the periphery of the RAMS network. Between the 0900 and 1400 CST hours the RTI-EML was near, but not actually in, the area having a high density of RAMS sites. Interpolated RAMS data for other times are less certain due to the small number of stations in the vicinity of the flight track. In addition, because the RTI-EML was traveling on roadways, it sampled air contaminated to an undefined extent with vehicular exhaust that was rich in O_3-destructive agents. The slight discrepancy between the two profiles for the 1800, 1900, and 2000 CST hours may be due both to nonrepresentative station location relative to the route and to possible roadway contamination of air sampled by the RTI-EML. The RTI-EML moved outside the RAPS area at approximately 2140 CST; therefore, RAMS data are not included for times after the 2000 CST hour.

It is interesting to note the elevated nighttime ozone concentration observed on the RTI-EML between the 2100 CST hour on 8 June and the 0100 CST hour on 9 June. Based on the hourly data of figure 20, the magnitude of the peak is 0.072 ppm, which represents a net increase of 0.038 ppm. Fifteen-

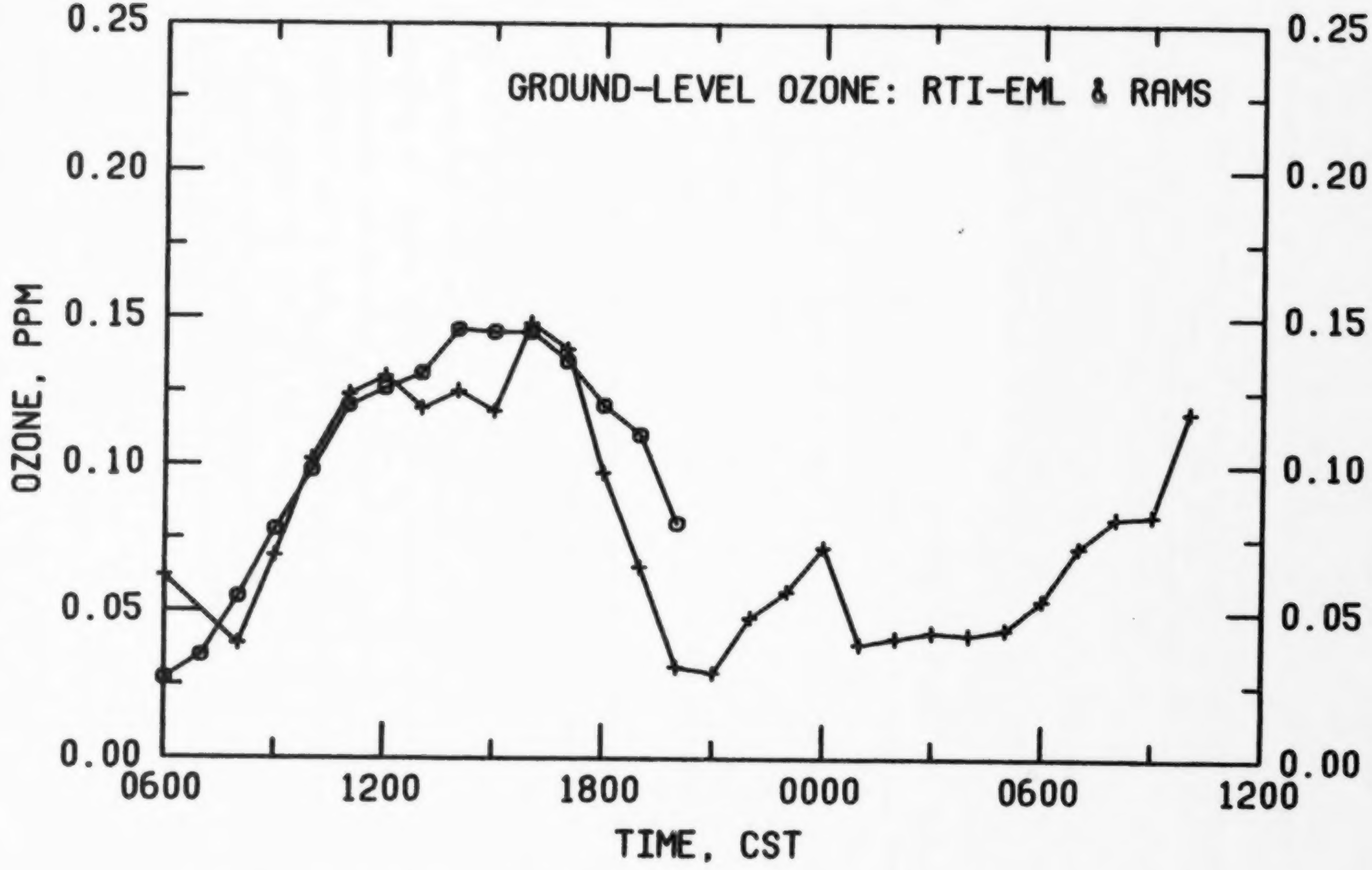

Figure 20. Ground-level ozone concentrations measured by RTI-EML (+) and nearest RAMS Station (o) during flight of Da Vinci II.

minute average data, not shown, suggest that the elevated ozone condition lasted for at least 2 h, from approximately 2315 until 0115 CST.

This phenomenon was investigated by visual inspection of plots of both RTI-EML and RAMS data for the period 1-7 June 1976. Nighttime ozone peaks were observed at Arrowhead Airport on most of the first 7 days of June (see figure 11). At RAMS sites during the same period, nighttime O_3 peaks representing a net increase of greater than 0.010 ppm occurred in approximately 80 cases. Additional RAMS parameters were examined for associations. Sharp nighttime ozone peaks were accompanied by equally sharp declines of NO_x and CO. Although somewhat more obscure, similar associations were observed with NO, NO_2, THC, and CH_4. Nighttime ozone peaks were weakly associated with increased wind speed and temperature, and with reduced temperature gradient.

Species such as CO, NO_x, THC, and CH_4 that have ground-based sources are expected to accumulate beneath the nocturnal radiation inversion. Air aloft, insulated from ozone-destructive agents emitted at ground level, is expected to be higher in ozone concentration than air near the ground. Vertical mixing would act to reduce the temperature gradient near the ground and could be indicated by increased wind speeds. If this turbulence is sufficient to penetrate the inversion layer, then increased ozone levels and air temperature may be accompanied by reduced CO, NO_x, THC, and CH_4 levels. These simultaneous phenomena were observed in many cases. This suggests that the nighttime ozone peaks observed on 1-7 June resulted from vertical transport through the nocturnal radiation inversion.

Air quality data collected at several ground stations on the night of 8 June were examined for associations with the nighttime ozone peak observed at the RTI-EML (see figure 11). Ozone peaks were observed at many of the RAMS sites. Associations similar to those noted above for CO, NO_x, THC, CH_4, wind speed, temperature, and temperature gradient were also observed in many cases. A summary of ozone behavior at many of the ground stations is presented in table 12. Occurrences of nighttime ozone peaks were widespread: net increases of at least 0.010 ppm were observed at 10 RAMS, 4 Kentucky, and 9 Illinois ground stations. A mean maximum net increase of 0.024 ± 0.012 ppm was observed, and the condition of elevated ozone lasted for 4 ± 2 h.

Based on the RAMS data in table 12, the strong nighttime O_3 increases may occur more frequently at suburban and nonurban sites than at urban locations. This hypothesis should be examined and explored using portions of the

Table 12. Nocturnal increases in ozone concentration at the surface during the flight of Da Vinci II[a]

Station	H_1, hour before elevated $[O_3]$ was first observed, CST	H_2, hour after the elevated $[O_3]$ was last observed, CST	Average $[O_3]$ observed at H_1 and H_2, ppm	Peak $[O_3]$, ppm	Net increase of $[O_3]$, ppm	Duration of elevated $[O_3]$ (H_2-H_1-1), h
St. Louis RAPS[b]						
RAMS 102	0100	0500	0.003	0.033	0.030	3
RAMS 106	0200	0600	0.015	0.032	0.017	3
RAMS 107	0100	0600	0.009	0.045	0.036	4
RAMS 112	0000	0600	0.015	0.066	0.051	5
RAMS 114	2100	2300	0.007	0.020	0.013	1
RAMS 117	0400	0800	0.033	0.047	0.014	3
RAMS 118	0200	0600	0.038	0.052	0.014	3
RAMS 119	0100	0700	0.018	0.045	0.027	5
RAMS 122	2000	2300	0.039	0.052	0.013	2
RAMS 122	0200	0500	0.022	0.033	0.011	2
RAMS 125	0000	0500	0.049	0.064	0.015	4
Kentucky Stations[c]						
Louisville	2100	2300	0.010	0.040	0.030	1
Louisville	2300	0600	0.003	0.035	0.032	6
Henderson	2200	0500	0.007	0.053	0.046	6
Owensboro	0100	0400	0.001	0.012	0.011	2
Illinois Stations[d]						
Alton	0100	0500	0.002	0.039	0.037	3
Decatur	2100	0500	0.023	0.048	0.025	7
Joliet	1900	2300	0.004	0.018	0.014	3
LaSalle	2200	0600	0.012	0.036	0.024	7
Normal	2000	0500	0.012	0.044	0.032	8
Peoria	2100	0000	0.000	0.013	0.013	2
Quincy	2000	0600	0.017	0.033	0.016	9
Rock Island	2300	0500	0.002	0.015	0.013	5
Springfield	2100	0600	0.026	0.066	0.040	8

---

[a] Hourly average data were examined.

[b] Nocturnal net increases of O_3 were observed to be less than 0.010 ppm at RAMS stations 103, 104, 105, 106, 109, 110, and 123; Peaks were not observed at stations 108, 111, 115, and 116; and valid data were not available at stations 101, 113, 120, 121, and 124.

[c] Data from nine Kentucky stations were examined.

[d] Data from twenty Illinois stations were examined.

RAMS data set. The behavior is probably governed by the ozone concentration above the nocturnal radiation inversion, the concentration of both O_3 and O_3-destructive agents beneath the inversion, and the meteorological processes that define the severity and the duration of the mixing. The net result of the interaction of increased downward mixing with such local situations as an urban heat island circulation system is unclear.

The data suggest that the nighttime ozone peak observed at the RTI-EML was due to downward mixing. The implications of this apparently widespread condition are poorly defined. This phenomenon, however, may provide mechanisms for depleting ozone aloft during nocturnal transport and for distributing nocturnal emissions of ozone precursors aloft. A major question, then, regards the impact that nighttime injections of ozone precursors can have on the ozone-producing potential within the daytime mixed layer.

4.3.5 Air Contaminant Behavior Aloft During the Flight

4.3.5.1 NOAA Aircraft

Data collected on the NOAA aircraft can be used to describe events that occurred aloft. Two vertical flights were conducted within 2 km of Da Vinci II: the first from 0915 until 0933 CST and the second between 1148 and 1211 CST. Ozone, B_{scat}, relative humidity, and NO_2 concentration profiles from these flights are presented in figures 21 through 24. For comparison, time-resolved data from the nearest RAMS station (hourly average), the RTI-EML (15-min average), and Da Vinci II (2-s average) are included, as available, on these graphs.

The discrepancies between the aircraft and the Da Vinci II ozone data shown in figure 21 may be real or they may be indicative of a calibration or other measurement error. Both NOAA profiles were adjusted by the amount required to align the noontime NOAA ozone level with the concentration measured on Da Vinci II, a factor of 0.64. These adjusted data are presented in figure 25. The adjusted ozone data appear to be more consistent with the RTI-EML and RAMS data for both periods. The 0915 profile coupled with the data point from Da Vinci II show a slight ozone bulge below 914 m (3,000 ft). This may be due either to an enhancement beneath the rising mixed layer presumably due to synthesis aloft or to inherent inhomogeneities that reflect incomplete mixing of the layered atmosphere. The distinct layering of ozone that existed at 0915 CST had disappeared by noon as the atmosphere became well mixed. The

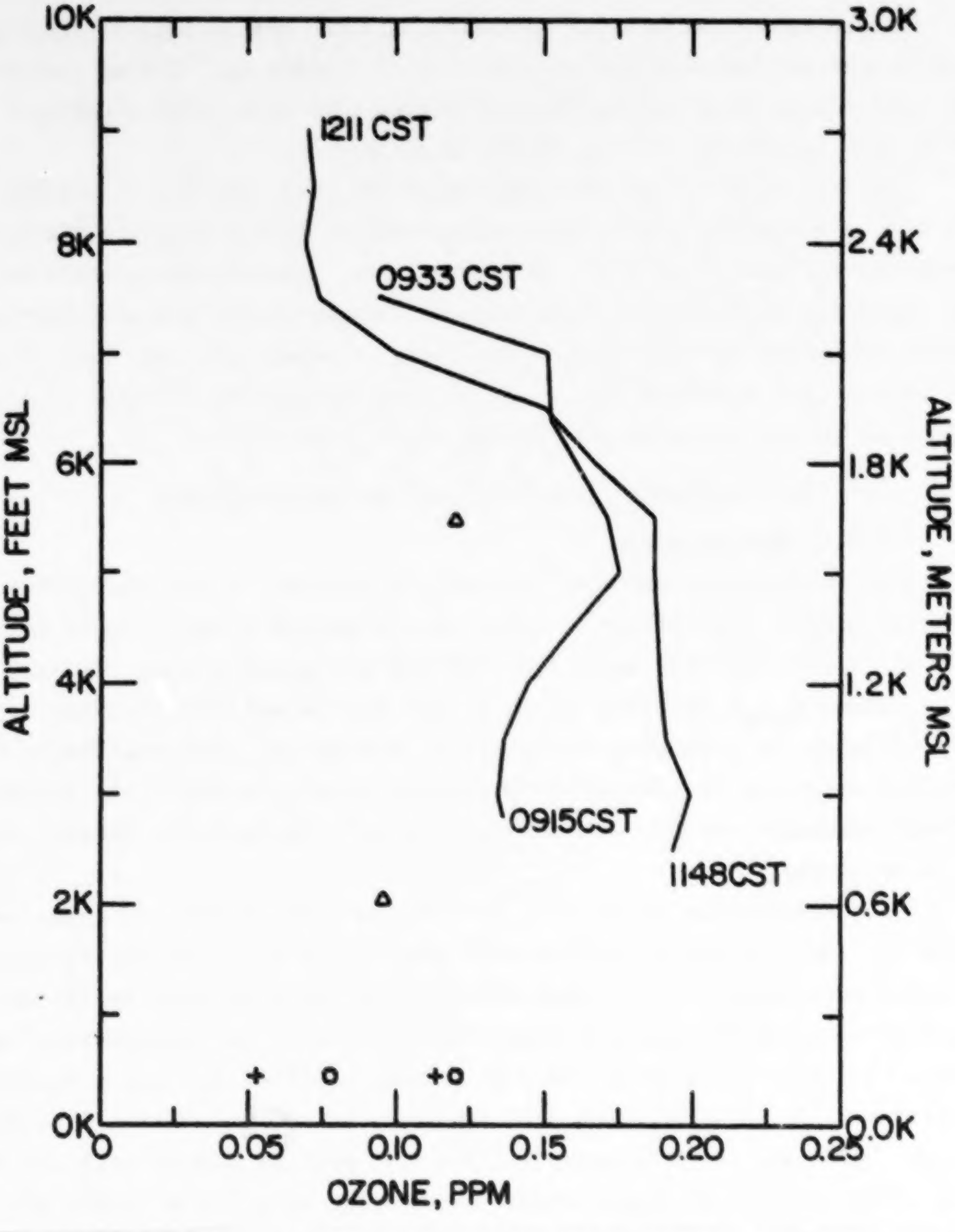

Figure 21. Unadjusted ozone profiles as measured in St. Louis on 8 June 1976 during vertical flights of the NOAA aircraft that started at 0915 and 1148 CST. Time-resolved ozone data from Da Vinci II (Δ), RTI-EML (+), and RAMS stations (o) are included for comparison.

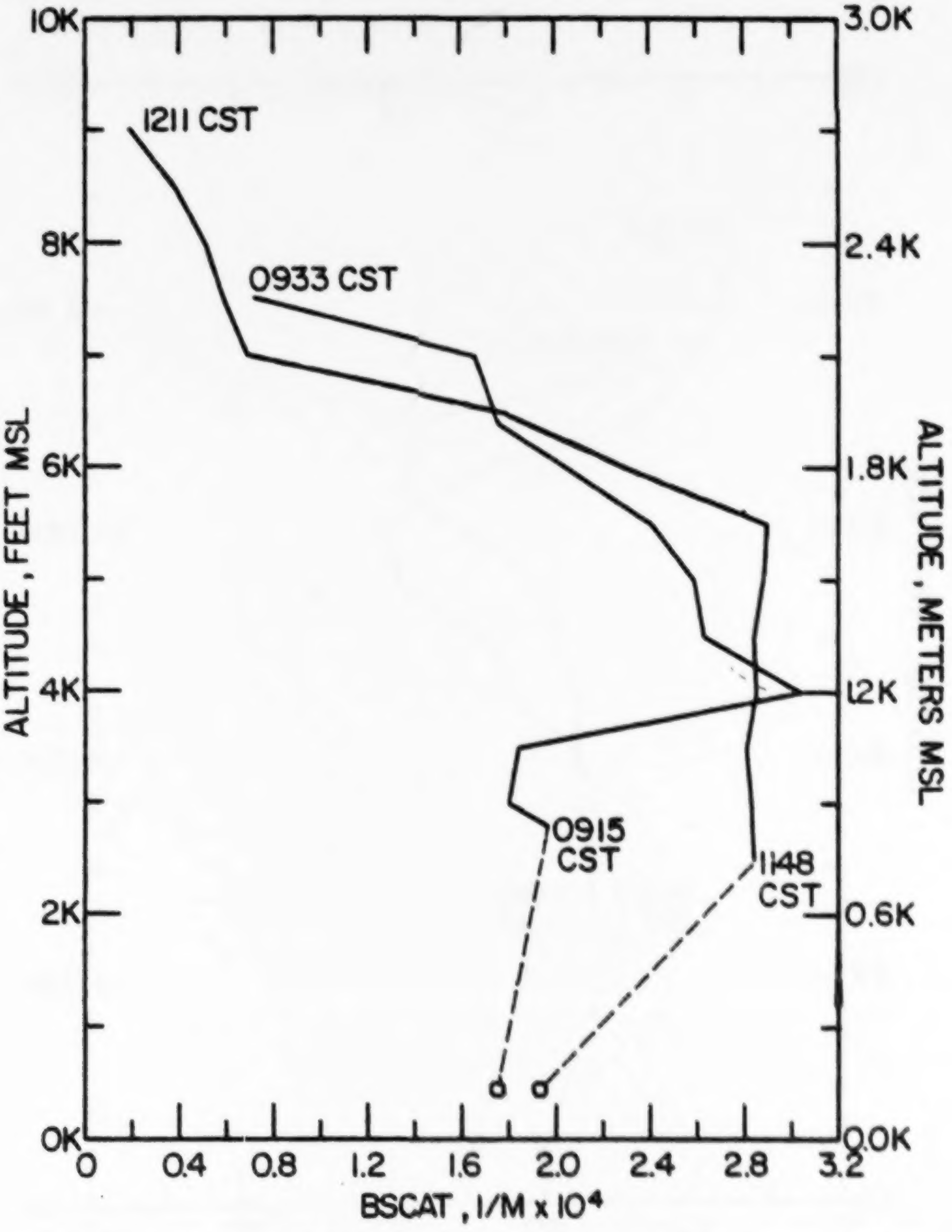

Figure 22. B_{scat} profiles as measured in St. Louis on 8 June 1976 during vertical flights of the NOAA aircraft that started at 0915 and 1148 CST. Time-resolved B_{scat} data from RAMS stations (o) are included for comparison.

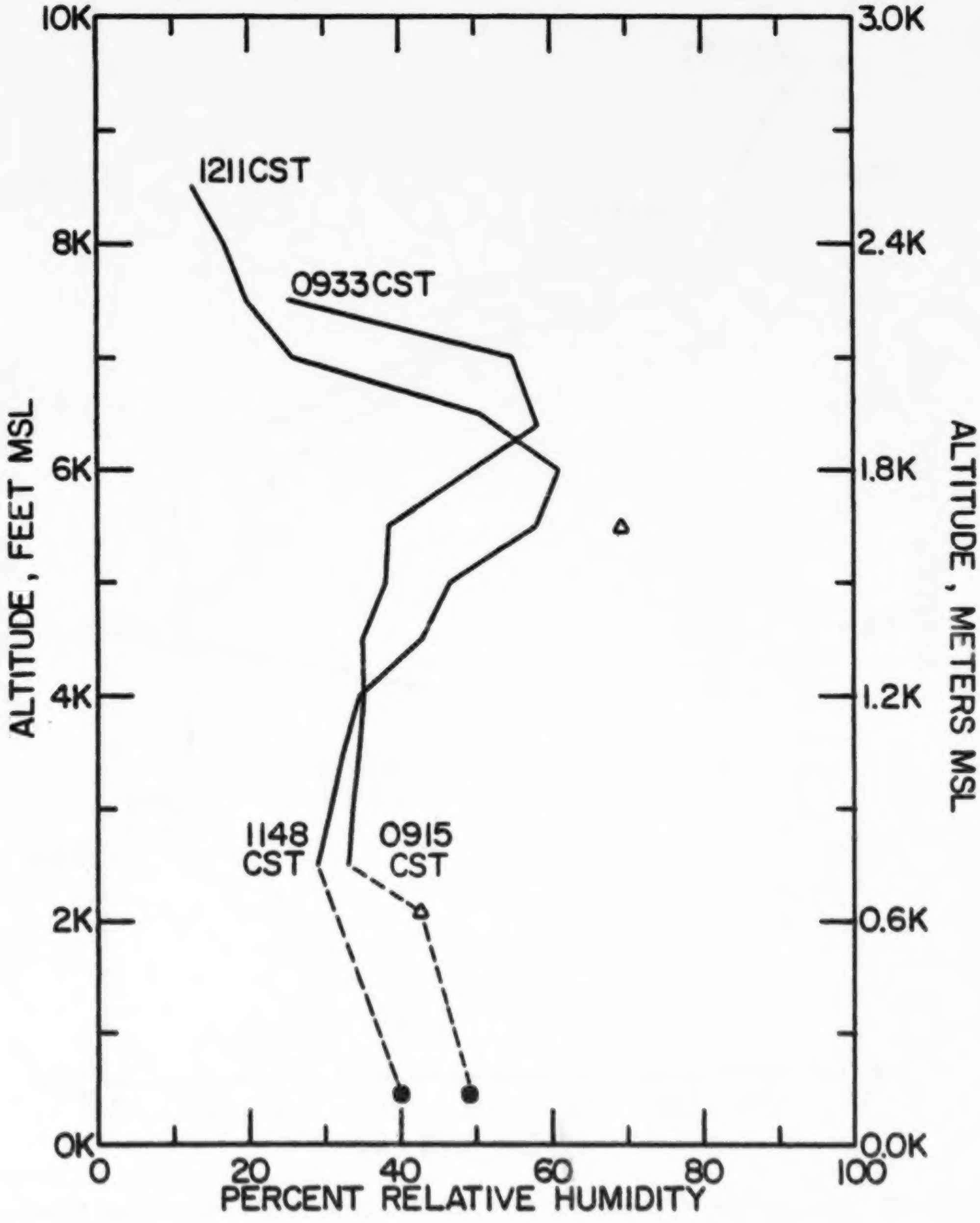

Figure 23. Relative humidity profiles as measured in St. Louis on 8 June 1976 during vertical flights of the NOAA aircraft that started at 0915 and 1148 CST. Time-resolved humidity data from Da Vinci II (Δ), RTI-EML (+), and RAMS stations (o) are included for comparison.

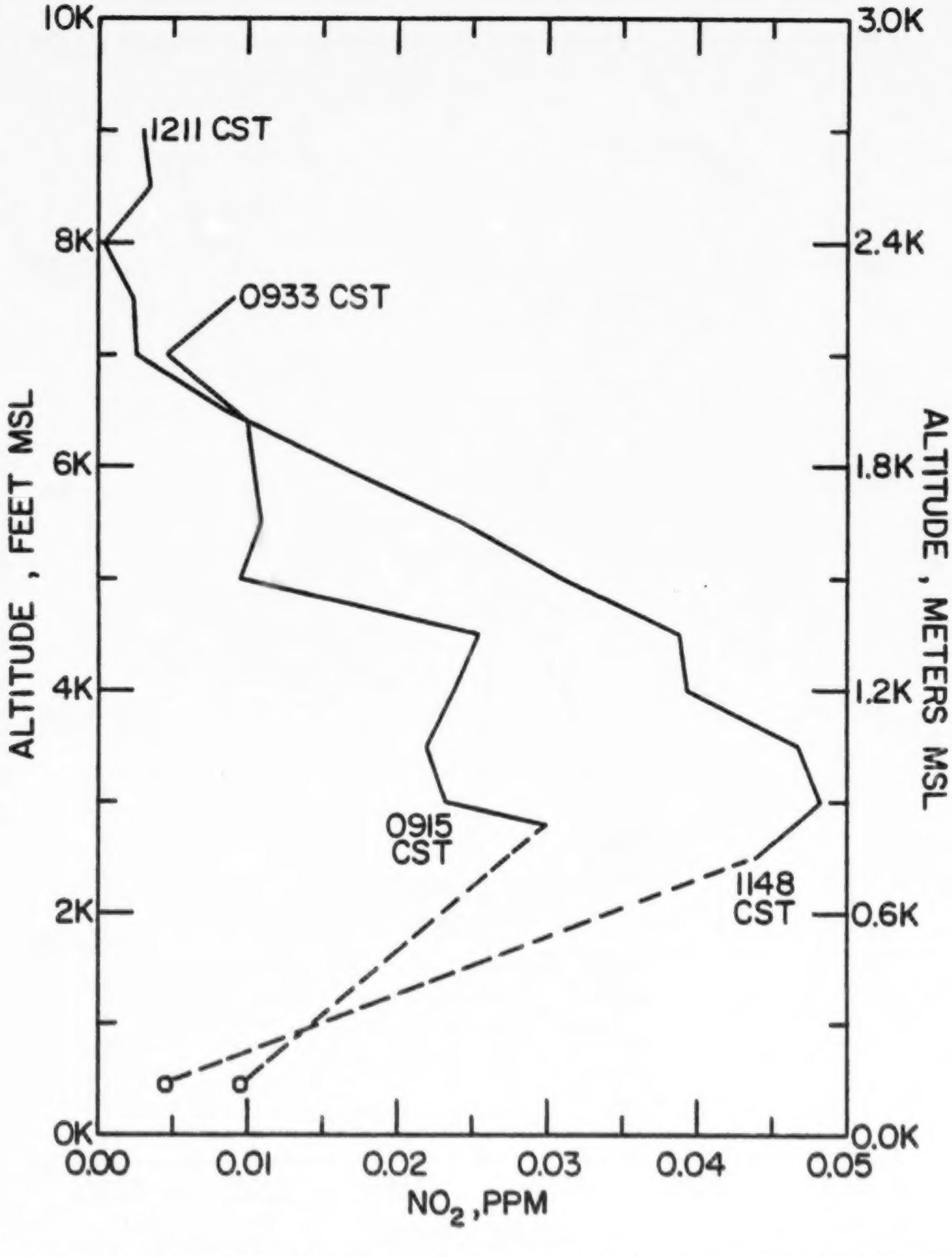

Figure 24. Nitrogen dioxide profiles as measured in St. Louis on 8 June 1976 during vertical flights of the NOAA aircraft that started at 0915 and 1148 CST. Time-resolved NO_2 data from RAMS stations (o) are included for comparison.

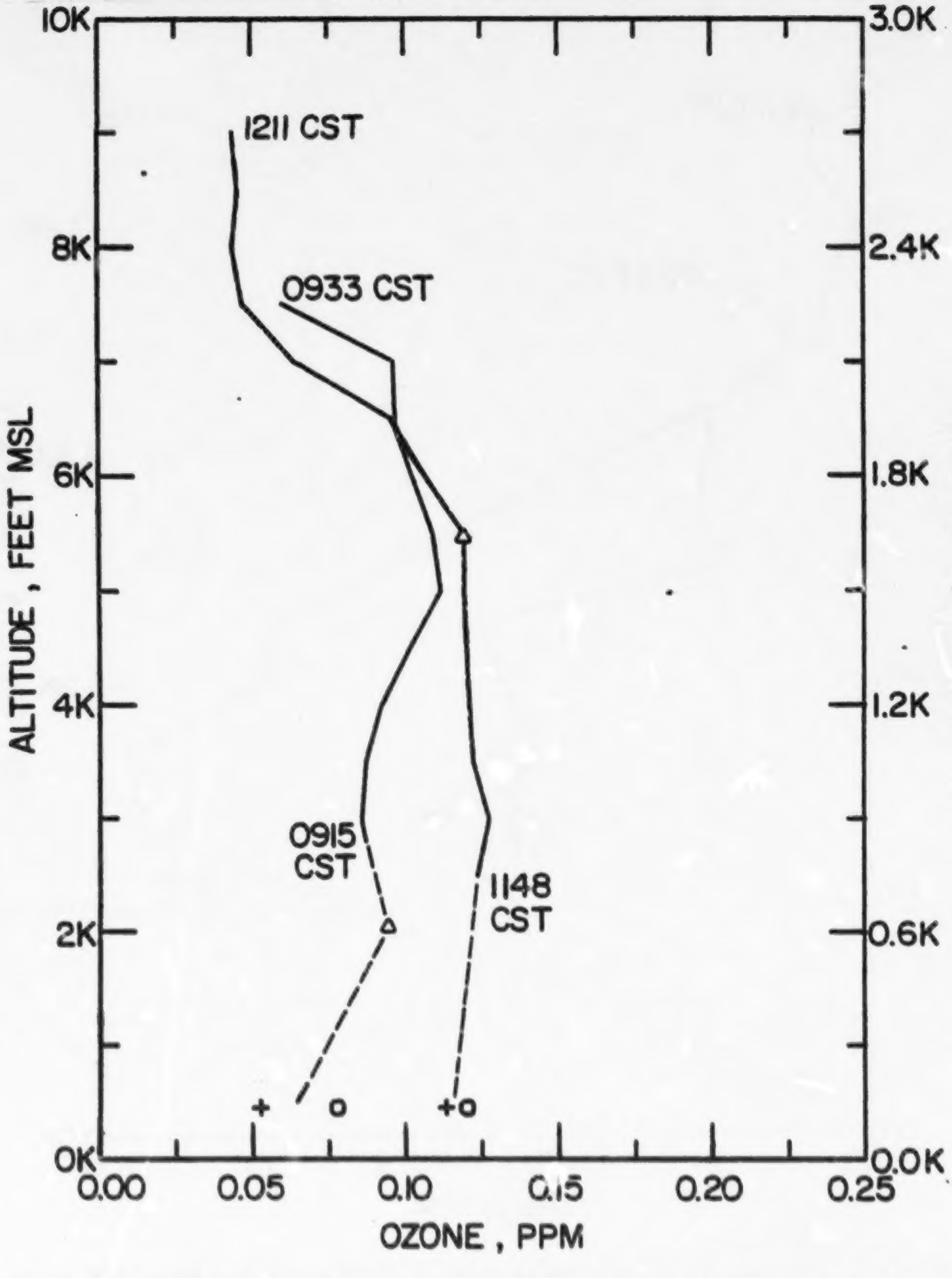

Figure 25. Adjusted ozone profiles as measured in St. Louis on 8 June 1976 during vertical flights of the NOAA aircraft that started at 0915 and 1148 CST. Time-resolved ozone data from Da Vinci II (Δ), RTI-EML (+), and RAMS stations (o) are included for comparison.

noontime ozone profile suggests that a near-zero gradient condition prevailed from the surface to 1,981 m (6,500 ft). The mean adjusted O_3 concentration aloft between 762 and 1,981 m (2,500-6,500 ft) was 0.097 ± 0.010 ppm at 0915 CST and was 0.117 ± 0.010 ppm at noon. This corresponds to an adjusted net increase of 0.020 ppm and an unadjusted increase of 0.032 ppm.

Portions of the above interpretation that rely on the adjusted data of figure 25 are somewhat speculative. Several general features are apparent, however, from either the raw or the adjusted data:

1. Substantial amounts of ozone existed aloft in a layer between 1,219 and 2,133 m (4,000-7,000 ft) at 0915 CST. This is probably indicative of the elevated ozone levels that prevailed from the midwest to the east coast during the time of the study.
2. Furthermore, this ozone could not have been synthesized from precursors released in St. Louis on 8 June, because by 0915 CST, the balloon was still upwind of St. Louis and the mixing layer had not yet reached the 1,219-m (4,000-ft) level.
3. Due to the early hour it is also improbable that the high levels of ozone prevalent at 0915 CST were photochemically synthesized on the morning of 8 June.
4. A net ozone increase of approximately 0.020-0.032 ppm occurred aloft during the 2.5-h interval between the two vertical flights. This ozone was either synthesized or transported into the area. Photochemical synthesis is thought to be primarily responsible for observed increase.
5. Ozone concentrations increased on the ground by 0.056 ppm at the RTI-EML and by 0.042 ppm at the nearest RAMS station between the 0900 and 1100 CST hours. These increases probably reflect both mixing and photochemical synthesis.

B_{scat} data were collected on the aircraft and at the nearest RAMS sites. These data, shown in figure 22, are in fair agreement. Substantial atmospheric layering is indicated by the 0915 CST profile. In general agreement with the ozone profiles, well-mixed conditions were established by noon up to 1,676 m (5,500 ft). Only a slight increase in B_{scat} from 2.5 to 2.8 x 10^{-4} m^{-1} occurred aloft at 1,524 m (5,000 ft) over the 2.5 h interval between vertical flights. These values are somewhat low in comparison to urban levels.[5] However, it may be too early in the day to use B_{scat} as an indicator of urban influence, because in typical photochemical systems, increased B_{scat} normally lags ozone. The highest noontime RAMS B_{scat} value was 3.0 x 10^{-4} m^{-1} and the highest daytime value was 4.0 x 10^{-4} m^{-1}.

Relative humidity data are presented in figure 23. These data were collected on the aircraft and Da Vinci II aloft and at RAMS stations and the RTI-EML on the ground. The data are in good agreement and indicate layering aloft. Elevated RH between 1,219 and 1,981 m (4,000-6,500 ft) was also indicated by rawinsonde data. A humidity increase of approximately 10 percent is observed at this level between 0915 CST and noon. The noontime profile suggests that the layering present at 0915 CST persisted until noon. This is puzzling in view of the well-mixed conditions indicated by both the ozone and B_{scat} noontime vertical profiles.

The NO_x concentration is expected to decrease with altitude due to the preponderance of ground-based NO_x sources. Nitric oxide and NO_2 concentration data were collected on the NOAA aircraft. In both vertical flights, the NO concentration was relatively constant with altitude at approximately 0.01 ppm. The mean NO concentration between 762 and 1,981 m (2,500-6,500 ft) was 0.009 ± 0.001 ppm in the 0915 flight and increased only slightly to 0.010 ± 0.002 ppm by noon. The invariant behavior of the NO with altitude is somewhat surprising in view of the apparent layering of other chemical species and may reflect instrument error. The 0900 and 1100 CST hourly average ground-level NO concentrations at the nearest RAMS stations were below the minimum detection limit of 0.005 ppm. The reported NO concentrations aloft are also near the instrumental minimum detection limit and therefore may be somewhat suspect.

The vertical NO_2 profiles shown in figure 24 are inconsistent with the RAMS data and may also be suspect. Both profiles are internally consistent and show decreasing NO_2 concentrations with altitude. Although behavior may be indicative of upward mixing from ground-based sources, the persistence of the vertical gradient at noon is contrary to the well-mixed conditions indicated by the O_3 and B_{scat} vertical concentration profiles noted earlier. Over the 2.5-h interval between flights, a net increase of 0.014 to 0.018 ppm NO_2 was observed aloft. Although upward mixing of NO_2, an ozone precursor, may facilitate enhancement and replenishment of O_3 levels aloft, conflicting evidence and a limited data base prevent this speculation in the present study.

Although they are not pictured in this section, rawinsonde temperature data indicate that the base of the subsidence inversion was at 2,743 to 3,048 m (9,000-10,000 ft). A sharp decline in the rawinsonde dewpoint data at 1,981 to 2,133 m (6,500-7,000 ft) suggests the existence of a stable layer beneath the subsidence inversion at that level.

Vertical profiles of O_3, B_{scat}, and RH also show sharp declines at 1,981 to 2,133 m (6,500-7,000 ft). In the noontime profile, the mean ozone concentration between 2,133 and 2,743 m (7,000-9,000 ft) was reduced by a factor of 2.4 in comparison to that between 762 and 1,981 m (2,500-6,500 ft). In addition, relatively high water vapor concentrations existed below 1,981 m (6,500 ft). These observations do not suggest that stratospheric intrusion was responsible for the elevated ozone concentration between 762 and 1,981 m (2,500-6,500 ft).

4.3.5.2 Acoustic Sounder

Data from ANL acoustic sounders are presented in figure 26. These data suggest that Da Vinci II was launched prior to complete dissipation of the nocturnal radiation inversion.

On the morning of 8 June the inversion was destroyed by 0920 CST; this correlates well with the first thermal experienced by Da Vinci II between 0937 and 0956 CST (see table 5). This is some 2 to 3 h after mixing had been established within the lowest 30 m (100 ft) as indicated by RAMS temperature gradient measurements. This, however, is not inconsistent because acoustic sounders provide information on the thermal layering to altitudes of 1 km (3,280 ft). It is likely that an additional 2 h of solar heating were required before the inversion was completely dissipated.

On the afternoon of 8 June, establishment of the nocturnal radiation inversion was observed to commence during the 1800 CST hour. This coincides well with RAMS temperature gradient measurements.

The reduced thickness of the nocturnal radiation inversion before midnight coincides well with the nighttime ozone peak observed by the RTI-EML. This suggests that the resistance to downward mixing was minimized at this time and is consistent with the previous interpretation of the nighttime O_3 peak observed at the RTI-EML on the evening of 8 June.

4.3.5.3 Temperature, Relative Humidity, and Condensation Nuclei on Da Vinci II

Air temperature, relative humidity, and condensation nuclei as measured on Da Vinci II are presented in figures 27, 28, and 29. Sandia and ASL air temperature data plotted in figure 27 are in good agreement. Comparison of these data with the altitude profile shown previously in figure 7 indicate the expected inverse relationship between altitude and temperature. During the day, when Da Vinci II was above 1,219 m (4,000 ft), the temperature was low. After

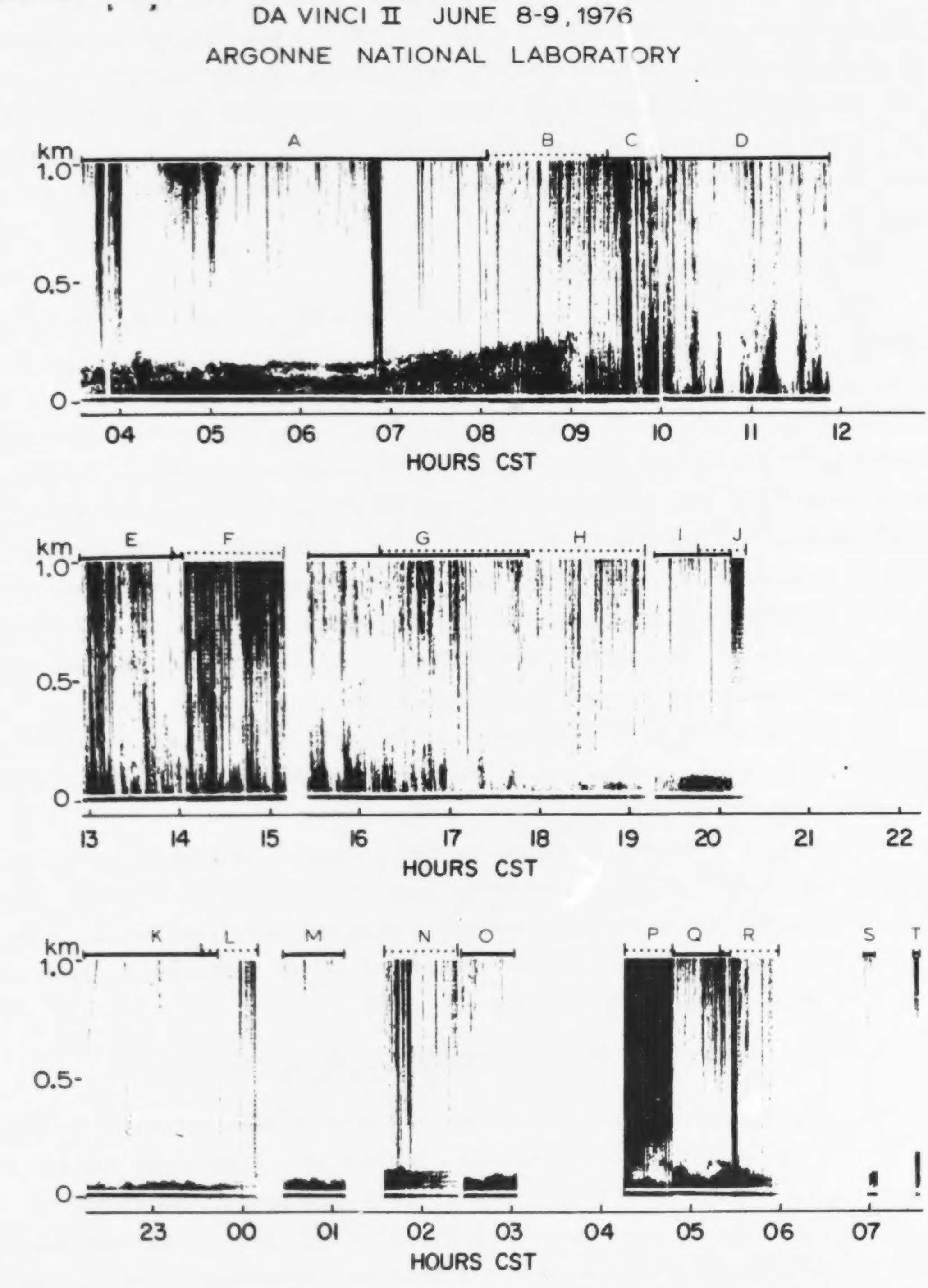

Figure 26. ANL acoustic sounder data along the flight track of Da Vinci II, 8 and 9 June 1976.

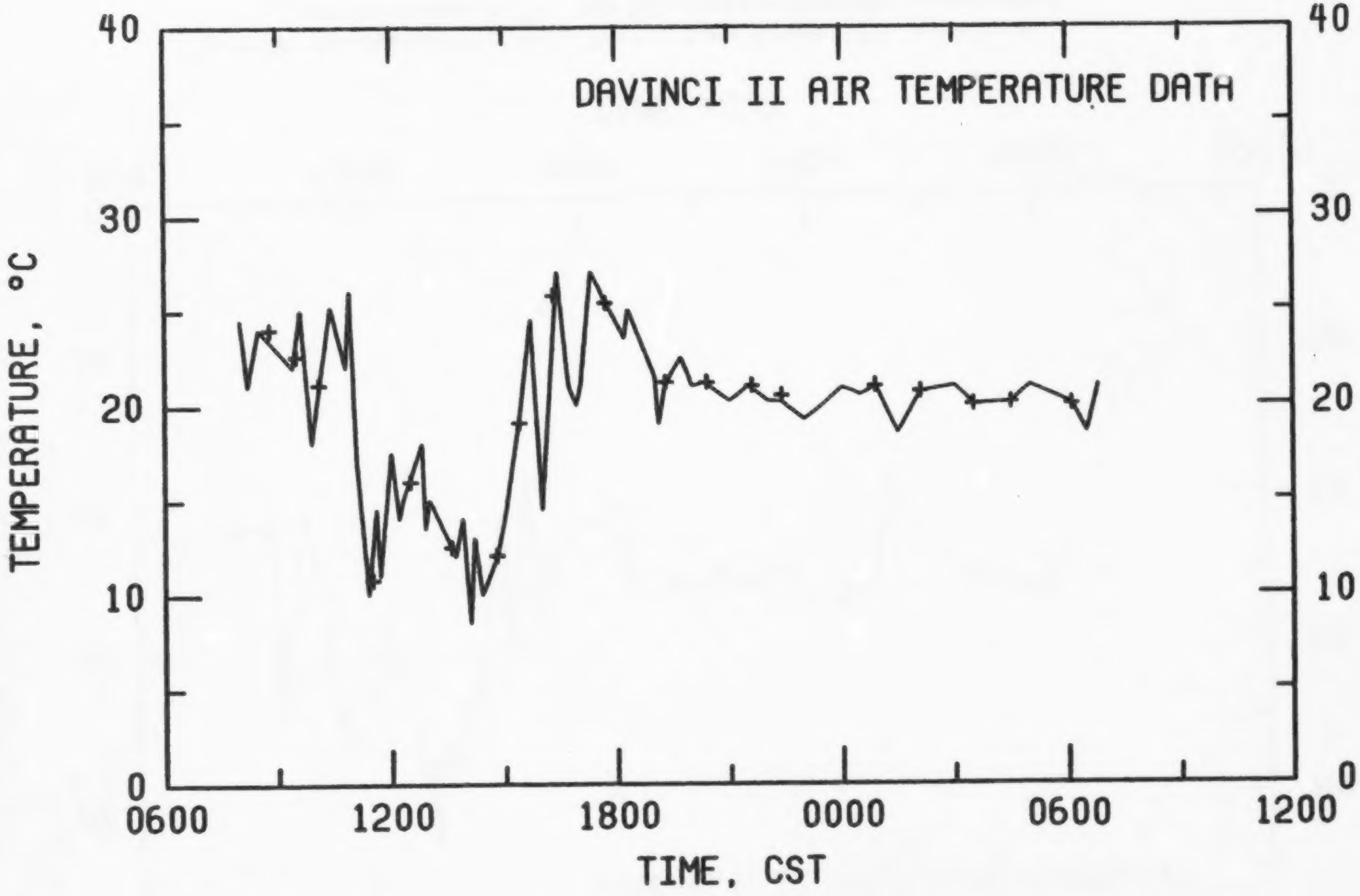

Figure 27. Air temperature on Da Vinci II, 8 and 9 June 1976. Sandia data are represented by " + " and ASL data are represented by connected dots.

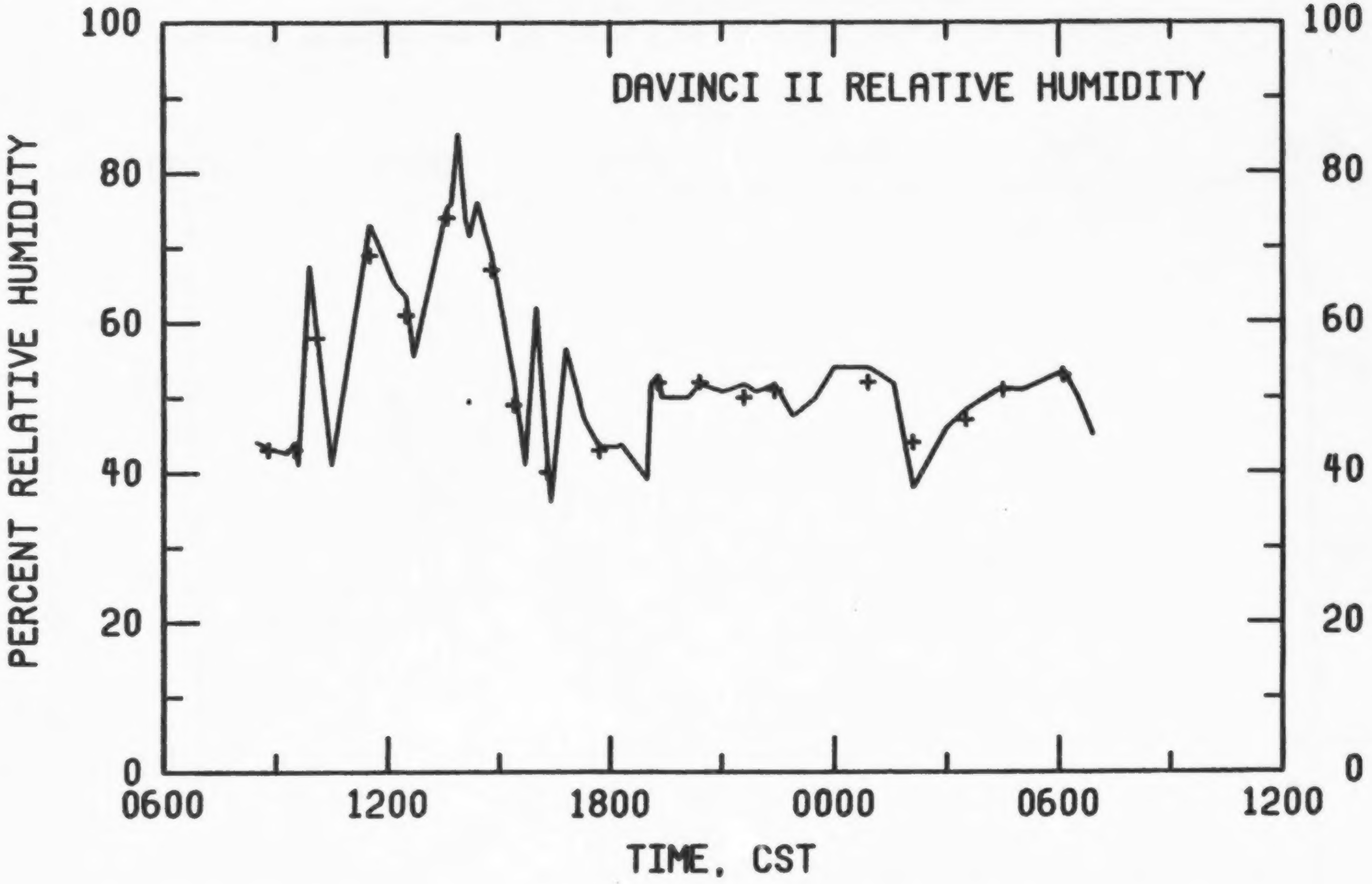

Figure 28. Relative humidity on Da Vinci II, 8 and 9 June 1976. Sandia data are represented by " + " and ASL data are represented by connected dots.

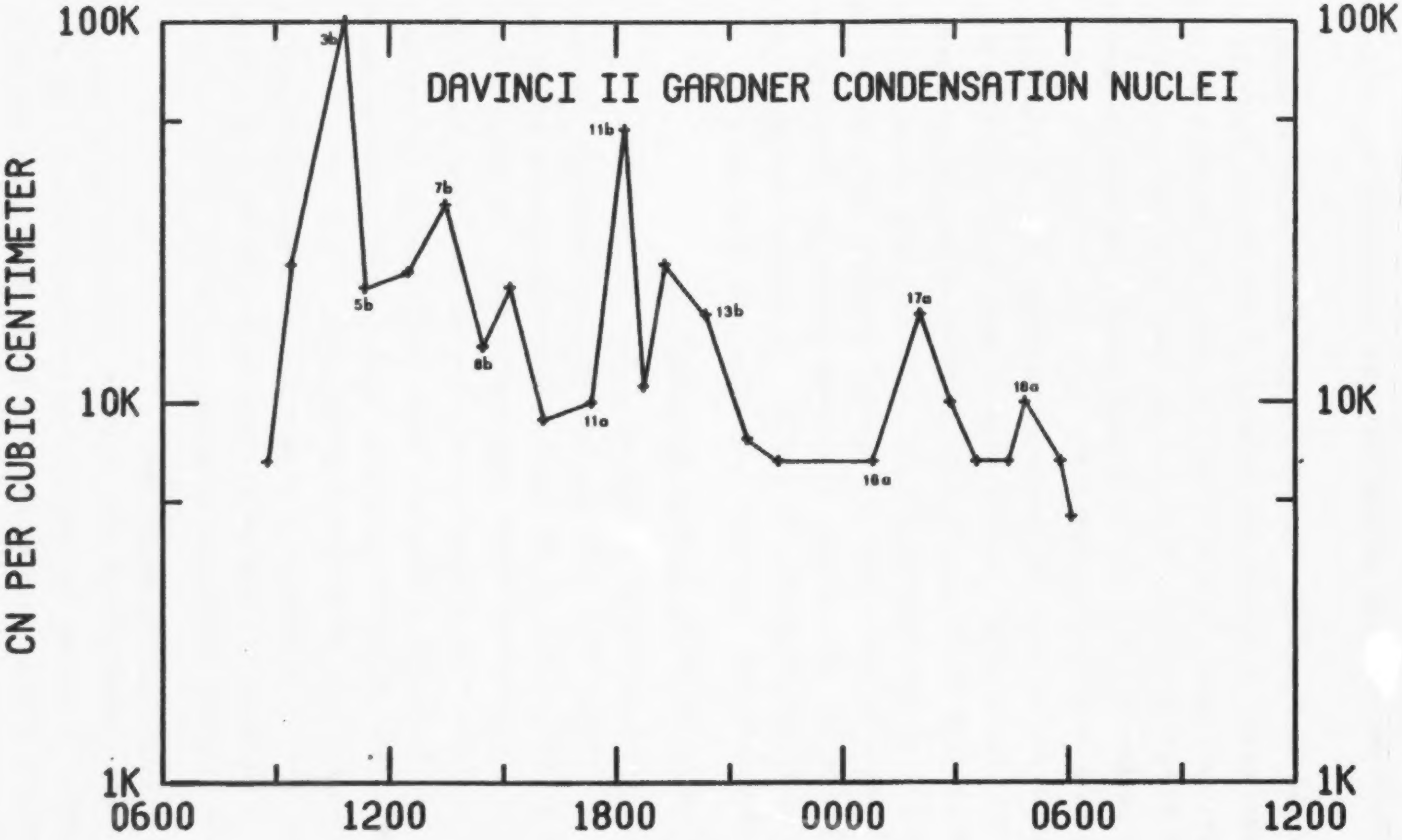

Figure 29. Condensation nuclei on Da Vinci II, 8 and 9 June 1976. Selected CN data that coincide with altitude excursions have been identified by the number of the corresponding altitude excursion from figure 7.

a stable altitude was achieved at 2000 CST, the temperature was relatively constant.

As indicated in figure 28, the ASL and the Sandia relative humidity data are in good agreement. A direct relationship between RH and altitude is indicated on comparing figures 29 and 7. When Da Vinci II was above 1,219 m (4,000 ft), elevated RH was observed. This is consistent with the aircraft data in figure 23 and rawinsonde data. As with temperature, the relative humidity profile is relatively stable after 2000 CST.

Condensation nuclei data are presented in figure 29. In the mean, excluding major excursions, a slight trend toward decreasing CN prevailed over the day. Selected CN data that coincide with altitude excursions have been identified by the number of the corresponding altitude excursion shown in figure 7. The highest CN level is associated with a small descent (3b to 4a) at 640 m (2,100 ft). Two of the lower midday CN concentrations are associated with two of the higher altitude excursions, 5b and 8b. In general, however, the limited frequency of CN measurements prevents comparison with other data.

4.3.5.4 Ozone and Sulfur Dioxide on Da Vinci II

4.3.5.4.1 Ozone and Sulfur Dioxide Profiles

Both ASL and Sandia ozone data are presented in figure 30. The agreement for these data is very good. In 28 cases of near-simultaneous measurements, ASL data are 5.5 ± 1.2 percent higher than Sandia data. To allow a visual assessment of temporal ozone behavior aloft, the ASL data have been replotted in figure 31 with the points connected. Major concentration excursions that coincide with altitude excursions have also been identified by the numbers of the corresponding altitude excursions from figure 7.

Sandia SO_2 data are presented in figure 32. Although SO_2 excursions are not associated with major altitude excursions, increased SO_2 levels coincide with small-scale altitude reductions in several cases.

4.3.5.4.2 Sulfur Dioxide Excursions

Sulfur dioxide concentrations were below 0.02 ppm (50 $\mu g/m^3$) for the first 12 h of the flight. A marked increase in SO_2 concentration occurred at 2035 CST, approximately 2 h after passing near the Sioux Power Plant and 45 min after passing near the Wood River Power Plant in the industrialized East Alton area. Three major SO_2 excursions occurred at 2047, 0005, and 0503 CST. The mean magnitude of these peak values is 0.134 ± 0.022 ppm. Smaller peaks asso-

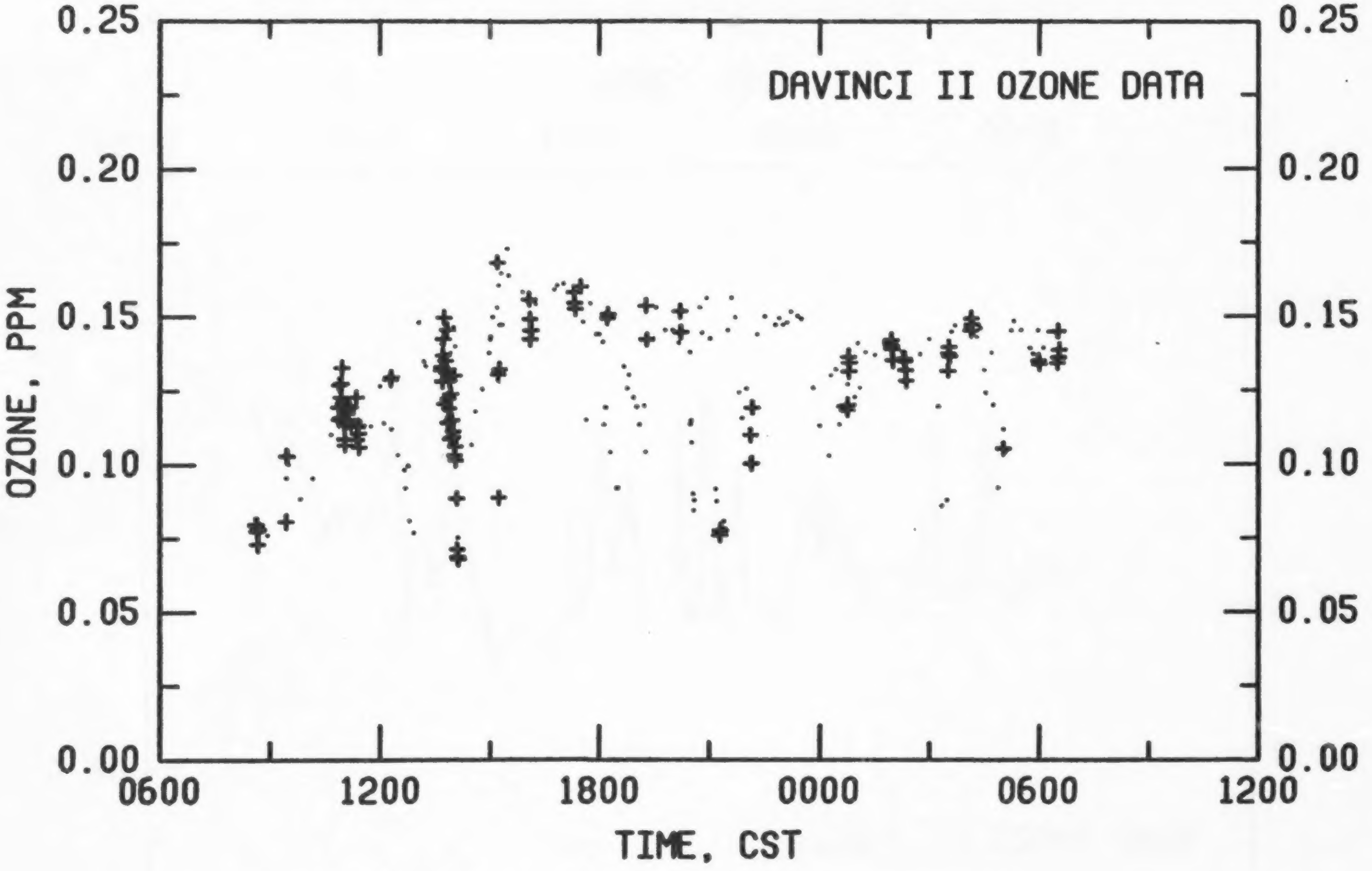

Figure 30. Ozone on Da Vinci II as measured by Sandia Laboratories (+) and ASL (•), 8 and 9 June 1976.

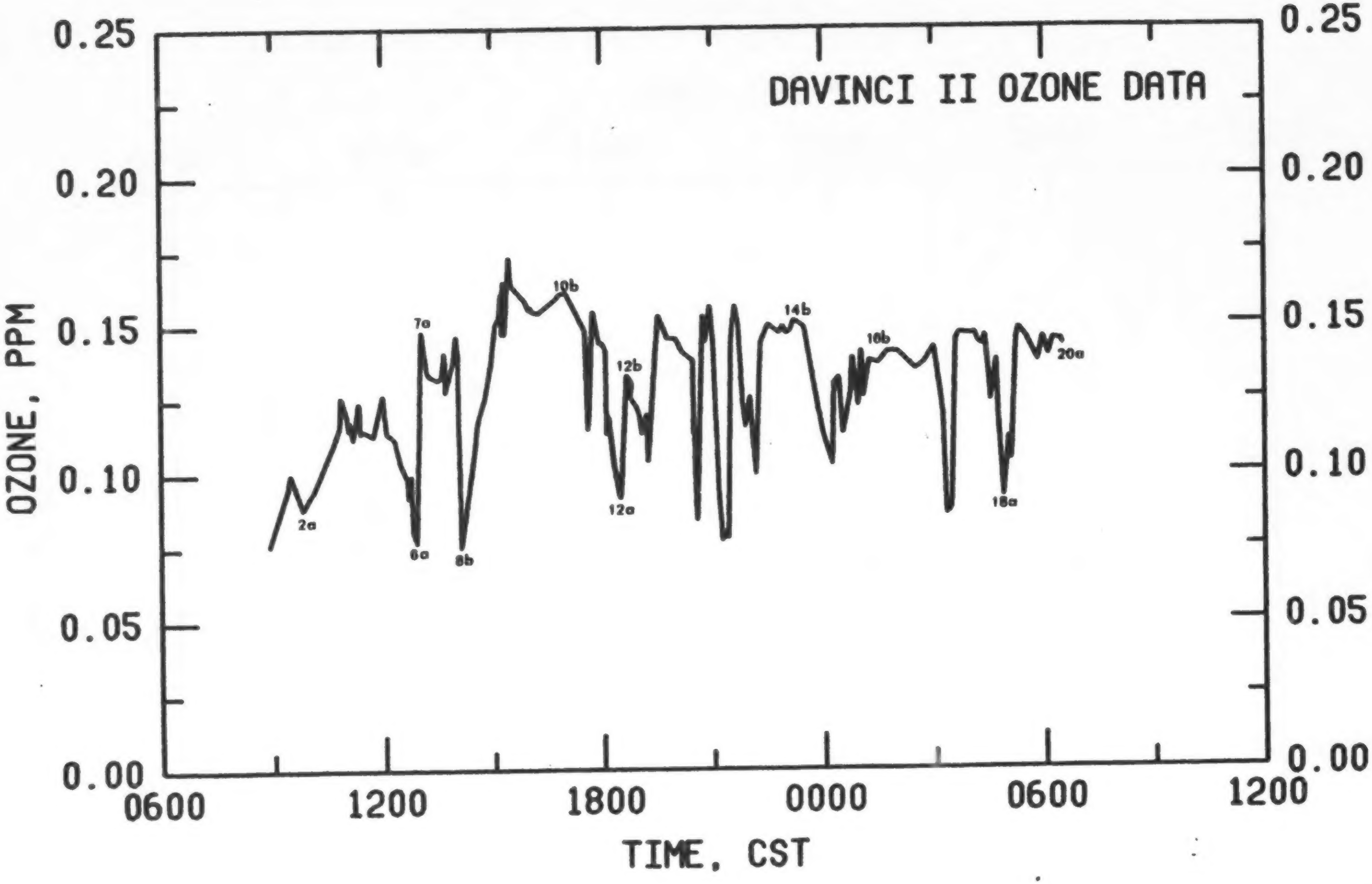

Figure 31. Ozone on Da Vinci II as measured by ASL and represented by connected dots, 8 and 9 June 1976. Selected ozone excursions that coincide with altitude excursions have been identified by the number of the corresponding altitude excursion from figure 7.

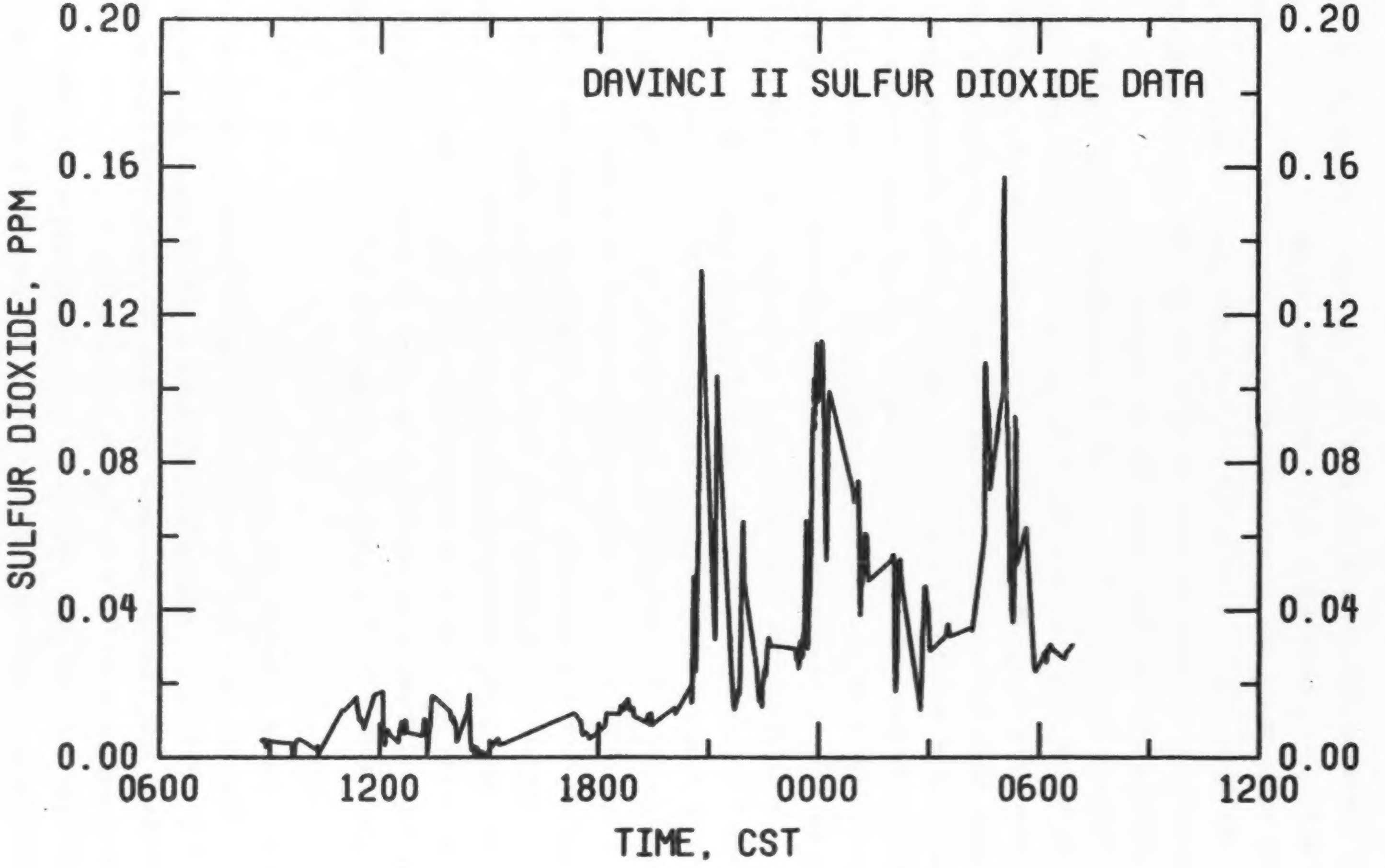

Figure 32. Sulfur dioxide on Da Vinci II as measured by Sandia Laboratories and represented by connected dots, 8 and 9 June 1976.

ciated with the major SO_2 excursions were also observed. Two small peaks were noted that were not associated with the major excursions.

For the three major SO_2 excursions, corresponding reductions of ozone occurred. The mean reduction of O_3 is 0.051 ± 0.010 ppm. In addition, reductions of ozone were observed at 2115 and 2210 CST for the two secondary SO_2 peaks associated with the first major SO_2 excursion.

The timing of the excursions and the corresponding position of Da Vinci II on the flight track suggests that the first two major SO_2 peaks were contributed by sources located in the greater St. Louis area. The only major SO_2 source located downwind from St. Louis that could have contributed to the 0503 CST excursion was the Coffeen Power Plant. The currently available data, however, do not allow reconciliation of the SO_2 excursions with specific sources.

Sulfur dioxide does not react appreciably with ozone. However, both SO_2 and NO_x are emitted in high concentrations from both power plants and petroleum refineries (see tables 6 and 7). If the SO_2 excursions are caused by Da Vinci II's entering a portion of such plume, then correspondingly high NO_x levels would also have been present. Ozone reacts quite rapidly with NO and somewhat more slowly with NO_2. For example, in the presence of a constant 0.15 ppm of O_3, NO has a half-life of 12 s. Molar NO_x/SO_2 ratios from power plant emissions calculated from the emissions inventory data range from 0.25 to 0.50. The ratio for petroleum refineries also falls within this range at 0.45. Thus, 0.034 to 0.067 ppm of NO_x could be simultaneously present with an SO_2 peak concentration of 0.134 ppm. If it is assumed that this NO_x is completely consumed by reaction with O_3, then a net reduction of 0.034 to 0.067 ppm is expected in the O_3 concentration. The mean observed O_3 decrease falls within the expected range.

4.3.5.4.3 Ozone Behavior and Excursions

Between 0900 and 1100 CST, hourly average ozone levels on Da Vinci II increased from 0.095 to 0.115 ppm, a net increase of 0.020 ppm. This is in excellent agreement with the net increase of 0.020 ppm calculated from adjusted NOAA data averaged between 762 and 1,981 m (2,500-6,500 ft).

Between 0900 and 1700 CST, ozone levels aloft generally increased. Hourly average concentrations increased from 0.095 ppm at 0900 CST to the flight maximum value of 0.153 ppm at 1600 CST, a net increase of 0.058 ppm. Thus, a net increase of 0.058 ppm ozone was observed aloft at or near Da Vinci II on 8 June.

The mean O_3 concentration aloft during the flight was 0.125 ± 0.018 ppm. On the average, slightly higher O_3 concentrations were observed aloft at night than during the day. The 1100-1500 CST mean value on 8 June was 0.121 ± 0.018 ppm in comparison to the 0100-0600 CST mean of 0.135 ± 0.005 ppm on the morning of 9 June. This is probably due to the differences in vertical movement and the resulting highly variable ozone concentrations measured during the first half of the flight.

During the flight, many excursions occurred in the ozone concentration. This suggests that Da Vinci II failed to behave as a perfect Lagrangian marker. Several ozone excursions were associated with altitude movement (see figures 31 and 7). The highest altitude excursion, 8b, is associated with a distinct reduction of ozone concentration. Da Vinci II may have penetrated the stable layer at 1,981 m (6,500 ft) and entered the ozone-deficient regime shown in the vertical ozone profiles, figures 21 and 25. The highly erratic vertical movement of Da Vinci II between 1500 and 1800 CST was not reflected in the ozone profile.

The altitude profile stabilized at 2000 CST, but the ozone profile became highly erratic. This behavior is closely associated with Da Vinci II's passing near the Sioux and Wood River power plants and the Wood River-Roxana petrochemical complex. The first of several coincident nighttime excursions of SO_2 and O_3 occurred at 2047 CST. The next two O_3 reductions, occurring at 2115 and 2210 CST, were coincident with two secondary SO_2 peaks associated with the first major SO_2 excursion.

In addition to being associated with a major increase of SO_2 at 0005 CST, the negative O_3 excursion between 2330 and 0145 CST is associated with a decrease in altitude of between 150 and 270 m (500-900 ft). As noted earlier, elevated ozone was observed between 2315 and 0115 CST on the ground at the RTI-EML (see figure 20). The coincident downward movement of the balloon, reduced ozone aloft, and elevated ground-level ozone concentrations provide tempting opportunities for associations with downward mixing.

The third ozone excursion occurred at 0320 CST and was not associated with an altitude excursion. Sulfur dioxide was not measured during a 27-min period encompassing this event and thus prevented a comparison of O_3 and SO_2 behavior during this period.

The final major ozone excursion occurred at 0453 CST. This reduced ozone behavior was associated with a major SO_2 excursion. These coincident excursions are difficult to assign to any specific source. As noted previously, this behavior was not caused by chemical reaction of ozone with SO_2. It is thought to have been caused by the chemical reaction of ozone with the NO_x that was emitted along with SO_2 by various sources. Atmospheric layering can allow several plumes as well as a balloon to travel long distances in parallel before vertical turbulence promotes interaction and mixing.

4.3.5.4.4 Ozone Half-Lives

It is of interest to speculate on the half-life of ozone under various conditions in the atmosphere. In the absence of the O_3 precursors (HC and NO_x), ozone in a mixture of air and water vapor will decay slowly in the dark--half-lives in excess of 100 h have been observed.[6] Under exposure to sunlight, ozone will, in the same system, decay more rapidly and will exhibit a half-life of approximately 10 h.[6] This suggests that if O_3 and water vapor were present in an HC- and NO_x-free atmosphere, half of this ozone would be naturally destroyed during a single sunny day by photoinitiated processes. In the troposhere, however, both anthropogenic and natural ozone precursors are present. Photochemical synthesis from these precursors can permit O_3 to accumulate during the day.

In the ambient atmosphere, the HC and NO_x that act as ozone precursors during the day, act as ozone-destructive agents at night. A question then arises concerning the behavior of ozone during nighttime hours in the presence of HC and NO_x. The nighttime decay rate to a large extent defines the maximum impact that ozone, which is generated on one day in an urban area, will have on downwind air quality on the next day.

The ideal approach for answering this question would involve in situ measuring of $[O_3]$ aloft under transport conditions. This would require a Lagrangian platform that could monitor ozone concentrations within an undiluted air parcel as it travels overnight. Data from the Da Vinci II experiment provide an opportunity to do just this. Two caveats must be emphasized, however: Da Vinci II was not a perfect Lagrangian marker, as shown in figure 31, and the extent of dilution experienced by the air parcel cannot be quantified for this experiment. With these shortcomings in mind, the ASL ozone data between 2000 CST on 8 June and 0500 CST on 9 June were examined to determine a nighttime ozone decay rate (see figure 31).

Ozone data were employed to define an envelope of maximum nighttime ozone concentrations. A least-squares regression of ln $[O_3]$ versus time permitted the calculation of a nighttime ozone half-life of 116 h. This approach neglects non-Lagrangian behavior of Da Vinci II and negative O_3 excursions presumably caused by isolated pockets of species that act as ozone scavengers. An early half-life estimate of approximately 30 h was based on a preliminary limited set of raw data in which negative excursions were difficult to distinguish.[7] Refinement of the nighttime half-life to our current estimate of 116 h has been permitted by an enlarged data base.

Nitrogen oxides and HC can act as both ozone precursors and ozone-destructive agents. The lack of NO_x measurements on Da Vinci II prevents an assessment of NO_x concentrations aloft. The examination of Da Vinci II HC data that is discussed in a subsequent section of this report suggests that the concentration of ozone-destructive and other HC species aloft was low during the flight. Thus, except for apparent encounters with remnants of industrial plumes, the conditions for which the above ozone half-life estimate was made is thought to be representative of suburban-to-urban air. The dark phase half-life of ozone under these conditions of presumed low levels of both NO_x and HC is entirely sufficient to allow ozone from one urban area to be transported overnight to another populated area without significant diminishment due to decay.

4.3.5.5 Hydrocarbons on Da Vinci II

Concentration profiles for many of the hydrocarbons are presented in figures 33a-33k. Each of these data points is representative of the few seconds of the flight during which each corresponding grab sample was collected. In view of this, a comprehensive picture of events for the flight cannot be prepared. Nevertheless, HC data were examined to determine the extent to which Da Vinci II was traveling in the urban plume and to document the behavior of Da Vinci II's environment for the flight. The approaches employed a mean value analysis, an excursion analysis, and a trend analysis.

4.3.5.5.1 Mean Value Analysis

Mean concentrations and concentration ratios, excluding excursions, were calculated for each species. These results were compared with ground-level values typical of urban, suburban, and nonurban RAMS sites.

Detailed HC data were not collected at ground level during the flight of Da Vinci II. To provide a basis for comparison, however, mean concentrations were calculated from 3 to 4 days of data collected at three RAMS sites during August 1976.[8] These data are presented in table 13 along with data collected

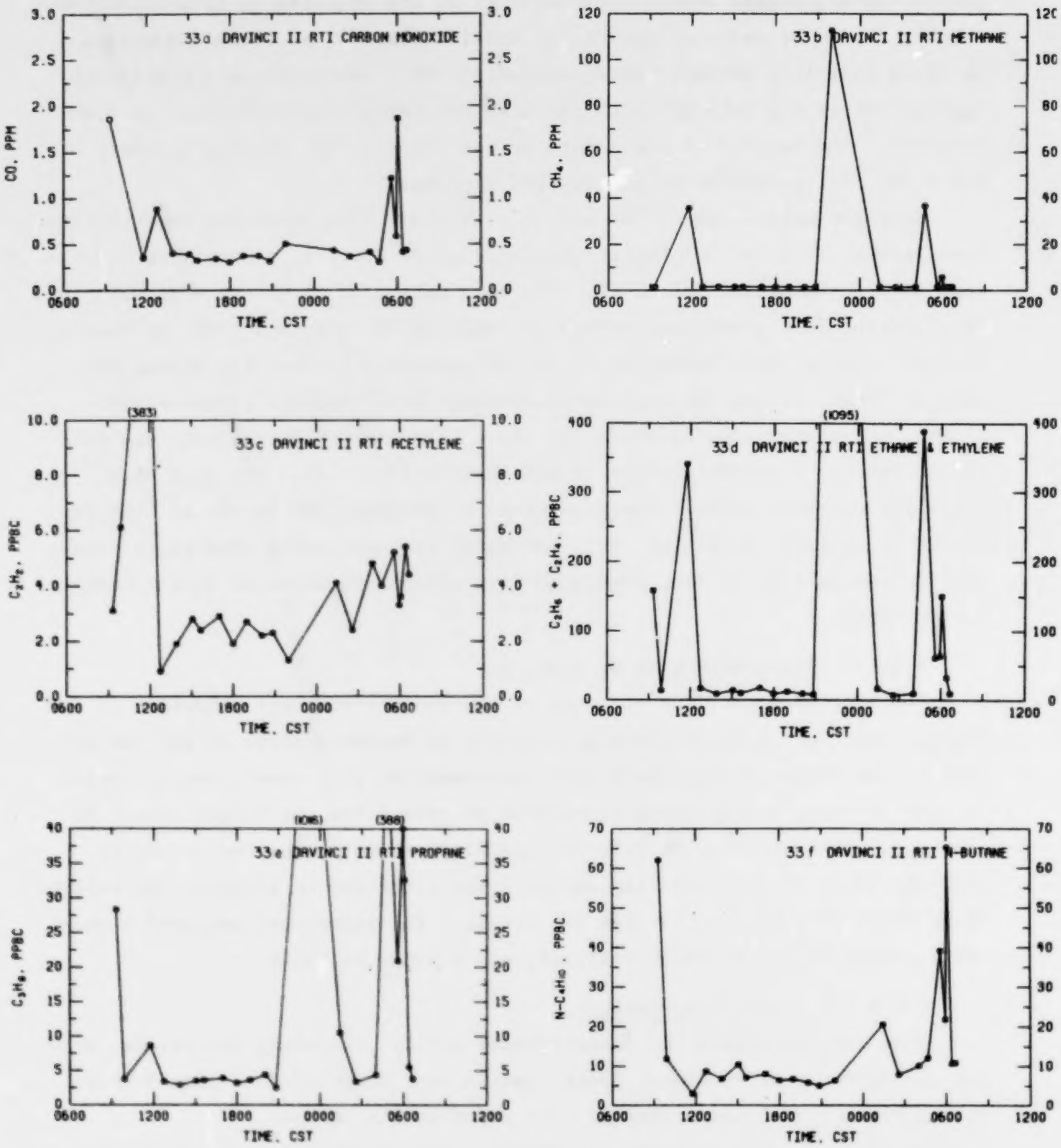

Figure 33. Pollutant concentrations as determined by RTI from grab samples collected on Da Vinci II, 8 and 9 June 1976.

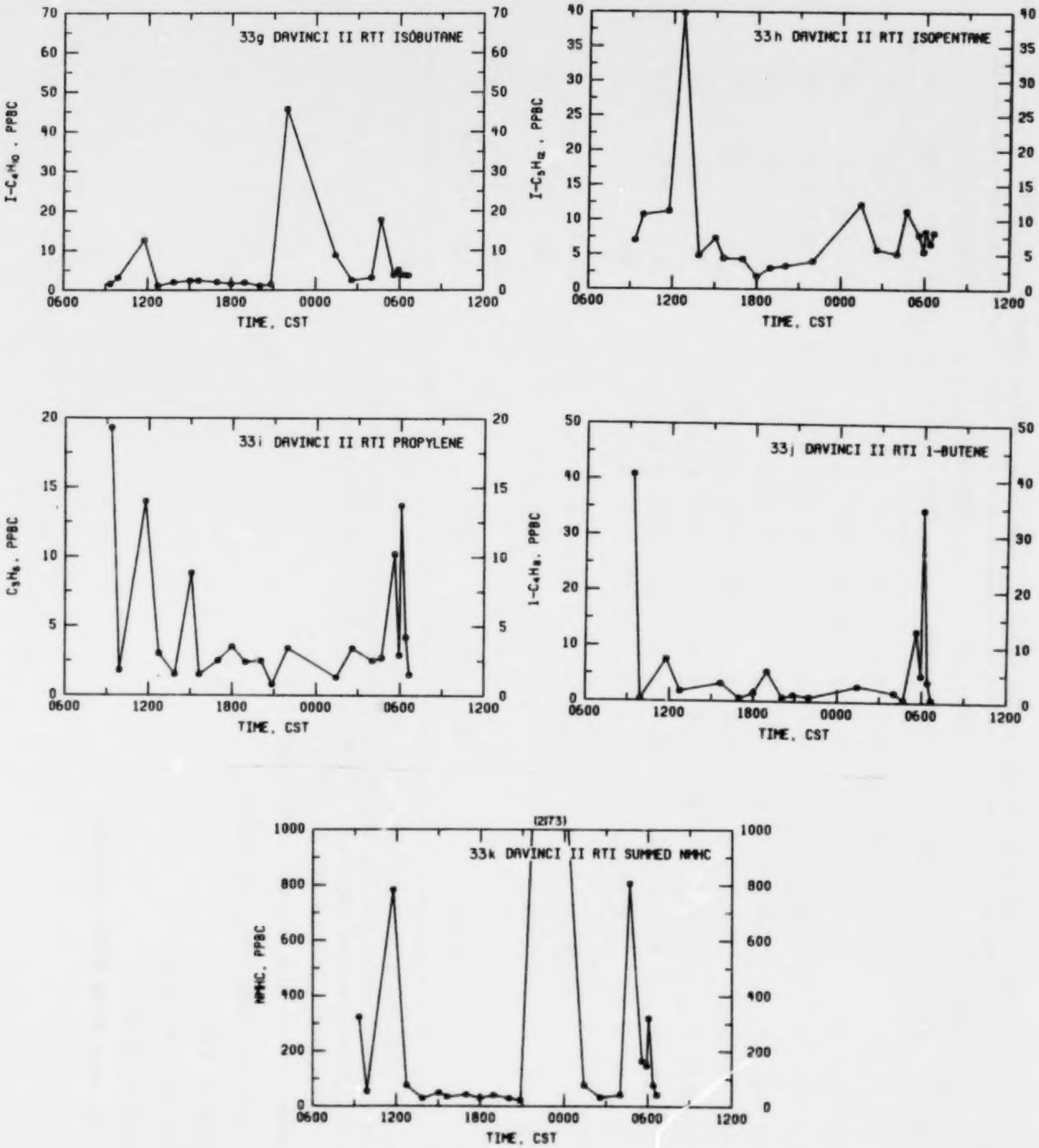

Figure 33. (con.)

Table 13. Mean HC concentrations at Da Vinci II and at selected RAMS stations[a]

Location	RAMS 101				RAMS 114		RAMS 124		DaVinci II	
Species	0700-0900[b]	n[c]	1100-1500	n	1100-1500	n	0700-1500	n	8,9 June 1976[d]	n
C_2H_2	21.1 ± 6.5	4	7.8 ± 2.5	8	3.8 ± 1.7	6	1.7 ± 0.49	5	3.2 ± 1.4	21
C_2H_6	12.5 ± 5.0	4	7.3 ± 1.2	8	5.3 ± 0.69	6	5.8 ± 1.7	5	(11.7 ± 3.5	14[e]
C_3H_6	8.7 ± 3.0	4	2.2 ± 1.1	8	0.88 ± 0.27	5	0.68 ± 0.20	5	2.5 ± 0.85	16
C_3H_8	21.1 ± 8.9	4	7.8 ± 2.2	8	7.2 ± 1.3	6	5.7 ± 1.0	5	3.7 ± 0.73	14
iC_4H_{10}	10.5 ± 2.6	4	5.5 ± 1.3	8	2.8 ± 1.4	6	1.5 ± 0.36	5	2.4 ± 0.95	17
nC_4H_{10}	50.2 ± 14.8	4	26.9 ± 7.7	8	12.2 ± 6.7	6	4.2 ± 0.95	5	8.4 ± 2.3	16
iC_5H_{12}	44.5 ± 8.6	4	23.4 ± 5.4	8	8.7 ± 5.1	6	3.4 ± 1.1	5	5.4 ± 1.9	16
nC_5H_{12}	22.3 ± 3.9	4	10.6 ± 2.2	8	3.8 ± 1.7	6	2.5 ± 0.92	5	ND	
ΣHC	190.9		91.5		44.7		25.5		37.3	
CO	1515 ± 417	2	678 ± 79	3	ND		338 ± 82	4	386 ± 73	17
									(488 ± 31	9)[f]
CO/C_2H_2	72		87		ND		200		120, (153)[g]	

---

[a] RAMS data were not available for the period of the Da Vinci II experiment. These RAMS data were collected during August 1976 and should be representative of summertime HC concentrations expected at urban, suburban, and nonurban sites in St. Louis. All concentrations are in ppbC.

[b] Time period during which samples were collected.

[c] n ≡ number of samples comprising the mean.

[d] Samples analyzed by RTI.

[e] Value is ethane plus ethylene.

[f] Samples analyzed by NCAR.

[g] Based on mean CO data from NCAR analyses.

aloft during the flight. RAMS station 101 is considered to be urban, station 114 is a suburban site, and station 124, located well south of St. Louis, is a nonurban site. At the urban site, data from early morning samples are higher than those from samples collected during the well-mixed portion of the day by factors of from 2 to 4. The decrease of HC concentration with increased distance from the CUA that was noted previously in figure 18 is also evident from the data in table 13.

In seven of eight cases, the mean HC concentrations aloft are smaller than those presumed to be representative of suburban St. Louis. This is consistent with the previous observations based on comparisons of ozone concentrations on Da Vinci II with RAMS data. These data indicate that, in the mean, Da Vinci II was within a suburban-to-nonurban air parcel.

Kopczynski et al.[9] reported a mean CO/C_2H_2 ratio of 73 in St. Louis roadway samples and respective urban and nonurban ratios of 48 and 90. The more recent results from St. Louis sites presented in table 13 suggest representative urban and nonurban CO/C_2H_2 ratios of 80 and 200. The mean values from Da Vinci II data range between 120 and 153. This provides additional evidence suggesting that Da Vinci II was in suburban-to-nonurban air.

4.3.5.5.2 Excursion Analysis

The hydrocarbon data analyzed by RTI were examined for apparent excursions from their mean behavior. The mean values and the type and timing of the excursions are identified in table 14. Comments concerning coincident excursions of altitude, O_3, and SO_2 are also presented.

The WSU acetylene, ethane, and ethylene data cited in the footnote on table 14 were not considered in this analysis due to a possible calibration discrepancy. The respective mean values for these species, 13.2, 18.9, and 34.7 ppbC, are approximately a factor of 4 higher than the corresponding RTI mean values. The ratios of ethane plus ethylene to acetylene, however, compare closely: 4.06 (WSU) vs. 4.10 (RTI), suggesting calibration differences. In addition, comparison of the WSU acetylene and ethane concentrations and the carbon monoxide to acetylene ratio with the corresponding RAMS data in table 13 would indicate that for the whole flight, Da Vinci II was exposed to air characteristic of that trapped in an urban area beneath the nocturnal radiation inversion. Based on the flight track and the altitude profile of Da Vinci II, it seems unlikely that the air was contaminated to this extent, thus providing further support for the hypothesis of calibration differences.

Table 14. Mean hydrocarbon concentrations and excursions from the mean on Da Vinci II

Compound	Mean Concentration[a/] ± 1 S.D. (ppbC)	n	Time of Excursion.[b/] 0919	0954	1145	1244	1503	1759	1857	2050	2158	0126	0441	0535	0556	0603	0624
CO[c/]	386 ± 73	17	+	ND		+								+		+	
CH_4[d/]	1526 ± 23	17		ND	+						+		+		+		
C_2H_2[e/]	3.2 ± 1.4	21			+												
C_2H_4[f/] + C_2H_6[g/]	11.7 ± 3.5	14	+		+						+		+	+	+	+	+
C_3H_8	3.7 ± 0.7	14	+		+						+	+	+	+	+	+	
C_4H_{10}	8.4 ± 2.3	16	+		-							+		+	+	+	
iC_4H_{10}	2.4 ± 0.9	17			+						+	+	+		+		
iC_5H_{12}	5.4 ± 1.9	16		+	+	+		-		ND		+	+				
cC_5H_{12}	0.0	20	ND	+	+	ND		ND		ND	ND	ND	ND	ND	ND	ND	ND
Propylene	2.5 ± 0.8	16	+		+		+			-				+		+	
1-Butene	1.3 ± 0.9	12	+		+		ND		+					+	+	+	+
Trans-2-Butene	0.0	15	+	ND	ND	ND	ND	+	+	ND	ND	ND	ND	+	+	+	+
$(C_2H_4+C_2H_6)/C_2H_2$	4.1 ± 1.3	14	+		-	+					+		+	+	+	+	
CO/C_2H_2	137 ± 45	16	+	ND	-	+					+		-			+	-
Comments																	
Altitude			Low, Stable	Ascent to 2b	Descent from 5b	Descent to 6a	Descent from 8b	Descent from 11b	Ascent to 12b	Stable	Stable	16b	Descent to 18a	Ascent to 18b	Stable	Stable	Stable
O_3						Low					Low	Low	Low				
SO_2											High	High	High				

[a/] Mean concentrations were determined from RTI data.

[b/] + ≡ positive excursion; - ≡ negative excursion; ND ≡ not detected.

[c/] Mean CO as determined by NCAR is 488 ± 31 ppb from 9 samples.

[d/] Mean CH_4 as determined by NCAR is 1770 ± 34 ppb from 9 samples.

[e/] Mean C_2H_2 as determined by WSU is 13.2 ± 3.1 ppb from 16 samples.

[f/] Mean C_2H_4 as determined by WSU is 34.7 ± 6.4 ppb from 17 samples.

[g/] Mean C_2H_6 as determined by WSU is 18.9 ± 1.1 ppb from 12 samples.

In general, no clear associations are evident between the times of the hydrocarbon and altitude excursions. However, increased SO_2, reduced O_3, and HC excursions occurred at 2158, 0126, and 0441 CST.

During the first 13 h of the flight only two HC excursions occurred that were widespread across many species. In the 0919 CST sample, excursions occurred for 7 of 12 species, and 10 of 12 species exhibited excursions in the 1145 CST sample.

The frequency of widespread excursions is substantially greater during the last half of the flight, the nighttime period. Six such excursions occurred during this period at 2158, 0126, 0441, 0535, 0556, and 0603 CST. This is also the interval of the flight during which generally high SO_2 levels were observed. Da Vinci II passed near the industrialized East Alton-Wood River area at approximately 2000 CST. The nighttime hydrocarbon excursions may be associated with various plumes from this area.

In five of the eight cases of widespread hydrocarbon excursions, elevated concentrations of both paraffins and olefins occurred. The remaining three cases displayed excursions of paraffinic hydrocarbons only. Interestingly, both O_3 and SO_2 exhibited excursions at these times. This behavior suggests that the HC excursions that occurred at 2158, 0126, and 0441 CST originated from different sources than those for the remaining widespread excursions.

Excluding excursions, mean methane concentrations of 1.53 and 1.77 ppm were determined by RTI and NCAR. These data are slightly higher than the global background methane concentration of 1.4 ppm.[10] The four excursions in the RTI methane data exceed the background by factors of 4 to 80. These peaks coincide with excursions of ethane and ethylene, propane, and isobutane. The ratios of ethane plus ethylene to methane (~0.01), to propane (~1.0), and to isobutane (~20) for the samples at 2158, 0441, and 0556 CST suggest common HC sources. Acetylene is usually considered to be an ideal tracer of automotive emissions. Because neither methane nor propane are associated with automotive emissions and because no acetylene excursions occurred in these samples, it is unlikely that the sampled air parcels were heavily contaminated by automotive emissions.

The first methane excursion (1145 CST) is associated with the major acetylene excursion. This suggests, at least in this case, that two sources of hydrocarbons contributed to the overall composition of the sampled air parcel.

Propane excursions coincide with excursions for the sum of butanes. This tends to suggest a similar source for both categories of emissions. Excursions of the individual butanes, normal and isobutane, however, do not coincide universally with propane peaks. This suggests at least two sources--both emitting propane, one emitting butane, and the other emitting isobutane.

The alkane hydrocarbon, isopentane, comprises a large fraction of gasoline vapor. Isopentane excursions at 1145 CST may be associated with automotive evaporative losses. The peaks at 0126 and 1441 CST may be associated with evaporative emissions from a petrochemical complex. The largest excursion of isopentane occurred at 1244 CST. No corresponding C_3 or C_4 paraffin peaks were apparent, although CO exhibited a coincident excursion. Implications of this behavior are not clear.

Condensation nuclei data were compared to CO and C_2H_2 data. Theoretically, CN should be indicative of combustion sources; however, the limited data base prevented a time-resolved analysis of both CN and the appropriate HC that might conclusively identify various combustion sources.

The limited data base prevents detailed reconciliation of sources from the HC data. Analysis of emissions from major sources is required to assign fractional contributions of specific sources to each sampled air parcel. In a study of this type, however, it may not be possible to obtain HC data from the major sources. Nevertheless, a major shortcoming of the current data base was the lack of coincident HC samples for comparing concentration behavior with air quality parameters, altitude, and source location. More frequent HC samples should therefore be collected in future studies to provide a more comprehensive data base.

4.3.5.5.3 Trend Analysis

The behavior of a chemical species in the atmosphere is governed by emissions, horizontal advection, dilution due to dispersion and to increased mixing height, and chemical reaction. It is difficult to quantify this information for the flight of Da Vinci II with the current data base. However, trends in hydrocarbon behavior were examined for the following relatively unreactive species: CO, C_2H_2, $C_2H_4 + C_2H_6$, C_3H_8, iC_4H_{10}, nC_4H_{10}, iC_5H_{12}, Freon® 11, and Freon® 12.

Visual inspection of concentration-time profiles for these species suggests that concentrations declined between 1300 and 2100 CST. Linear regression of concentrations with time were performed with the excursions excluded. Predicted concentration changes and r^2 values were determined for each species.

Concentration reductions were indicated for eight of the nine species examined. Declines ranging from 38 to 58 percent were found for the butanes, isopentane, and the Freons.® The r^2 values ranged from 0.42 to 0.67 for these five species. Since this behavior is not expected to occur for both hydrocarbons and Freons® solely from chemical reaction in the atmosphere, dispersion processes may be implicated.

As noted in a previous section, Da Vinci II may have entered a plume at 2100 on 8 June that was enriched in HC and may have remained in HC-rich air for the remainder of the flight. Mean concentrations of the nine species considered above were calculated for two time intervals: 1300-2100 and 2100-0700 CST. Ratios of data for the period after 2100 to that before 2100 were all greater than one. Mean concentrations of ethane plus ethylene and of the Freons® were enhanced by only 2 to 5 percent in comparison to the greater than 20 percent enhancement calculated for the remaining six species. A statistical test with the null hypothesis of no difference between the means was performed for each species. The hypothesis was rejected ($\alpha = 0.05$) for CO, C_2H_2, i-C_4H_{10}, n-C_4H_{10}, and i-C_5H_{12}. This provides strong evidence supporting an earlier contention that Da Vinci II entered an air parcel on the evening of 8 June that was enriched in hydrocarbons.

4.3.6 Air Quality Aloft and at the Ground

4.3.6.1 Sulfur Dioxide

Profiles of hourly average SO_2 concentrations measured on Da Vinci II, on the RTI-EML, and at the RAMS stations nearest Da Vinci II are presented in figure 34. Agreement among these profiles is poor.

Sulfur dioxide concentrations at RAMS sites were low. The daily RAMS network maximum of 0.04 ppm occurred at 1100 CST at station 115, although along the flight track, concentrations measured at RAMS stations were below 0.005 ppm. This is in qualitative agreement with concentration data from Da Vinci II.

It has been noted that the SO_2 monitors employed on Da Vinci II and on the RTI-EML were subject to positive interference by hydrocarbons. The RTI-EML traveled on roadways and sampled air that was contaminated to an undefined extent with vehicular exhaust that was rich in hydrocarbons. The RTI-EML SO_2 data are therefore considered to be somewhat suspect.

The SO_2 monitor aboard Da Vinci II was subject to the same interferences.

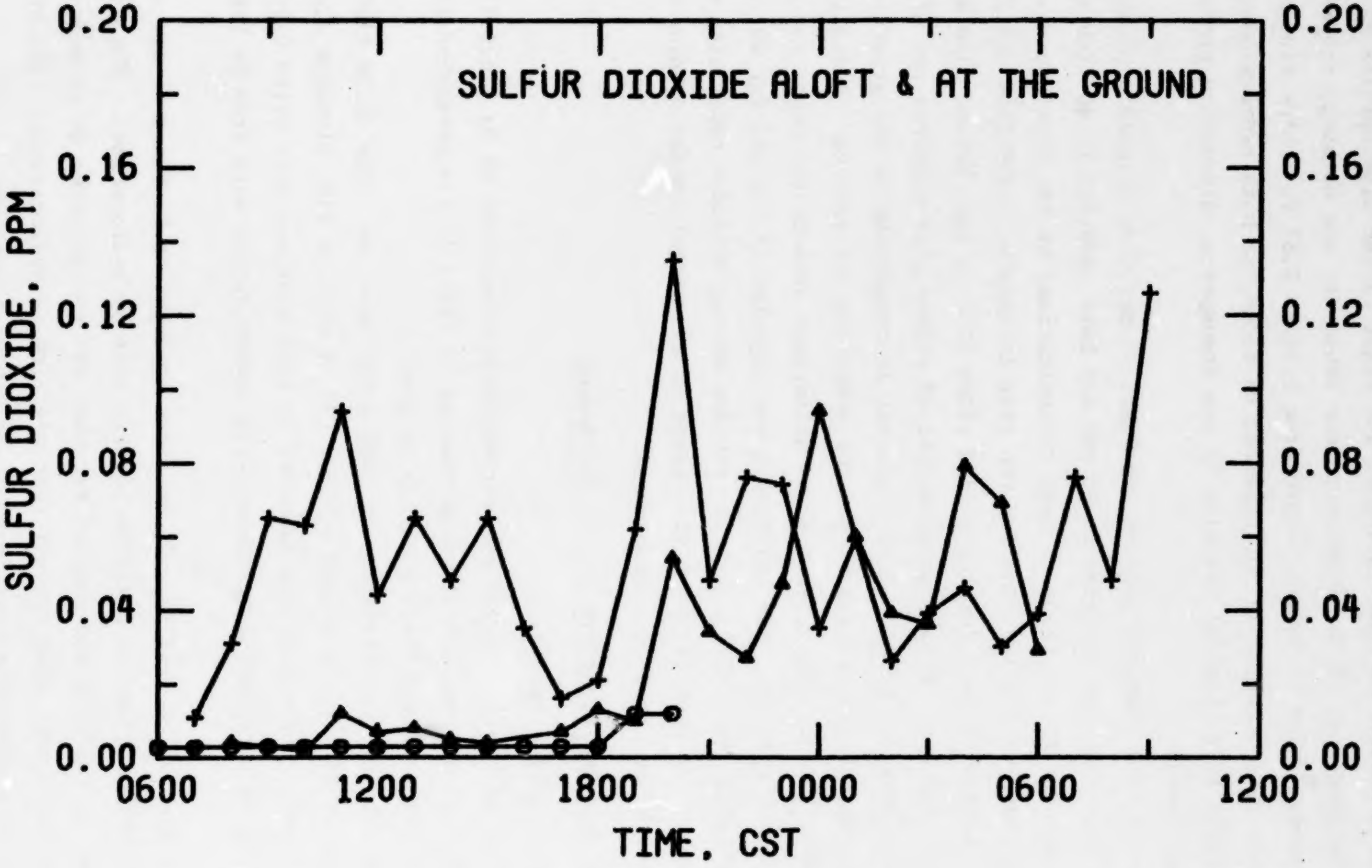

Figure 34. Hourly average sulfur dioxide aloft and at ground level, 8 and 9 June 1976; (Δ) Da Vinci II, (+) RTI-EML, (o) and RAMS.

Analyses of grab samples collected on Da Vinci II, however, have shown the hydrocarbon concentrations aloft to be low. On this basis, the SO_2 profile measured on Da Vinci II is considered to be more reliable than data from the RTI-EML. The SO_2 data collected on Da Vinci II were examined previously and will not be discussed further.

4.3.6.2 Ozone

Profiles of hourly average ozone concentrations measured on Da Vinci II, on the RTI-EML, and at the RAMS stations nearest Da Vinci II are presented in figure 35. As noted previously, the RTI-EML data and the interpolations from isopleths of RAMS data are in good agreement.

Early morning ozone concentrations aloft on Da Vinci II were greater than those at the ground. This is presumably due to reduced concentrations of O_3-destructive agents above the nocturnal radiation inversion. It should be noted that O_3 levels at the RTI-EML and the westernmost RAMS stations, while reduced in comparison to levels aloft, were significantly higher than levels in downtown St. Louis. This reflects the differences in concentrations of O_3-destructive agents in nonurban and urban air beneath the nocturnal radiation inversion.

As the surface-based nocturnal inversion was destroyed, ground-level ozone concentrations approached those aloft. Concentrations at these two locations became almost indistinguishable by the 1100 CST hour. This is also illustrated by the adjusted vertical ozone profiles in figure 25. The stratification that was apparent in the 0915 CST profile had disappeared by the time the 1148 CST vertical flight was conducted.

Sunrise occurred at 0436 CST on 8 June. Temperature gradient data suggest that the inversion breakup began to occur through the first 30 m (100 ft) during the 0600 CST hour. According to acoustic sounder records, the inversion was destroyed by 0920 CST. The ozone profiles in figure 35 suggest that well-mixed conditions prevailed from the 1100 to the 1700 CST hour. The 1100-1500 CST mean concentration on Da Vinci II of 0.121 ± 0.018 ppm is in excellent agreement with the corresponding 0.123 ± 0.005 ppm from the RTI-EML.

Based on the RTI-EML ozone data, the first indication of the reestablishment of two ozone regimes occurred during the 1800 CST hour. On 8 June, sunset occurred at approximately 1924 CST, and temperature gradient data show the first indications of the formation of the radiation inversion during the 1800 CST hour. Acoustic sounder data show similar behavior during the 1800 CST hour.

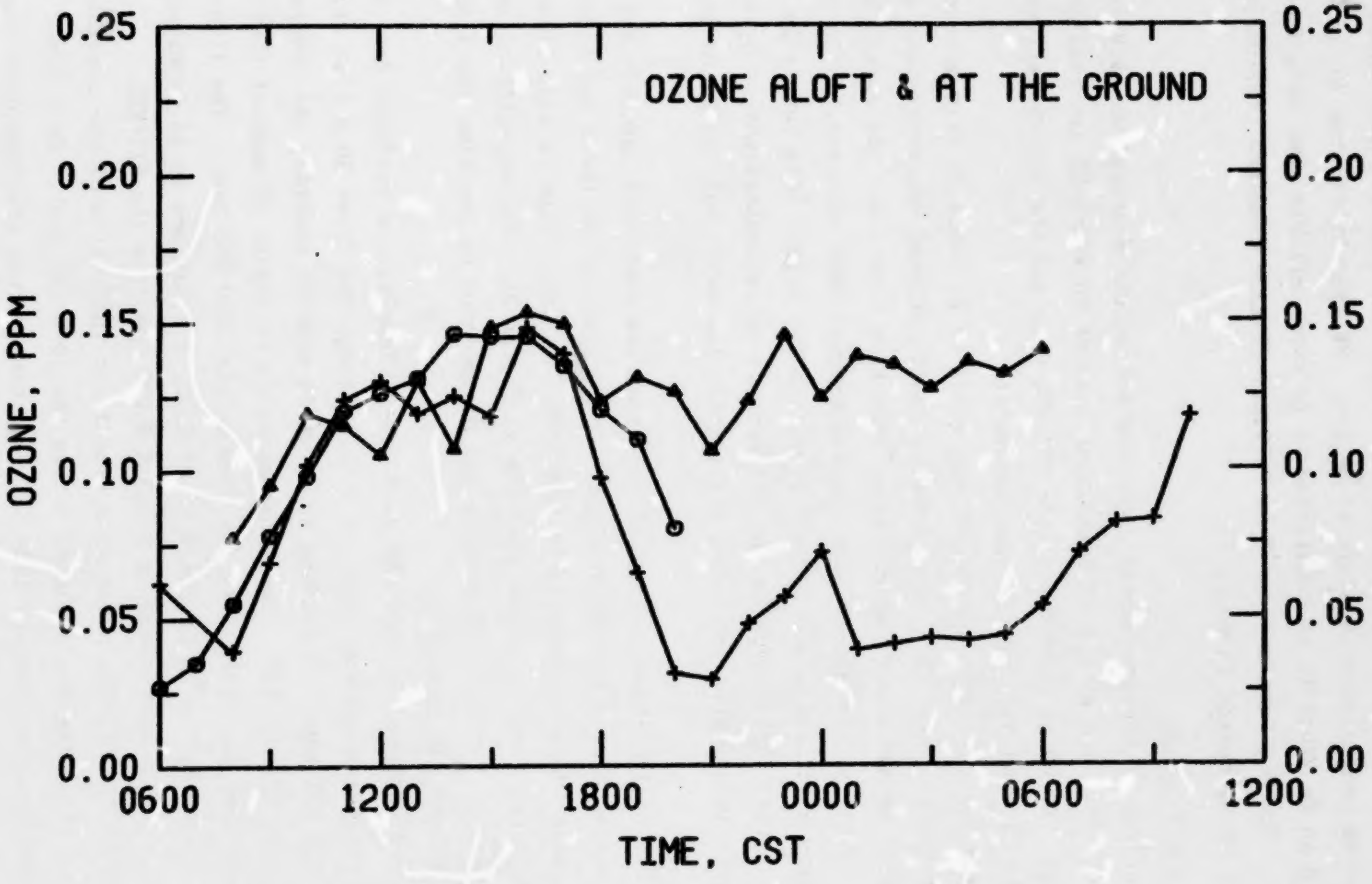

Figure 35. Hourly average ozone aloft and at ground level, 8 and 9 June 1976; (Δ) Da Vinci II, (+) RTI-EML, (o) and RAMS.

At the 1900 CST hour and throughout the night, the Da Vinci II and RTI-EML data clearly demonstrate existence of two regimes of ozone. Aloft, ozone remains insulated from ground-based destructive agents, and the concentration remains relatively constant except for periodic encounters with industrial plumes. Beneath the inversion, ozone concentrations are reduced both by surface deposition and by chemical reaction with destructive agents emitted from local sources that are trapped within this layer. The relative importance of these two mechanisms remains to be defined.

Just prior to midnight, the inversion was penetrated as a result of mechanical turbulence, which brought air containing high concentrations of ozone down to the surface. The simultaneous reduction in ozone concentration aloft was coincident with SO_2 excursions and hence the associated, but unmeasured, NO_x excursions that accompany SO_2 in power plant plumes. The extent that upward mixing of ozone-deficient air from the surface perturbed concentrations aloft at the 762-m (2,500-ft) level remains to be determined.

Sunrise occurred at approximately 0427 CST on 9 June. This correlates with the increase in ground-level ozone measured on the RTI-EML during the 0600 CST hour. Similar behavior is noted in figures 12 and 35 on 8 June at RAMS stations. This increase in ozone is presumably due both to mixing of high concentrations of ozone to the surface from aloft during the dissipation of the nocturnal radiation inversion and to photochemical synthesis.

Ozone concentrations at the RTI-EML increased on the morning of 9 June as if to converge with O_3 levels aloft as measured on Da Vinci II. On the basis of the O_3 behavior on 8 June in St. Louis, convergence is expected on the morning of 9 June with the establishment of well-mixed conditions. Termination of the experiment prevented an assessment of this hypothesis.

On the afternoon after Da Vinci II had landed, additional ozone measurements were conducted aloft by ICFAR. Ozone concentrations measured at 457 m (1,500 ft) AGL from 225 km northeast to 290 km southwest of Indianapolis are presented in figure 36. Between 1527 and 1656 CST on 9 June, ozone concentrations aloft ranged between 0.14 and 0.19 ppm. These data coupled with those from Da Vinci II, the NOAA aircraft, RAMS stations, and ground stations in the northeastern quadrant of the country provide strong evidence for the existence of high regional-scale concentrations of ozone aloft during the period encompassing the Da Vinci II experiment.

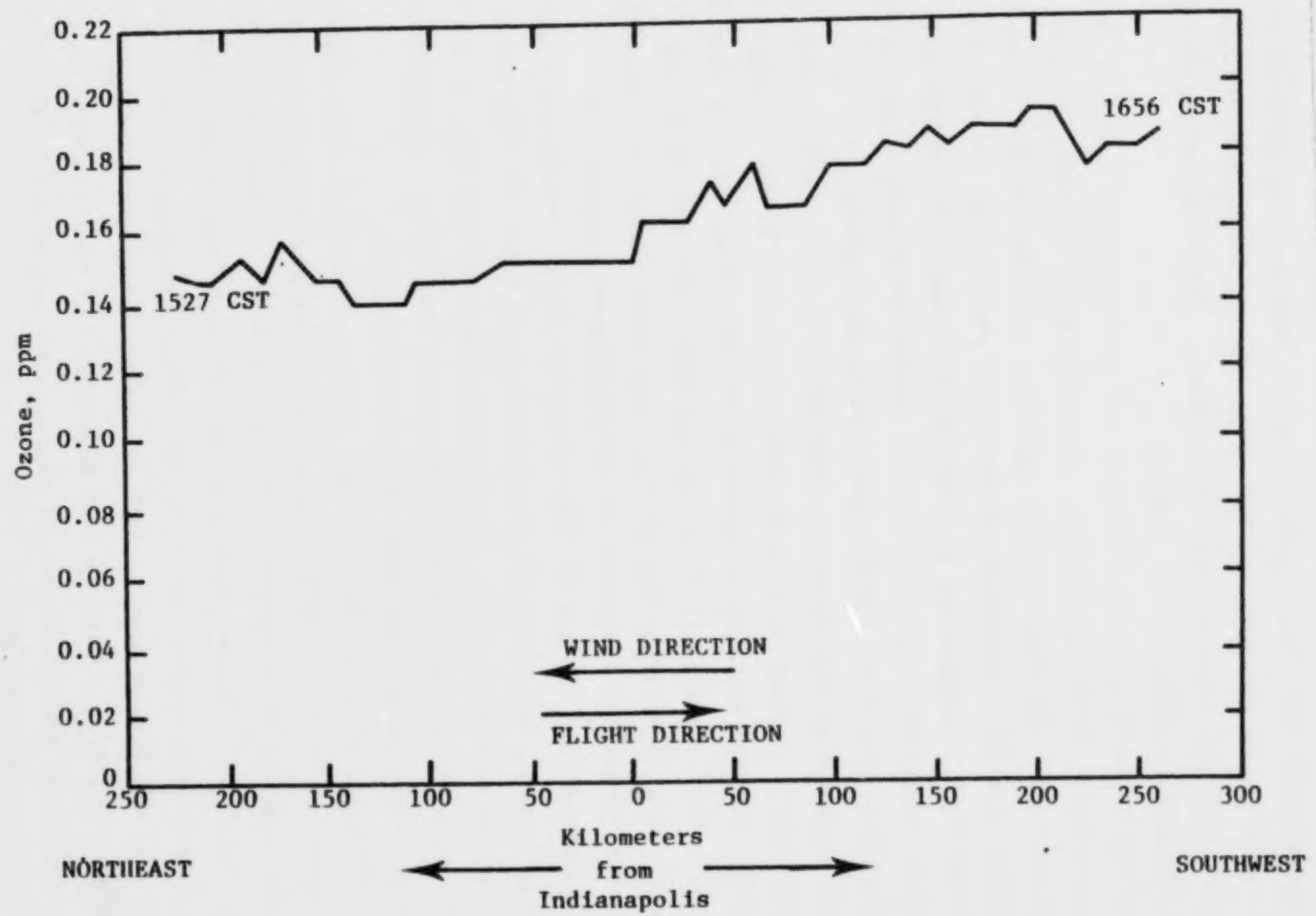

Figure 36. Ozone upwind and downwind of Indianapolis at an altitude of 457 m (1,500 ft) above ground on 9 June 1976 as measured on the ICFAR aircraft.

4.3.6.2.1 Transported Ozone

Evidence for the regional-scale existence of high concentrations of ozone aloft during the study period have been presented. The mean of the 1100-1500 CST hourly average ozone concentrations at an upwind site was used as an estimate of ozone transported into the study area. The 1100 to 1500 CST interval is considered because it occurs during the portion of the day when the boundary layer is well mixed, and it occurs late enough in the day for synthesis of ozone from transported precursors to have occurred as well.

On 8 June the winds were generally from the west. RAMS station 125 is the westernmost site. The mean of the 1100-1500 CST hourly average ozone concentrations at this site was 0.108 ± 0.007 ppm. Thus, a considerable amount of ozone, approximately 0.108 ppm, was transported into St. Louis on flight day.

The mean of the 1100-1500 CST hourly average ozone concentrations observed on Da Vinci II was 0.121 ± 0.018 ppm. This is only slightly higher than the 0.108 ppm transported into the area. The maximum mean 1100-1500 CST ground level ozone concentration within the RAMS network was 0.177 ppm. Comparison of these data (also see figure 17a) suggests that the balloon was not in the center of the urban plume as defined by ozone concentrations.

4.3.6.2.2 Ozone Synthesis

During the morning, ground-level ozone concentrations were less than concentrations aloft. The observed increase of ozone concentrations aloft, therefore, could not have resulted from upward mixing of ozone from the ground, but was probably due to photochemical synthesis aloft.

The magnitude of synthesis aloft on 8 June is estimated to have been 0.058 ppm. This estimate is based on the difference between the 0900 CST and the daily maximum hourly average measured on Da Vinci II.

A net increase of 0.020 ppm has been noted on Da Vinci II between the 0900 and 1100 CST hourly average ozone concentrations. Between 0915 and 1148 CST, net increases ranging from 0.020 to 0.032 ppm have been found based on averaged ozone data collected between 762 and 1,981 m (2,500-6,500 ft) MSL on the NOAA aircraft. During this same period, ozone levels at the RTI-EML and RAMS sites nearest the flight track increased by 0.042 and 0.056 ppm. Thus, the net increase of ozone at the ground was approximately twice the net increase that occurred aloft.

Well-mixed conditions prevailed from noon until some time in the afternoon. During this period, synthesis is presumed to be a major contributor to increases in the observed ozone level. On Da Vinci II, the ozone increase between the 1100 CST hour and the daily maximum value was 0.038 ppm. The corresponding increases at the nearest RAMS station and at the RTI-EML were 0.026 and 0.024 ppm. These results suggest that between noon and the end of the day, a net amount of approximately 0.030 ppm of ozone was synthesized along the flight track.

Based on ozone isopleths drawn from RAMS data and presented in figure 19, the buildup and movement of an ozone "hot spot" was documented for 8 June and was attributed to precursors released in the St. Louis urban area. A specific source was not identified.

4.3.7 Considerations for Future Programs

The current study was successful at consolidating data collected by many separate investigators and at providing a cohesive interpretation of the results. During the data analysis effort, however, several points became apparent that should be considered in future programs of this type.

1. The limited area encompassed by the RAPS monitoring network in comparison to the scale of air movement that can occur during a 1-day period prevented detailed definition of the St. Louis urban plume. A comprehensive measurement program conducted on an aircraft in support of future balloon-borne experiments could fill this gap by defining the vertical and aerial extent of the urban plume, the influence of major sources on that plume, and the maximum ozone concentration within the plume. The lack of such an effort hampered the data analysis effort in the current study.
2. Nitrogen oxides are ozone precursors and are instrumental in atmospheric photooxidation processes. They are also emitted by both automotive and industrial sources. In future studies, balloon-borne measurements of NO_x could enhance the quality of the data base by permitting assessment of the impact of ground-based automotive sources or industrial plumes on NO_x concentrations aloft.
3. The atmosphere behaves in a dynamic fashion. The behavior of atmospheric chemical species is also highly variable. Continuous measurement of such species as O_3, NO_x, SO_2, and CN as well as frequent CO and HC sampling are desirable.
4. Detailed RAPS emissions inventory data were not available in the current study. High-quality data of this type are needed to relate ambient concentrations of chemical species to their emission rates.
5. An assessment of the degree to which a balloon behaves as an ideal Lagrangian marker is important. Relative air velocity data should be examined in future studies to permit this evaluation.

4.4 Findings

The following observations have been drawn from the atmospheric chemistry analysis:

1. Conditions of elevated ozone concentrations persisted aloft for the study period. These conditions were widespread and extended for several hundred kilometers.
2. Ozone and water vapor concentrations determined in vertical aircraft flights do not suggest that stratospheric intrusion was responsible for the elevated ozone concentrations that existed aloft on 8 June.
3. Air containing high concentrations of ozone, approximately 0.11 ppm, was transported into the study area on the flight day.
4. Da Vinci II was launched into air that had an immediate history in nonurban environs, although the total experiment was conducted within a stagnant, polluted, high pressure system.
5. Da Vinci II did not travel in the heart of the St. Louis urban plume as defined by ozone concentrations. Examination of the hydrocarbon concentrations sampled on the balloon suggests that the flight occurred in air characteristic of suburban-to-nonurban areas.
6. During the morning, ground-level ozone concentrations were less than concentrations aloft. The observed increase of ozone concentrations aloft, therefore, could not have resulted from upward mixing of ozone from the ground, but was probably due to photochemical synthesis.
7. The impact of anthropogenic emissions on ambient concentrations within the urban area is variable and depends strongly on the time of day. Ground-level CO and NO_x were diluted by factors of 5 to 9 between morning and afternoon. This behavior reflects the significant increase in the mixed volume that occurs with the dissipation of the surface-based radiation inversion and the establishment of well-mixed conditions.
8. As vertically well-mixed conditions were established during the morning, both downward mixing and photochemical synthesis contributed to the observed net increase in ground-level ozone concentration. The ground-level net increase was approximately twice that aloft.
9. Between the 1100 and 1700 CST hours on flight day, a near zero ozone concentration gradient existed from the ground into the mixed layer. This is, to a large extent, based on the close comparison of ozone measurements determined on the balloon with those beneath the balloon at ground level.
10. After well-mixed conditions were established and until they began to dissipate, the increase in ozone concentrations aloft and at ground level were approximately equal and probably resulted from photochemical synthesis.
11. The stratification of the daytime mixed layer that occurred at night with the establishment of the nocturnal radiation inversion resulted in the formation of two regimes of ozone concentrations.

12. Ozone concentrations beneath the radiation inversion were much reduced compared to levels above it. This is presumably due to destruction by surface deposition and reaction with ozone-destructive agents trapped beneath the inversion.

13. The dark-phase stability of ozone at the Da Vinci II level above the nocturnal surface-based radiation inversion suggests that transport of ozone can occur aloft over long distances at night without significant diminishment. It is possible for the ozone to be transported overnight several hundred kilometers and be mixed to the ground on the next day with a significant impact on ground-level air quality.

14. Penetration of the nocturnal radiation inversion occurred frequently during May and June of 1976 and resulted in the mixing of high levels of ozone to the ground and of precursors from the ground to aloft. This was suggested by the sharp nighttime ozone peaks and the associated declines of NO_x and CO observed at selected ground stations. This phenomenon was widespread and occurred over several hundred kilometers. It may also provide mechanisms for increasing nighttime ozone destruction aloft and for enhancing early morning ozone synthesis by distributing ozone precursors aloft above the inversion before sunrise.

15. The balloon may have entered an air parcel that was enriched in hydrocarbons after 2100 CST on 8 June and traveled within this parcel for the remainder of the flight.

16. Sharp reductions in ozone concentrations that occurred during the nighttime portion of the flight were associated with increases in SO_2 concentration. Both SO_2 and NO_x are emitted by power plants and petroleum refineries. Although NO_x was not measured in this study, the observed ozone behavior is probably the result of destruction by reaction with NO_x.

17. The influence of ozone precursors emitted in the urban area were manifest at ground-level by ozone concentrations enhanced over non-urban concentrations. The net magnitude of this enhancement was 0.06 to 0.11 ppm. Both the buildup and movement of the region of enhanced ozone were documented, although detailed definition of the extent and magnitude were severely hampered by the lack of a comprehensive supporting measurement program conducted on an aircraft.

18. The feasibility of balloon-borne experiments for obtaining the data needed to address atmospheric chemistry problems has been demonstrated. However, this study has also shown that detailed interpretation of the results from such a study requires data from several complementary platforms: the Lagrangian marker, a ground-level chase vehicle, a network of ground stations, and a chase aircraft. The omission of any one of these facets severely limits the interpretation effort.

5.0 MESOMETEOROLOGICAL AND AIR POLLUTION STUDY RELATIVE TO DA VINCI II

5.1 Introduction

The objective of section 5.0 is to characterize the three-dimensional meteorological and air pollution distribution on 8 June 1976 in St. Louis, during the period Da Vinci II was in close proximity to the city. For the study, ozone was used as the primary trace gas for air pollution. Upper level (but in the boundary layer) concentrations of ozone were obtained by the Da Vinci II system, which was launched at 0756 CST on 8 June from the Arrowhead Airport, some 24 km west of St. Louis. In the period 0756 to 2100 CST, the balloon drifted in and around the immediate vicinity of St. Louis.

In the period of interest, the meteorology in St. Louis was dominated by a strong, daytime heat island circulation. It is normally considered that the most intense urban heat island circulation should be found when the urban heat island is most intense. Past evidence as well as current evidence shows that the urban heat island is generally most intense at night.[11] Past data have also shown that at times the urban heat island persists during the day, particularly in the winter, which is believed to be due to anthropogenic heating. Previously, there has only been scattered evidence that a daytime heat island persists in the summertime.

If the heat island exists during the day, there is the potential to produce a stronger heat island circulation than during the night. During the daytime period, the boundary layer is generally characterized, particularly in the summertime, by a deep adiabatic or superadiabatic layer. The presence of this layer will allow heating from the urban surface to be mixed through a deeper layer. From basic hydrostatics, it can be shown that if the heating is distributed through a deeper layer, a greater pressure perturbation will be produced at the surface over the city. This will lead to greater horizontal and vertical accelerations. The general motion associated with the urban heat island circulation is complex[12] and may have a marked effect on the air pollution distribution in and around the city.

One of the purposes of the Da Vinci II system was to characterize the time history of air pollution in the urban plume as it moved downstream from St. Louis. However, due to synoptic and local flow characteristics, the balloon drifted around the city for approximately 13 h yielding a unique opportunity to determine three-dimensional structure of air pollution where a marked heat island circulation existed. Following are the results of the data analyses.

5.2 Data Sources

One of the basic sources of data for this analysis was the Regional Air Pollution Study (RAPS). The location of RAPS surface and upper air stations operating on 8 June are shown in figure 37. Five of the RAPS stations are not shown in the figure because they were outside of the region of immediate interest. However, these stations were used in the analysis of data.

For the analysis, hourly averaged temperature, winds, and ozone concentrations from the RAPS surface stations were used for the period 0300 CST, 8 June, to 0500 CST, 9 June. The surface wind data were used as input for an objective analysis algorithm, which produced an interpolated wind speed field on a 4-km by 4-km grid over the area of interest. The radiosonde data provided vertical profiles of potential temperature, wind speed, and wind direction for 0345 CST, 0945 CST, 1545 CST, and 2145 CST at two upper air stations. One of the upper air stations is located in downtown St. Louis and the other in the rural region to the west (figure 37).

The principal source of ozone data aloft was the Da Vinci II system. The Da Vinci II system made a variety of environmental and gas chemistry measurements; however, of particular importance to this study were the ozone measurements.

Surface ozone concentrations were also obtained by the RTI-EML. The RTI-EML followed the track of Da Vinci II as closely as possible from takeoff to landing (figure 38) making a number of environmental measurements. Only the ozone measurements were used in this study. A detailed description of the Da Vinci II system and the RTI-EML is given in section 3.0.

The ozone data from the Da Vinci II system and the RTI-EML were obtained in the period 0756 CST, 8 June, to 1000 CST, 9 June 1977. However, for this study, only the data for the period 0800 CST, 8 June, to 0600 CST, 9 June, were used. Between 0756 and 2100 CST, 8 June, the Da Vinci II system and the RTI-EML were in the immediate vicinity of St. Louis, Missouri.

5.3 Surface Temperature Distribution

Hourly surface temperature from twenty-five RAPS stations were used to delineate the St. Louis urban heat island on 8 June. Figure 39 represents the diurnal variation of the temperature difference between the urban and rural

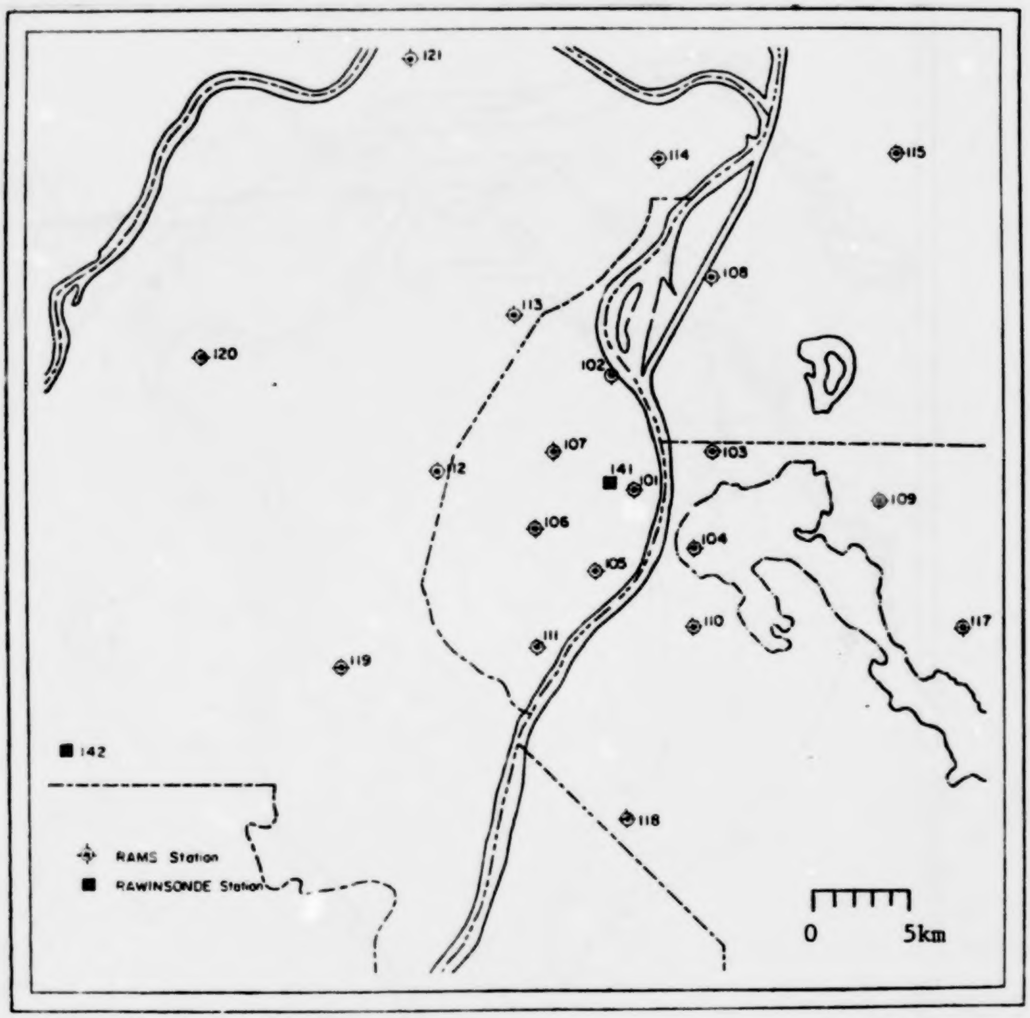
121
114
115
108
113
120
102
107
103
141
101
112
109
106
104
105
110
117
111
119
142
118
RAMS Station
RAWINSONDE Station
0
5km

Figure 37. The area of immediate interest around St. Louis showing the locations of the RAPS stations and the two upper air sounding stations.

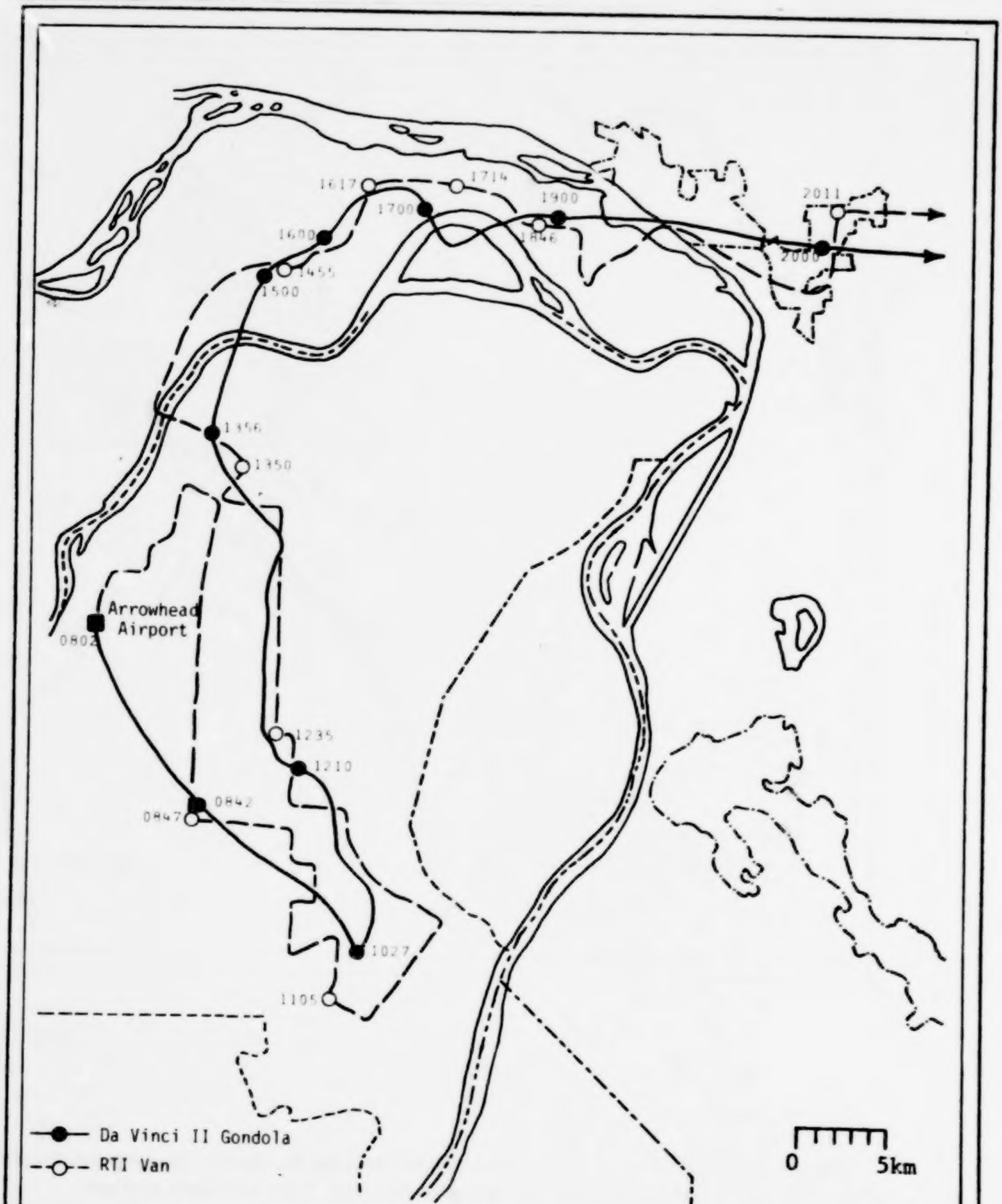
1617
1714
1700
1900
2011
1600
1455
1500
1846
2000
1356
1350
Arrowhead Airport
0802
1235
1210
0842
0847
1027
1105
Da Vinci II Gondola
RTI Van
0
5km

Figure 38. The ground track of the Da Vinci II gondola and the track of the RTI-EML from lift-off at Arrowhead Airport through 2000 CST. The RTI-EML maintained visual contact with the gondola for the entire mission.

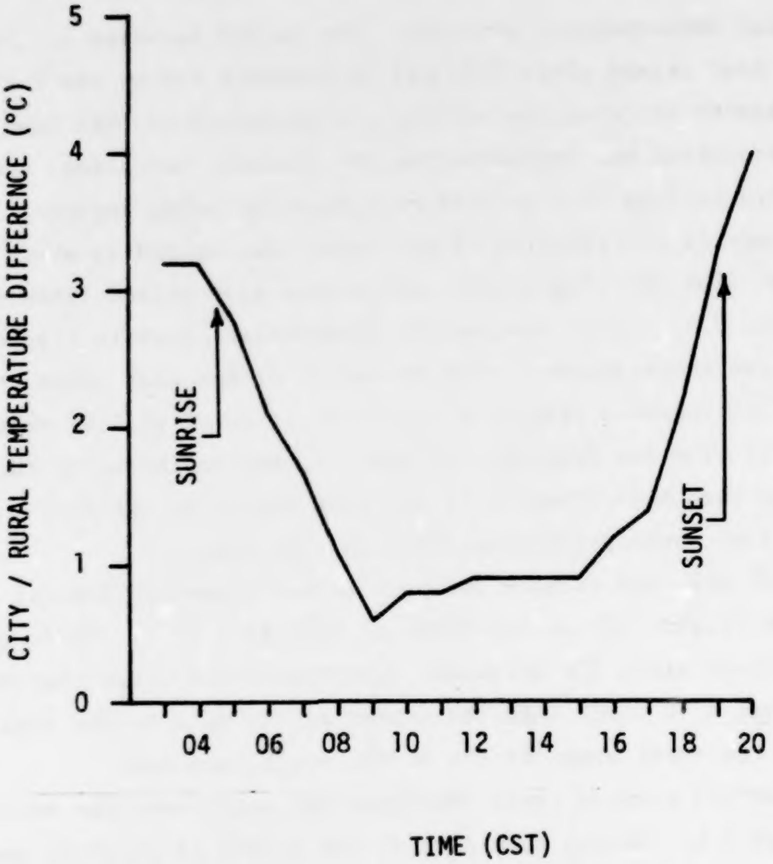

Figure 39. Tne hourly temperature difference between the St. Louis center city and the rural/suburban area some 15 mi away.

region for the period 0300 to 2000 CST on the 8th of June. Temperature at the surface in the urban region was represented by the average of four RAPS stations in the center of the city (stations 101, 105, 106, and 107). The rural surface temperature was represented by the average, using data from stations 117, 118, 119, and 120. The diurnal variation is typical of that found by other investigators.[11,13]

The data show that at 0300 and 0400 CST, the heat island intensity (measured by the urban-rural temperatures difference) was, on the average, slightly more than 3° C. By 0500 CST, warming began and the magnitude of the urban heat island intensity began to decrease (sunrise occurred at 0445 CST). The heat island existed throughout the daytime period, reaching a minimum at 0900 CST of approximately 0.6° C. Afterwards, it increased somewhat, probably due to increased anthropogenic activity. The marked increase in the intensity of the urban heat island after 1500 CST is probably due to the fact that the solar intensity reaching the surface had decreased at this time, the infrared outgoing radiation was overbalancing the incoming radiation, and the rural regions were cooling at a greater rate than the urban regions.

The spatial distribution of the urban heat island is shown in figures 40 and 41. At 0500 CST (figure 40), the actual heat island intensity was somewhat greater than 3.5° C (the heat island intensities shown in figure 39 are based upon averaged temperatures). The extension of the heat island to the north is not to be considered a result of advection since it will be shown that the flow at this time was from the northwest to the southeast at the surface. It is believed that the extension of the heat island to the north was due in part to intensified anthropogenic activity in that region.

At 0900 CST, the surface analysis showed a weak horizontal contrast in temperature (figure 40) on the order of 1.5° to 2.0° C. There was a region of low temperature along the northwest boundary of the urban complex, which was slightly over 1° C lower than the center of the city to the east and 0.5° C lower than the rural areas to the north, south, and west.

The surface warming trend continued uniformly over the entire study area for the next 5 h. During this period, the pocket of slightly lower surface temperature along the western edge of the urban complex remained identifiable although it was never more than 0.5° C lower than the surrounding rural regions. During the early afternoon, the center of the urban heat island shifted back and forth between RAPS station 107 (approximately the geographic center of the St. Louis downtown area) and station 105 (some 6 km to the south southeast near the west bank of the Mississippi River). It was located at station 107 at 1000 CST to 1100 CST, but shifted to station 105 for the next 3 h. It then shifted back to station 107 at 1400 CST when the highest surface temperature of the day (30.2° C) was recorded (figure 40). At 1400 CST, the horizontal contrast in temperature had increased somewhat but not to a great extent. The cooler area to the northwest was still evident.

From about 0800 to approximately 1600 CST, the area east of the river and to the northeast of the center of the city remained warmer than the suburban areas to the north, west, south, and southeast of the city. Stations 103, 108, 109, and 115 consistently recorded temperatures within a few tenths of a degree of the temperatures found in the center of the city and nearly a degree

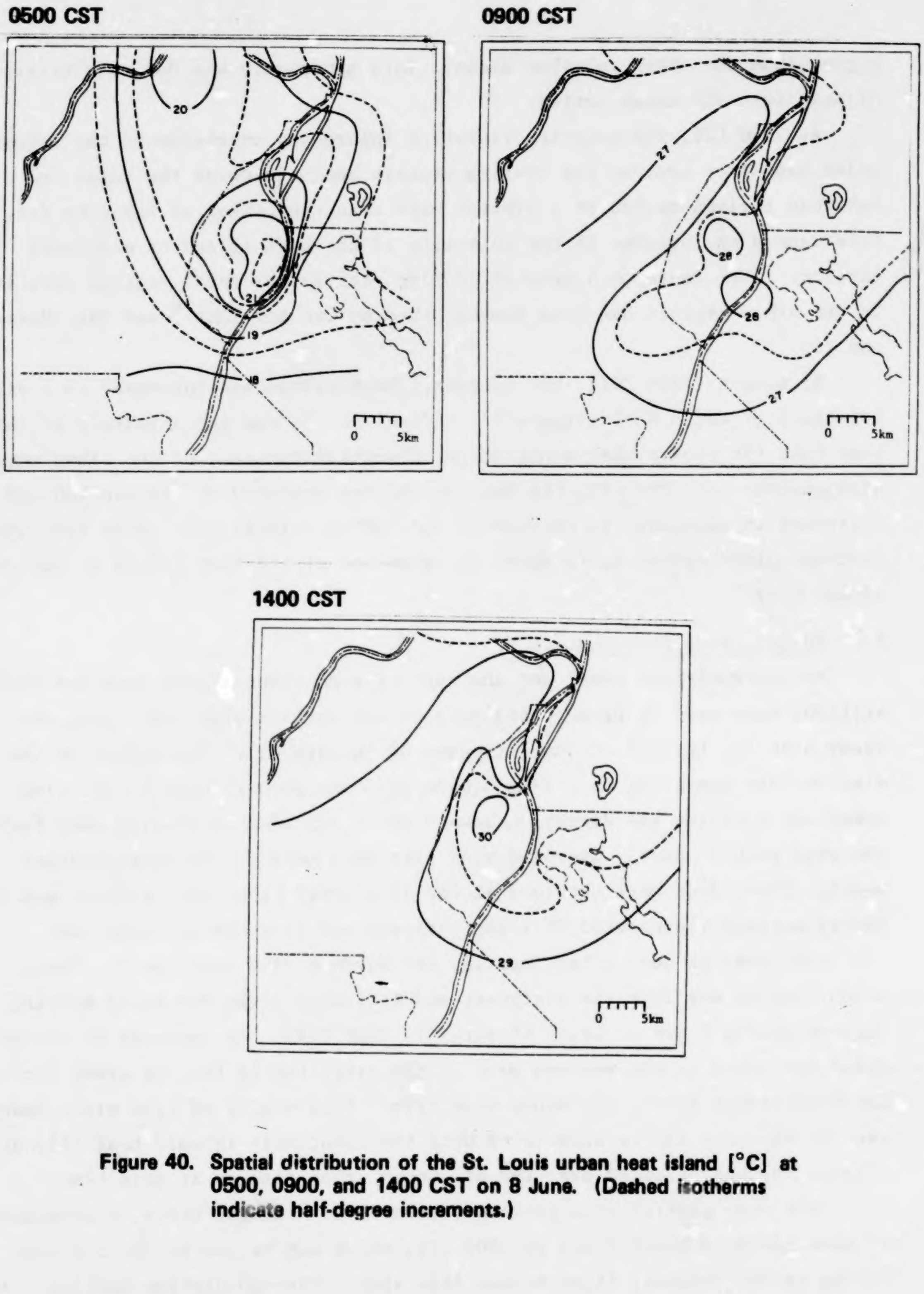
0500 CST
20
21
19
18
0
5km
0900 CST
27
28
28
27
0
5km
1400 CST
30
29
0
5km

Figure 40. Spatial distribution of the St. Louis urban heat island [°C] at 0500, 0900, and 1400 CST on 8 June. (Dashed isotherms indicate half-degree increments.)

higher than the other suburban areas. This apparently was due to a transport of heat from the urban center.

At 1500 CST, the outgoing radiation apparently overbalanced the incoming solar radiation because the cooling process began in which the rural and suburban regions cooled at a greater rate than the center of the city did. This caused an increase in the intensity of the heat island as mentioned earlier. That there is a greater cooling rate in the rural regions relative to the urban regions has been demonstrated by Oke and East[14] and Oke, Maxwell, and Yap.[15]

By sunset (1900 CST), the intensity heat island had increased to a value between 2.5° and 3.0° C (figure 41, 1800 CST). It was approximately at this time that the cool pocket along the northwestern boundary of the urban complex disappeared. At 2000 CST, the heat island was centered at station 105 and had increased in intensity to between 5° and 5.5° C (figure 41). Note that the isotherm distribution again shows an extension of the heat island to the north of the city.

5.4 Surface Wind Distribution

An interpolation model and the surface wind observations from the RAPS stations were used to produce analyses of the surface wind field over the study area for the 8th of June (figures 42 through 43). The length of the wind vectors appearing on a 4-km square grid are proportional to the wind speed and indicate the direction toward which the wind is blowing away from the grid point. Hourly averaged wind data were used in the interpolation model. These data were obtained at the 10-m level above the surface, and the hourly average represented 60 1-min observations from the previous hour.

Just over an hour after sunrise, the surface flow over the St. Louis urban complex was from the northwest and typically light for early morning (approximately 1 m/s or less) (figure 42, 0500 CST). An increase of the wind speed was noted in the western part of the city; but in the low areas east of the Mississippi River, the winds were calm. This region of calm winds downwind of the city may be associated with the relatively intense heat island (figure 40) that existed over the St. Louis urban complex at this time.

This same general flow pattern continued for several hours, strengthening in wind speed to about 3 m/s by 0800 CST, which may be due to the increase in mixing as the boundary layer became less stable through daytime heating. As

1800 CST

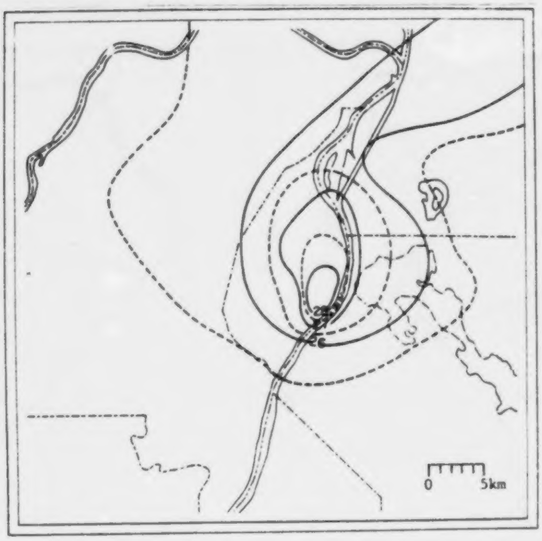

2000 CST

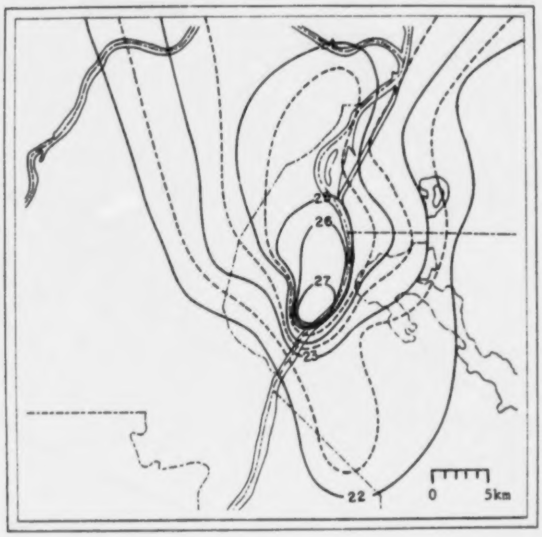
28
26
27
23
22
0
5km

Figure 41. Spatial distribution of the St. Louis urban heat island [°C] at 1800 and 2000 CST on 8 June. (Dashed isotherms indicate half-degree increments.)

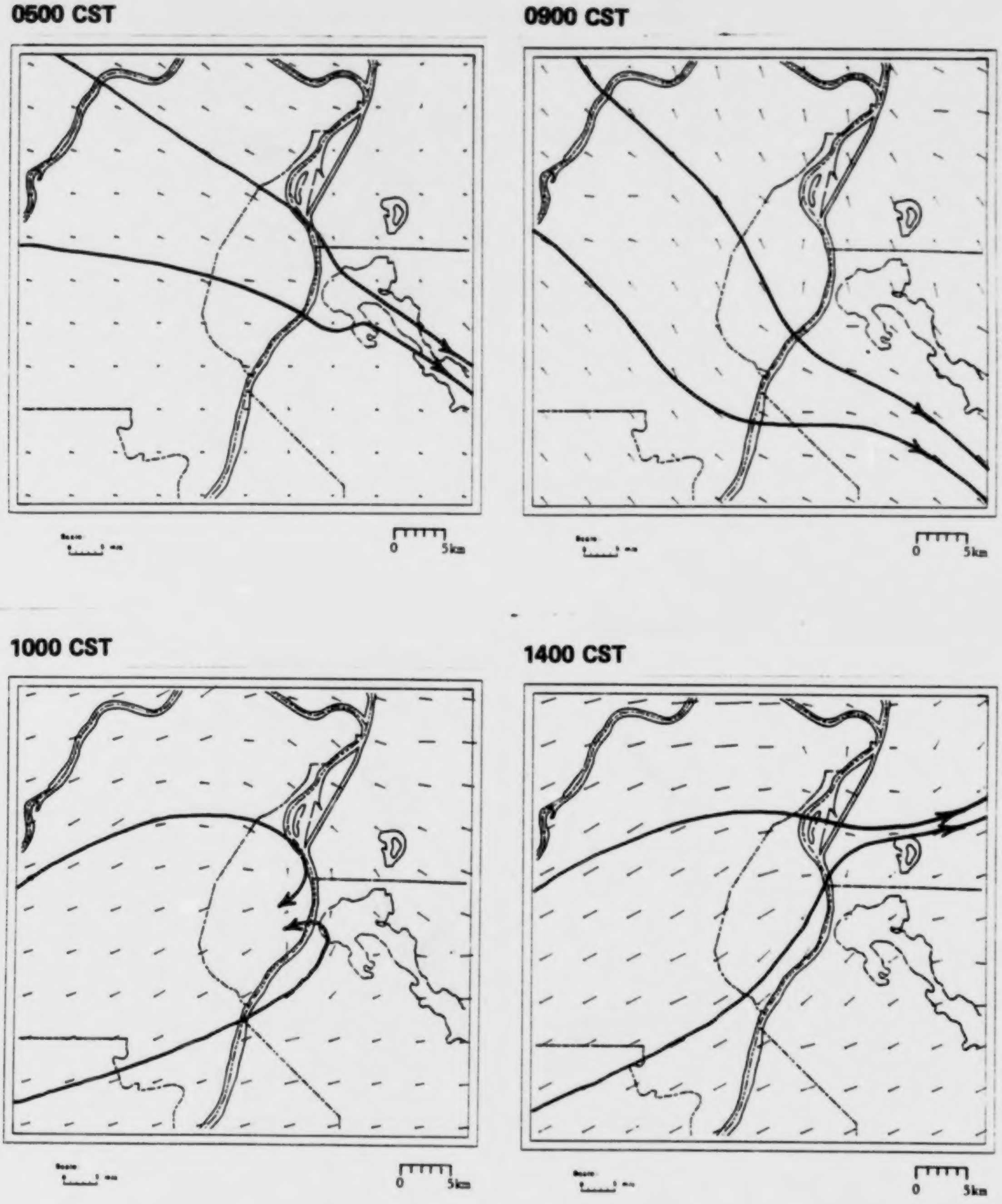
0500 CST
0900 CST
1000 CST
1400 CST
0
5km

Figure 42. Interpolated surface wind field [m/s] at 0500, 0900, 1000, and 1400 CST on 8 June. Vectors are proportional in length to wind speed and extend from the grid point in the direction of the flow.

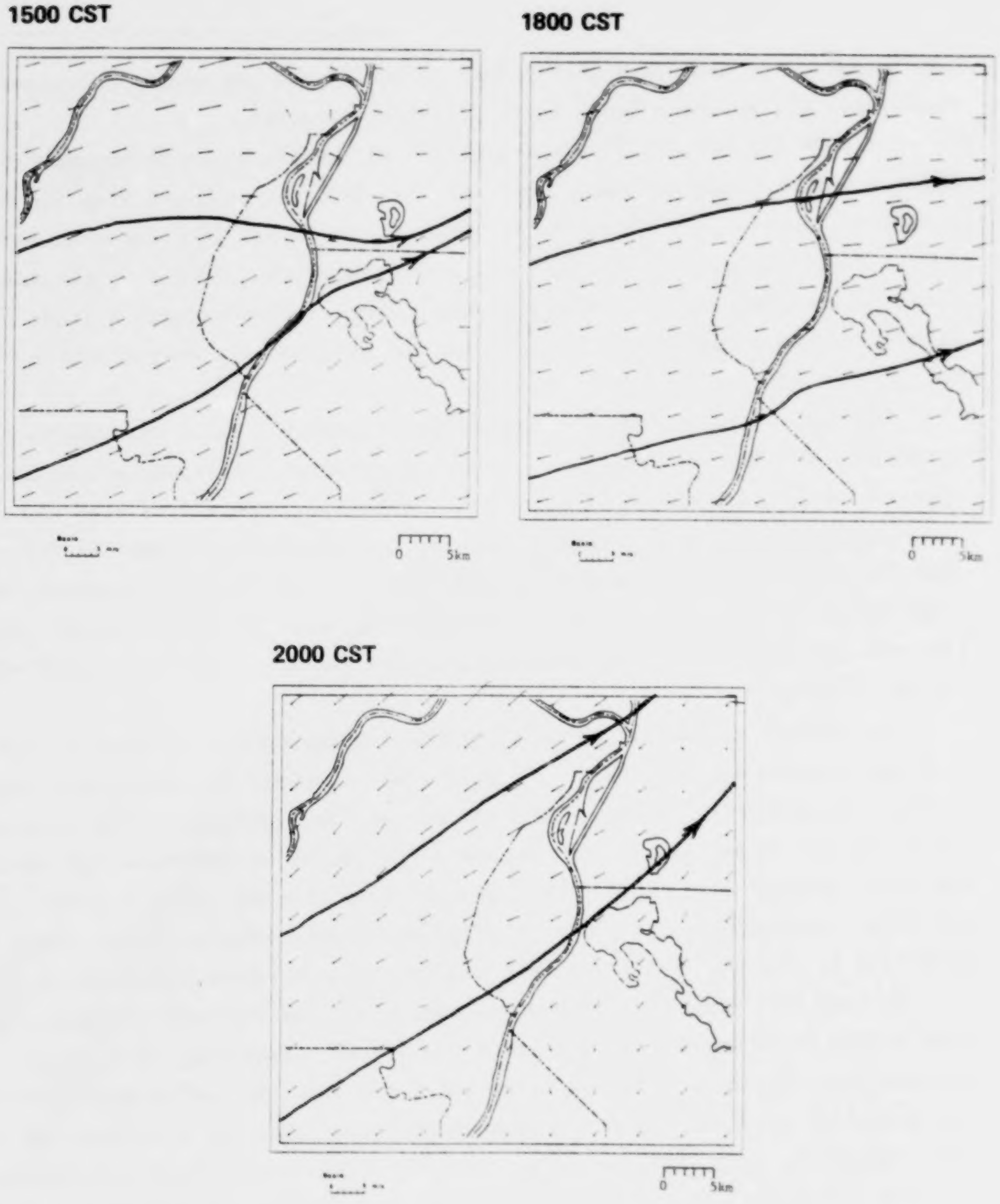
1500 CST
1800 CST
2000 CST
0
5km

Figure 43. Interpolated surface wind field [m/s] at 1500, 1800, and 2000 CST on 8 June. Vectors are proportional in length to wind speed and extend from the grid point in the direction of the flow.

the intensity of the urban heat island decreased and the mixing increased, measurable air movement began in the low-lying regions.

At 0900 CST (figure 42), a transition in the direction of the surface mesoscale flow began to take place. At 0800 CST, the wind was from the west northwest; however, by 1000 CST, the wind direction was from the west southwest. This factor, combined with the influence of the effects on the momentum field by the urban heat island, produced a complex flow pattern varying in direction from northerly to the north of the city and westerly to the south of the city at 0900 CST.

The wind field at 1000 CST (figure 42) showed the first convergence effects of the daytime urban heat island circulation. A region of inflow was apparent over and downwind of the city. This flow pattern persisted and at 1400 CST (figure 42) the center of convergence was north and east of its 1000 CST position. Note in both the 1000 CST and the 1400 CST analyses, the winds north of the city were more westerly than those to the south and west. This was probably due to the pressure gradient accelerations associated with the heat island.

The intense effect of the heat island circulation persisted to at least 1600 CST (figure 43, 1500 CST). At that time, the zone of convergence began to weaken considerably. The time 1500 CST marked the beginning of the intensification of the urban heat island through differential cooling when the suburban and rural regions were cooling at a greater rate than the urban region. Low-level cooling suggests the initiation of a surface-based stable layer. Stability in the boundary layer will weaken the heat island circulation.[16,17]

By 1700 CST, when the effects of surface cooling were more evident, the heat island circulation had diminished considerably resulting in a fairly uniform west-southwesterly flow of around 3 m/s over the entire area. There was a zone of weak convergence evident downwind of the city's center. By 1900 CST (figure 43, 1800 CST), no evidence of the urban heat island circulation could be determined in the flow even though the heat island intensity had increased markedly by this time (figures 39 and 41). At 2000 CST (figure 43), the overall wind speeds were diminishing to about 1 to 2 m/s accompanied by a slight backing. The decrease in the wind speed and the backing of the wind direction are indicative of decreased mixing in the boundary layer. The urban heat island circulation was not evident in the 10-m wind field, even though a 5° C surface temperature difference existed between the center of the city and the surrounding rural regions. In light of the results of Vukovich and Dunn[17], this has to be attributed to the dampening effects of a strong surface-based inversion.

5.5 Temperature and Wind Profiles

The temperature and wind profiles at RAPS upper air stations 141 and 142 were examined to determine the diurnal variability of the potential temperature distribution and the wind distribution with height. Figure 44 shows the diurnal variability of potential temperature with height at station 141 in the center of the city. At 0346 CST, a surface-based inversion was noted with the top at approximately the 200-m level. Above the 200-m level to approximately 2.7 km, the boundary layer was characterized by weak stability. By 0949 CST, a shallow superadiabatic layer developed between the surface and the 100-m level. Above the 100-m level, the atmosphere was quasiadiabatic to 1.2 km. Stability characterized the layer above 1.2 km. As the analysis of the surface temperature distribution indicates, after 1500 CST, surface cooling began to occur. The 1545 CST temperature profile shows a stable layer had developed in the urban region from the surface to the 200-m level, confirming the earlier suggestion that the surface cooling was producing low-level stability. Above the 200-m level, the boundary layer was superadiabatic to 400 m, quasiadiabatic in the layer from 400 m to 1.2 km, weakly stable from 1.2 km to 3.0 km, and strongly stable above the 3.0-km level. At 2151 CST, the shallow surface-based stable layer had strengthened but its top was still at the 200-m level. Above the 200-m level, the boundary layer was characterized by weak stability up to 2.4 km and strong stability above the 2.4-km level.

In the rural regions (station 142) at 0358 CST (figure 44), a shallow inversion was also evident from the surface to the 300-m level. Weak stability characterized the region from 300 m to 2.8 km and strong stability was found above the 2.8-km level. Comparing the temperature profiles at 0346 CST at station 141 and 0358 CST at station 142, it can be seen that the urban region was warmer than the surrounding rural regions in the layer from the surface to the 400-m level.

A shallow superadiabatic layer developed from the surface to the 200-m level by 0945 CST in the rural regions. Weak stability was found in the layer from 200 m to 2.0 km, and strong stability was noted above the 2-km level. At this time, the urban region was warmer than the rural region in the layer from the surface to about the 1.0-km level.

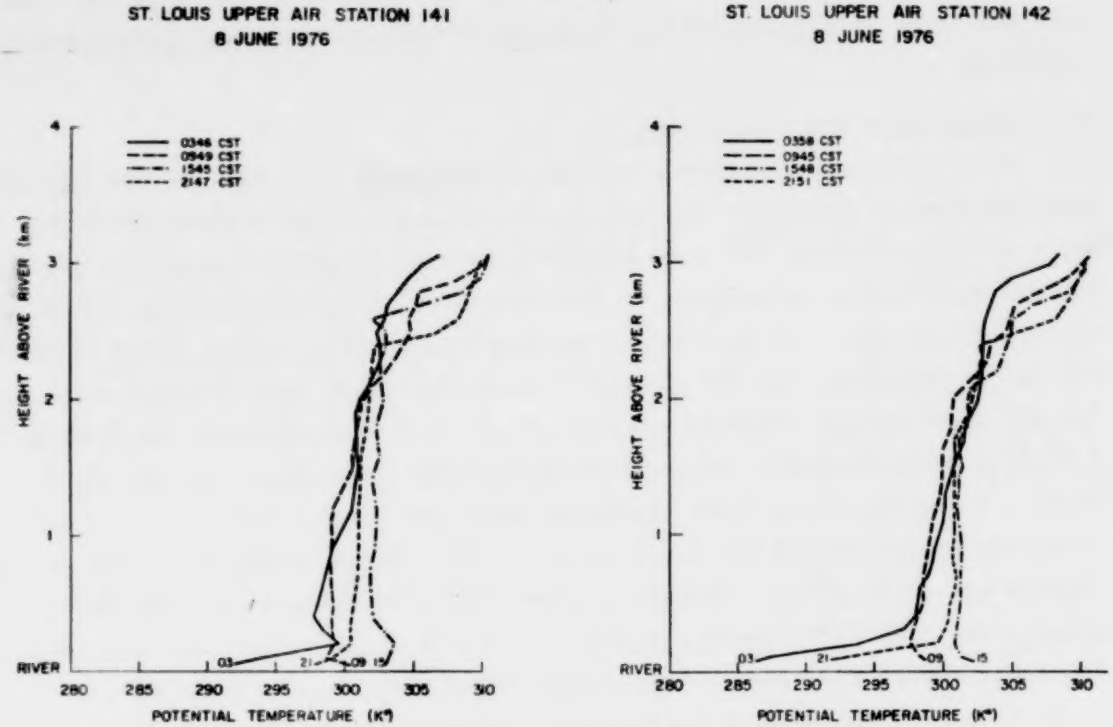

Figure 44. Diurnal variability of the potential temperature [°K] profile on 8 June over the St. Louis center city (Station 141) and over the rural area southwest of St. Louis (Station 142). Figure 37 shows the exact locations of these two sounding stations.

At 1548 CST, a shallow superadiabatic layer existed from the surface to the 200-m level in contrast to the weak stable layer found in the same region over the urban area. No explanation could be found for the difference. Perhaps mixing coupled with surface heating had momentarily removed the stable layer at station 142 and produced the superadiabatic layer. Above the 200-m level, a quasiadiabatic region was noted up to 1.7 km with strong stability above that level. At this time, the urban region was warmer than the rural region up to a height of 2.2 km.

A shallow layer of strong stability had developed by 2151 CST in the rural regions from the surface to the 200-m level. Above 200 m, the boundary layer was quasiadiabatic up to 1.7 km and weak to strong stability was found above that region. At this time, the urban heat island extended up to approximately 600 m according to the radiosonde data.

The wind speed profile over the center of the city (station 141) indicated the presence of a low-level jet above the inversion top (200-m level) at 0346 CST (figure 45). The wind direction (figure 45) through the low-level jet was fairly uniform with winds out of the west. Above 800 m, the wind direction changed markedly, retaining some uniformity in the layer from 1.2 km to 2.4 km with winds from the south to southwest. In this layer, a secondary speed maximum was found at the 2.1-km level.

The low-level jet was also evident over the rural region at 0358 CST (figure 46) but was centered at a higher elevation (300-m level). The wind direction (southwest) was also uniform through the layer where the low-level jet was found in the rural region (figure 46). Above 700 m, wind direction underwent marked changes as it did over the urban regions. There was a layer from 1.2 km to 3.8 km of relatively uniform wind direction (south to southeast). In that layer, a secondary wind speed maximum was noted from 2.4 to 2.9 km.

At 0949 CST, the low-level jet was still present over the rural region. It is suggested that the relatively high wind speeds found at low levels over the urban areas were not remnants of the low-level jet but were the results of pressure gradient accelerations associated with the urban heat island circulation.

There was a change in the wind direction in the surface layer around 1000 CST. It is noted that the wind direction over the urban area at 0945 CST was rather uniform from the surface to the 1.0-km level with winds out of the northwest. In the same layer over the rural region, wind direction varied from north to northwest to northeast. A number of changes in the wind direction occurred above the 1.0-km level over both regions, but there was a layer of relatively uniform wind direction from the south to southeast from 1.2 to 2.8 km.

. Wind speeds were small at all levels over the urban and rural regions at around 1545 CST. In the urban region, the strongest wind speeds were found near the surface, suggesting effects associated with the heat island circulation. The wind direction over the urban and rural regions underwent marked changes with height. The region of relatively uniform wind direction was noted over the rural region in the layer from 400 m to 2.4 km. In that layer the wind direction was from the south. No such layer was evident over the

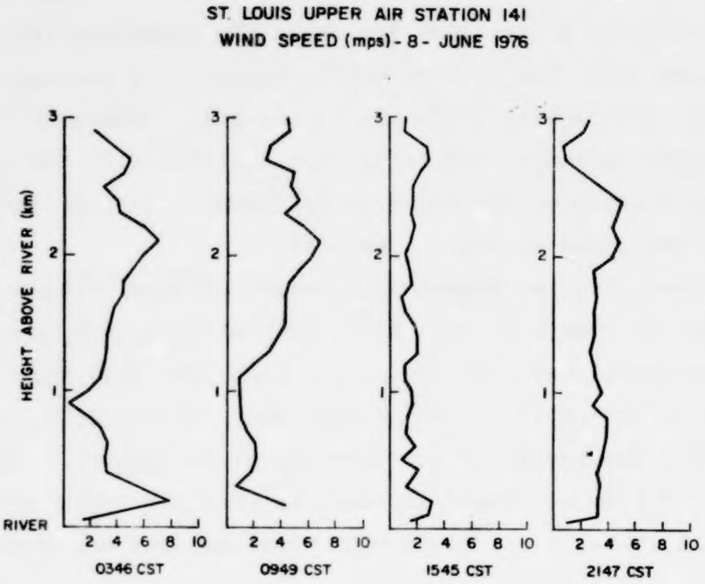

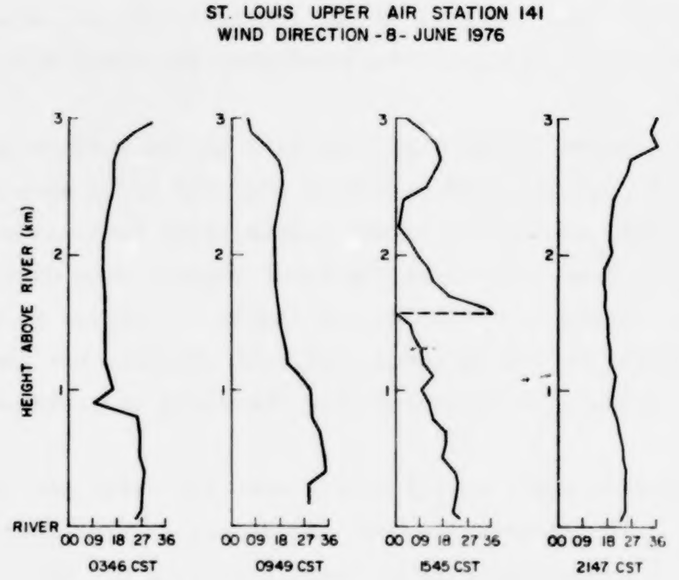

Figure 45. Diurnal variability of the wind speed [m/s] and wind direction profiles over the St. Louis center city on 8 June.

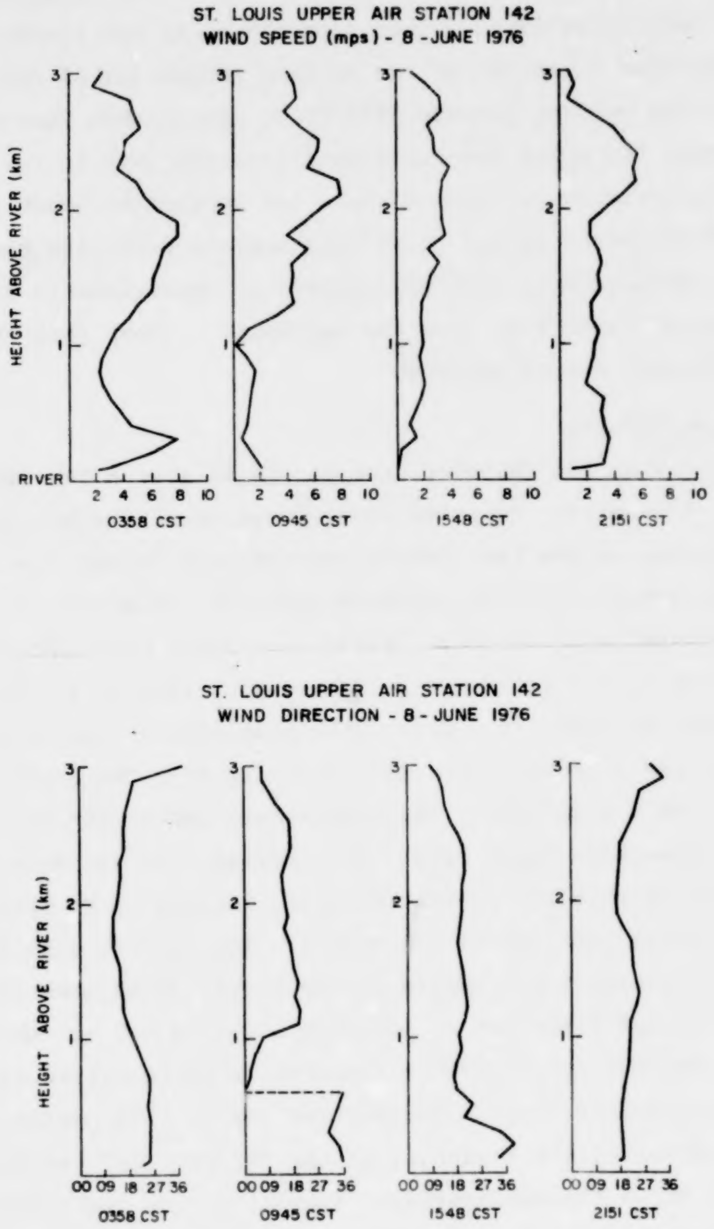

Figure 46. Diurnal variability of the wind speed [m/s] and wind direction profiles over the rural area southwest of St. Louis on 8 June.

urban region. It is interesting to note that over the urban region, the wind direction at the 1.0-km level (winds from the east) was almost 180° out of phase with the wind direction at the surface (winds out of the west southwest).

Later in the evening (around 2147 CST), wind speeds increased at most levels over both the urban and rural locations relative to the 1545 CST profiles, and were relatively uniform above the surface to about the 3.5-km level. The wind direction was relatively uniform over both the urban and rural regions in the layer from the surface to approximately the 2.6-km level. In this layer the winds were from the southwest. Above that layer the wind direction underwent marked changes.

5.6 Simulation Results

The analysis of the observed data yields at most a two-dimensional view of the flow. A primitive equation model[12] was used to simulate the time-dependent behavior of the heat island and the heat island circulation in order to obtain some insight into the three-dimensional structure of the flow over the city associated with the heat island circulation and into the effect of the perturbation on the local air pollution distribution in the period 0900 CST to 2100 CST when Da Vinci II was in close proximity to the city. Initially for the model, the boundary layer was adiabatic from the surface to the 1.0-km level. Above the 1.0-km level, the temperature lapse rate was identical to the standard atmosphere lapse rate. The initial wind was zero at the surface and was 2.0 m/s through the adiabatic layer, increasing to approximately 5 m/s at the 4.0-km level (the top of the model). The initial wind direction was from the west throughout the domain of the model, which generally characterizes the geostrophic wind direction at low levels (below 1.0 km) through the period of interest. The maximum allowable temperature perturbation at the surface due to the urban heat island in the daytime period (the period from 0900 to 1500 CST, which marked the beginning of the differential cooling) was 2.4° C.

Figure 47 shows the near-surface, simulated flow reminiscent of the period around 1000 CST on 8 June. Though the initial wind direction was from the west, frictional effects produced a general flow from the southwest. Figure 47 shows the strong zone of convergence over the central area of the city and a region of inflow over and downwind of the city associated with the urban heat island circulation similar to that shown in the analysis of the RAPS wind data for 1000 CST (figure 42). The strongest wind speeds were found near the central regions of the city upstream of the center of convergence,

100 m

1,000 m

600 m

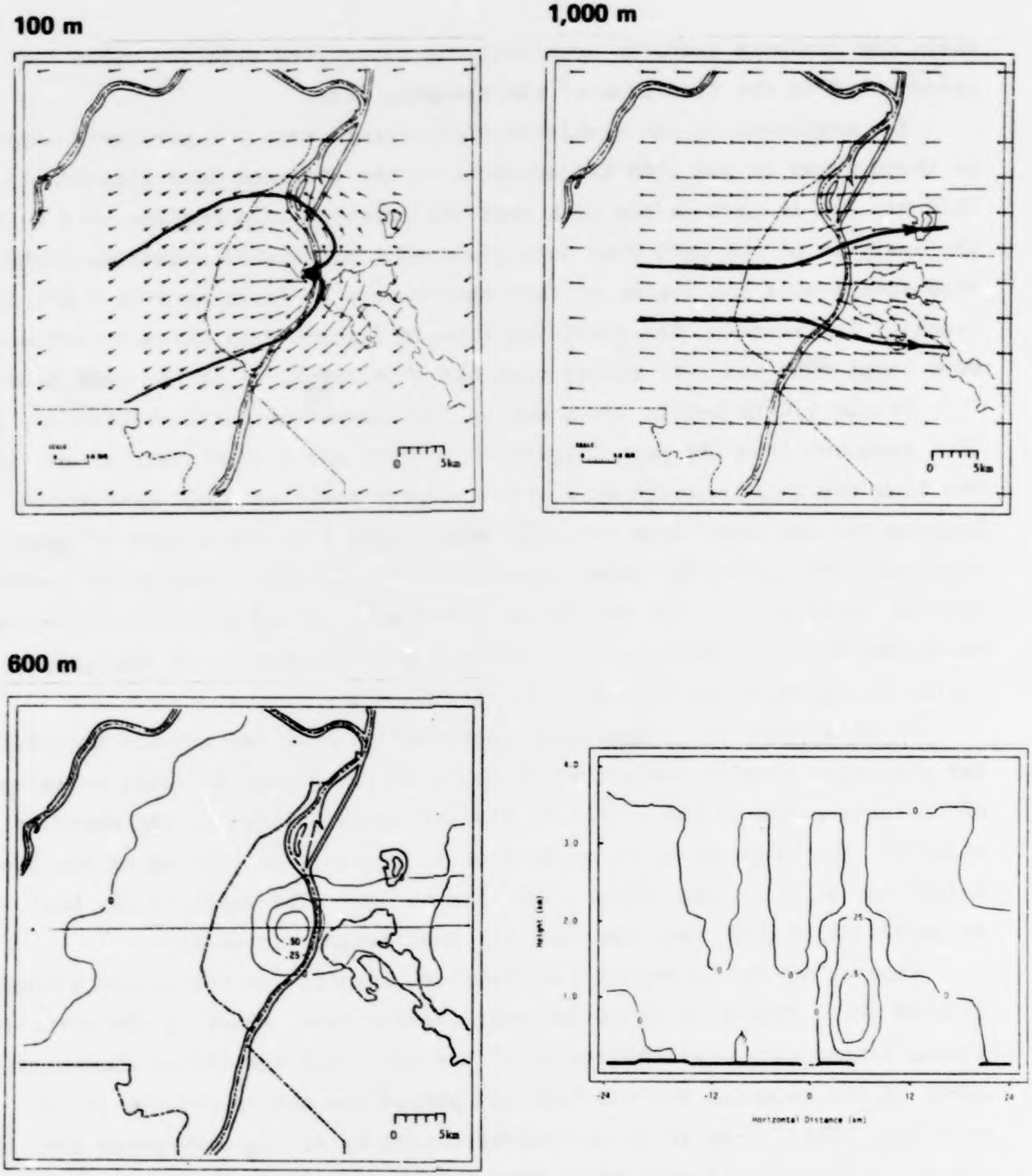
0
5km
0
5km
0
5km
.50
.25
4.0
3.0
2.0
1.0
Height (km)
0
.25
.5
-24
-12
0
12
24
Horizontal Distance (km)

Figure 47. Simulated horizontal flow at 1000 CST is shown at 100 m above the surface of the river (upper left) and at 1,000 m above the river (upper right). Vectors are proportional in length to wind speed and extend from the grid point in the direction of the flow. Horizontal distribution of the vertical velocity [m/s] at 1000 CST is shown for the 600-m level (lower left) with a section line along which a vertical cross section of the vertical velocity profile is shown (lower right). Positive values indicate upward motion.

where the pressure gradient accelerations associated with the urban heat island were in the direction of the synoptic flow.

The magnitude of the simulated wind vectors were not precisely comparable to those shown in the 1000 CST analysis of the observed data (figure 42). This was due in part to the fact that the interpolation routine used to create the analysis of the RAPS wind data produced considerable smoothing (actual wind speeds near the region of convergence were as large as 3 to 4 m/s in many cases). Furthermore, the simulated flow in figure 47 is characteristic of the 60-m level over the city rather than the 10-m level, as is the RAPS data.

At the 1.0-km level, which was not influenced by surface friction, the flow remained from the west (figure 47). Over the central part of the city the flow was characterized by a strong directional and speed divergence. Linking the low-level flow with the upper-level flow was a zone of upward vertical motion centered about the city with a maximum speed on the order of 0.5 m/s (figure 47). The top of the urban heat island circulation (the region where the vertical velocity approximately goes to zero or is negligible) was in the vicinity of the 2.0-km level (figure 47).

At this time, the temperature perturbation near the surface according to the simulated results was approximately 1.0° C. Figure 48 shows an extension of the heat plume to the northeast similar to that shown in the observed results. The temperature cross section indicates that the top of the heat island was at about the 400-m level (figure 48). The depth of the heat island is generally smaller than that for the heat island circulation.

Figures 49 and 50 depict the simulated results for the period around 1300 to 1500 CST. Figure 49 shows the near-surface flow, which is characterized by strong convergence near the center of the city, but the inflow characteristics shown in the solution for the 1000 CST period are not as evident in this solution. The 1.0-km level was characterized by strong divergence over the center of the city (figure 49). Note that the winds at the 1.0-km level over the downtown area were about 180° out of phase with the near-surface flow in the same region, a factor noted in the observed data. Positive vertical velocities were centered over the central portions of the city with magnitudes on the order of 1.0 m/s (figure 49). Top of the heat island circulation was still found around the 2-km level (figure 49).

The near-surface temperature perturbation associated with the urban heat island was on the order of 1.5° C in the central area of the city (figure 50).

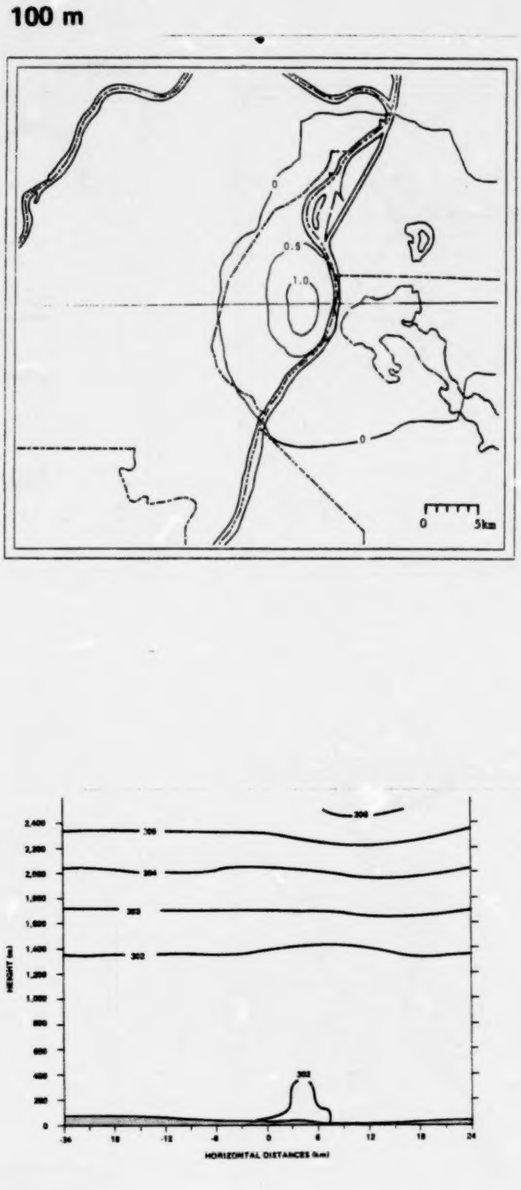
100 m
0
0.5
1.0
0
0 5km
306
305
304
303
302
302
2,400
2,200
2,000
1,800
1,600
1,400
1,200
1,000
800
600
400
200
0
HEIGHT (m)
-24
-18
-12
-6
0
6
12
18
24
HORIZONTAL DISTANCES (km)

Figure 48. Horizontal distribution of the potential temperature [°K] perturbation at the 100-m level above the river surface at 1000 CST on 8 June (above). Below is the vertical cross section of the potential temperature [°K] field constructed along the section line shown on the horizontal distribution map.

100 m

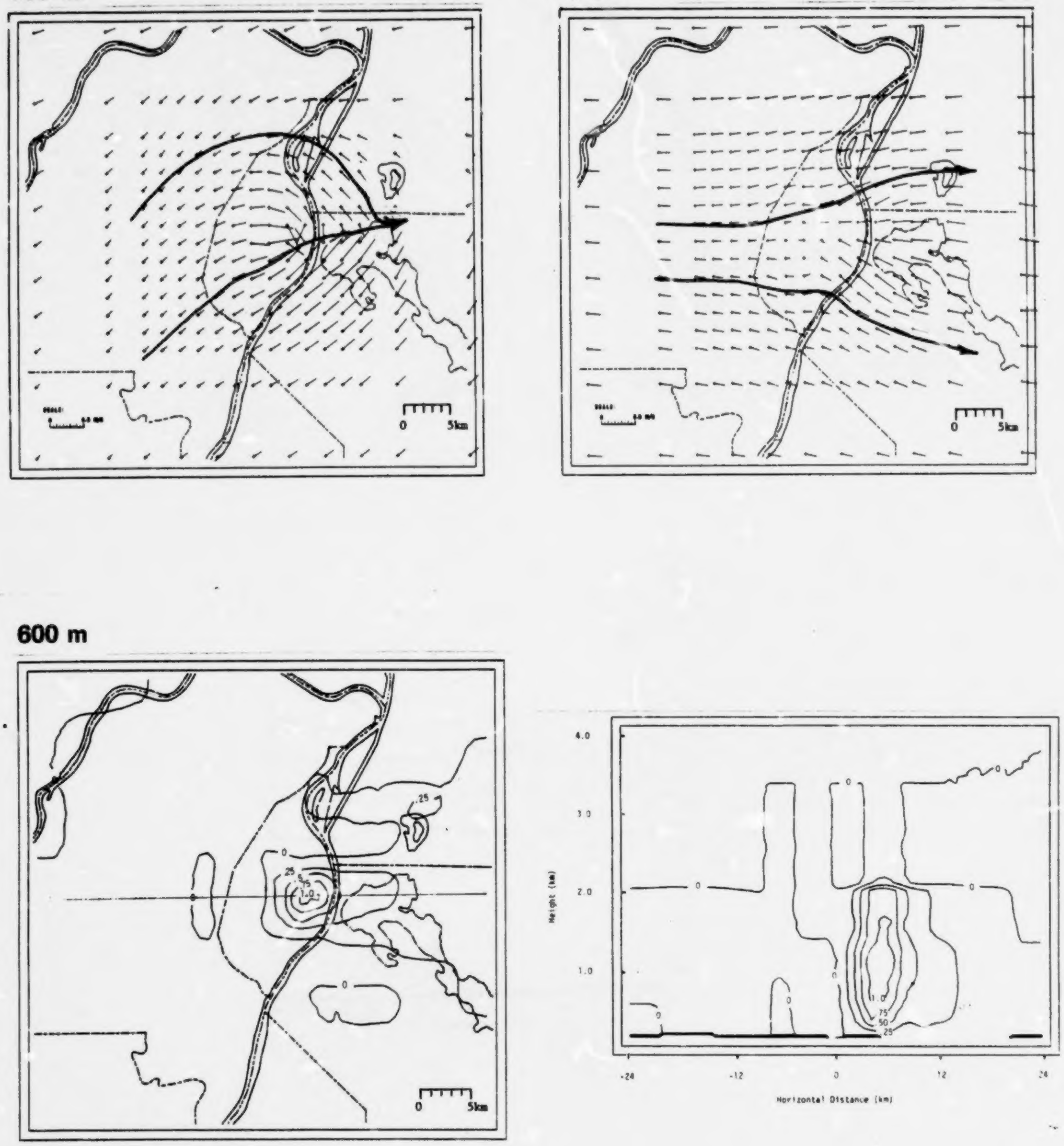
100 m
1,000 m
600 m
0 5km
0 5km
0 5km
0
.25
.75
1.0
4.0
3.0
2.0
1.0
Height (km)
0
.75
.50
.25
-24
-12
0
12
24
Horizontal Distance (km)

Figure 49. Simulated horizontal flow at 1400 CST is shown at 100 m above the surface of the river (upper left) and at 1,000 m above the river (upper right). Vectors are proportional in length to wind speed and extend from the grid point in the direction of the flow. Horizontal distribution of the vertical velocity [m/s] at 1400 CST is shown for the 600-m level with a section line along which a vertical cross section of the vertical velocity profile is shown (lower right). Positive values indicate upward motion.

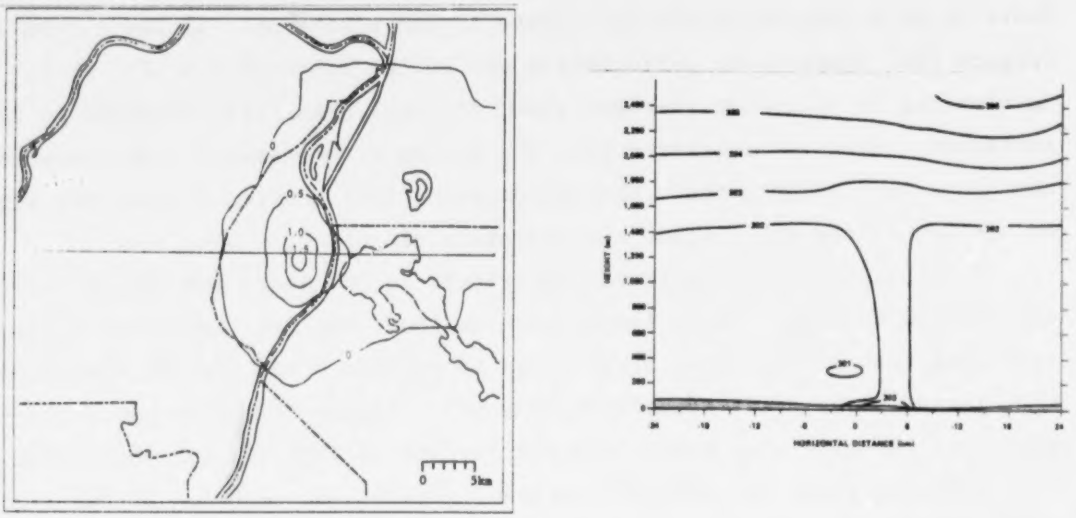

1,000 m

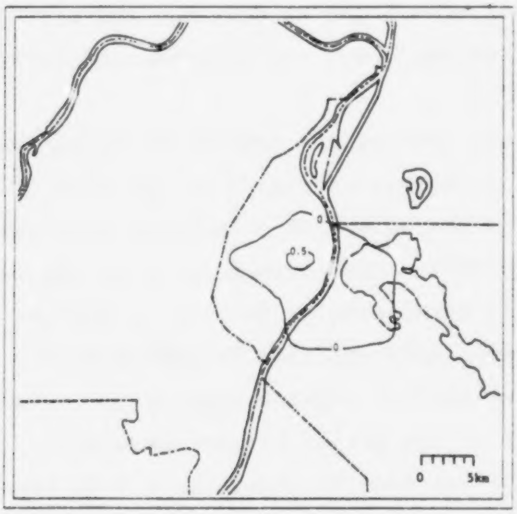

Figure 50. Horizontal distribution of the potential temperature [°K] perturbation is shown at the 100-m level above the river surface at 1400 CST on 8 June. In the upper right is the vertical cross section of the potential temperature [°K] field constructed along the section line shown on the horizontal distribution map. Below is the horizontal distribution of the potential temperature [°K] perturbation at the 1,000-m level above the river at 1400 CST.

There is an extension of the heat plume to the northeast. At the 1.0-km level (figure 50), temperature perturbation was on the order of 0.5° C. It is interesting to note that the heat plume at the 1.0-km level extended to the southeast. This is associated with the strong southeastward flow produced by the upper level divergence. The temperature cross section (figure 50) suggested the top of the heat island was approximately at the 1.6-km level.

After 1500 CST, the surface temperature in the model was forced to cool differentially (the surface temperature in the rural area cooled at a greater rate than that in the urban area) so as to produce a heat island comparable to that found in the observed data at 2000 CST. Figure 51 yields the distribution of the simulated winds near the surface at 1600 CST and shows that the zone of convergence had weakened (stream lines do not unite). At the 1.0-km level, the divergence aloft had also become weaker. The vertical velocity had decreased to a value of 0.5 m/s, and the zone of updraft had been displaced downstream of its position found at 1400 CST. The depth of the heat island circulation remained at approximately the 2.0-km level. (See figure 51.) The thermal perturbation also began to decrease and move downstream (figure 52). An inversion had developed over the suburban and rural regions, but not over the urban region.

The near-surface convergence zone found downstream of the urban area at 1600 CST continued to weaken according to the 1800 CST results (figure 53). The 1.0-km level was characterized with speed divergence but directional divergence was not evident. The maximum vertical velocity was located over East St. Louis, Illinois, downstream of St. Louis, and the magnitude of vertical velocity had decreased substantially to approximately 0.10 m/s. There were secondary centers of updraft located west of the downtown section of the city and north and south of the center of maximum updraft. The weaker updraft found upstream of the city extended to about the 2.0-km level (figure 53), whereas the updraft center over East St. Louis only extended to the 1.5-km level. The thermal perturbation associated with the urban heat island (figure 54) had decreased substantially but apparently there still was a flux of heat to the 100-m level from the surface since there was an extension of the heat plume over the city. It would have been expected that if there were no heat flux to the 100-m level from the city, the heat plume would have moved downstream by this time, and there would be no extension of the heat plume over the city. Vertical cross section (figure 54) indicates a weak stable layer from the sur-

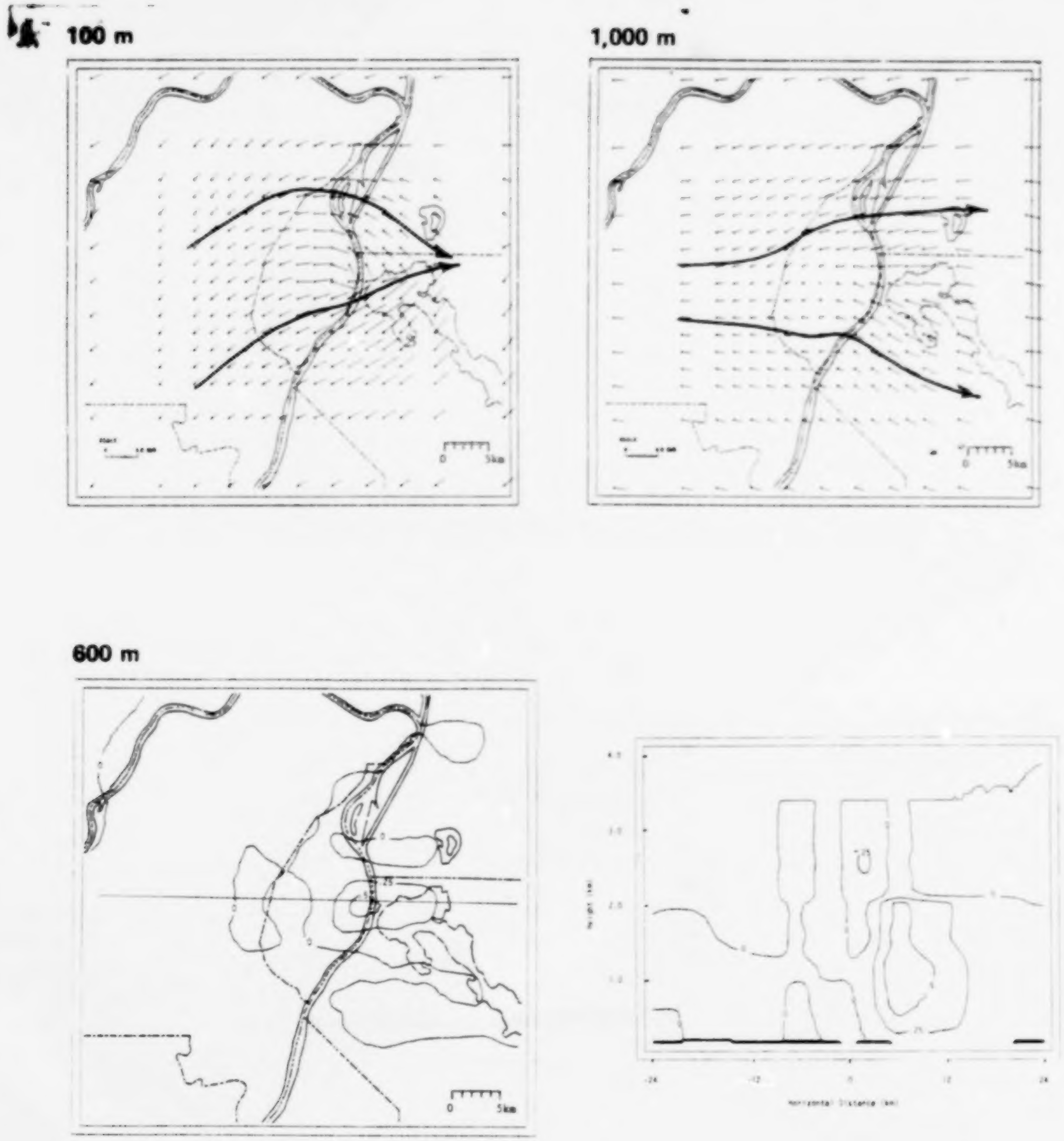

100 m

1,000 m

600 m

Figure 51. Simulated horizontal flow at 1600 CST is shown at 100 m above the surface of the river (upper left) and at 1,000 m above the river (upper right). Vectors are proportional in length to wind speed and extend from the grid point in the direction of the flow. Horizontal distribution of the vertical velocity [m/s] at 1600 CST is shown for the 600-m level (lower left) with a section line along which a vertical cross section of the vertical velocity profile is shown (lower right). Positive values indicate upward motion.

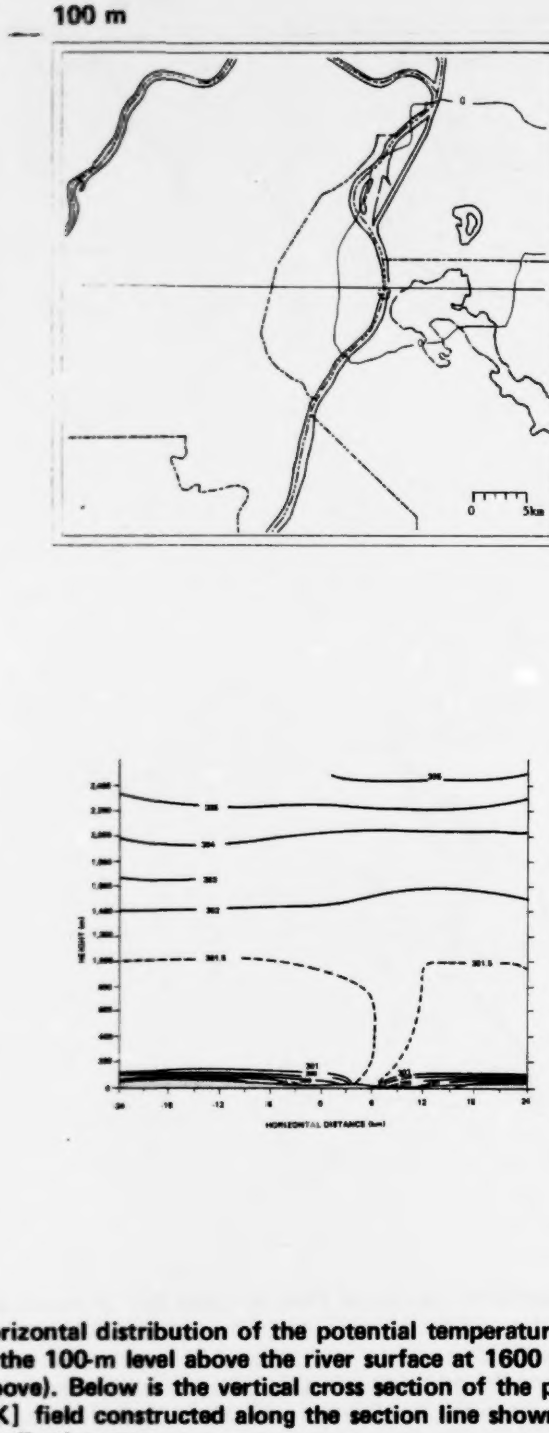

Figure 52. Horizontal distribution of the potential temperature [°K] perturbation at the 100-m level above the river surface at 1600 CST on 8 June (above). Below is the vertical cross section of the potential temperature [°K] field constructed along the section line shown on the horizontal distribution map.

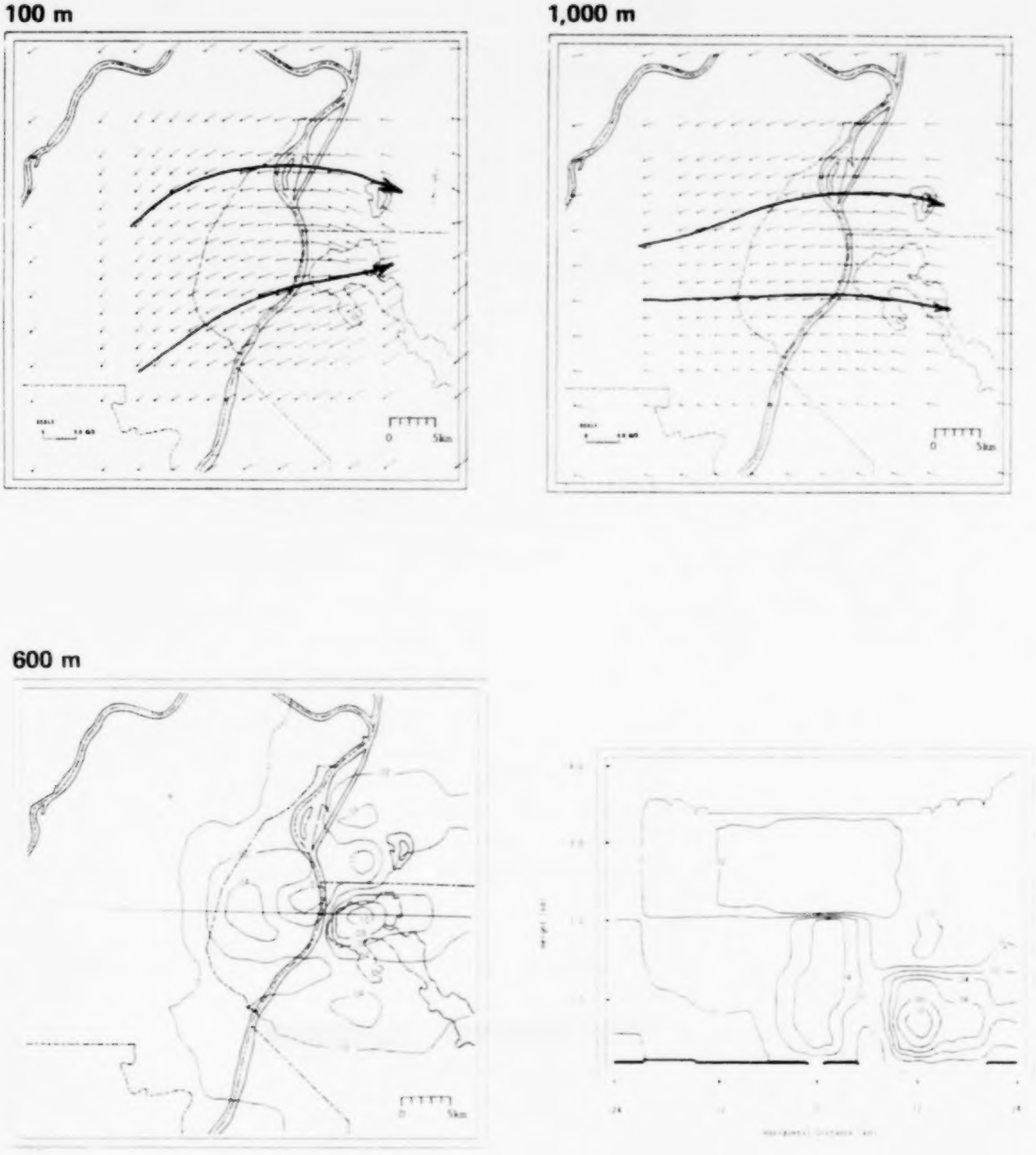

Figure 53. Simulated horizontal flow at 1800 CST is shown at 100 m above the surface of the river (upper left) and at 1,000 m above the river (upper right). Vectors are proportional in length to wind speed and extend from the grid point in the direction of the flow. Horizontal distribution of the vertical velocity [m/s] at 1800 CST is shown for the 600-m level (lower left) with a section line along which a vertical cross section of the vertical velocity profile is shown (lower right). Positive values indicate upward motion.

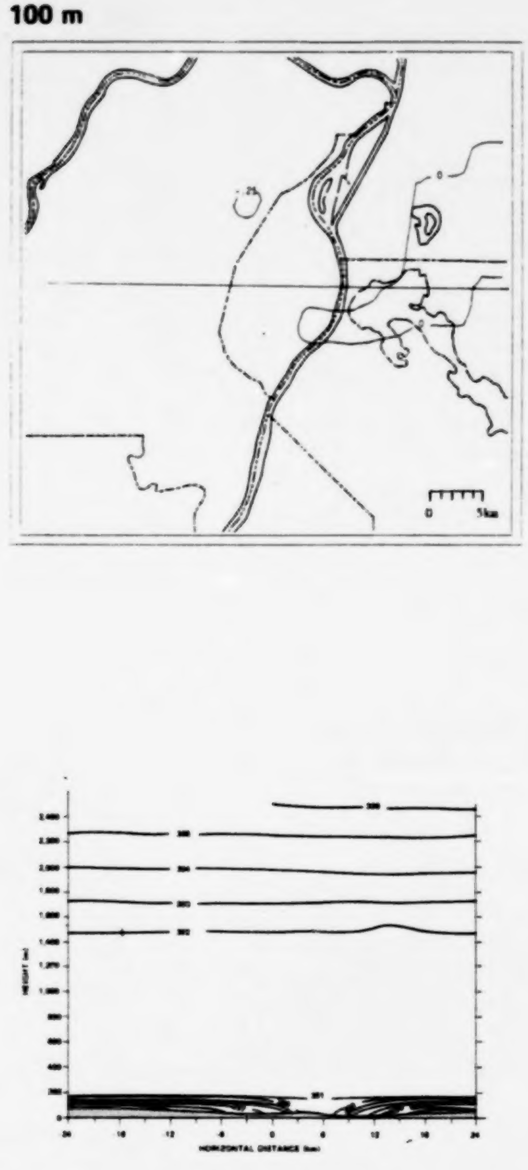
100 m
-.25
0
0
0 5km
HEIGHT (m)
HORIZONTAL DISTANCE (km)

Figure 54. Horizontal distribution of the potential temperature [°K] perturbation at the 100-m level above the river surface at 1800 CST on 8 June (above). Below is the vertical cross section of the potential temperature [°K] field constructed along the section line shown on the horizontal distribution map.

face to approximately the 150-m level over the urban area with an inversion in approximately the same layer over suburban and rural regions surrounding the city.

Simulation results that characterize 2100 CST show little indication of the urban heat island circulation (figure 55). The wind speed had increased at most locations over and surrounding the city. Furthermore, there was no indication of divergence aloft, but there was a center of upward motion (approximately 2 cm/s) centered over the city (figure 55). The top of the region of upward motion was at about the 800-m level (figure 55). Stronger stability had developed over the urban region (figure 56) but the lifting of the isopotentialtherms over and downwind of the city indicate upward mixing of heat.

5.7 Surface Ozone Distribution

At 0500 CST (figure 57), the ozone distribution was fairly uniform to the west of the city, averaging around 0.03 ppm. In the downtown region, along the river, and immediately to the east, ozone was barely detectable, which is indicative of a strong ozone-destructive process that occurs in a surface-based nocturnal temperature inversion layer in the inner city. Ozone trapped in such a stable layer would be destroyed by contact with surface objects and by reactions with ozone-destructive agents such as NO and NO_2 emitted by combustion processes and certain hydrocarbons emitted by petrochemical plants located along the river.

From 0500 through 0800 CST, the lowest ozone in the area consistently was recorded in the east central portions of the downtown business districts. Higher readings were noted to the north and west of the city. By 0900 CST (figure 57), the ozone had become fairly uniform over the study area with slightly lower readings still occurring over the downtown area. Higher ozone concentrations were found in an area to the southeast of the city that had been downwind of the center of the city for most of the morning, suggesting photochemical generation of ozone from precursors transported downwind from the city.

After 0900 CST, the wind direction changed from northwesterly to southwesterly. The location of the highest ozone concentration began to move from southeast of the city to northeast of the city and, in the period 1000 to 1400 CST, appeared immediately downwind of the center of the city in the approximate location of the zone of convergence associated with the urban heat

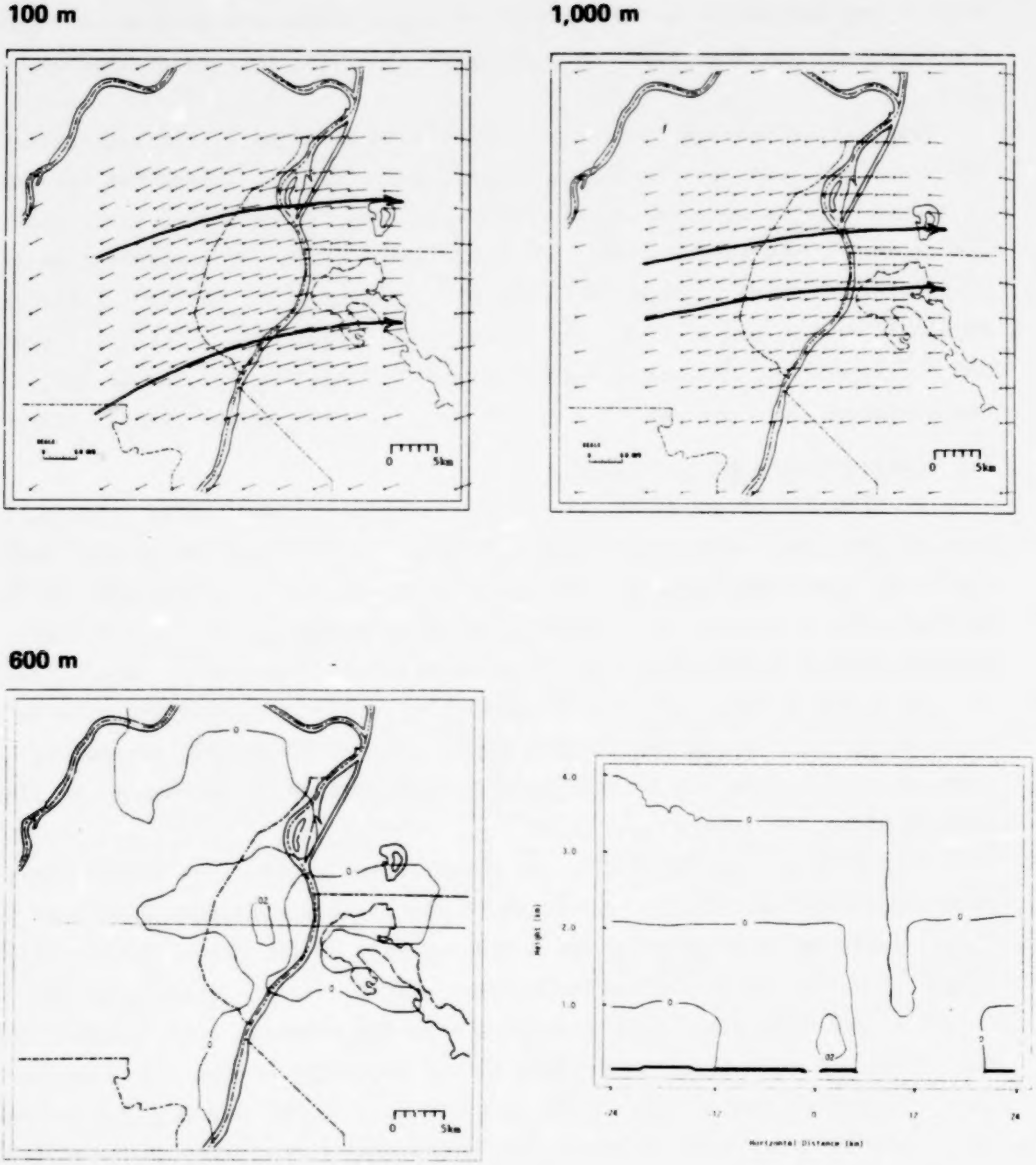
100 m

1,000 m

600 m

0 5km
0 5km
0 5km
4.0
3.0
2.0
1.0
Height (km)
0
.02
-24
-12
0
12
24
Horizontal Distance (km)

Figure 55. Simulated horizontal flow at 2100 CST is shown at 100 m above the surface of the river (upper left) and at 1,000 m above the river (upper right). Vectors are proportional in length to wind speed and extend from the grid point in the direction of the flow. Horizontal distribution of the vertical velocity [m/s] at 2100 CST is shown for the 600-m level (lower left) with a section line along which a vertical cross section of the vertical velocity profile is shown (lower right). Positive values indicate upward motion.

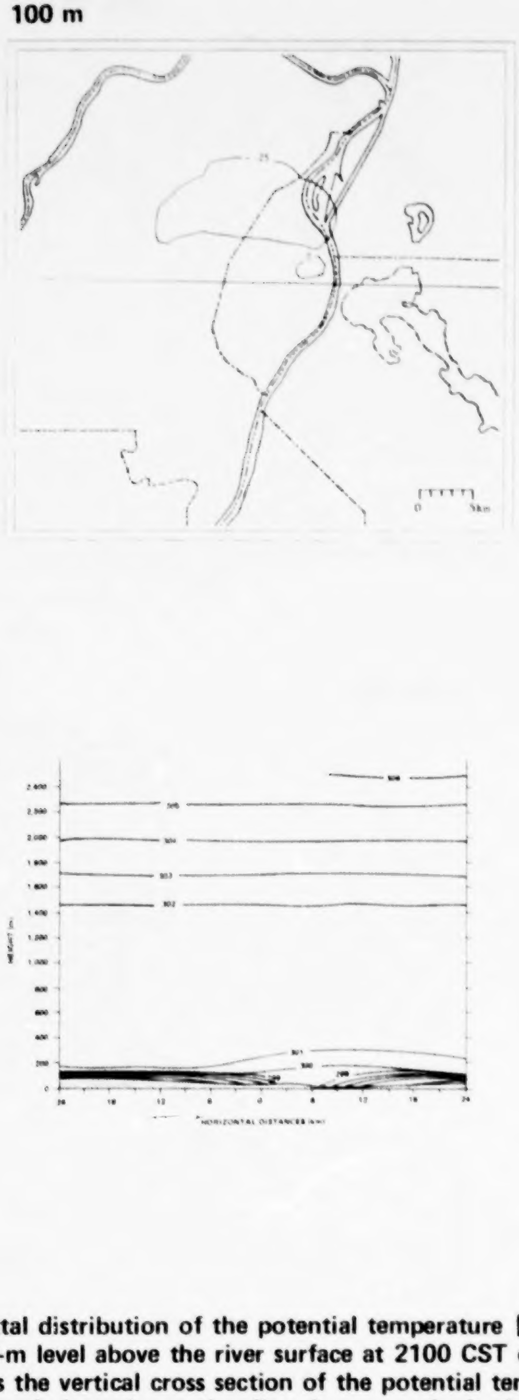

Figure 56. Horizontal distribution of the potential temperature [°K] perturbation at the 100-m level above the river surface at 2100 CST on 8 June (above). Below is the vertical cross section of the potential temperature [°K] field constructed along the section line shown on the horizontal distribution map.

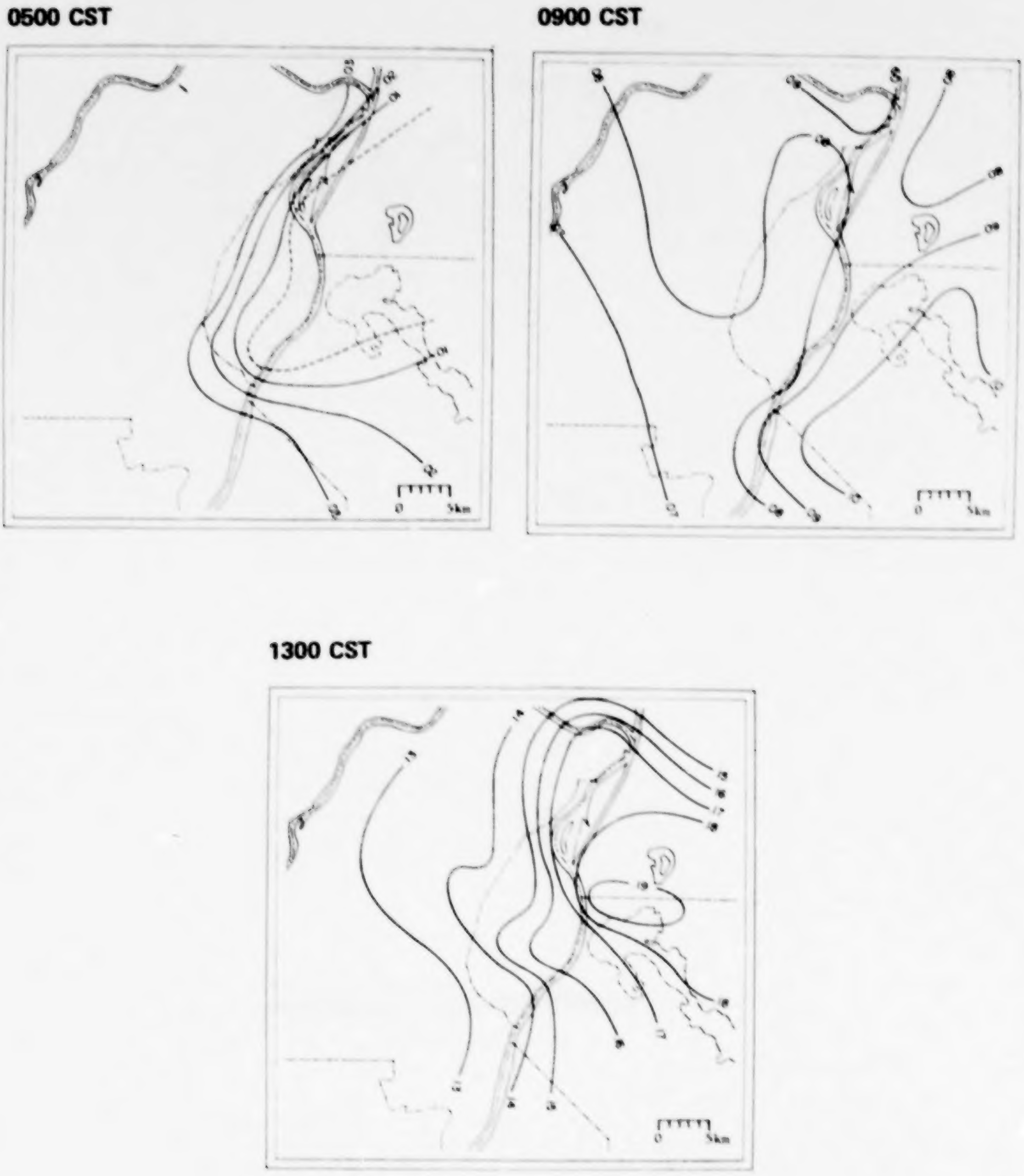
0500 CST

0900 CST

1300 CST

Figure 57. Surface ozone distribution [ppm] in the study area at 0500, 0900, and 1300 CST on 8 June. (Dashed line represents .005 ppm.)

island circulation (data not shown). Areas of lower ozone concentration were found upwind of the city. An example of this distribution is shown in figure 57, which is the ozone distribution at 1300 CST.

By 1600 CST, a rather broad urban plume was found along a southwest-northeast axis through the center of the city (figure 58). At this time, the maximum ozone concentration was displaced farther downstream than previously. The downstream displacement of the maximum ozone concentration occurred at about the same time that the strong convergence characterized by inflow into the city downwind of the city and associated with the urban heat island weakened and the inflow region no longer existed. This general pattern for the ozone distribution persisted, and by 1800 CST the maximum ozone in the plume decreased from 0.22 at 1600 CST to 0.15 ppm, while the minimum value in the surrounding suburban and rural regions dropped by about 0.03 ppm to around 0.09 ppm in the same period. This indicates the presence of more ozone-destructive agents in the urban plume than in the surrounding suburban and rural regions.

By 1900 CST (figure 58), several distinct features appeared in the pattern of ozone distribution: highs were noted to the northeast and southeast. The high to the northeast was associated with the still distinct urban plume stretching out in that direction from the center of the city. The fairly high ozone noted to the southeast of the city was probably due to the lack of ozone-destructive agents in that area relative to the western suburban and rural region.

By 2100 CST (figure 58), the nocturnal destruction of ozone had markedly affected the ozone distribution. Although the urban plume was still evident, the suburban areas to the west of the city through the southern downtown area, and east into Belleville, showed very low ozone concentrations. This was most likely due to destructive effects of NO and NO_2 emitted by the rush hour and early evening traffic into the stable surface layer. Areas to the south and southeast of the city still showed relatively higher ozone concentration at this hour.

5.8 Da Vinci II and RTI-EML Ozone Data

In the period 0800 to 2100 CST on 8 June, Da Vinci II and the RTI-EML collected ozone data in the immediate vicinity of St. Louis. Figure 38 shows the track of Da Vinci II and the RTI-EML. Figure 59 yields the time variation of the height of Da Vinci II in the period of interest.

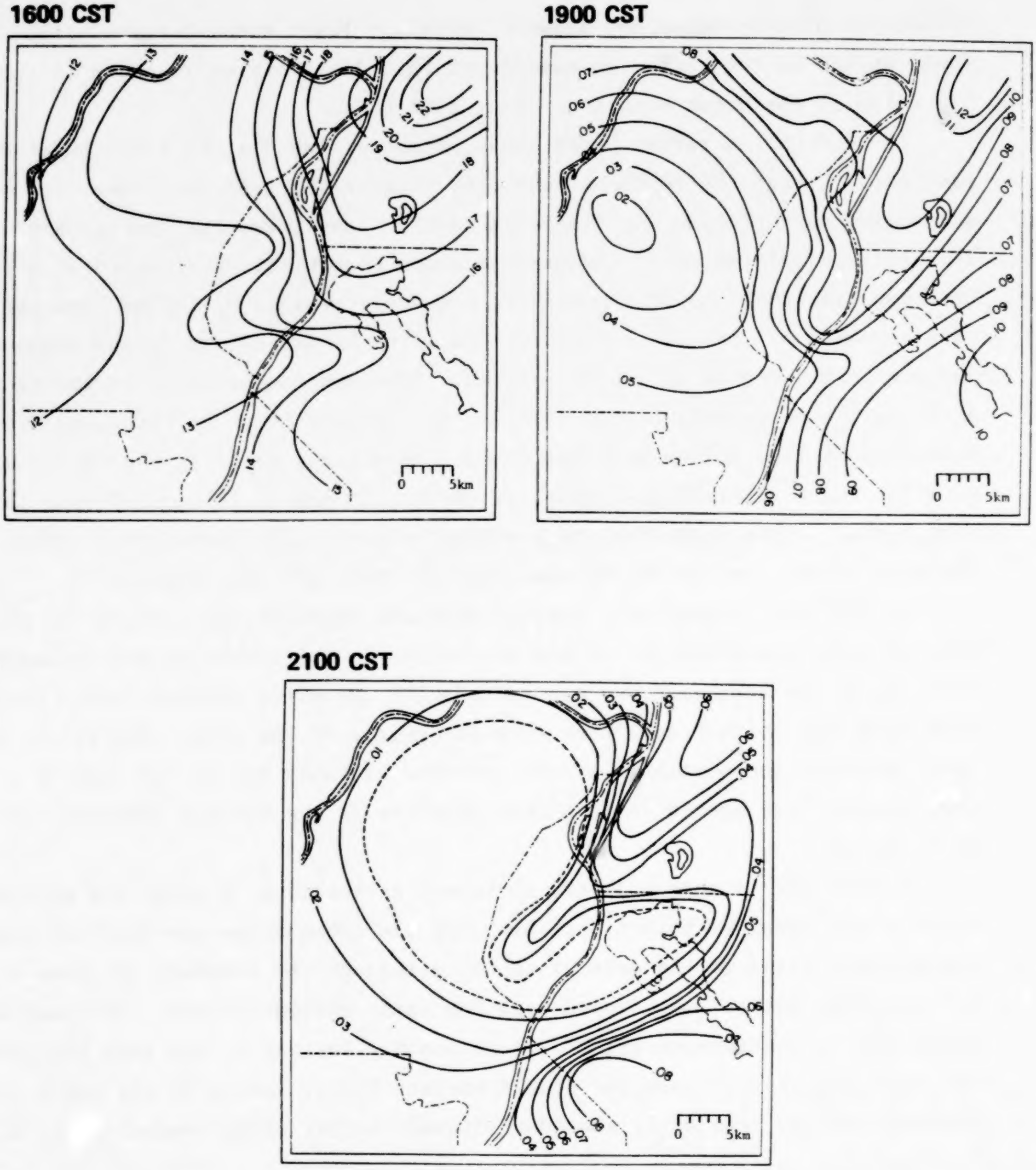
1600 CST
12
13
14
15
16
17
18
19
20
21
22
0 5km
1900 CST
02
03
04
05
06
07
08
09
10
11
12
0 5km
2100 CST
01
02
03
04
05
06
07
08
0 5km

Figure 58. Surface ozone distribution [ppm] in the study area at 1600, 1900, and 2100 CST on 8 June. (Dashed line represents .005 ppm.)

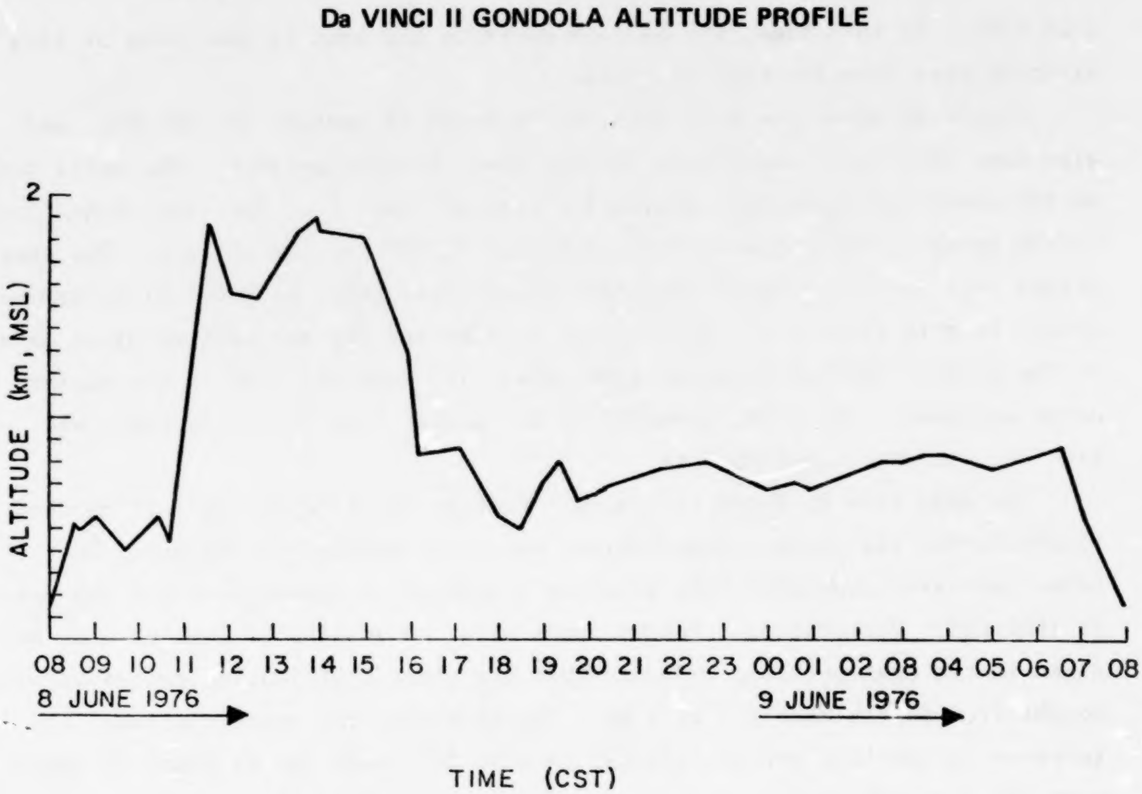

Figure 59. Variation of altitude with time for the flight of Da Vinci II.

Da Vinci II was launched at 0756 CST on 8 June from Arrowhead Airport, which is approximately 24 km west of St. Louis. It took the balloon approximately 30 min to reach flight altitude. In the period 0830 to 1030 CST, the balloon drifted southwestward at an approximate altitude of 700 m MSL. Winds at flight altitude were from the northwest at approximately 1 to 2 m/s. Because of severe thermal convection encountered by the balloon at around 1030 CST, the balloon changed flight altitude. The transition took place between 1030 and 1130 CST. From 1130 CST to approximately 1500 CST, the balloon cruised at an approximate altitude of 1,700 m, where the winds were from the south to southeast at 2 to 3 m/s and the balloon moved to the northwest. As the stability began to develop in the boundary layer between 1500 and 1600 CST, the severe convection ceased, and the altitude of the balloon lowered to 700 m. The balloon remained at 700 m for the rest of the period of interest (1600 to

2100 CST). At this time, the balloon moved to the east as the winds at flight altitude were from the west at 3 m/s.

Figure 60 shows the data from the Da Vinci II system, the RTI-EML, and also some additional ozone data derived from the RAPS network. The solid line is the ozone concentrations obtained aboard Da Vinci II. The long dashed line is the ozone concentrations obtained by the RTI-EML at the surface. The short dashed line is the surface concentration of ozone under Da Vinci II determined using the path of Da Vinci II relative to time and the analyses of ozone data at the surface derived from the RAPS data. The dash-dot line is the surface ozone maximum in the plume downwind of St. Louis. The latter analysis was also derived from the RAPS data.

The data from Da Vinci II indicate that at the time Da Vinci II reached flight level, the ozone concentrations were approximately 0.080 ppm. The ozone increased from 0800 CST, reaching a maximum of approximately 0.152 ppm at 1600 CST. Vertical profiles of ozone obtained at 1145 CST, which will be given in the next section, indicate that the ozone distribution decreased with height from approximately 1 to 2 km. The fact that the ozone continued to increase in the time period 1030 CST to 1130 CST, when the Da Vinci II underwent its altitude changes from 400 to 1,700 m, suggests that some overriding factor, possibly synthesis, was influencing the time variation of ozone during that period.

After 1500 CST, the balloon descended. The major portion of its descent occurred between 1500 and 1600 CST. Afterwards, there was a rapid decrease in ozone (1700 to 2100 CST). At the time of the rapid decrease of ozone, the Da Vinci II system was over the Alton-Wood River Industrial Region. It is suggested that the balloon entered into a region where there were significant amounts of ozone-destructive agents, the apparent source of which was the Alton-Wood River Industrial Region. Since the decrease in ozone ceased at 1900 CST and since the ozone increased from 1900 CST, reaching a value of approximately 0.145 ppm at 2300 CST, it is suggested that most, if not all, of the destructive agents were removed through reaction with ozone by 1900 CST, and that the increase in ozone that followed was due to mixing with the surrounding environment.

The data from the RTI-EML also indicated that ozone increased initially reaching a maximum at 1600 CST also. The maximum concentration of ozone was 0.149 ppm. After 1600 CST, the ozone decreased rapidly, reaching a minimum at

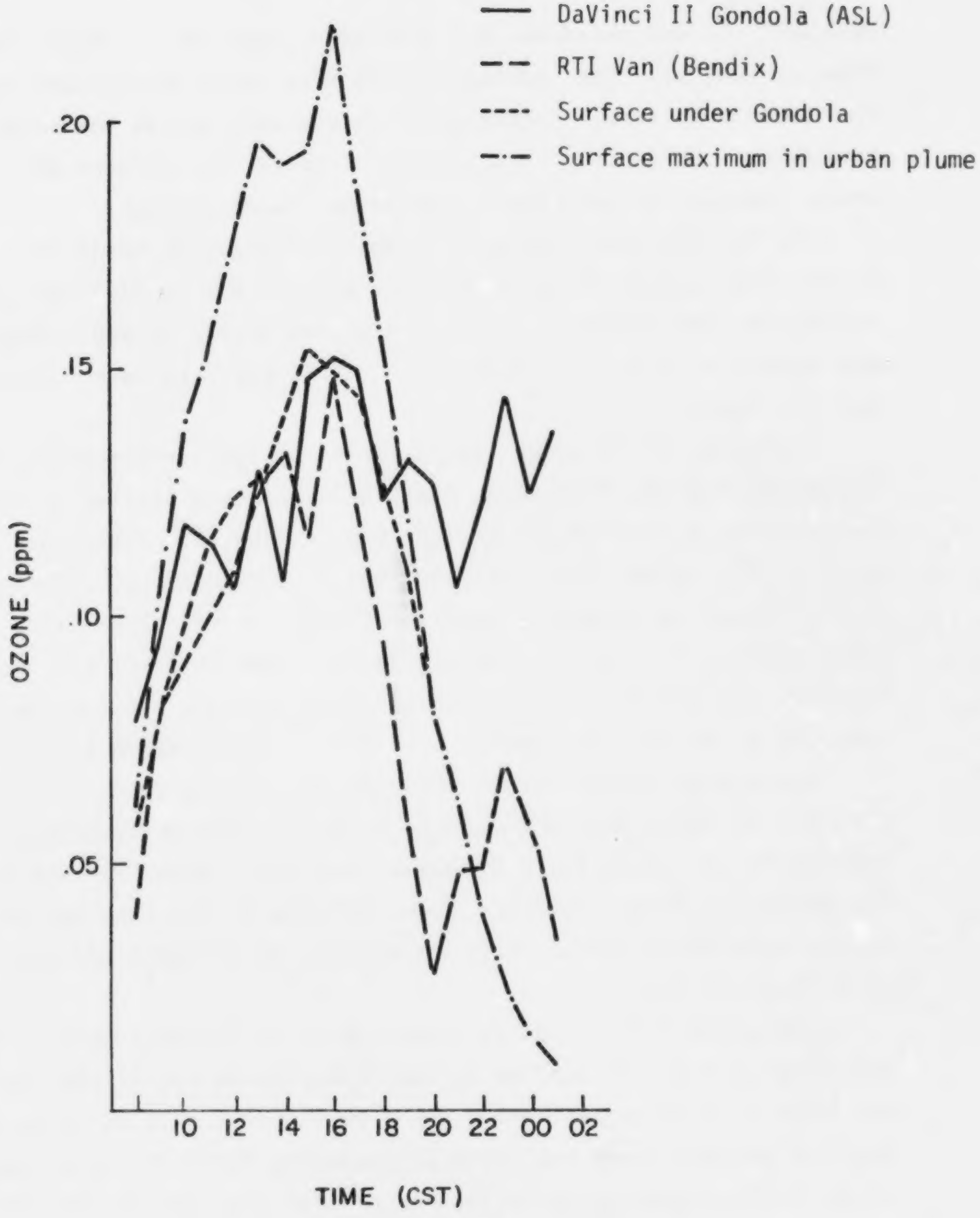

Figure 60. Hourly average ozone concentrations [ppm] measured along the Da Vinci II flight track, including measurements taken from the gondola, the RTI van, and the RAPS monitoring network.

2000 CST. It was noted earlier that after 1400 CST, a surface-based inversion began to develop. The inversion would trap ozone-destructive agents emitted from surface sources. Furthermore, during this period the solar intensity was decreasing. Evidently a destruction of ozone overbalanced the synthesis of ozone, causing the decrease in the ozone concentration.

The RTI-EML data indicated a rapid increase, followed by a rapid decrease in the ozone concentration in the period 2000 CST to 0100 CST. At this time, the RTI-EML was northeast of St. Louis (see figure 38 and figure 58) in the approximate location of the remnants of the major surface ozone plume emitted from St. Louis.

Variation of the ozone concentration at the surface under Da Vinci II as determined from the RAPS data, indicated a pattern similar to that found in the Da Vinci II data in the period 0800 to 1500 CST. There was an increase in ozone in the period, and after 1100 CST, the values at the surface under Da Vinci II were approximately equal to those observed on Da Vinci II. Maximum ozone concentration was approximately 0.154 ppm at 1500 CST. From 1500 to 2000 CST, the surface ozone under the gondola had a pattern similar to that observed by the RTI-EML; namely, the ozone concentration decreased rapidly.

The maximum ozone concentration at the surface in the plume downwind of the city increased from 0800 CST to 1600 CST. The maximum ozone concentration observed in the plume was 0.22 ppm at 1600 CST. From 0900 CST to 1900 CST, the ozone concentration in the plume downwind of the city was in excess of the values observed by the Da Vinci II system, the RTI-EML, and surface values under Da Vinci II.

After 1600 CST, the surface maximum ozone concentration in the plume decreased in a manner similar to that observed by the RTI-EML and similar to the surface ozone concentration under Da Vinci II. It is interesting to note that the surface ozone concentration under Da Vinci II approached the maximum ozone concentration in the plume around 1900 CST, but the RTI-EML was observing lower concentrations until 2300 CST. Between 2100 and 0100 CST, the RTI-EML experienced an increase in ozone. It is also important to note that the ozone concentration in the plume northeast of the city (RAPS station 115) was considerably smaller than that observed by the RTI-EML in that period. The RTI-EML was farther to the northeast of the city (see figure 38) at this time.

5.9 Aircraft Ozone Profiles

Two vertical profiles of ozone were obtained by a NOAA aircraft within

2.0 km of Da Vinci II on the morning of 8 June (figure 61). The profiles were based upon ozone concentrations recorded during the ascending portions of the aircraft missions, the first from 0915 to 0933 CST and the second from 1148 to 1211 CST. Both of these missions were conducted during the time Da Vinci II was moving rather slowly through an area about 20 km southwest of the center of downtown St. Louis (figure 38).

The two profiles suggest the mixed layer extended up to about 6,500 ft MSL. The ozone destruction that occurred within the surface layer during the previous night was still in evidence at 0915 CST even though the inversion had, by this time, dissipated. Examination of the two profiles reveals evidence of synthesis of ozone in the layer during the hour and a half between ascents. Over the period, there was an average increase in ozone in the layer 762-2,286 m of approximately 0.035 ppm. Vertical mixing would produce a fairly uniform ozone concentration throughout the mixed layer of about 0.145 ppm based on the 0915 CST profile. As the 1148 CST profile clearly shows, the average ozone concentration in the layers was around 0.180 ppm. These data suggest that a significant amount of ozone was generated in the layer between 0915 and 1148 CST. Precursors of ozone may have been mixed upward from the urban region; but it is also possible that they were mixed upward upstream of the urban region, horizontally transported into the region, and through horizontal mixing, affected the ozone concentration observed by Da Vinci II.

5.10 Summary and Conclusions

The analysis indicated that the surface ozone distribution during the period 1100 to 1700 CST was affected by an intense urban heat island circulation that existed during that period. It was shown that from approximately 1000 CST to 1400 CST, the highest concentration of ozone was found immediately downwind of the downtown region of St. Louis over the East St. Louis, Illinois, region and parts of north St. Louis. It was also shown that a convergence zone characterized by wind reversals and inflow associated with the urban heat island circulation was immediately downwind of the city, and in the same location where the highest concentration of ozone was found. This suggests that the convergence prevented rapid downwind transport of ozone and ozone precursors.

After 1500 CST, the heat island circulation began to dissipate. Differential cooling intensified the urban heat island, but also produced a surface-based stable layer that was responsible for the weakening and eventual

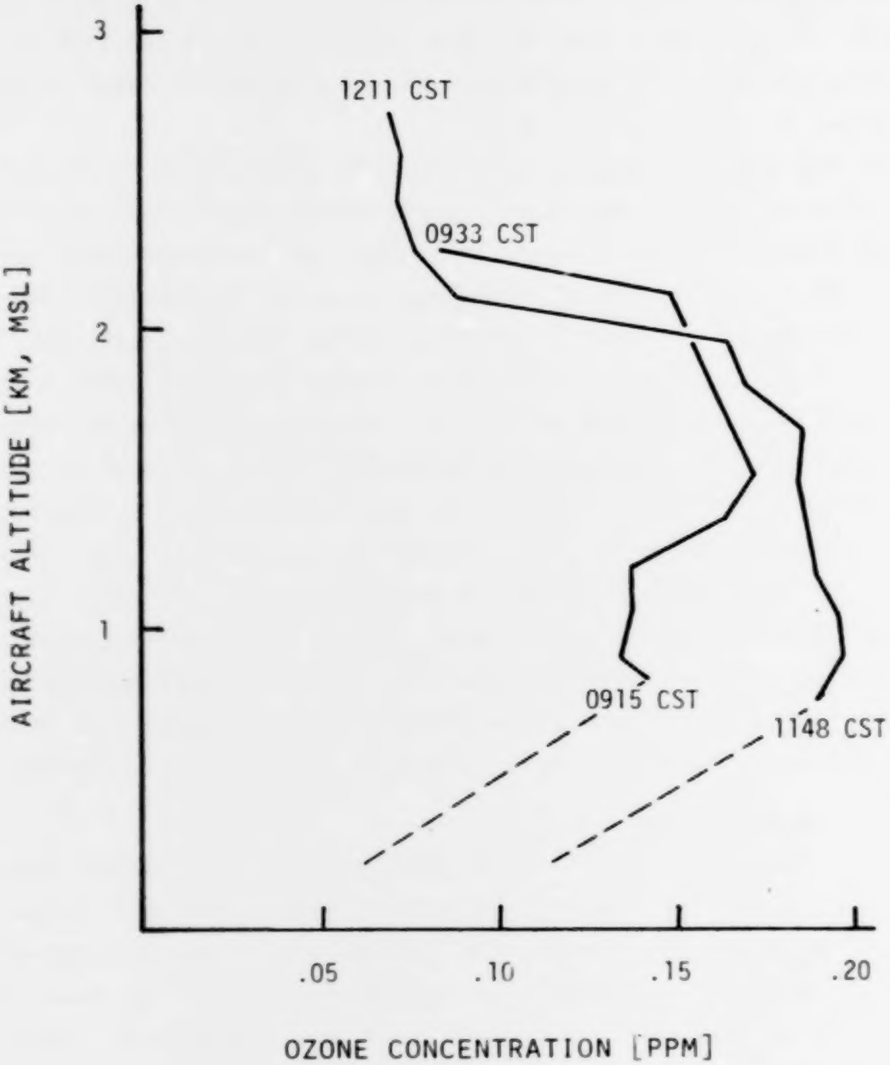

Figure 61. Vertical ozone profiles flown by a NOAA aircraft in the vicinity of the Da Vinci II gondola on the morning of 8 June 1976. Surface ozone concentrations measured beneath the gondola are also plotted and are projected up to the aircraft level.

dissipation of the urban heat island circulation. During the dissipation stage, the near-surface zone of convergence found immediately downwind of the city dissipated in stages. Initially, the region of inflow over and downwind of the city was no longer apparent. In the final stages of dissipation, no directional or speed convergence was found at the surface and the results of the primitive equation model suggested that there were no perturbations aloft. During this period the highest ozone concentration in the plume moved significantly farther downstream than previously. Dissipation of the urban heat island circulation and the accompanying convergence zone allowed the ozone precursors and ozone to be transported farther downstream.

Movement of Da Vinci II was governed by changes in the wind direction associated with synoptic weather changes and with changes in the flight level of Da Vinci II. At approximately 1000 CST, wind direction at the surface changed from northwest to southwest. From 1100 CST and until 1500 CST, Da Vinci II was located at approximately the 1,700-m level where radiosonde data indicated that the winds were from the south to southeast.

However, even if Da Vinci II could have moved eastward toward St. Louis, the results from the primitive equation model suggested that the strong divergence field over the city associated with the urban heat island circulation would not have allowed Da Vinci II to pass directly over the city. If it had moved eastward, Da Vinci II would only have come in contact with the major urban plume from the city if it passed south of the center of the city. Strong upward motion in the center of the surface-based convergence zone would have transported air pollutants aloft. Using the heat perturbation as a tracer, the results indicated that the upper plume would have moved southeastward immediately downstream of the city. The surface observations and simulated results indicated the major surface plume moved to the northeast. This suggests that the major upper plume and the major surface plume could have been as much as 90° out of phase in their respective directions of motion.

It was also noted that during the period 0900 to 1700 CST, the ozone concentration observed by Da Vinci II increased. Since Da Vinci II is a Lagrangian system, changes in the ozone concentrations measured aboard Da Vinci II can only be due to turbulent transport, synthesis, and destruction of ozone and only turbulent mixing and synthesis could account for increases in the ozone concentration. Existing vertical profiles of ozone (figure 61) indicate the region above 2.0 km to have lower concentrations of ozone than that observed at the flight level of Da Vinci II (below 2.0 km). The theory of turbulent transport indicates that under those circumstances, if there were mixing between the region above 2.0 km and the region around the flight level of Da Vinci II, ozone would be transported from the region below 2.0 km to the region above 2.0 km, and the region below 2.0 km would experience a decrease in the ozone concentration, if there were no means of compensation for the effects of this particular exchange process, which is in contrast to what was observed.

From 0800 to about 1200 CST, the ozone concentration at the surface was smaller than that at the flight level of Da Vinci II (figure 60). In this case, turbulent flux of ozone would be downward, and mixing would increase the ozone concentration at the surface at the expense of the ozone aloft; i.e., the ozone concentration at the flight level of Da Vinci II should decrease. This again is in contrast to what was observed. From about 1300 to 1700 CST, the ozone concentrations at the flight level of Da Vinci II were, for all practical purposes, equal to that at the surface. Therefore, the turbulent flux (proportional to the vertical gradient) was zero, or any mixing of ozone between the surface and the flight level of Da Vinci II could not influence the ozone concentration one way or another.

These arguments indicated that in no way could mixing of ozone account for an increase in the ozone concentrations aloft. This only leaves synthesis as the potential mechanism. Precursors may come from the city because strong vertical convection occurred during the daytime period over St. Louis, or may be mixed upward from surface sources upstream of the city and transported horizontally over the city. Furthermore, a great percentage of the ozone observed at the time of maximum ozone must be considered background ozone since 0.080 ppm ozone existed at flight level when Da Vinci II reached it.

After 1500 CST, the cooling process began. Differential cooling increased the intensity of the urban heat island. It also developed a surface-based stable layer over the city and the rural region. It was noted that a surface-based stable layer was present over the city at 1545 CST. Observed data and the results using the primitive equation model indicated that though the urban heat island intensity increased, the urban heat island circulation weakened and dissipated due to the surface-based stability, which was the overriding factor influencing the urban heat island circulation. Stability also trapped ozone-destructive agents near the surface causing the ozone concentration at the surface to decrease rapidly in the vicinity of the RTI-EML and under Da Vinci II; but the ozone concentrations aloft remain at levels above the NAAQS.

The ozone concentration observed by Da Vinci II decreased markedly in the period 1800 to 1900 CST. Though the change was great, the concentration of ozone remained at a level above the NAAQS. Da Vinci II was over the industrial regions of Alton-Wood River at this time, and it is suggested that the gondola may have lowered into the remnants of a plume from that region or there was injection of air pollutants from smoke stacks that penetrated through the surface inversion into the air mass that influenced Da Vinci II. Ozone concentration observed by Da Vinci II increased as Da Vinci II moved farther downstream, suggesting mixing with the surrounding environment.

At 2100 CST, Da Vinci II and the RTI-EML moved into a region where remnants of a major surface ozone plume from St. Louis may have been located; i.e., northeast of St. Louis. The ozone data from the RTI-EML suggested that it was in a region of elevated ozone at the surface between 2100 CST and 0100 CST. No such indications were evident in the Da Vinci II data. The radiosonde data indicated that the stability would have trapped the surface ozone plume in the layer below 200 m (the top of the inversion). In any case, the ozone data from the Da Vinci II and the RTI-EML indicated that the mixing would have been downward since the ozone concentrations aloft were greater than that in the plume at the surface. The fact that the ozone concentration in the plume was significantly lower than that observed by the RTI-EML suggests that downward mixing through a break in the inversion was responsible for the elevated ozone observed by the RTI-EML.

Analysis of the data and the simulation results indicate a complicated structure for the three-dimensional ozone distribution over the city of St. Louis. This structure may also exist for other pollutants. Because of this complex structure, changes in the synoptic weather distribution, and changes in the flight level of Da Vinci II, Da Vinci II never came in contact with the major air pollution plume emanating from the city of St. Louis when it was in the vicinity of the city.

6.0 METEOROLOGICAL ANALYSIS FOR DA VINCI II

In order to understand the atmospheric chemistry measurements made aboard Da Vinci II, it is also necessary to understand the physical environment where those measurements were made. The environment can be examined in several ways: At a given time and altitude, what is the history of the air which currently surrounds Da Vinci II? Has that air been in the St. Louis urban area? Was it affected by emissions from St. Louis? How does the understanding of the meteorological processes, as revealed by measurements, help to interpret the air chemistry measurements? These general questions have been investigated by attempting to define the three-dimensional plume emanating from St. Louis, using a trajectory analysis approach. That approach is necessary since there were no measurements normal to the airflow at Da Vinci II altitudes. Secondly, the vertical structure of the atmosphere along the flight track was examined for the effects of wind shear and atmospheric stability, which can be derived from standard measurements. The atmospheric stability of the lowest kilometer of air was examined by analyses of the acoustic sounder records made during the field program. These analyses are interpreted to assess the impact of vertical diffusion and transport upon contents of the air. Finally, in recognition of the complex behavior of the atmospheric boundary layer, a simple one-dimensional model of that layer, developed by other investigators, was tested and applied to a portion of the Da Vinci II flight.

6.1 Plume Identification

6.1.1 Introduction

The "urban plume" is an analogy to the isolated plume emanating from a point source of material into the atmosphere. The concept is that the total plume, composed of the combination of area and point sources of all types of pollutants, behaves as an isolated plume would behave. This is not totally the case because of the multiple scales of motion affecting the urban emissions. When dealing with the concept of an urban plume, it is extremely important to recognize that the transport wind speed and direction varies horizontally, vertically, and with time. Consequently, emissions from one portion of the city may take different paths than emissions from another part of the city, while air at one altitude will take a different direction and speed than the air at another altitude. Because of this inhomogeneous motion, the emissions from the urban area may spread over a large depth and width of the atmosphere and be at different locations at different altitudes although they were initially within the same column of air. Nevertheless, individual plumes within the urban plume may maintain their identity.

Da Vinci II did not operate in a totally Lagrangian mode. Soon after launch it became apparent that controlling the altitude of the balloon was far more difficult than anticipated for this particular situation. After the onset of strong convection, the balloon was permitted to seek its own altitude. Later in the day it was maneuvered to near the planned altitude. During the evening and into the next morning, Da Vinci II remained at a relatively stable altitude between 700 and 850 m. Because of the changes in altitude and the wandering path, it is difficult to appraise whether Da Vinci II was actually in the effluent of the city of St. Louis during the flight. The multiple level analysis presented attempts to reconcile the movement of Da Vinci II at various altitudes within the limits of the available data.

The objective of section 6.1 is to develop streak lines of air movement for up to 24 h at five altitudes--10, 100, 500, 1,000, and 2,000 m--beginning at 0700, 1300, 1900, and 0100 CST hours on 8-9 June for selected locations around St. Louis. This analysis will help to define the three-dimensional boundaries of the St. Louis "urban plume." These objectives were slightly modified in terms of altitudes, beginning times, and duration to make the analyses more pertinent to defining the three-dimensional plume.

6.1.2 Data Sources

Single theodolite pilot balloon (pibal) observations were taken at 17 different locations, 42 different times before and during the flight of Da Vinci II. (See figure 62 and table 15). The two mobile crews taking the observations tried to anticipate the movement of Da Vinci II and to be in the position to make a sounding when Da Vinci II moved over. These data were taken to assist with flight operation and with postflight diagnostic studies. Because of the unusual flight tract, the pibals were not always taken in the immediate vicinity of the gondola. These wind data at 50-m increments above the ground were obtained through Mr. John Bujnoch, the meteorologist for the Da Vinci II field program.

6.1.3 Method of Computation

A streak line is the instantaneous locus of points at time t_f (air par-

Table 15. Pilot balloon observations

Date	Release #	Time (CST)	Location	Map Site #
6/7/76	24	0242	Arrowhead Airport, Mo.	1
6/7/76	25	2330	Arrowhead Airport, Mo.	1
6/7/76	26	2345	Arrowhead Airport, Mo.	1
6/8/76	27	0000	Arrowhead Airport, Mo.	1
6/8/76	28	0030	Arrowhead Airport, Mo.	1
6/8/76	29	0100	Arrowhead Airport, Mo.	1
6/8/76	30	0130	Arrowhead Airport, Mo.	1
6/8/76	31	0300	Arrowhead Airport, Mo.	1
6/8/76	32	0430	Arrowhead Airport, Mo.	1
6/8/76	33	0500	Arrowhead Airport, Mo.	1
6/8/76	34	0530	Arrowhead Airport, Mo.	1
6/8/76	35	0600	Arrowhead Airport, Mo.	1
6/8/76	36	0610	Jct. I70 and Lucas and Hunt Rd.	2
6/8/76	37	0630	Arrowhead Airport, Mo.	1
6/8/76	38	0700	Arrowhead Airport, Mo.	1
6/8/76	39	0700	Jct. I70 and Lucas and Hunt Rd.	2
6/8/76	40	0730	Jct. I70 and Lucas and Hunt Rd.	2
6/8/76	41	0730	Arrowhead Airport, Mo.	1
6/8/76	42	0801	Arrowhead Airport, Mo.	1
6/8/76	43	0830	Bi State Airport, Ill.	6
6/8/76	44	1022	5 Miles South of Dupo, Ill.	5
6/8/76	45	1025	Fairview Heights, Ill.	9
6/8/76	46	1120	5 Miles South of Dupo, Ill.	5
6/8/76	47	1130	Fairview Heights, Ill.	9
6/8/76	48	1223	3 Miles North of Red Bud, Ill.	11
6/8/76	49	1300	St. Libory, Ill.	12
6/8/76	50	1600	Jct. Route 61 and P, Mo.	4
6/8/76	51	1646	Old Monroe, Mo.	7
6/8/76	52	1730	Bowling Green, Mo.	17
6/8/76	53	1730	Grafton, Ill.	8
6/8/76	54	1820	Grafton, Ill.	8
6/8/76	55	1830	Bowling Green, Mo.	17
6/8/76	56	2000	Bowling Green, Mo.	17
6/8/76	57	2020	Grafton, Ill.	8
6/8/76	58	2115	Grafton, Ill.	8
6/8/76	59	2340	Edwardsville, Ill.	10
6/9/76	60	0200	Greenville, Ill.	13
6/9/76	61	0230	Vandalia, Ill.	14
6/9/76	62	0440	Flora, Ill.	15
6/9/76	63	0620	Flora, Ill.	15
6/9/76	64	0630	Samsville, Ill.	16
6/9/76	65	0720	Flora, Ill.	15

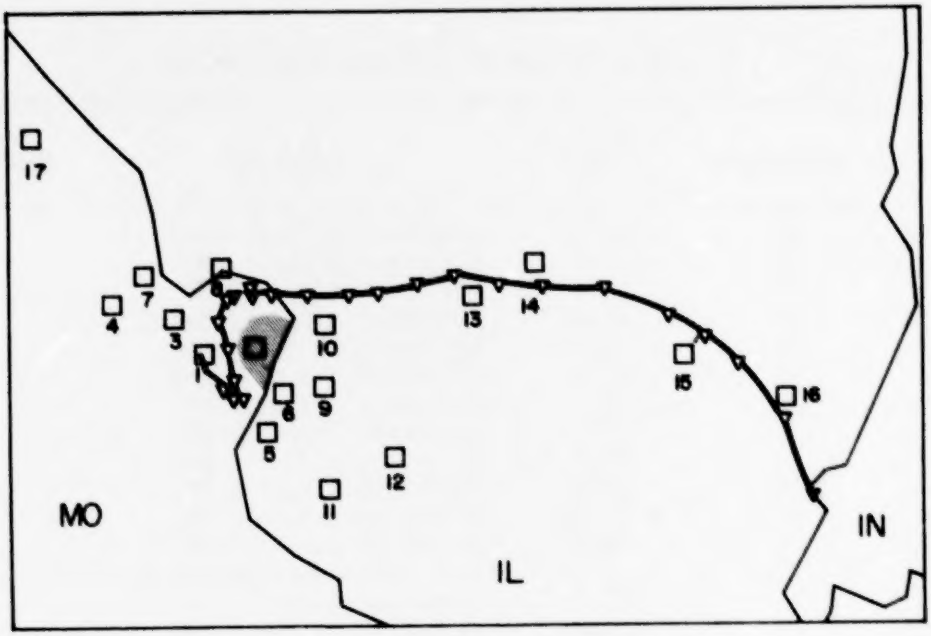
17
7
4
3
1
6
10
9
5
8
12
11
13
14
15
16
MO
IL
IN

Figure 62. Pilot balloon launch sites.

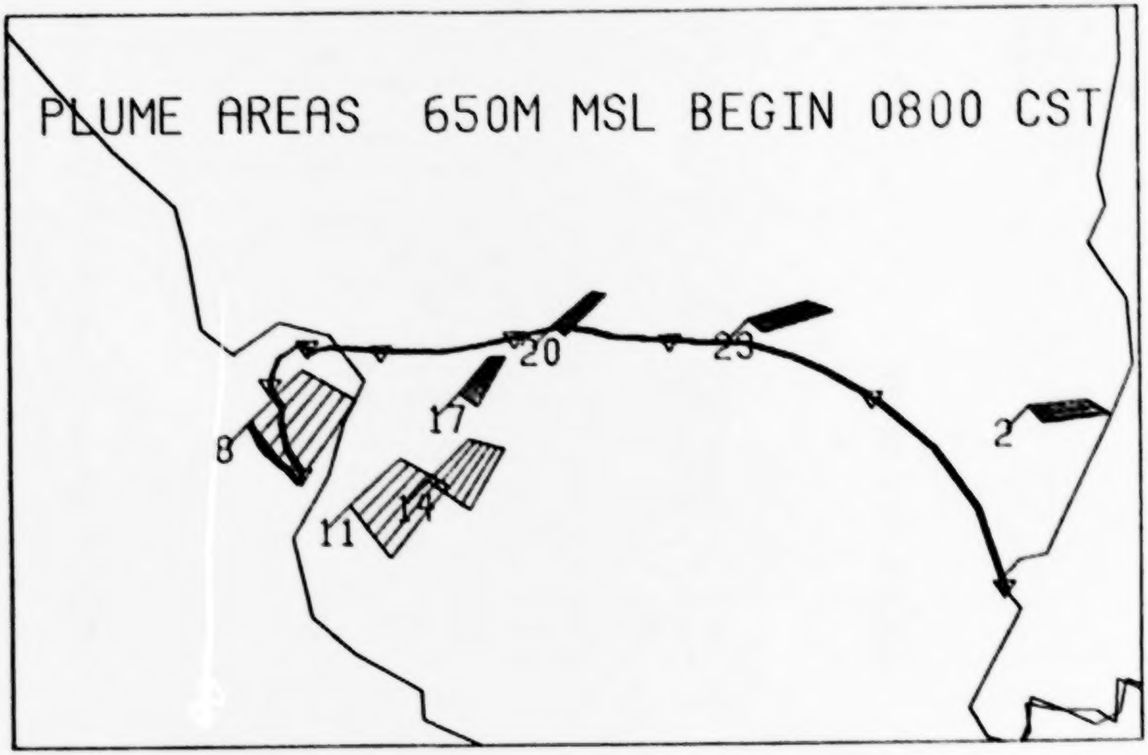
PLUME AREAS 650M MSL BEGIN 0800 CST
8
11
14
17
20
23
2

Figure 63. Typical analysis of air leaving St. Louis during Da Vinci II flight. Da Vinci II positions every third hour are shown.

cels), having passed a fixed point at some previous time. Mathematically stated, the streak line position vector, $\vec{S}$, is given by

$$\vec{S} = \int_{t_f}^{t_o} \vec{V}\, dt$$

where $\vec{V}$ is the velocity experienced by the parcel. A trajectory is the path taken by a given point (air parcel) to achieve its present position. Mathematically stated, the trajectory position vector, $\vec{T}$, is given by

$$T = \int_{t_o}^{t_f} \vec{V}\, dt$$

At a time, t_f, the position vectors of a parcel leaving the fixed point at $t = t_o$ are equal in length and opposite in direction, $\vec{T} = - \vec{S}$.

Given the type of available data, a trajectory is easier to compute than a streak line. Streak lines can be determined from the trajectories. The position of points at a given time having a common space origin but different "starting times" can be found from the trajectory analysis. The locus of those points is the streak line. In this analysis, the trajectory approach is generally taken so that the fate of the air in the St. Louis urban area at a particular time and altitude can be examined.

The trajectories at 50 m and 300 m above ground level and at 650 m, 1,000 m, and 1,400 m MSL were computed for air parcels leaving four locations approximately surrounding the metropolitan St. Louis area (see figure 63). Those locations form a rectangle that encloses many primary emission sources of the St. Louis urban area. The western and southern points coincide with the release point and southernmost points of the flight track.

The computational procedure for a trajectory began by specifying the latitude and longitude, altitude, and time of a given air parcel. For that altitude, a u and v component of the wind were interpolated to that location using the Barnes' space and time interpolation technique (appendix D). The parcel is then moved with that speed such that the latitude, $\Delta\Phi$, and longitude, $\Delta\lambda$, changes (in radians) are given by:

$$\Delta\Phi = u\Delta t/R_E$$

$$\Delta\lambda = v\Delta t/(R_E \cos \Phi)$$

where R_E is the radius of the earth (6.4×10^6 m). This procedure allows for convergence of the meridians and the change of u and v with location on the map. Throughout the computations, an Albers equal area projection on specifiable scale was used to convert from spherical to Cartesian coordinates. For each altitude, each trajectory was integrated for 18 h beginning at 0800, 1100, 1400, 1700, 2000, and 2300 CST hours, 8 June. These computations were performed using $k = 38$ km, $\nu = 1.5$ h, $\gamma = 2.0$, and $V_* = -5.0$ (parameters of Barnes' method) at a scale of 1:5,000,000. These parameters were chosen so that two or more observations would contribute to each interpolated value. Consequently, the procedure smoothed the analyses in data-rich areas to obtain analyses in data-sparce areas.

6.1.4 Results

The trajectory computations were carried out to show these features of the air flow:

1. the effects of wind shear on a plume,
2. the identification of a low altitude plume, and
3. the position of the plume relative to Da Vinci II at the altitude of Da Vinci II.

A typical interpretation of the computations is given in figure 63. The States of Missouri, Illinois, and Indiana are outlined. The Da Vinci II track is indicated by a heavy line with the hourly or three-hourly Da Vinci II position indicated by an inverted triangle. The positions of the air moving from the four locations are shown every third hour. The air that had previously been over St. Louis is indicated by the striped area. The effects of the convergence (divergence) and deformation of the wind field are easily shown as the area changes size and orientation. There was no attempt to add a diffusive spreading to the analyses, although diffusion certainly occurs. The air path is an estimate, not an exact determination of position. The errors of position are proportional to errors of the wind interpolation. If the wind speed is off by 1 m/s, a positional error of 3.6 km occurs after 1 hour. The Da Vinci II position error is known to about 2 km.[18] Thus the typical error in the parcel displacement is about equal to the expected diffusive component.

6.1.4.1 Wind Shear

The effect of wind shear upon the dispersal of the urban air at launch time is clearly shown in figure 64a. In the lower altitudes, the flow is

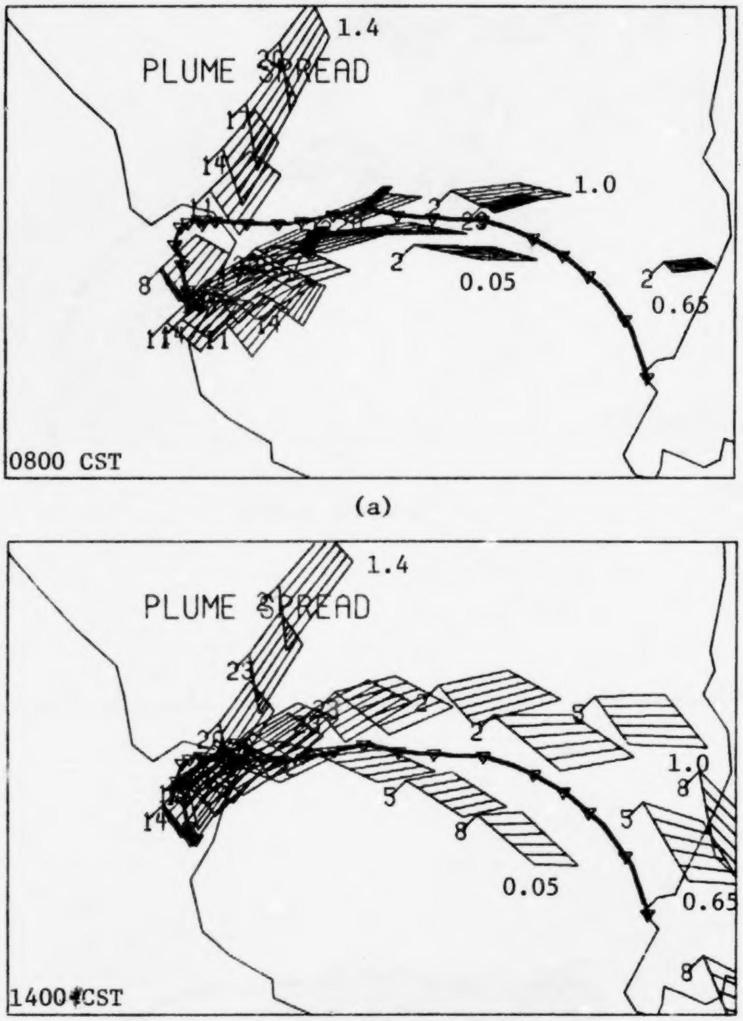
1.4
PLUME SPREAD
23
17
14
11
1.0
2
0.05
0.65
8
0800 CST
1.4
PLUME SPREAD
23
2
5
1.0
8
14
0.05
0.65
1400 CST

(a)

(b)

Figure 64. Dispersion of air, initially, over St. Louis at indicated altitudes (km) and times, resulting from wind shear.

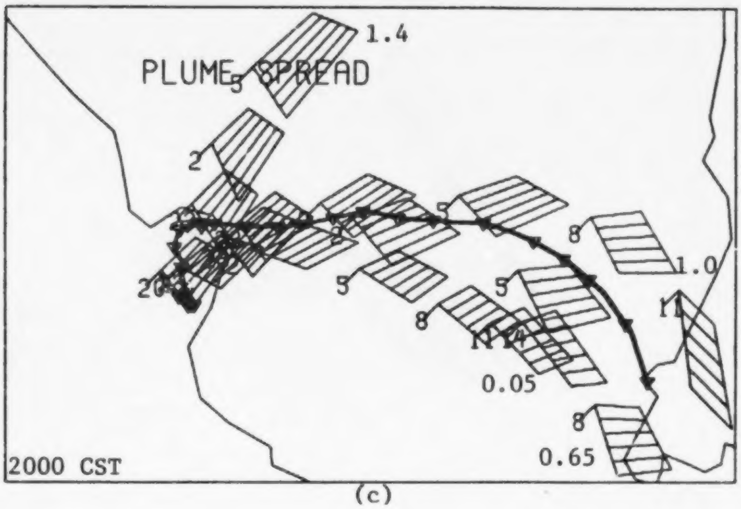
1.4
PLUME SPREAD
5
2
2
5
8
1.0
20
5
5
8
11
11
14
0.05
8
0.65
2000 CST
(c)

Figure 64. (con.)

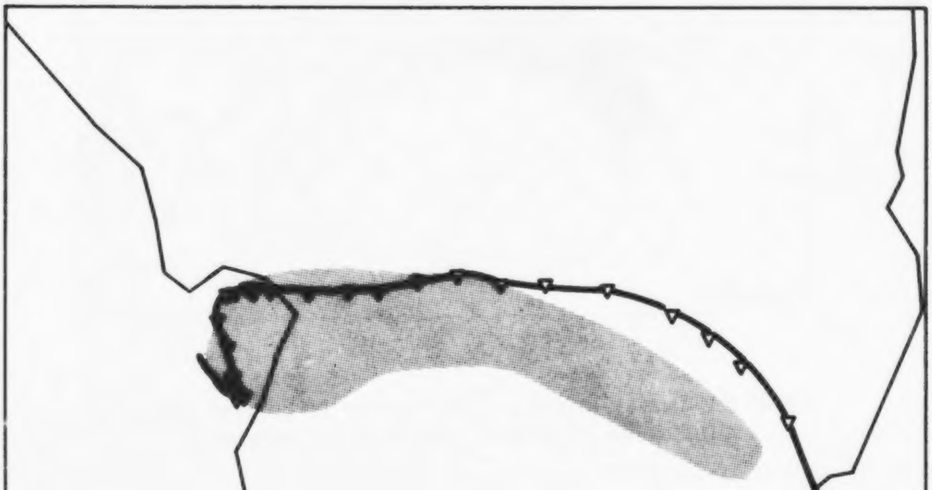

Figure 65. Movement of air at 50 m from St. Louis between 0800 and 2000 CST, 8 June 1976 and for 18 h of transport. Envelope of air at 50 m passing over St. Louis between 0800 and 2000 CST, 8 June, and transported for 18 h.

generally from the northwest, but at 1.4 km, the flow is from the southwest. At 0800, the wind speeds were low at all levels, so the directional shear was predominant in dispersing the air over St. Louis. Since the winds were disorganized, the thermally induced motion played a stronger role in the dispersion of the pollutants. The change in the thermal structure became most noticeable as the nocturnal inversion was lifted and destroyed by vertical turbulence (and diffusion) arising from surface heating. Thus the surface-based emissions were easily mixed through a deepening surface layer. The development of the nocturnal low level jet moved the 650-m air much farther than the air at 50 or 1,000 m, emphasizing the effect of wind speed shear.

The relatively weak, disorganized flow persisted into the early afternoon. The analysis of figure 64b shows the shearing and dispersion of the column of air over St. Louis at 1400 CST. By 2000 CST (figure 64c), the flow became more organized throughout the column. The air at all levels (below 1,400 m) moved toward the northeast. The column of air was not so strongly subjected to shear by direction as by speed (figure 64c).

These results agree with the cross-sectional analysis (section 6.2) and emphasize the effects of horizontal and vertical shear of the wind upon the dispersal of the St. Louis urban plume.

6.1.4.2 Low Altitude Plume

The air nearest the ground is expected to contain the highest concentration of pollutant species and affects the greatest number of people. The superposition of the trajectory analyses at 50 m beginning at 0800 CST and extending through 2000 CST of 8 June (figure 65) clearly shows the area of impact of the emissions from St. Louis. The emissions nearly saturate the area just to the east and northeast of the St. Louis urban region because of the low wind speeds during the first 8 h of the flight. The RTI-EML maintained visual contact with Da Vinci II and stayed within about 2 km of the Da Vinci II position. The RTI-EML was subjected to only a small portion of the major urban plume between 0800 and 2000 CST.

After 1600 CST, Da Vinci II began to move eastward. The RTI-EML followed closely. The emissions associated with the city moved east northeasterly until the RTI-EML appeared to encounter that air about 2300 CST and remained in it until approximately 0100 CST. Thereafter, the low altitude movement of the air was slightly slower and from a more northerly direction than the air aloft, thereby moving from the area of operations of the RTI-EML.

6.1.4.3 The Plume at Altitude

The Da Vinci II balloon-gondola system is very nearly a Lagrangian platform insofar as horizontal motion is concerned. Turbulent eddies with sizes of the order of Da Vinci II or larger will affect the balloon motion. Just after launch, Da Vinci II rose above the level of thermally induced turbulence near 500 m. As the depth of mixing increased, overtaking Da Vinci II, flight altitude became more difficult to control and maintain. During this time Da Vinci II drifted southeastward about the outskirts of the urban emissions, the ozone concentration increased with time at altitude and at the ground, and the air at 650 m moved southeastward as indicated in figure 66a.

By 1100 CST, turbulence had increased to such intensity that Da Vinci II was permitted to rise to about 2 km where the turbulence was less intense and less altitude control was required or exercised. Da Vinci II drifted northward during the next 3 h. Its relationship to the air (at 1.4 km) over St. Louis during that time is shown in figure 66b. Pilot balloon data did not extend above 1,500 m for logistical reasons; although Da Vinci II went to higher altitudes.

Over the next 3 h (1400 to 1700 CST), Da Vinci II was generally descending to 600 m. Choosing the 1 km winds as representative of the mean winds encountered during this period, the air initially over St. Louis at 1400 CST moved northeastward, roughly paralleling the Da Vinci II horizontal motion (figure 66c).

Between 1700 and 2000 CST, Da Vinci II, operating in the 800- to 500-m altitude range, began a slow eastward motion that gradually accelerated. The analysis (figure 66d) indicates that the air at 650 m over St. Louis moved northeastward, so that the midpoint of the emissions area was co-located with Da Vinci II at 2000 CST.

For the remainder of the flight, Da Vinci II stayed near 650 m and the air that was over St. Louis between 2000 and 2300 CST moved with Da Vinci II (figure 66e).

6.1.5 Interpretation

There are two apparent contradictions in this analysis. During the 1700-2000 CST period, the air at 650 m moved northeastward while Da Vinci II, near the same altitude, moved eastward. If Da Vinci II is a Lagrangian platform, then horizontal motion cannot bring the air from St. Louis into the Da Vinci II path, as the analysis indicates. Thus either Da Vinci II is non-La-

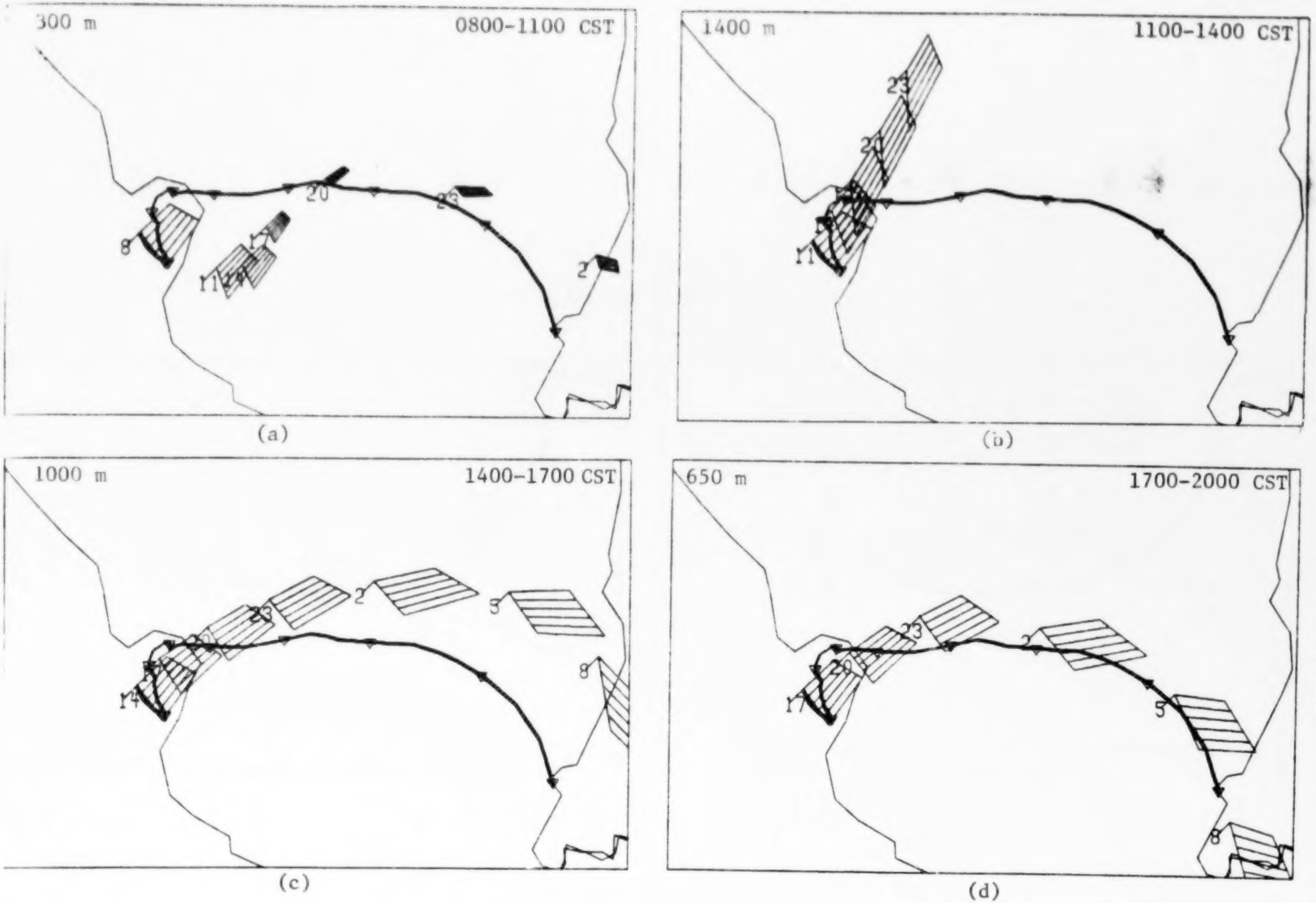
300 m
0800-1100 CST
8
11
14
17
20
23
2
(a)
1400 m
1100-1400 CST
11
14
20
23
(b)
1000 m
1400-1700 CST
14
20
23
2
5
8
(c)
650 m
1700-2000 CST
17
20
23
2
5
8
(d)

Figure 66. Motion of air initially over St. Louis at the indicated altitudes and times and near the Da Vinci II altitude. Three-hourly positions along the flight track are indicated.

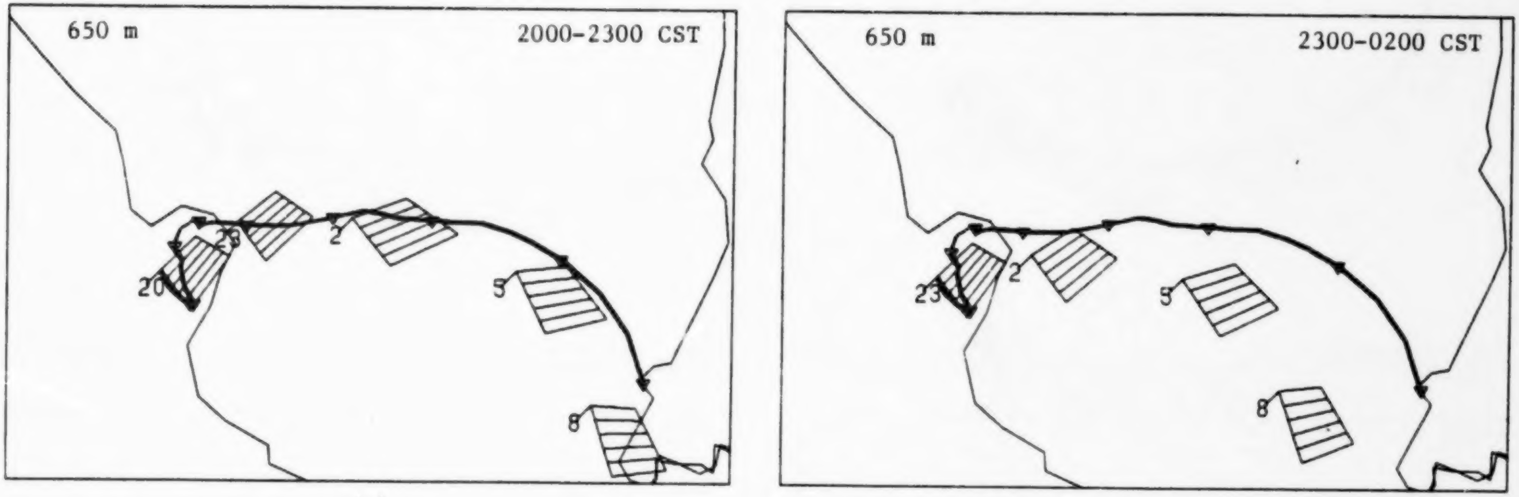
650 m
2000-2300 CST
20
23
2
5
8
650 m
2300-0200 CST
23
2
5
8

(e) (f)

Figure 66. (con.)

grangian or the analysis is incorrect, or both. Furthermore, the analysis suggests that the air at 650 m is moving about 1 m/s faster than Da Vinci II, which is very near the same altitude. This appears to contradict the Lagrangian characteristics of Da Vinci II.

The probable reason for these contradictions comes from the pilot balloon observations, their spatial and temporal variations, and the interpolation procedure for the winds. Single theodolite measurements require assuming a constant rise of the pilot balloon, so that altitude is directly proportional to time since release. Studies of sequential wind profiles with double theodolite measurements of pilot balloons show a variable rise rate and, more importantly, show that significant changes in speed and direction occur between observations.[19] Both of these factors play a role in the discrepancy. Pilot balloon observations (single theodolite) made southwest of St. Louis (RAMS site 142) and in downtown St. Louis (RAMS site 141, see figure 37) between 1800 and 2300 CST show a substantial difference in the wind direction at 650 m MSL. (Those observations were not included in the analysis.) In the downtown measurements (table 16), the wind was principally from the west-southwest while the southwest measurements indicated a southerly wind. This type of variability is difficult to incorporate into an objective analysis over several hours and tens of kilometers. Effectively, the wind data are not dense enough to describe the air motion at the same scale as Da Vinci II. The 1 m/s difference of the Da Vinci II speed and the interpolated wind speeds gives a realistic estimate of the resolution of the interpolation procedure.

The rise and fall of the altitude of Da Vinci II during the nocturnal portion of the flight may also contribute to the discrepancy betwen analysis and observation. During most of this portion of the flight, Da Vinci II was above the 650-m level and, according to the cross section analysis, experienced slower air speeds, just above the developing low level jet.

6.1.6 Conclusions

This analysis has identified the probable location of the envelope of the area containing emission from the St. Louis urban area, the St. Louis "plume," at selected times and altitudes. These analyses suggest that Da Vinci II did not encounter a significant portion of that envelope during the daytime and that Da Vinci II may have encountered some of the plume during the nighttime portion of the flight.

Table 16. Winds at 650 m MSL from RAMS pilot balloon stations

Time (CST)	Location Downtown direction/speed (m/s)	Southwest
1800	221/3.1	216/1.5
1900	254/2.3	172/1.1
2000	260/4.4	170/2.2
2100	253/4.1	183/3.5
2300	249/4.2	194/4.5

There is insufficient evidence from this portion of the analysis to identify the cause of the increase in surface layer ozone concentration during the period 2200 to 0100 CST.

6.2 Cross Section Analyses

6.2.1 Introduction

In the lower atmosphere, two predominant processes affect the vertical distribution of atmospheric variables and in particular the distribution of pollutants near the ground. A continual downward flux of momentum replaces the momentum lost to the ground by friction. This process results in a vertical profile of the wind velocity that generally increases in speed and changes direction as altitude increases, in the familiar Ekman spiral. The heat flux at the air-ground interface adds or extracts heat from the atmosphere resulting from solar heating or radiational cooling. This heat transfer near the ground plays an important role in the scaling of atmospheric turbulence and thus the rate at which the momentum and heat are mixed within the lower atmosphere.

By scaling variables, it is possible to show that vertical diffusion of materials is more significant to the time rate of change of concentration than is the horizontal diffusion. This is especially true considering a Lagrangian type measurement platform the size of Da Vinci II.

Evidence is mounting that ozone, generated during the day and distributed through the mixed layer, is transported long distances at night aloft, separated from destruction by ground contact or destructive agents at ground level by a nocturnal radiative inversion. Concurrently, surface-based emissions of precursors into the radiative inversion layer destroy the ozone there and tend to accumulate precursors. As the solar insolation increases the following morning, precursors are available to produce ozone in that lowest layer. When the inversion layer is raised and dissipated by the insolation, there is an abundant reservoir of ozone aloft available to mix downward, giving a rapid increase in surface concentrations. The observed concentrations aloft are not significantly depleted by mixing the shallow "below inversion" air with the much deeper reservoir aloft. Since urban areas such as St. Louis are the principal sources of anthropogenic ozone precursor materials, it is reasonable to expect that a similar phenomenon might be observed downwind of the St. Louis area. Da Vinci II monitored the ozone at altitude, the RAMS stations monitored ozone continuously at fixed ground stations, and the RTI-EML measured ozone near the ground while following the balloon. Other sections of this report discuss those data in some detail. The combination of the Da Vinci II data at altitude and near the ground support the idea of the separated layers of ozone at night. The data also show some interesting discrepancies from the scenario outlined above. Therefore, in this section the role of the vertical structure of the lower atmosphere and its diurnal changes upon the measured concentrations of ozone will be examined.

6.2.2 Analysis Approach

The vertical flux of heat in the St. Louis area is related to time of day. Therefore, this analytical approach quantifies the vertical structure of the atmosphere within the column of air containing Da Vinci II at hourly increments of time along the path of Da Vinci II. Since Da Vinci II did not move at a constant speed, the distance traveled in these intervals varied substantially. The position of Da Vinci II at each hour was interpolated from RTI's time and position data.

The set of 42 pilot balloon observations used to compute the analyses of section 6.1, a special set of six-hourly upper air observations at the regular rawinsonde stations of the National Weather Service, and a set of acoustic sounder data prepared from operations of Dr. E. Miller of Argonne National Laboratory were the principal sources of data for this analysis.

6.2.2.1 Analysis of Winds Aloft

Pilot balloon data were interpolated to 50-m increments above the ground along the flight track for each hour during the Da Vinci II flight using

Barnes' technique. These data are displayed as wind vectors in figure 67. The wind vectors are drawn using the standard meteorological connotation, i.e., showing the direction from which the wind is blowing. The speed is indicated by the length of the vector. North is at the top of the figure.

During the first hour after launch (0800 CST), the winds in the lowest 300 m increased in speed before decreasing wind direction turned slightly more northerly through the first kilometer. Thereafter, the winds became quite light, turning to a southwesterly flow. Over the next few hours, wind speeds at lower levels continued to decrease while remaining northwesterly, whereas winds farther aloft became a little stronger from the southwest. Three hours after launch, Da Vinci II ascended to an altitude well above the operation level of the pilot balloon data. During the time that Da Vinci II was aloft, winds below it were quite light and variable.

About 9 h after launch (1700 CST), the wind flow throughout the entire area became more organized. The winds, initially light and from the southwest, began to increase in speed from the ground upward. Winds near the very top of the layer (1.5 km) showed a little more southerly flow. As nighttime progressed, the winds in the lower altitudes increased in speed and became more westerly, the greatest increases in speed occurring near 250 to 300 m above the ground. With the advent of morning (21 h after launch), the lower level winds continued to turn to a northwesterly and then a northerly flow throughout the first kilometer. These interpolations, of course, agree quantitatively with the trajectory analyses and also with the movement of the balloon, since the same data set and interpolations were used.

The air flow was disorganized for the first 8 to 10 h of the flight because of the stagnant anticyclone centered in the St. Louis area. Toward the later part of the day, the surface high pressure system drifted southwestward, slightly increasing the pressure gradient and developing the flow near the ground. This turning of the wind and the increase in wind speeds overnight accompanied a redevelopment of a low level jet just above the nocturnal inversion layer. This jet was clearly evident on the night before the launch and the remnants of it were apparent in the first 2 h of the Da Vinci II flight. At 2300 CST (15 h after launch), a substantial increase in wind speeds occurred in the lowest 150 m; a minimum in the wind speed occurred about 19 h after launch (0300); and a wind speed increase and wind direction shift (more northwesterly) occurred during the remainder of the flight. This change of the

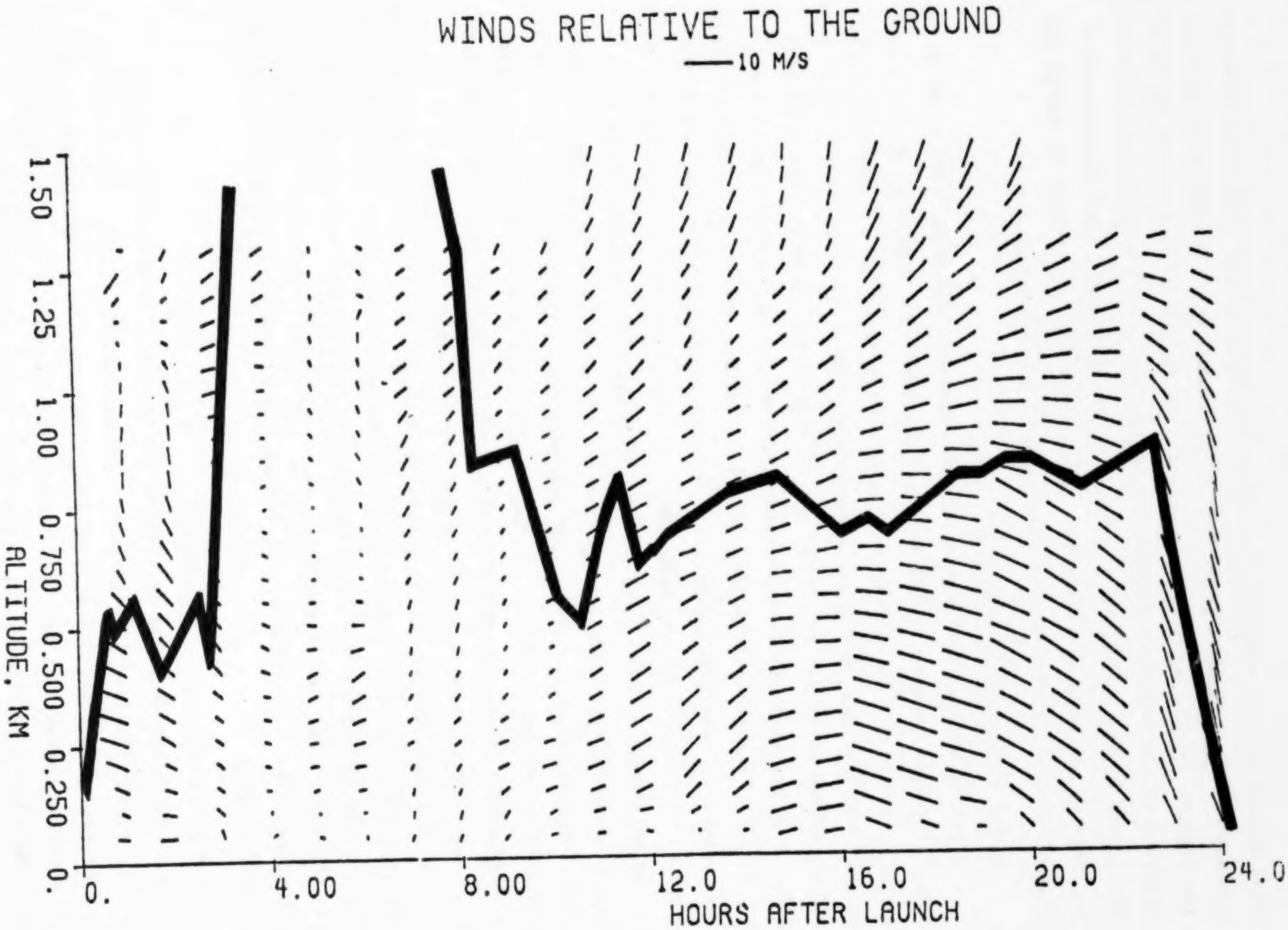

Figure 67. Wind vectors aloft along Da Vinci II's track, from pilot balloon observations.

wind characteristic suggests that there may have been an additional momentum transferred down to the ground near midnight and later in the early morning of the flight. A similar trend in surface wind speeds and directions was also observed at Terre Haute, Indiana, Champaign, Illinois, and Decatur, Illinois, during the nighttime and early morning hours of 9 June. The coincidence of increase in the wind speed and the higher ozone concentrations at the ground suggest that a downward mixing of ozone-rich air occurred.

6.2.2.2 Rawinsonde Analyses

A set of special rawinsonde observations were taken in support of the Da Vinci II flight program at the National Weather Service Offices at the times given in table 17. These data were made available to RTI as computer printouts of the altitude, pressure, temperature, dew point temperature, wind speed and direction at 50-mb increments and at significant levels. The data were ordered by altitude and interpolated to 100-m increments from the ground to 3.5 km MSL. The rawinsonde data offers a distinct advantage in understanding the dynamics of the lower atmosphere because air temperature and humidity are measured in addition to the wind speed and direction and data are available to 3.5 km or higher. Time-altitude cross sections were developed using the Barnes' technique outlined in appendix D. These analyses were done for wind speed, regardless of direction, and for potential temperature, θ. Since θ is conserved in adiabatic processes, the vertical gradient of θ is proportional to atmospheric stability, and atmospheric stable layers are easily identified. It is superior to temperature as an analysis variable.

The dominant factor in the resulting analyses was the set of observations made at Salem, Illinois, approximately 75 km east of St. Louis and about 20 km south of the midnight position of Da Vinci II. Since the data are more sparse than the pibal data, the analyses are not sensitive to short-term or local influences. These analyses do not include rawinsonde data taken in support of the RAMS program.

6.2.2.2.1 Potential Temperature

The time-altitude cross section of the potential temperature along Da Vinci II's path is given in figure 68. Throughout the flight, a very stable layer persisted just below 3 km resulting from atmospheric subsidence in the high pressure system. It had been evident for the past 3 days in the St. Louis area. This layer represents the upper limit of any vertical motion that may have occurred in the planetary boundary layer during that time.

Table 17. Rawinsonde data used in analyses

	Time, CST				
	June 8			June 9	
Station	0600	1200	1800	0000	0600
Omaha, Nebr.	x	x	x	x	x
Monett, Mo.	x	x	x	x	N/A
Topeka, Kans.	x	x	x	x	N/A
Peoria, Ill.	x	x	x	x	x
Salem, Ill.	x	x	x	x	x
Flint, Mich.	x	N/A	x	N/A	x
Nashville, Tenn.	N/A	x	N/A	x	N/A

N/A: Not available.

On the morning of the flight, the analysis of figure 68 shows static stability increasing from the ground upward. The destabilization of the lower 1.5 to 2.0 km of air occurs by midday, as a result of the solar heating. The destabilization was enhanced by very weak wind patterns within the lower atmosphere. Without a wind shear to transport momentum downward, the surface heat flux plays a dominant role in the vertical transport of heat and momentum. Thus, during the afternoon, it appears that a free convection regime could easily be established. In that circumstance the convection motion is predominant and vertical mixing takes place very quickly and freely over a wide area. The analysis suggests that the lowest 2.0 to 2.5 km are well mixed.

By evening a superadiabatic layer is indicated near 1.5 km. Over the duration of the night, the feature tends to rise to higher altitudes, retaining its tendency for instability. At these altitudes at night, the atmosphere loses or gains heat by radiation or advection rather than from surface processes. It is difficult to envision the physical processes that would maintain a superadiabatic layer in the absence of a heat source. Thus, since the air was unstable in the late afternoon, the air aloft remained very nearly unstable with a potential for good vertical mixing, but lacked the impetus to initiate the exchange.

Significant radiational cooling began at the ground at about 1700 CST. This cooling continued into the night, giving a shallow, stable inversion

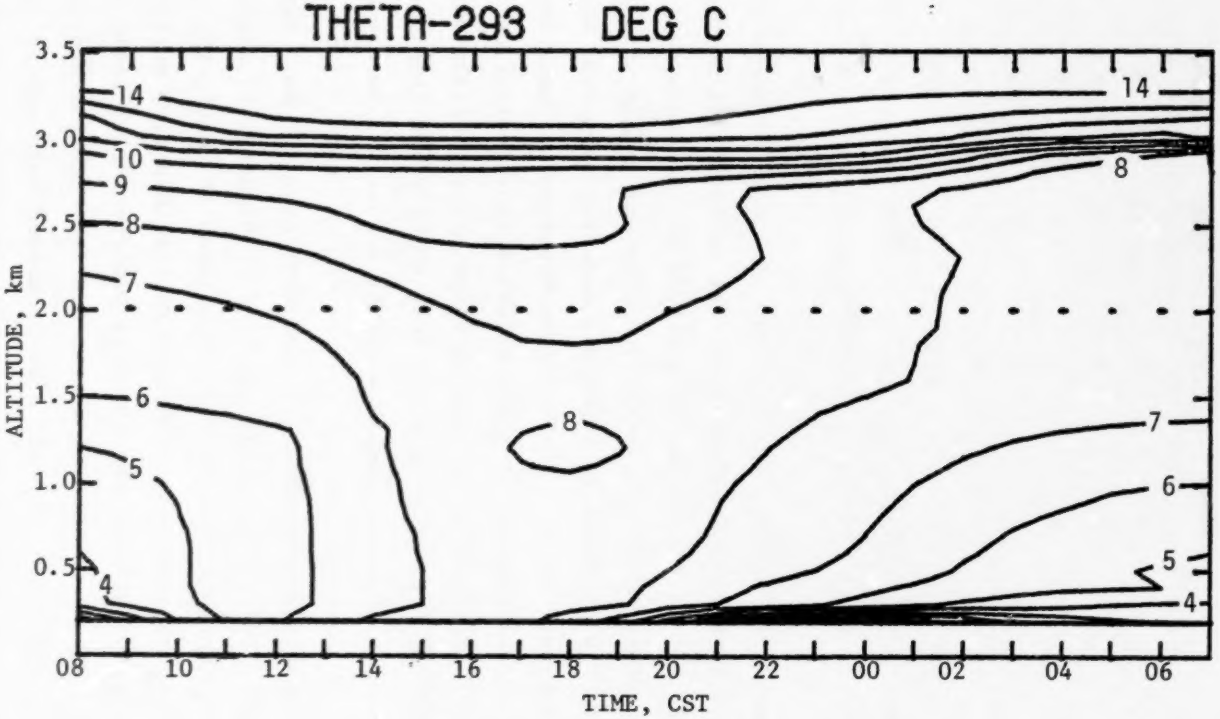

Figure 68. Cross section of potential temperature along Da Vinci II path (from rawinsonde data).

layer by midnight. Thereafter, the stability of that lower layer tended to decrease until by morning (0600 CST), a warming process was clearly taking place. By 0800 CST of 9 June, the vertical structure of the air was similar to but slightly less stable than that observed the morning before.

This analysis of potential temperature is further substantiated by the rawinsonde observations from the St. Louis area and from the soundings at Salem, Illinois. Both sets of data indicate a moist layer of air having a slowly decreasing water vapor mixing ratio from the ground to approximately 2 km throughout the flight. Above 2 km, the mixing ratio decreased up to the subsidence inversion at 2.9 km and decreased more rapidly in the superior air. The aircraft vertical profiles, discussed in section 4.3.5.1, also indicate that the upper extent of the high ozone concentration was near 2 km with a substantial decrease above. Vertical mixing of surface effluents effectively extended up to that level but did not extend all the way to the subsidence inversion about 500 to 800 m above. Assuming that the oxidant and the water vapor result from emissions near the ground and that they are susceptible to the same transport processes, the effective mixing depth of the atmosphere during the daytime must have been 2.0 to 2.5 km.

6.2.2.2.2 Wind Speeds

The vertical distribution of wind speeds as interpolated to the hourly positions of Da Vinci II through the first 3.5 km of the atmosphere from the rawinsonde data is shown in figure 69. The lack of detail in wind speeds in this analysis is compensated for by the added depth of the atmosphere, revealing further insight into the behavior of the winds during the day. This analysis clearly shows that the disorganized, low wind speed pattern in the lower 1.5 km extends throughout the depth of the atmospheric boundary layer. The wind speeds reached their minimum just below the upper level inversion layer. After sunset (2000 CST), a low level jet began to form near 500 m MSL (300 m above ground), just above the surface radiative inversion. The jet built in intensity, reaching a maximum speed near 0100 CST. A secondary wind maximum that occurred in the 2.0- to 2.5-km layer was not related to the lower level jet but resulted from a slight southerly shift of the high pressure pattern at 850 mb, increasing the pressure gradient aloft.

6.2.2.3 Acoustic Sounder

A pair of acoustic sounders were operated by Dr. Ed Miller of Argonne

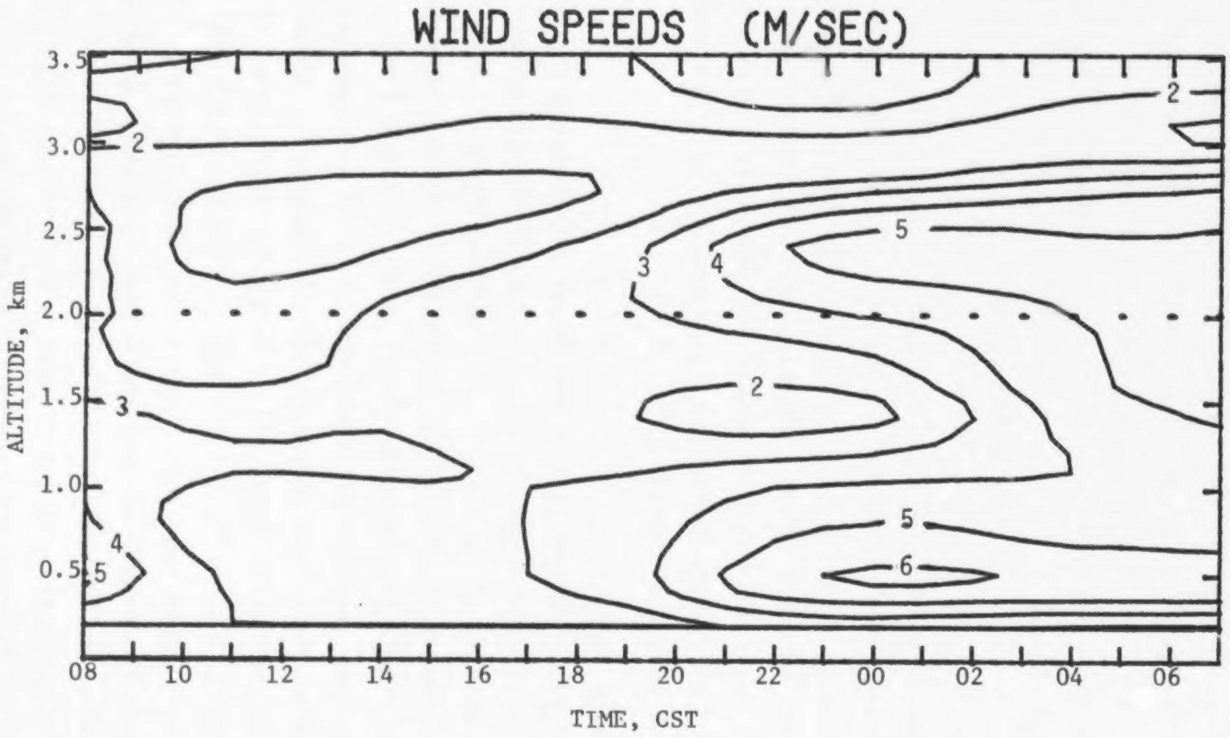

Figure 69. Cross section of wind speed along Da Vinci II path (from rawinsonde data).

National Laboratory in support of the Da Vinci II program. These mobile units were operated in a leap-frog fashion, sampling the Da Vinci II environment. An acoustic sounder operates on the principle of backscattering of a transmitted sound pulse by a change in the temperature of the atmosphere. The pulse of sound is transmitted vertically approximately every 20 s. Reflected sound energies are then recorded as a function of time, which is translatable to altitude. Figure 26 was prepared by Dr. Miller and given to RTI as preliminary data. Since there have been no other data forthcoming, it was assumed that this portrayal of the data has become final. RTI's interpretation follows.

During the morning hours preceding and shortly after launch, the acoustic sounder showed a stable low level inversion layer or layers in the lowest 200 m. The stable layer was gradually rising and weakening, until by 0920 CST the low level inversion had dissipated. Thereafter, until approximately 1730 CST, the record indicates numerous thermals.

During the early evening a stable layer developed and intensified. At 2300 CST the thin, wavy inversion layer appeared only in the first 50 m above the ground. This is a smaller thickness than was indicated in figure 68. By 0200 CST the layer was still less than 100 m thick; by 0300 to 0400, a little thicker and perhaps a little more intense inversion layer had developed. At 0530 CST, wave motion on the top of the inversion was strongly indicated, which suggests that destabilization was beginning and would probably persist. By 0700 CST, the weaker but thicker inversion layer was indicated.

6.2.3 Conclusions

The morning breakup of the inversion layer on 8 June 1976 was completed by about 0930 CST. A free convection regime seemed to have developed since the winds were light and disorganized. This combination of events eventually produced a well-mixed layer to about 2.2 km where the air began to stabilize, limiting the vertical mixing.

There seemed to be a breakdown in the low level, nocturnal stability on the night following the Da Vinci II launch. The acoustic sounder record and the development of the low level jet seemed to confirm the event. Thus it appears that during the period of 2300 to 0100 CST, there might have been a breakdown in the low level inversion, permitting the ozone-rich air from aloft to be brought to the ground.

6.3 Modeling Atmospheric Chemistry and Physics

6.3.1 Need for Modeling

The assimilation of meteorological and air chemistry data into a cohesive picture of the events of the Da Vinci II flight requires the analyst(s) to incorporate the ongoing physical processes and their qualitative contribution to "explain" the various nuances of the data. Both the air chemistry and the atmospheric physics are time- and space-dependent processes. Some proceed rapidly; others proceed slowly. Quantitative rather than qualitative results give far more insight into the processes, but are far more difficult to attain.

The Da Vinci II program has an extensive data base in both atmospheric chemistry and physics to support a quantitative analysis. As good as the data base may be, it is still insufficient to provide the detailed relationships among the variables. The program is undersampled and unable to fully describe the ongoing atmospheric processes. While it is not a panacea, a model of the atmospheric chemistry and physics can lend insight into pollutant transport, diffusion, and interaction. Atmospheric modeling of emissions, transport, and diffusion in urban areas into nonurban areas is not well developed at the present time. Such models also require an extensive emissions inventory, including a mobile source and fixed sources throughout the urban area. A steady, predictable wind field is usually required to simplify the model. The Da Vinci II program and the St. Louis area do not lend themselves to application of the large photochemical models. The analysis of the cross section data indicates significant vertical shear within the mixed layer and thus does not fit the other models. The models are incompatible with the space scale of the Da Vinci II flight. It soon became apparent that it would be necessary to adapt a simple, existing meteorological model and couple it with a simplified existing air chemistry model. In reality, neither model is simple. RTI's experience with an air chemistry model to simulate smog chamber studies appeared a proper choice for the air chemistry model. The one-dimensional planetary boundary layer (PBL) model of Busch, Chang, and Anthes[19] was chosen to simulate the atmospheric physics (e.g., meteorological conditions), since it incorporated the surface heating and cooling, friction, and a driving geostrophic wind in a nonactuating environment, which are the principal factors of the Da Vinci II environment.

6.3.2 Results of Model Application

The model was applied to the data of the morning of the Da Vinci II flight. The vertical profiles of u, v, and Θ from the cross section analysis at 0800 CST were used to initialize the meteorological fields at 100-m vertical increments. Hourly temperature observations at Lambert Field, St. Louis, were used to compute the surface heat flux. Geostrophic winds of 190° @ 2.0 m/s at the top of the model (3,210 m) and 325° @ 0.8 m/s at the ground were used. An inert material ($\Gamma = 0$) with constant concentration (C=1) throughout the atmosphere with a constant source ($\overline{w'c'} = 0.05$) was modeled, using 5-min time steps. A test run of 4 h was attempted. The results are shown in figure 70.

The test run was successful until about 1100 CST (see figure 70). Between 1000 and 1100 CST, the values of L became extremely small ($\sim$-0.1) because the friction velocity u_{*_0} was very small, and the surface heat flux was large but not excessive. The domination of heat flux over surface friction characterizes the free convection mode of the atmosphere. The atmospheric scaling used in the model does not apply to free convection, thereby invalidating further modeling results of the daytime convection. The small values of L, arising from the weak geostrophic flow, give large, negative values of z/L, which resulted in large eddy diffusivities ($K_h \sim 10^5$ m^2/s) in the mixed layer. Such diffusivities are encountered only at a highly turbulent, convective atmosphere.

Before the onset of the free convection, the boundary layer behaved as expected. The slightly stable layer gradually became adiabatic. The mixing depth increased with time. Very little change was observed in the concentration profile since it was initially uniform.

These model results agree very well with the evidence gathered and experiences of the Da Vinci II flight. The time of onset of the free convection corresponds to the acoustic sounder records, the cross section analysis, and the reasons for letting the balloon go to higher altitudes during the daytime.

Future simulations of the Da Vinci II PBL with the current model must be restricted to the late afternoon and nocturnal phases of the flight to avoid the free convection situation. Considerations of nonuniform profiles of materials and their elementary interactions should help the understanding of the measurements made during the flight. Coupling of the atmospheric physics model with the air chemistry model awaits further development work.

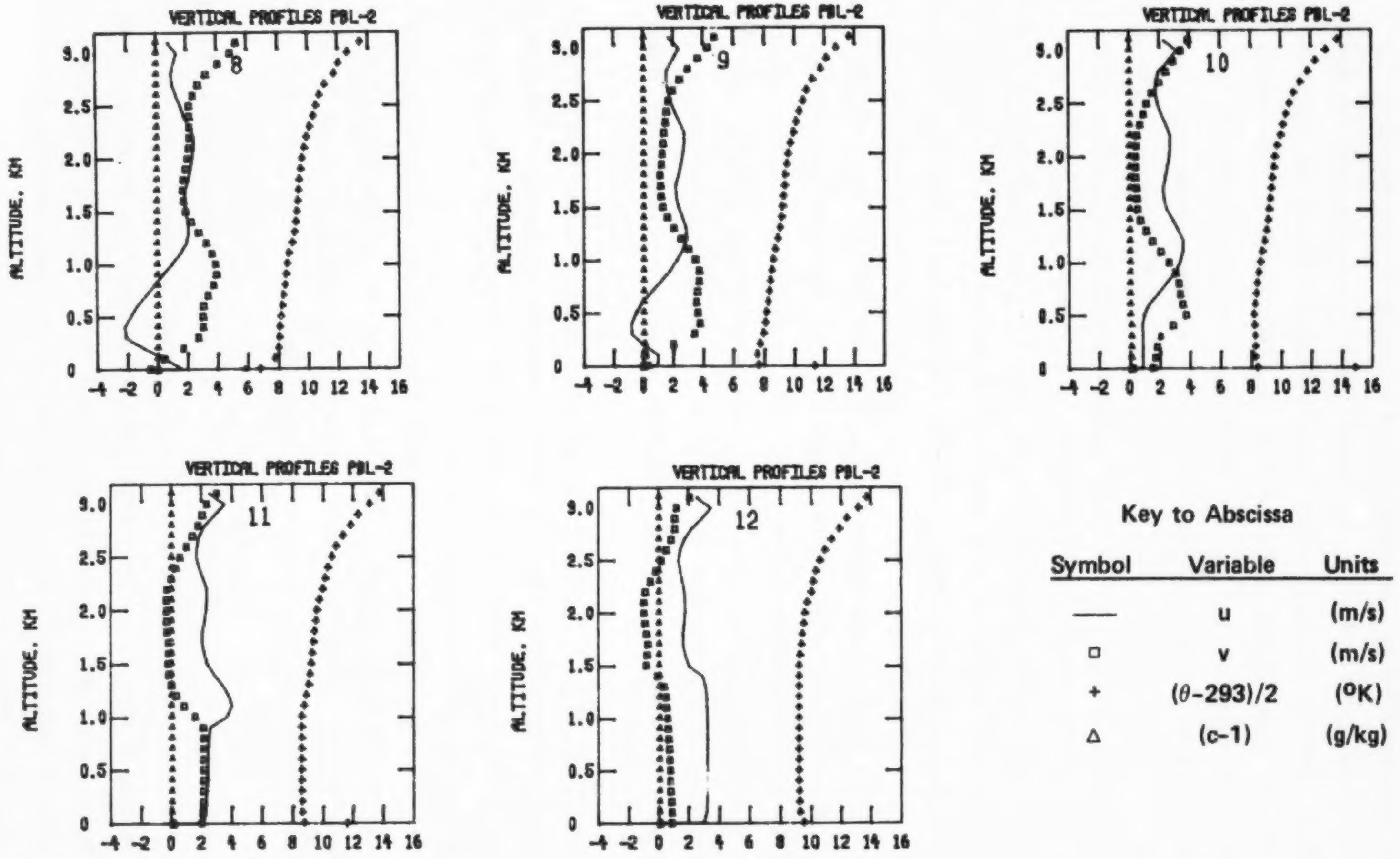

Key to Abscissa

Symbol	Variable	Units
—	u	(m/s)
□	v	(m/s)
+	$(\theta-293)/2$	(°K)
△	(c-1)	(g/kg)

Figure 70. Vertical profiles of u, v, θ, and c at indicated times from PBL model simulation of 8 June.

7.0 PRINCIPAL FINDINGS AND CONCLUSIONS

7.1 Principal Findings

Selected data collected by various participants during the flight of Da Vinci II were consolidated, summarized, and segmented into general subject areas for analysis and interpretation. These subject areas include atmospheric chemistry and meteorological analyses. Data were analyzed and interpreted according to the objectives for each analysis and have been incorporated to combine both a chemical and meteorological interpretation of results. Principal findings from these studies are summarized below.

1. Conditions of high ozone concentrations persisted aloft for the study period. These conditions were widespread and extended for several hundred kilometers. Air containing high concentrations of ozone, approximately 0.11 ppm, was being transported into the study area on the flight day.
2. Da Vinci II was launched into air that had an immediate fetch over a nonurban area, although the total experiment was conducted within a stagnant, polluted, high-pressure system. Air parcel trajectories suggest that Da Vinci II was launched into air that 72 h earlier had been in eastern Kentucky and the Ohio Valley.
3. Da Vinci II did not travel in the heart of the St. Louis urban plume as defined by ozone concentrations. Examination of the hydrocarbon concentrations sampled on Da Vinci II suggests that the flight occurred in air characteristic of suburban-to-nonurban areas.
4. The ozone concentration at the flight level (700 m) of Da Vinci II was greater than 0.08 ppm when Da Vinci II reached that altitude. Since it reached that level prior to 1030 CST when deep convective mixing was experienced in the urban boundary layer, a major portion of the upper level ozone concentration must have come from sources other than St. Louis on the morning of 8 June.
5. During the morning, ground-level ozone concentrations were less than concentrations aloft. The observed increase of ozone concentrations aloft, therefore, could not have resulted from upward mixing of ozone from the ground, but was probably due to tropospheric photochemical synthesis.
6. Vertical profiles show substantial ozone concentrations aloft between 762 and 1,981 m (2,500-6,500 ft) on the morning of 8 June with a sharp decline in ozone concentration above 2,133 m (7,000 ft). Mean ozone concentrations between 2,133 and 2,743 m (7,000-9,000 ft) were less than those measured between 762 and 1,981 m (2,500-6,500 ft) by a factor of 2.4. These observations suggest that stratospheric intrusion was not responsible for the elevated ozone concentrations that existed aloft on 8 June.
7. The impact of anthropogenic emissions on ambient concentrations within the urban area is variable and depends strongly on the time

of day. Ground-level CO and NO_x were diluted by factors of 5 to 7 between the morning and afternoon. This behavior probably reflects the significant increase in the mixed volume that occurs with the dissipation of the surface-based radiation inversion and the establishment of well mixed conditions.

8. As vertically well mixed conditions were established between 0500 and 1100 CST, both downward mixing and photochemical synthesis contributed to the observed increase in ground level ozone concentration. This ground level increase exceeded that aloft by a factor of approximately two.

9. Between 1100 and 1700 CST on flight day, a near zero ozone concentration gradient existed from the ground into the mixed layer. This is based, to a large extent, on the close comparison of ozone concentrations determined on Da Vinci II with those beneath Da Vinci II at ground level.

10. After well mixed conditions were established and until the nocturnal inversion began to form, the increases in ozone concentrations aloft and at ground level were approximately equal and probably resulted from photochemical synthesis.

11. The airflow in the immediate vicinity of St. Louis on 8 June was governed by the synoptic scale flow and an intense circulation produced by the urban heat island. Da Vinci II responded to both of these scales of motion.

12. A major air pollution plume (defined by the ozone distribution) was found at the surface. The maximum ozone concentration in this plume was immediately downstream (within 5 km) of the center of downtown St. Louis between 1000 and 1500 CST. Simulation results (meteorological model) suggest that if a plume existed in the upper portions of the boundary layer, it would have moved in a different direction than the surface plume.

13. Between 1000 and 1500 CST, the maximum ozone concentration in the major air pollution plume at the surface (as defined by ozone distribution) was found in a region where there was a zone of horizontal convergence in the wind field associated with the urban heat island circulation.

14. After 1500 CST, the maximum ozone concentration in the air pollution plume (as defined by the ozone distribution) moved farther downstream (greater than 15 km) when the heat island circulation and its accompanying convergence zone was dissipating.

15. Within the layer that had been well mixed during the daytime, stratification which occurred at night with the establishment of the nocturnal radiation inversion resulted in the formation of two regimes of ozone concentrations. Ozone concentrations within the radiation inversion were much reduced compared to levels above it. This is presumably due to destruction by surface deposition and reaction with ozone-destructive agents emitted into and trapped within the inversion.

16. Ozone data obtained aboard Da Vinci II were used to calculate a nighttime ozone half-life of 116 h. Examination of available hydro-

carbon precursor data obtained aboard Da Vinci II suggests that concentrations of ozone destructive and other HC species aloft were low during the flight. The dark phase half-life of ozone under the conditions of presumed low levels of precursors is sufficient to allow transport of ozone from an urban area overnight to another area without significant diminishment due to decay.

17. Penetration through the nocturnal radiation inversion resulted in the mixing of high levels of ozone to the ground and precursors from the ground to aloft. This was suggested by the sharp nighttime ozone peaks and the associated declines of NO_x and CO observed at selected ground stations. This phenomenon occurred frequently in May and June and was observed at ground stations covering an area of several hundred kilometers. It may also provide mechanisms for increasing nighttime ozone destruction aloft and for enhancing early morning ozone synthesis by distributing ozone precursors aloft above the inversion before sunrise.

18. The balloon may have entered an air parcel that was enriched in hydrocarbons after 2100 CST on 8 June and traveled within this parcel for the remainder of the flight.

19. Sharp, short-term reductions in ozone concentrations occurred aloft during the nighttime portion of the flight and were coincident with increases in SO_2 concentration. Both SO_2 and NO_x are emitted by power plants. Although NO_x was not measured in this study, the observed ozone behavior is probably the result of destruction by reaction with NO_x.

20. The influence of ozone precursors emitted in the urban area was manifested at ground level by ozone concentration enhancement over nonurban concentrations. The magnitude of this enhancement was 0.06 to 0.11 ppm. Both the buildup and movement of the region of enhanced ozone were documented, although detailed definition of the extent and magnitude were severely hampered by the lack of a comprehensive supporting aircraft measurement program.

21. High ozone concentrations measured aloft aboard Da Vinci II on the morning of 9 June in Southwestern Indiana are attributed to long distance transport of ozone. High ozone at the surface is influenced by synthesis and mixing downward of the ozone aloft in the morning. After a well-mixed layer is established, changes resulting from mixing are minimized. Further increases in ozone concentration at the surface can be attributed to synthesis.

22. The use of a Lagrangian system to document ozone transport and address atmospheric chemistry problems has been shown to be feasible. Interpretation of these data are severely limited, however, unless supporting data that define vertical and horizontal pollutant distributions are also available.

7.2 Conclusions

The conclusions listed below are derived from the analysis of the Da Vinci II data relative to the objectives of this project.

1. The synoptic wind flow pattern as modified locally by the urban heat island circulation prevented Da Vinci II from passing over the St. Louis urban area and taking up a position in the urban plume.
2. During the nocturnal phase of the flight, changes in ozone concentrations observed aboard Da Vinci II could not be directly attributed to the downtown St. Louis urban plume.
3. General meteorological conditions--a subsidence inversion aloft and a strong radiative inversion based at the ground--were nearly ideal for long-distance transport aloft of ozone at night, while keeping ozone separated from ground level emissions and destruction and limiting vertical mixing.
4. The dark-phase stability of ozone above the nocturnal surface-based radiation inversion suggests that transport of ozone can occur aloft over long distances at night without significant diminishment. It is possible for the ozone to be transported overnight several hundred kilometers and be mixed to the ground on the next day with a significant impact on ground-level air quality.
5. The occurrence of high ozone concentrations aloft on the morning of 9 June, in a rural area in southwestern Indiana, is attributed to long-distance transport of ozone.
6. Balloon-borne experiments are a feasible approach for addressing atmospheric chemistry problems, provided supporting data from ground stations, a ground-level chase vehicle, and an instrumented aircraft are available to complement the interpretation. The omission of any one of these measurement platforms severely limits the interpretation effort.

8.0 REFERENCES

1. Research Triangle Institute, Ambient Monitoring Aloft of Ozone and Precursors in the Vicinity and Downwind of a Major City, Environmental Protection Agency Report No. EPA-450/3-77-009.
2. Research Triangle Institute, Study of the Formation and Transport of Ambient Oxidants in the Western Gulf Coast and North-Central and Northeast Regions of the United States, Environmental Protection Agency Report No. EPA-450/3-76-033.
3. Research Triangle Institute, Investigation of Rural Oxidant Levels as Related to Hydrocarbon Control Strategies, Environmental Protection Agency Report No. EPA-450/3-76-035, March 1975.
4. G. T. Wolfe, personal communication, Interstate Sanitation Commission, New York, 1977.
5. W. H. White, J. A. Anderson, D. L. Blumenthal, R. B. Husar, N. V. Gillani, J. D. Husar, and W. E. Wilson, Jr., "Formation and Transport of Secondary Air Pollutants," Science, 194:187, 1976.
6. J. E. Sickles, II, "Ozone Precursor Relationships of Nitrogen Dioxide Isopentane and Sunlight Under Selected Conditions," Doctoral Dissertation, Department of Environmental Sciences and Engineering, University of North Carolina, Chapel Hill, North Carolina, 1976.
7. J. E. Sickles, II, L. A. Ripperton, and W. C. Eaton, "Oxidant and Precursor Transport Similation Studies in the Research Triangle Institute Smog Chambers," in Proceedings of International Conference of Photochemical Oxidant Pollution and its Control, Environmental Protection Agency Publication No. EPA 600/3-77-001a, p. 319, 1977.
8. S. L. Kopczynski, personal communication, Environmental Protection Agency, Research Triangle Park, North Carolina, 1977.
9. S. L. Kopczynski, W. A. Lonneman, T. Winfield, and R. Seila, "Gaseous Pollutants in St. Louis and Other Cities," J. Air Pollution Control Assoc., 25(3):251, 1975.
10. H. Levy, II, "Photochemistry of Troposphere," Advances in Photochemistry, 9, J. N. Pitts, Jr., G. S. Hammond, and K. Gollnick, Eds., John Wiley Interscience, New York, p. 369, 1974.
11. J. M. Mitchell, Jr., "The Thermal Climate of Cities," Symposium of Air Over Cities, Cincinnati, Ohio, November, 6-7, 1961, U.S. Public Health Service Report No. A62-5, Cincinnati, Ohio, November 1961, pp. 131-145.
12. F. M. Vukovich, J. W. Dunn, III, and B. W. Crissman, "A Theoretical Study of the St. Louis Heat Island: The Wind and Temperature Distribution," J. Appl. Meteor., 15(5):417-440, May 1976.
13. K. D. Hage, "Nocturnal Temperatures in Edmonton, Alberta," J. Appl. Meteor., 11(1):123-129, February 1972.
14. T. R. Oke and C. East, "The Urban Boundary Layer in Montreal," Boun. Layer Meteor., 1(4):411-437, April 1971, D. Reidel Publishing Company, Dordrecht, Holland.

15. T. R. Oke, D. Yap, and G. B. Maxwell, "Comparison of the Urban/Rural Cooling Rates at Night," Proceedings of the Conference on Urban Environment and 2nd Conference on Biometeorology, October 31-November 2, 1972, Philadelphia, Pennsylvania, 1972, pp. 17-22.

16. F. M. Vukovich, "A Study of the Effect of Wind Shear on a Heat Island Circulation Characteristic of an Urban Complex," Mon. Wea. Rev., 103(175): 27-33.

17. F. M. Vukovich, and J. W. Dunn, III, "A Theoretical Study of the St. Louis Heat Island: Some Parameter Variations," paper submitted to the J. Appl. Meteor., 1977.

18. B. D. Zak, personal communication.

19. N. E. Busch, S. W. Chang, and R. A. Anthes, "A Multi-Level Model of the Planetary Boundary Layer Suitable for Use with Mesoscale Dynamic Models," J. Appl. Meteor., 15:909-919, 1976.

APPENDIX A

EVALUATION OF SAMPLE COLLECTION CONTAINERS FOR HYDROCARBON SAMPLING

APPENDIX A

EVALUATION OF SAMPLE COLLECTION CONTAINERS FOR HYDROCARBON SAMPLING

A-1 Introduction

During the flight of Da Vinci II, grab samples (2- to 3-min sample duration) were collected in stainless steel containers and Tedlar® bags (protected from sunlight) using a common sample pumping system for analysis by Washington State University (WSU), National Center for Atmospheric Research (NCAR), and Research Triangle Institute (RTI). Listed in table A-1 are participants, sampling container type, and components analyzed by the respective organizations. From table A-1, comparisons could be made between RTI and NCAR for carbon monoxide and methane and between RTI and WSU for Freon® 11 and 12, acetylene, and ethane/ethylene.

Preliminary evaluation of the Da Vinci II ambient hydrocarbon data showed disagreement between absolute concentrations of various compounds that could be compared among the three participating organizations.

Figure A-1 shows a plot of acetylene concentrations reported by WSU and RTI for samples collected during the Da Vinci II flight. Samples were collected within 3-5 min of each other and since acetylene is a relatively unreactive compound, the difference between the two sets of numbers becomes significant.

Table A-1. Hydrocarbon sampling and analysis: Da Vinci II

Participant	Sample Container Type	Components Analyzed
RTI	Tedlar® bags covered with Scotchpak	CO, CH_4, Freon® 11, Freon® 12, ethane/ethylene, acetylene, and C_3-C_5 hydrocarbons
WSU	Stainless steel containers	Freon® 11, Freon® 12, methyl chloride, carbon tetrachloride, nitrous oxide, ethane, ethylene, and acetylene
NCAR	Stainless steel containers	CO, CH_4, N_2O, hydrogen, carbon tetrachloride

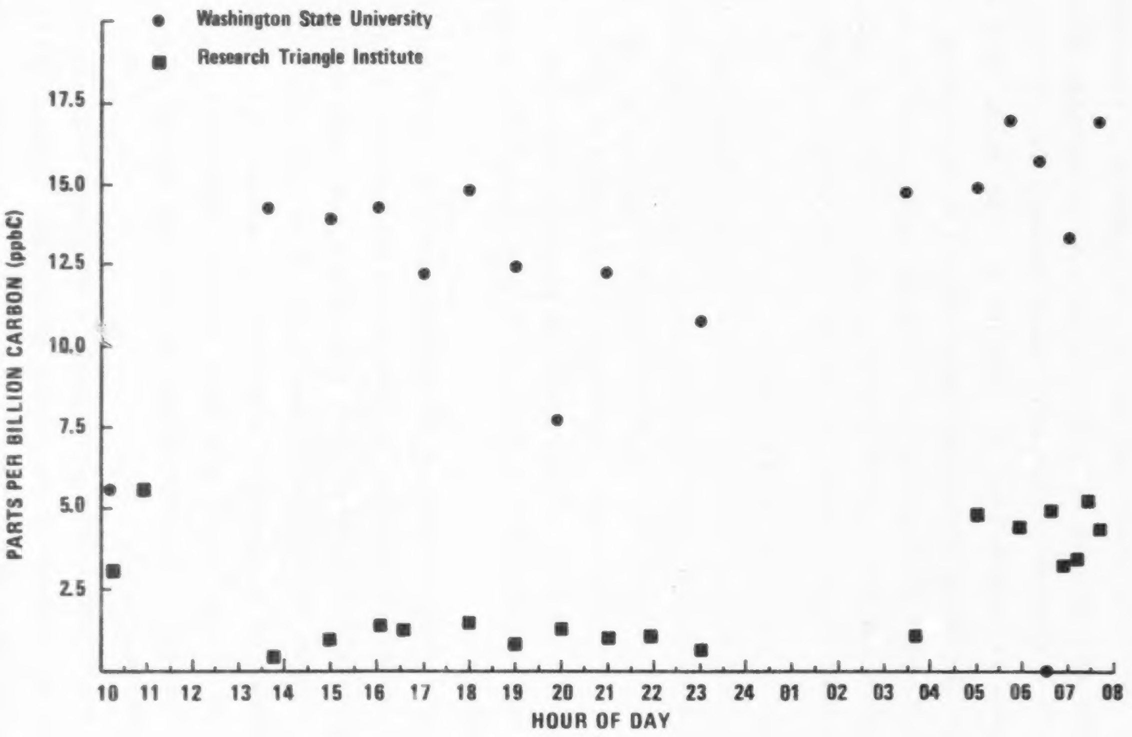

Figure A-1. Plot of WSU and RTI acetylene concentrations for samples collected during Da Vinci II

The differences could come from several sources, the most obvious being the use of different materials for sample collection and problems in the preparation or use of primary calibration standards. Before data analysis could begin, it was apparent that an investigation was needed to evaluate the properties of various materials routinely used in the collection and storage of hydrocarbons in the C_2-C_5 range and certain halocarbons. Secondly, the laboratory procedures and quality control practices were examined for all participants involved in hydrocarbon/halocarbon measurements for Da Vinci II. Results of that evaluation are summarized in appendix B. The discussion and results presented in the following paragraphs describe RTI's evaluation of glass bulbs, Tedlar® and Teflon® bags (protected from light), and treated stainless steel containers (purchased from WSU) for storage of ambient concentrations of various hydrocarbons (C_2-C_5 range) and certain halogenated compounds.

A-2 Sample Container Evaluation Program

Hydrocarbon measurements at the ambient concentration level have been made on a routine basis by numerous research groups. The analytical methodology, techniques, and approaches used are inconsistent from one research group to another. In many cases, interlaboratory comparisons have shown large discrepancies in the results. Each research group is confident of its approach and frequently has incorporated no quality control practices or procedures into its methodology.

A variety of sample collection techniques has been used during the past 10 yr to collect samples; however, a systematic evaluation of the stability of compounds in the sample container after the sample has been collected has not been performed. There are basically two types of devices for collection of C_2-C_{10} hydrocarbons and halogenated compounds in ambient air, namely polymeric films (Tedlar® and Teflon® bags) and hard surface containers, such as stainless steel and glass vessels. Each container has its own unique properties with advantages and disadvantages.

Controlled experiments were performed to evaluate both the containers and the stability of the various hydrocarbons at ambient concentration levels. Ambient air monitoring sample integrity has to be maintained to prevent sample degradation or sample contamination. To study these effects, a matrix of tests was designed. Table A-2 shows a list of the tests performed on four types of containers. Four containers of the same type were employed for each

Table A-2. Evaluation tests

Test #	(4) Stainless Steel	(4) Glass	(4) Teflon®	(4)Tedlar®
1	Zero Air	Zero Air	Zero Air	Zero Air
2	HC's + Zero Air	HC's + Zero Air	HC's + Zero Air	HC's + Zero Air
3	HC's + NO	HC's + NO	HC's + NO	HC's + NO
4	HC's + NO_2	HC's + NO_2	HC's + NO_2	HC's + NO_2
5	HC's + O_3	HC's + O_3	HC's + O_3	HC's + O_3

test. Two of the containers were spares in case the two containers evaluated developed leaks or unforeseen problems were encountered.

The hydrocarbon mixture employed in the matrix was composed of ethane plus ethylene, acetylene, propane, propylene, and n-pentane. Each test was conducted over an 18-day period with more intensive analyses during the earlier part of the test. Samples were withdrawn from the containers on day 0, 1, 2, 3, 4, 8, 13, and 18. After 4 days, only two containers of each type were tested for the extended part of the stability test. From day 1 to day 4 samples were analyzed on a random basis (see table A-3) to minimize any systematic error in the analyses.

A-3 Zero Air Evaluation Results

The zero air experiment provided data on the contamination of the sample stored in the four containers. The zero air had been previously analyzed for trace hydrocarbons and was found to contain only trace quantities (≈20 ppb) of ethylene. It was later discovered that the ethylene was due to a small piece of Teflon® tubing (FEP) in between the sampling containers and the zero air source. This problem was solved by replacing the Teflon® tubing with flexible stainless steel tubing. The zero air was introduced inside the containers after it had passed through a double dilution system, which was later employed in the rest of the study to generate low concentrations of hydrocarbons and other pollutants. Two different types of sampling containers were filled simultaneously to insure some cross reference between sample containers.

The zero air test samples collected from the containers were analyzed for both C_2-C_5 and C_5-C_{10} hydrocarbons. The data collected demonstrate clearly the difficulties that had been experienced previously by RTI and others.

Table A-3. Analysis schedule

Time	Day 1	Day 2	Day 3	Day 4
08:00	A_1	A_2	A_1	A_2
09:00	B_1	B_2	B_1	B_2
10:00	C_1	C_2	C_1	C_2
11:00	D_1	D_2	D_1	D_2
12:00	E_1	E_2	E_1	E_2
13:00	A_2	A_1	A_2	A_1
14:00	B_2	B_1	B_2	B_1
15:00	C_2	C_1	C_2	C_1

Note: Suffix number refers to container number. Numbers 3 and 4 of each type were spares.

A = stainless steel cylinders (2)
B = stainless steel cans (2)
C = glass bulbs (2)
D = Tedlar® bags with Viton quick connect (2)
E = Teflon® bags with stainless steel fitting (2)

Stainless steel containers showed a slight decrease in the ethylene concentration from 20 ppb to 12 ppb (18th day). After 18 days, no other components were detected in the analyses. It should be pointed out that the stainless steel containers had been pressurized to 40 psig with the use of an MB151 Metal Bellows pump. The absence of contamination over such an extended period is important. Since in many cases, sampling containers are transported in contaminated atmospheres, it is imperative that the samples retain their integrity even though the containers are exposed to pollutant levels several orders of magnitude higher than the collected sample.

Glass containers appeared to be as good as the stainless steel containers, but some disadvantages were encountered. Since the glass bulb could not be pressurized to any great extent (10 psi), retrieval of samples was more difficult and possible contamination could occur unless a great deal of care was taken in maintaining leak-free seals during transfer of samples from the containers to the gas chromatograph. Since only limited amounts of sample could be drawn from the bulb, it was found that some contamination did occur when the vacuum in the container became significant (~400 mmHg). Leaks occurred at both the Teflon® stopcocks or at the connections between the stopcock and the GC, drawing lab air inside the sampling bulb. Absolute conclusions could not be made about the glass containers except that without extreme care, the samples could be easily contaminated.

Results of zero air stability for Tedlar® bags, a commonly used polymer for the collection of air samples, reaffirmed our belief that the sampling container is adequate for sampling C_1-C_5 hydrocarbons. No increase in any hydrocarbon species was shown for up to 8 days. Trace quantities (~0.2 ppb [v/v]) of acetylene, propane, and propylene were observed by the 18th day; however, significant concentrations (1-2 ppmC) of FID responsive species were observed in the C_6-C_{10} range.

Teflon® (5 mil FEP) sampling bags that had been treated with zero air showed unexpected results. After 4 days, significant concentrations of various hydrocarbons were observed. The results of this test are shown below in table A-4.

The concentration of the C_5-C_{10} hydrocarbons in Teflon® bags ranged from

Table A-4. Zero air test results for Teflon® bags (ppb (v/v))

	Days in Container					
Hydrocarbon Compounds	1	2	4	8	13	18
Ethane + Ethylene	4.8	6.0	9.5	19.6	111.2	201.7
Acetylene	>0.1	>0.1	>0.1	0.3	0.6	3.1
Propane	0.5	0.8	1.2	2.9	3.6	4.8
Propylene	0.5	1.1	1.4	2.8	2.5	2.3
Isobutane	>0.1	>0.1	>0.1	>0.1	>0.1	>0.1
Butane	>0.1	0.3	0.3	0.8	2.9	2.2
1-Butene	>0.1	>0.1	>0.1	>0.1	>0.1	>0.1
Isopentane	>0.1	>0.1	>0.1	1.9	2.3	3.0
Trans-2-Butene	>0.1	>0.1	>0.1	>0.1	>0.1	>0.1
n-Pentane	>0.1	>0.1	>0.1	>0.1	>0.1	>0.1

1 ppmC on day 1 to 2 ppmC by day 18. The problem encountered with the Teflon® film sampling bag has been experienced by other researchers.* Severe treatment of the TFE film in some cases can ameliorate its performance. For example, repeated exposure to high ppm concentrations of ozone can improve performance. It has also been found that generation of ethylene by Teflon® film can be batch dependent.*

In summary, it was found that stainless steel containers could retain samples, uncontaminated, up to 18 days, while other containers such as glass bulbs are too fragile and require extreme care in order to retrieve the collected sample. Tedlar® sampling bags exhibited good results for C_2-C_5 but were inadequate for any other higher molecular weight species. Teflon® sampling bags were unsatisfactory for both C_2-C_5 and C_5-C_{10} hydrocarbon analyses.

A-5 Hydrocarbon Evaluation Results (C_2-C_5 Range)

Test 2 involved low concentrations of hydrocarbons and zero air. In this test, the analyses provide some idea of the interaction of the container with an ideal hydrocarbon sample. Previous evaluations have been made at ppm levels (references), but control testing had not been undertaken at concentrations close to those found in ambient air. The concentrations of the individual hydrocarbons were approximately 10 ppb (v/v). Measurements at that level have been shown to have a repeatability of 6 percent. This was experimentally determined by four successive analyses of the same sample. Results of repeatability tests are shown in table A-5.

---

*Mike Holdren, private communication, 1977.

Table A-5. Repeatability results for selected hydrocarbon analyses (ppb (v/v))

Hydrocarbon Compounds	1	2	3	4	Variance %
Ethane + Ethylene	26.9	28.7	26.8	27.3	3.2
Acetylene	10.5	11.6	11.4	11.2	4.3
Propane	12.9	14.4	14.0	15.2	6.8
Propylene	12.3	13.0	12.3	14.7	8.7
n-Pentane	10.6	11.3	10.0	12.2	8.6

It should be emphasized at this point that approximately 100 cm^3 of sample are cryogenically concentrated for these analyses. The variance in the analysis can be improved by increasing the trapped volume, but it was felt that a variance of 6 percent was sufficient. This also provided a base from which statistical evaluation of the data could be made, i.e., assuming that a variance greater than 6 percent would be reflective of interaction of the sample with the container.

During the test, all containers were kept inside aluminum suitcases to minimize any photochemical activity. When the containers were sampled, the laboratory lights were turned off. Results of the test are shown in table A-6 and are illustrated in figures A-2 through A-5.

In order to compare variance for each container and component analyzed, the mean of these variances was calculated for a particular test and container. The means are shown in table A-6. The results are fairly conclusive. The two containers that have the smallest variance are the Tedlar® bag and the stainless steel container. It should be noted that both of these containers have variances that approach the variance of the analytical procedure. The Teflon® bag and glass container have variances approximately twice that of the Tedlar® and stainless steel containers. The high variance of the glass container is probably not due to the container itself but to the difficulty of recovering samples from the container. The high variance observed with the Teflon® bag can only be explained by interaction of the container with the sample. In most cases, the concentration of each component analyzed increased. Observation during the zero air evaluation reconfirmed the problem of contamination of the Teflon® bags.

Table A-6. Hydrocarbon stability results

Hydrocarbon Compounds	Stainless Steel	Glass	Tedlar®	Teflon®
HC + Zero	10.2	19.5	12.4	16.2
HC + NO	6.9	13.7	4.7	13.7
HC + NO_2	5.9	20.8	3.6	11.1
HC + O_3	5.4	5.5	5.4	8.6
Mean Variance of All Tests	7.1	14.9	6.5	12.4

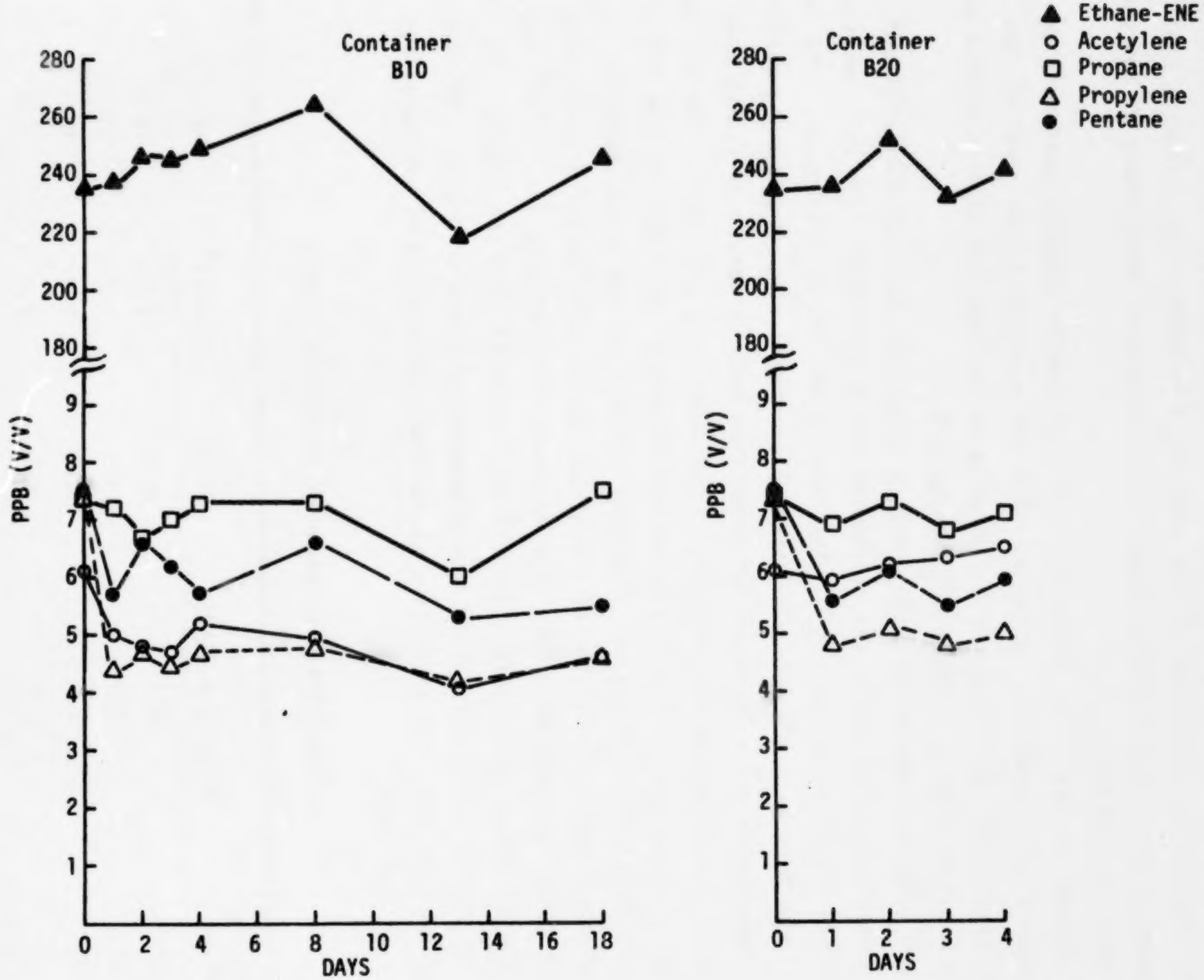

Figure A-2a. Stainless steel can evaluation (HC's and zero air).

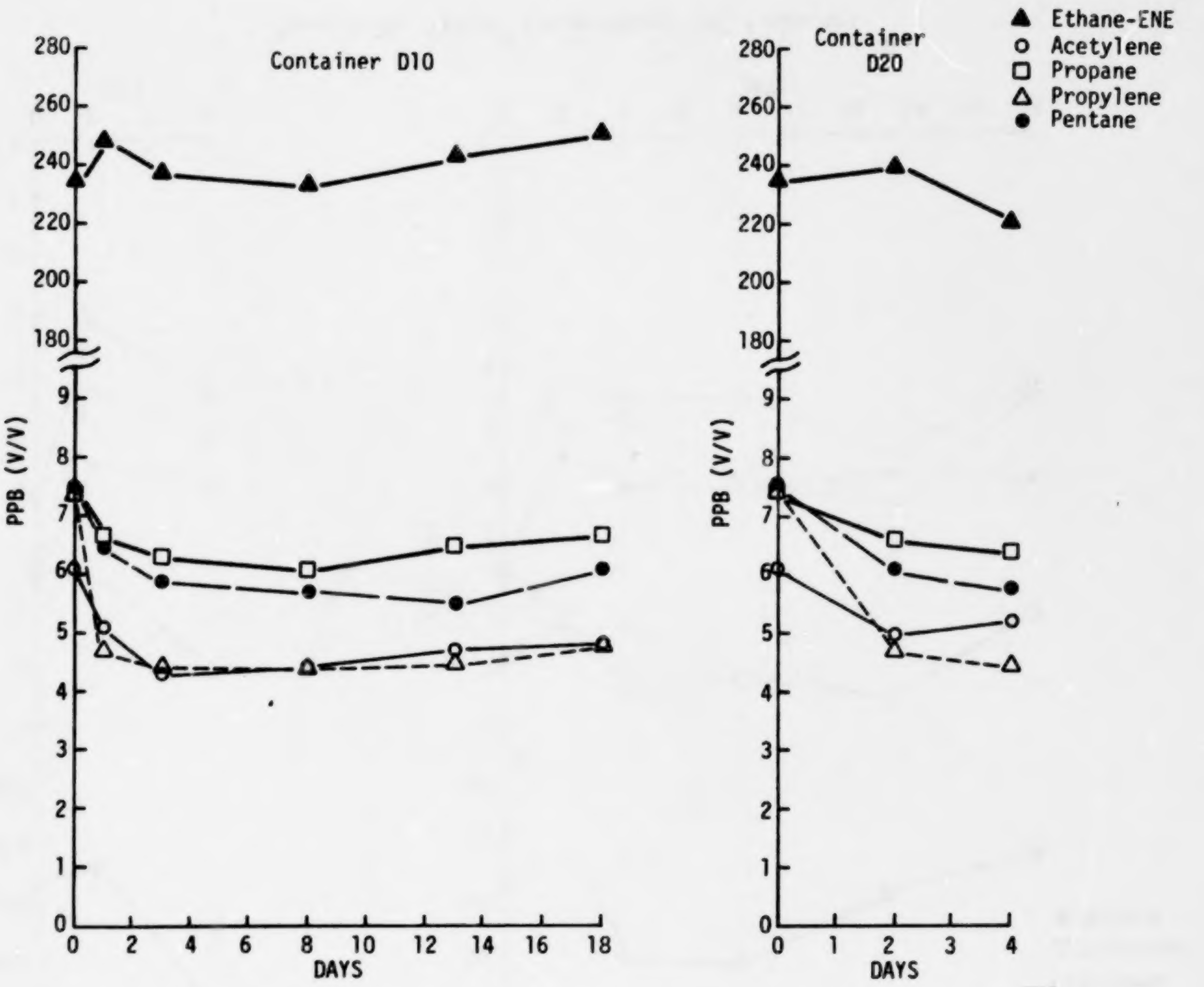

Figure A-2b. Tedlar® bag evaluation (HC + zero air).

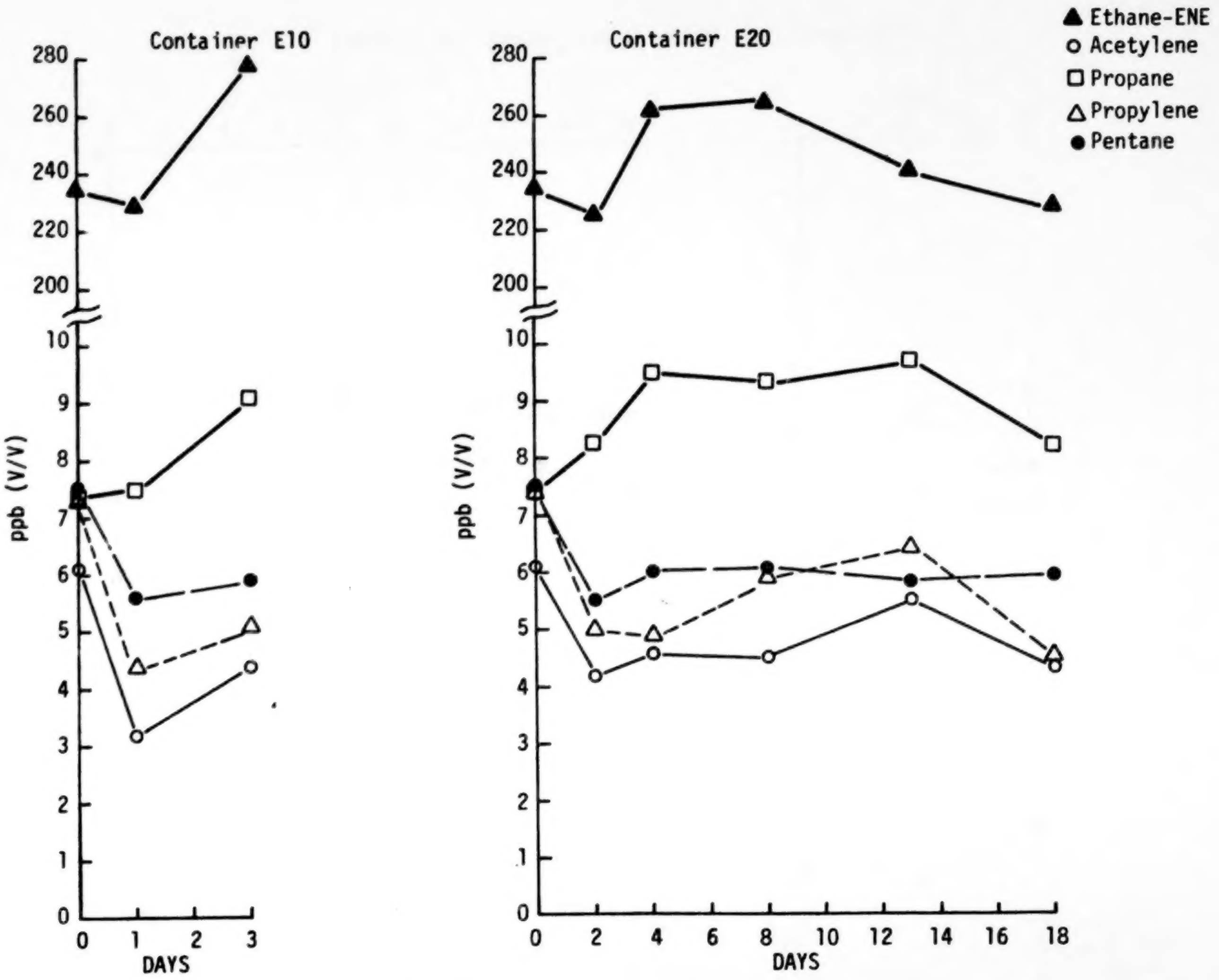

Figure A-2c. Teflon® bag evaluation (HC + zero air).

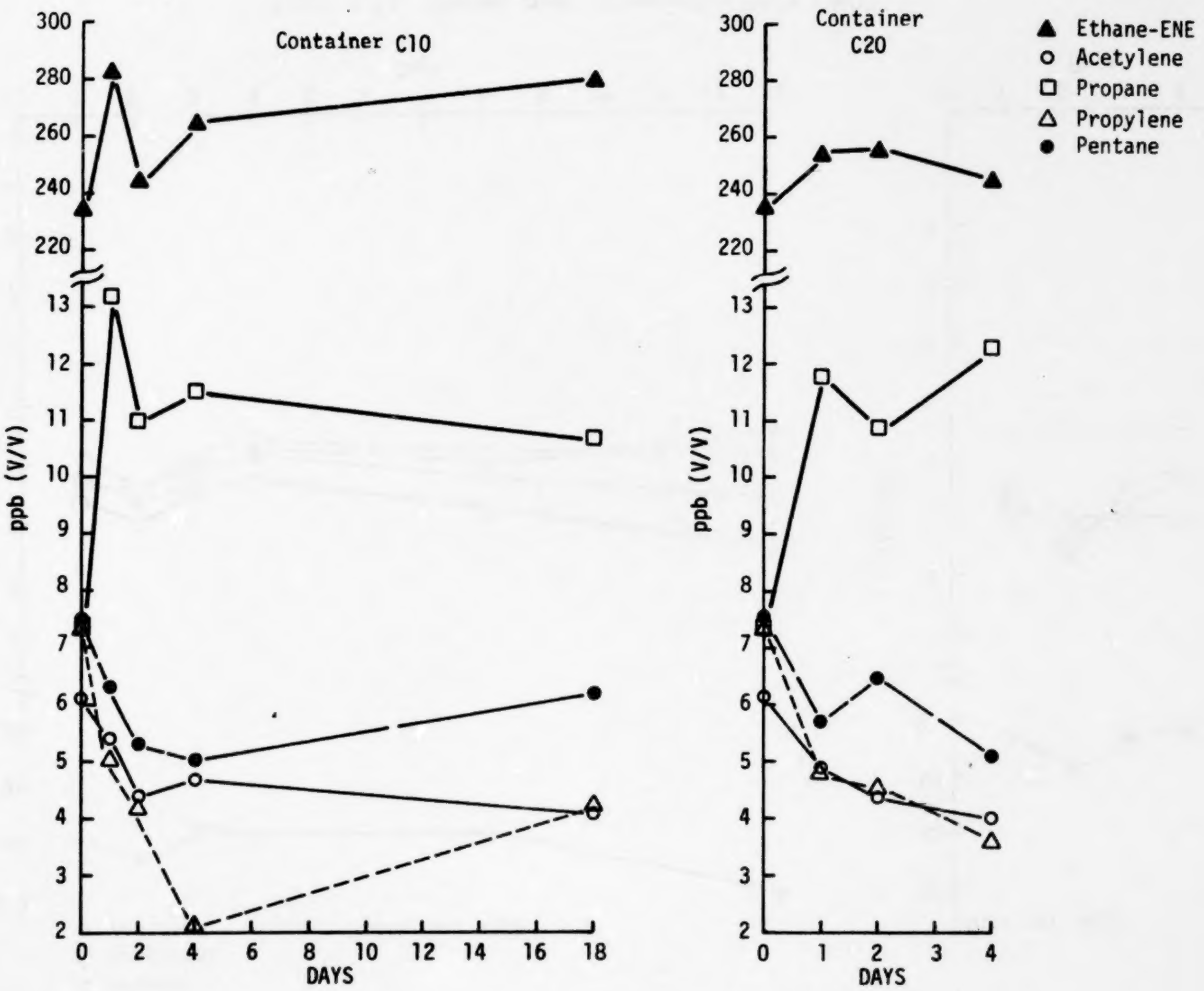

Figure A-2d. Glass container evaluation (HC's + zero air).

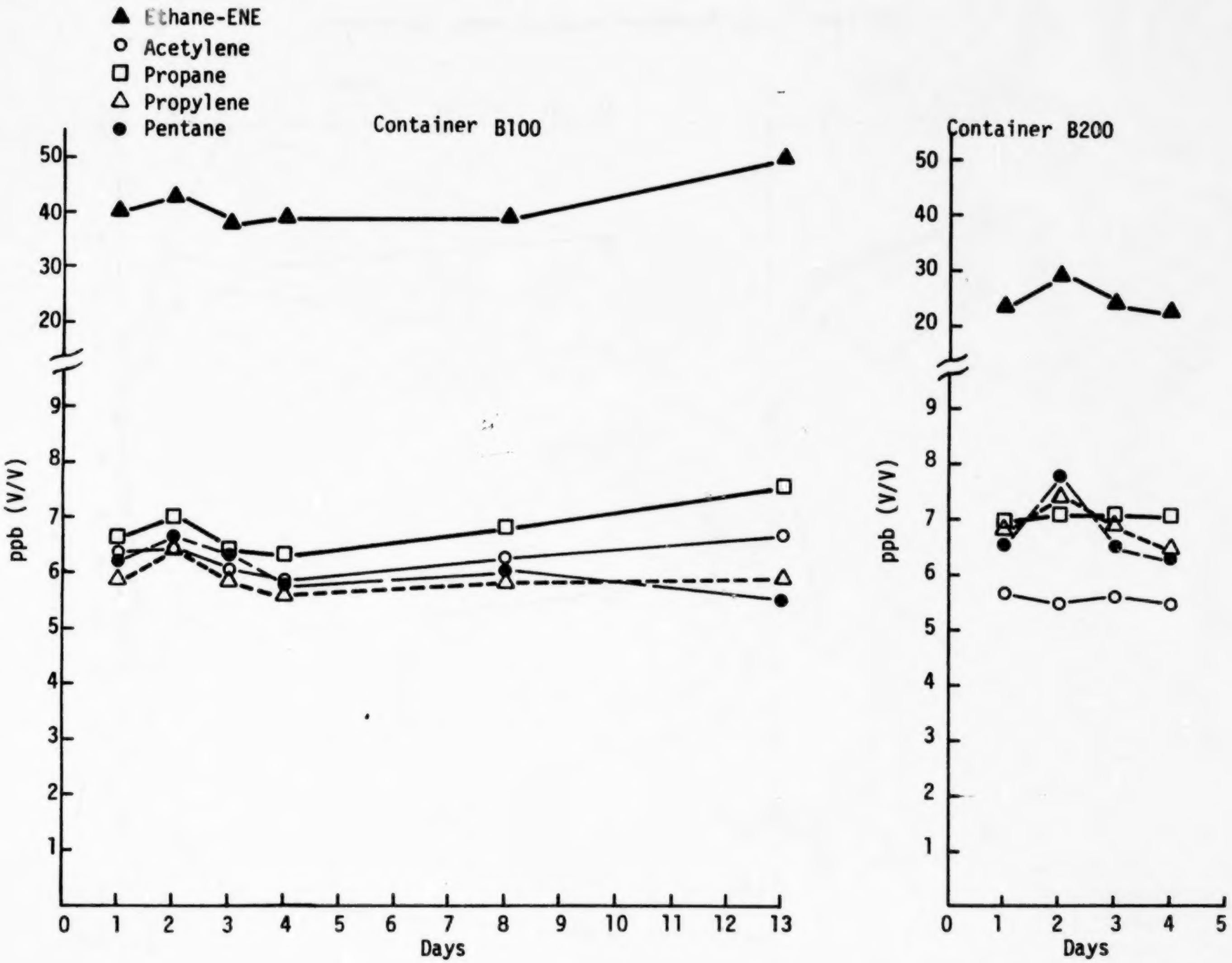

Figure A-3a. Stainless steel can evaluation (HC's + NO).

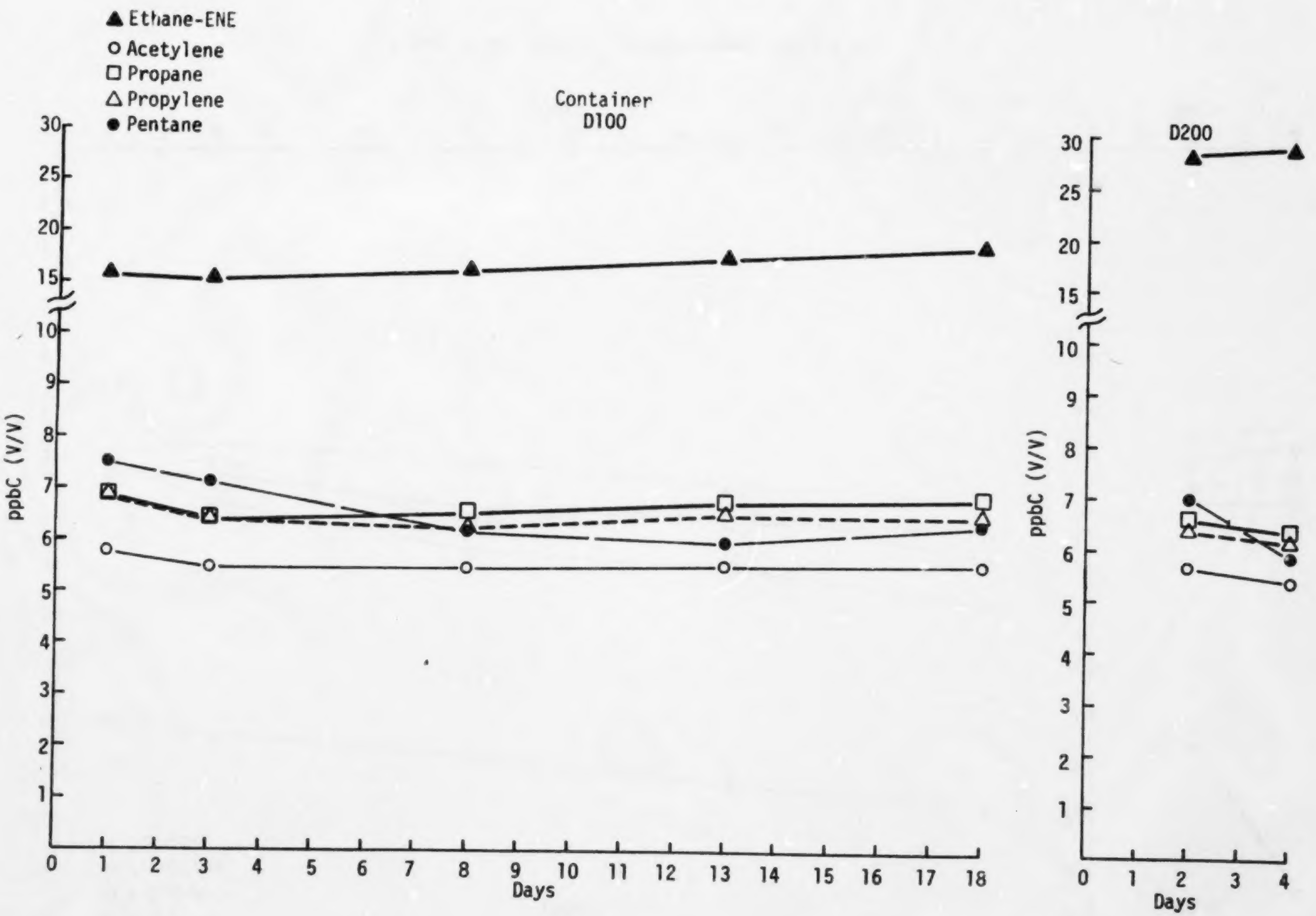

Figure A-3b. Teflon® bag evaluation (HC's + NO).

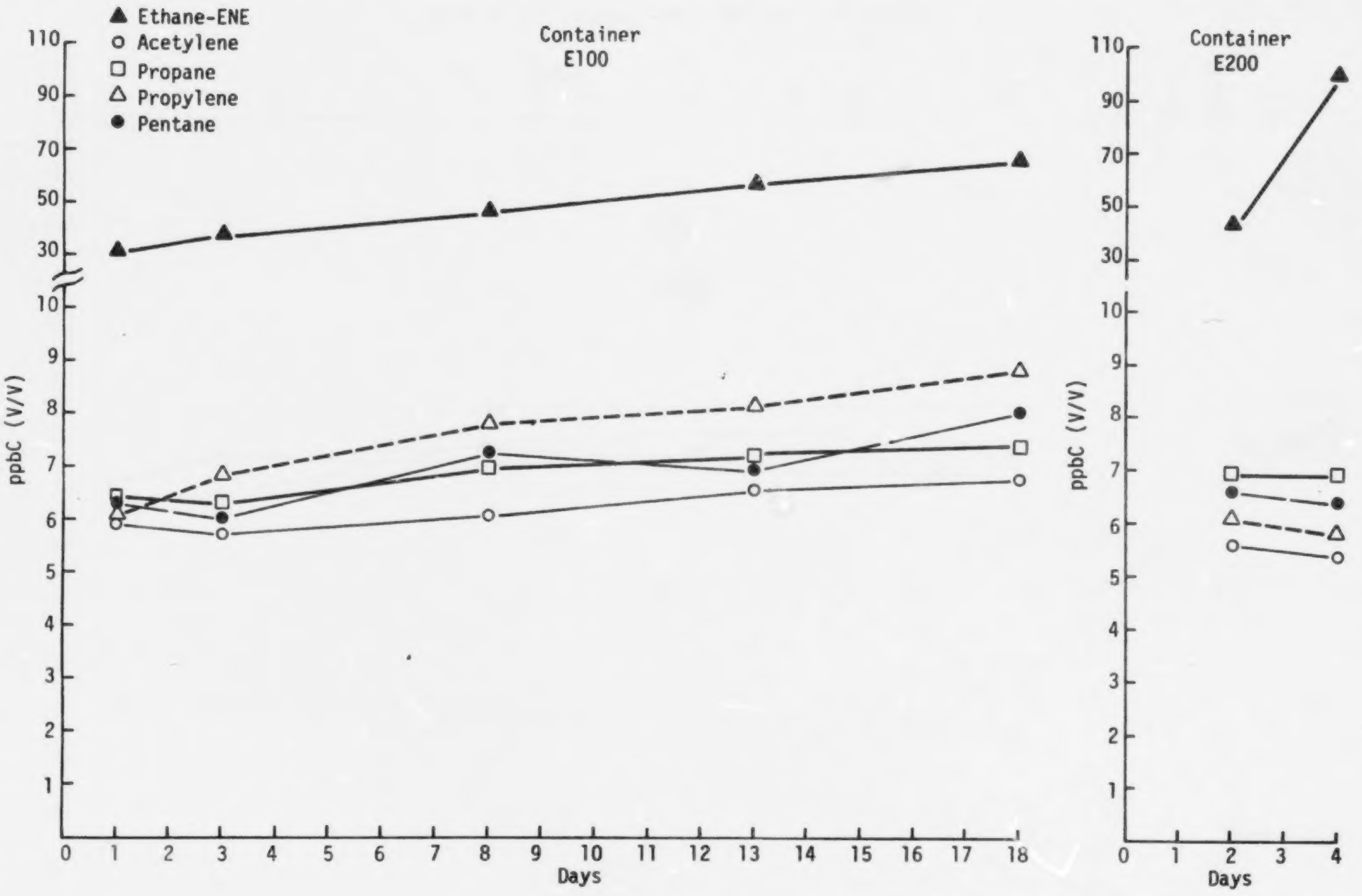

Figure A-3c. Teflon® bag evaluation (HC's + NO).

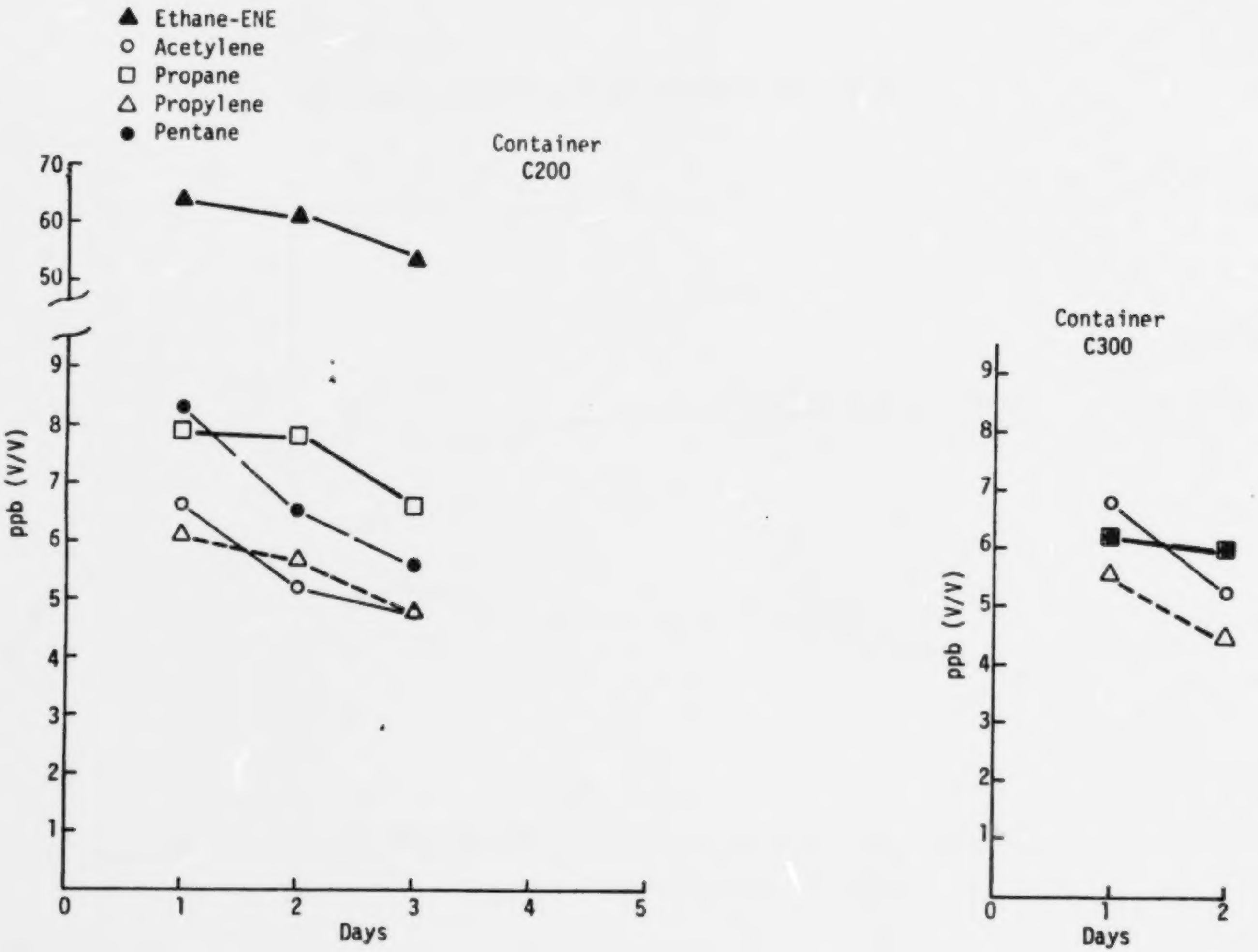

Figure A-3d. Glass bulb evaluation (HC's + NO).

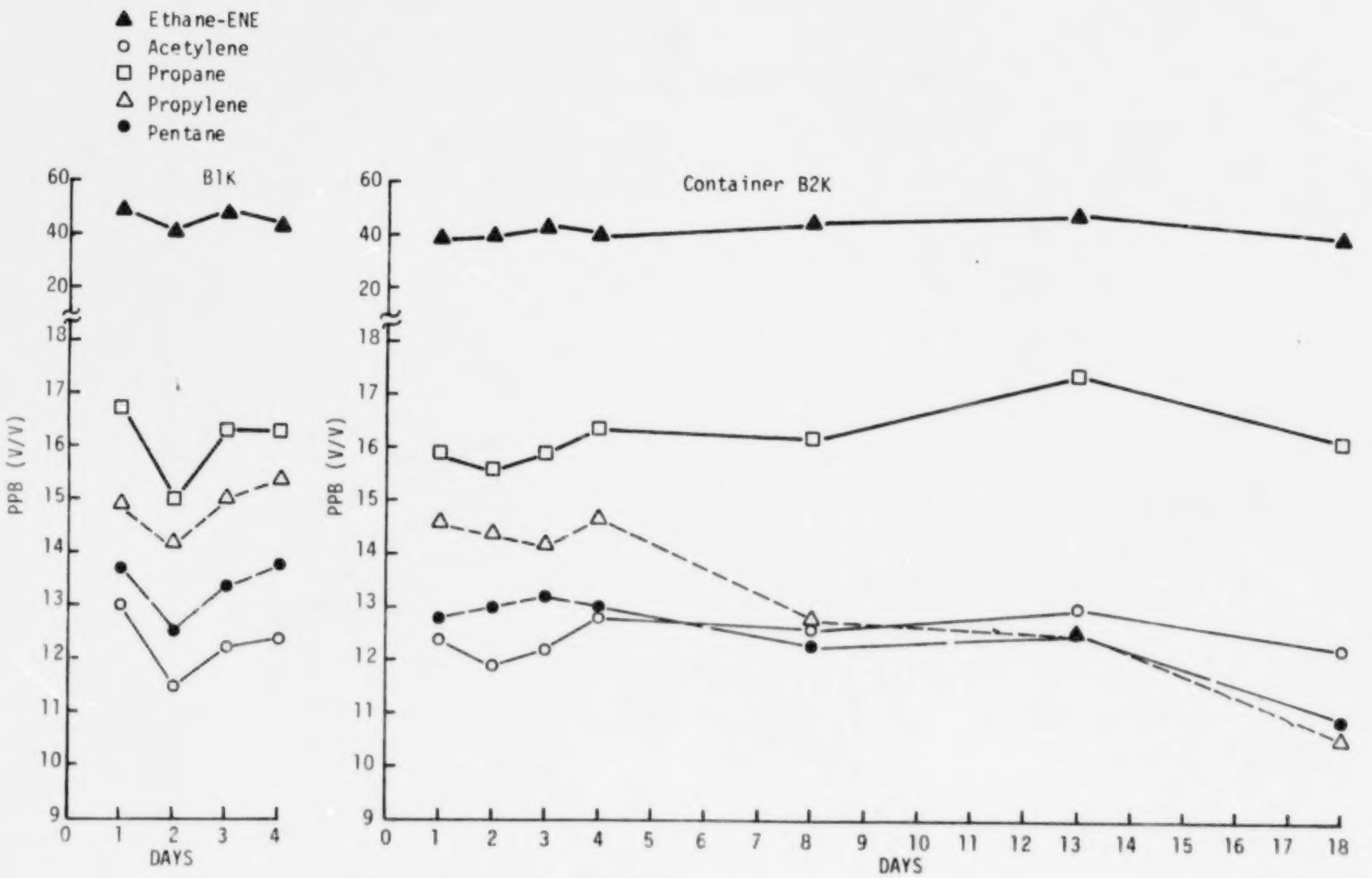

Figure A-4a. Stainless steel can evaluation (HC + NO_2).

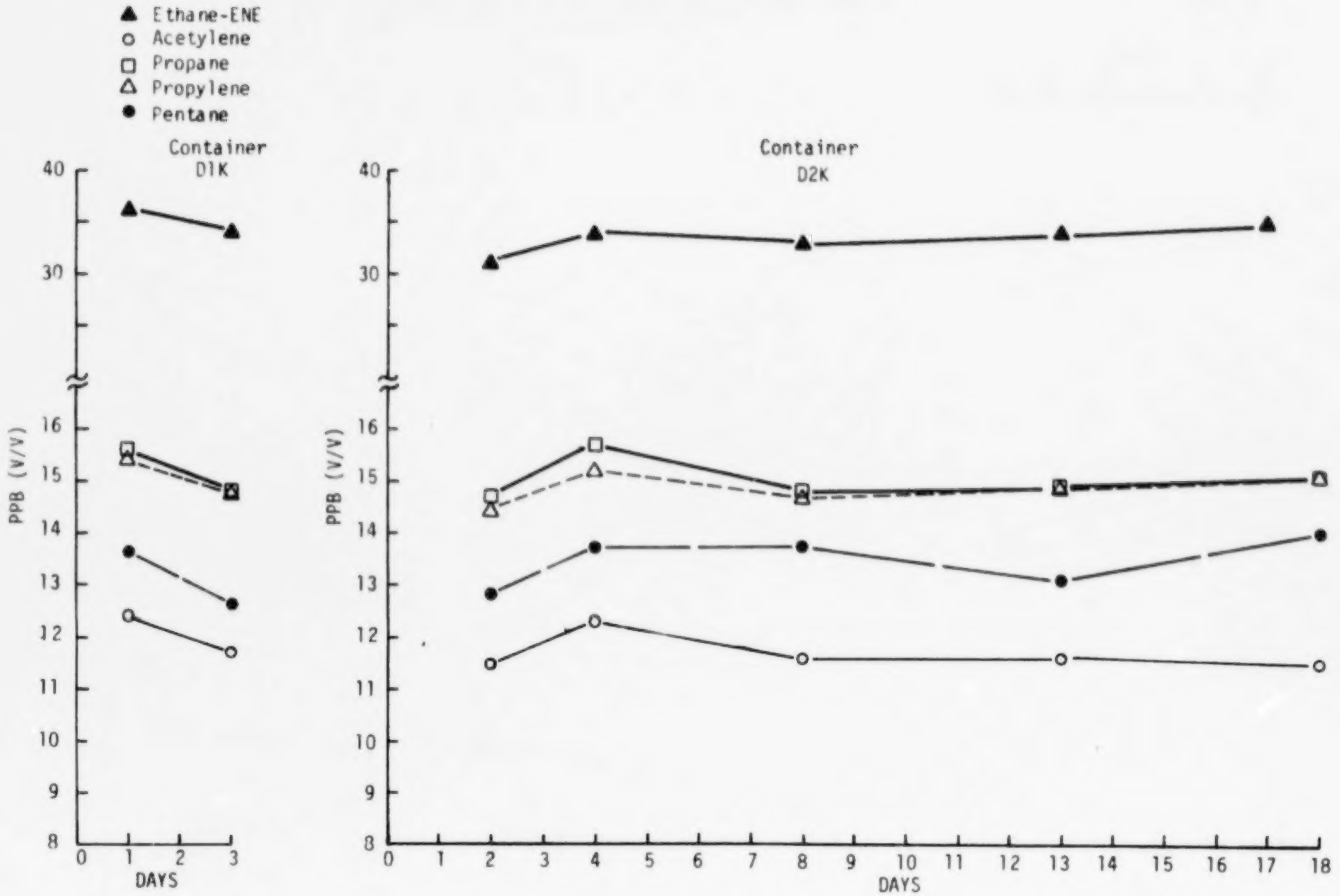

Figure A-4b. Tedlar® bag evaluation (HC + NO_2).

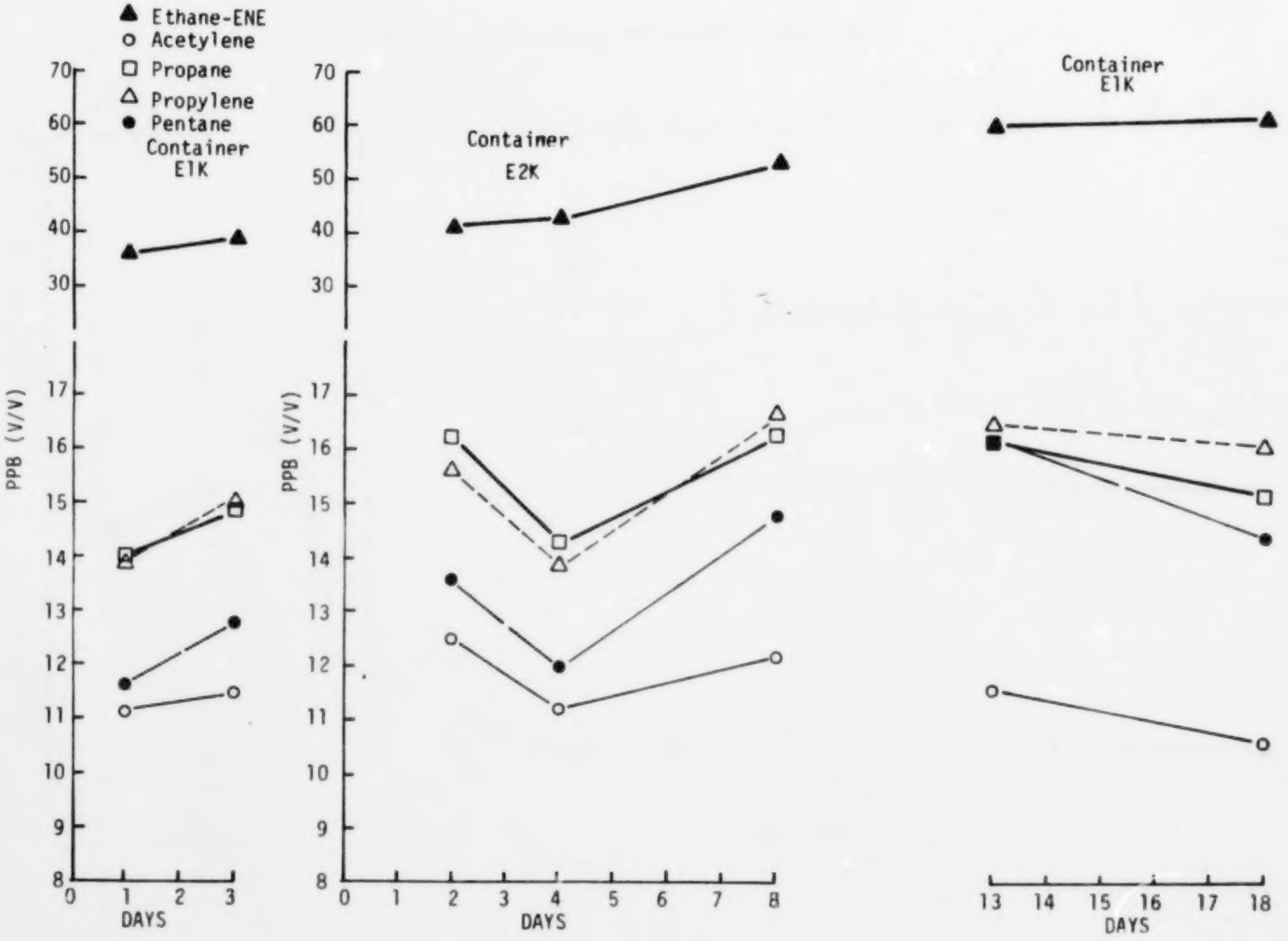

Figure A-4c. Teflon® bag evaluation (HC + NO_2).

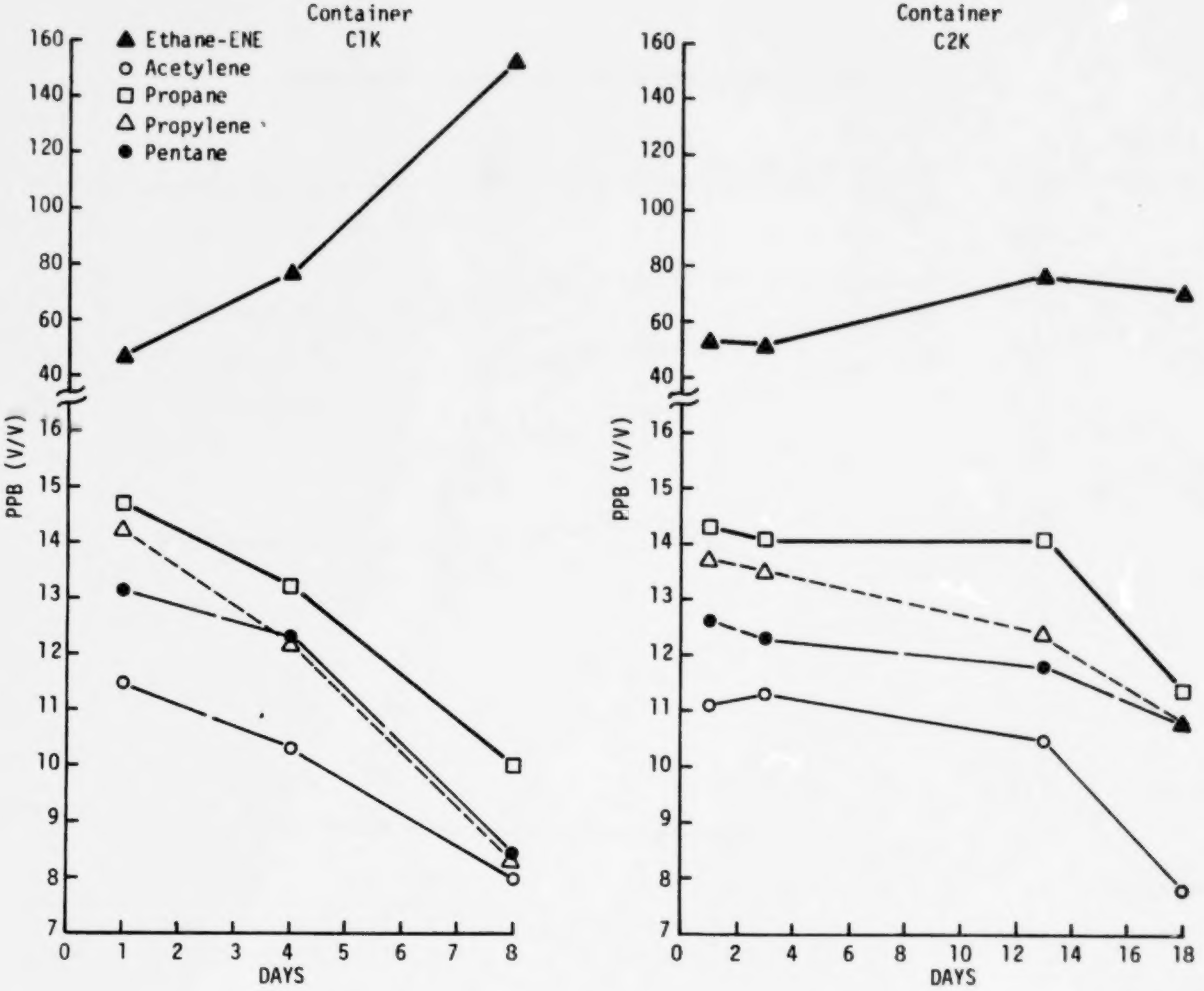

Figure A-4d. Glass container evaluation (HC + NO_2).

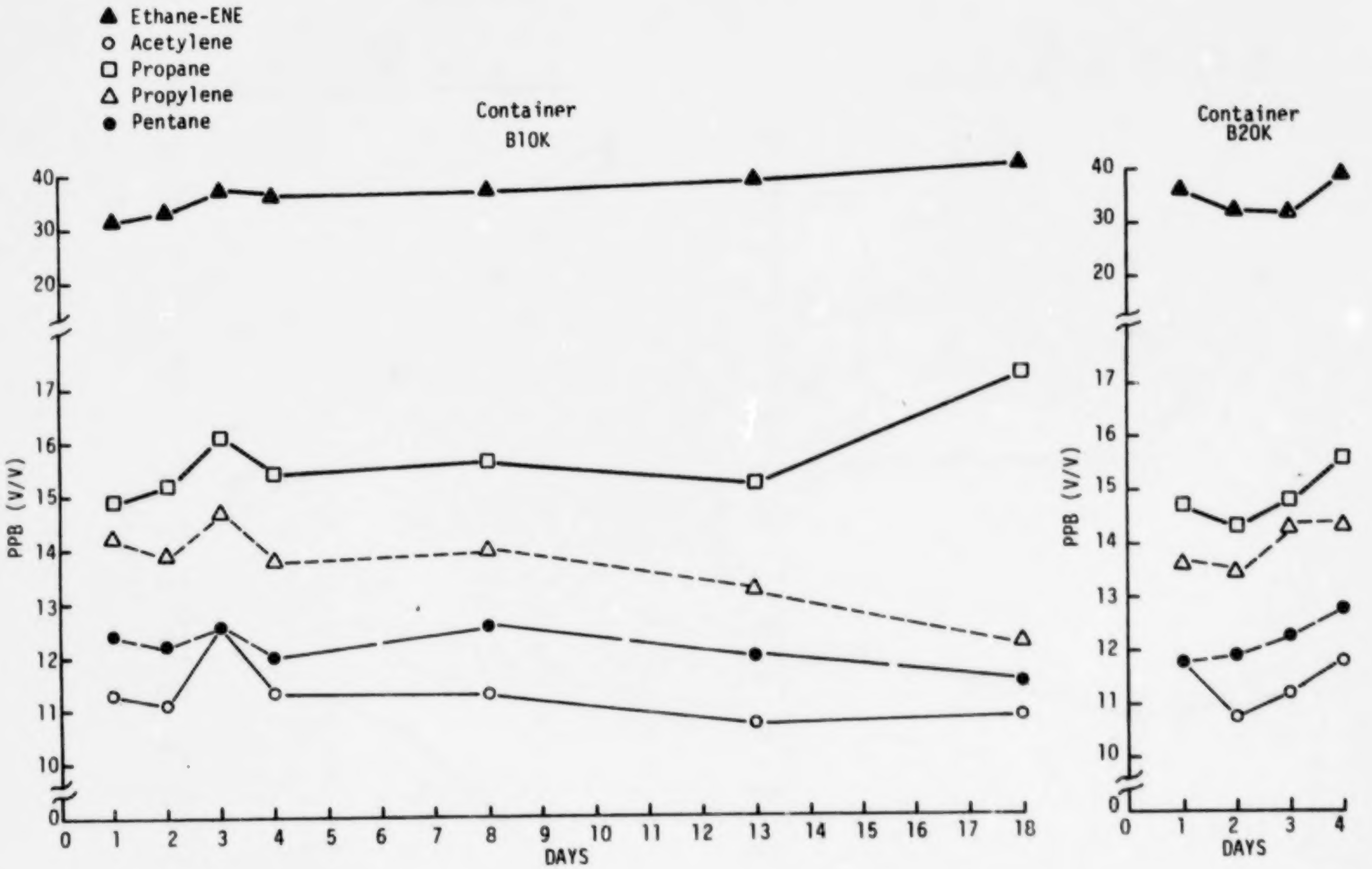

Figure A-5a. Stainless steel can evaluation (HC's + O_3).

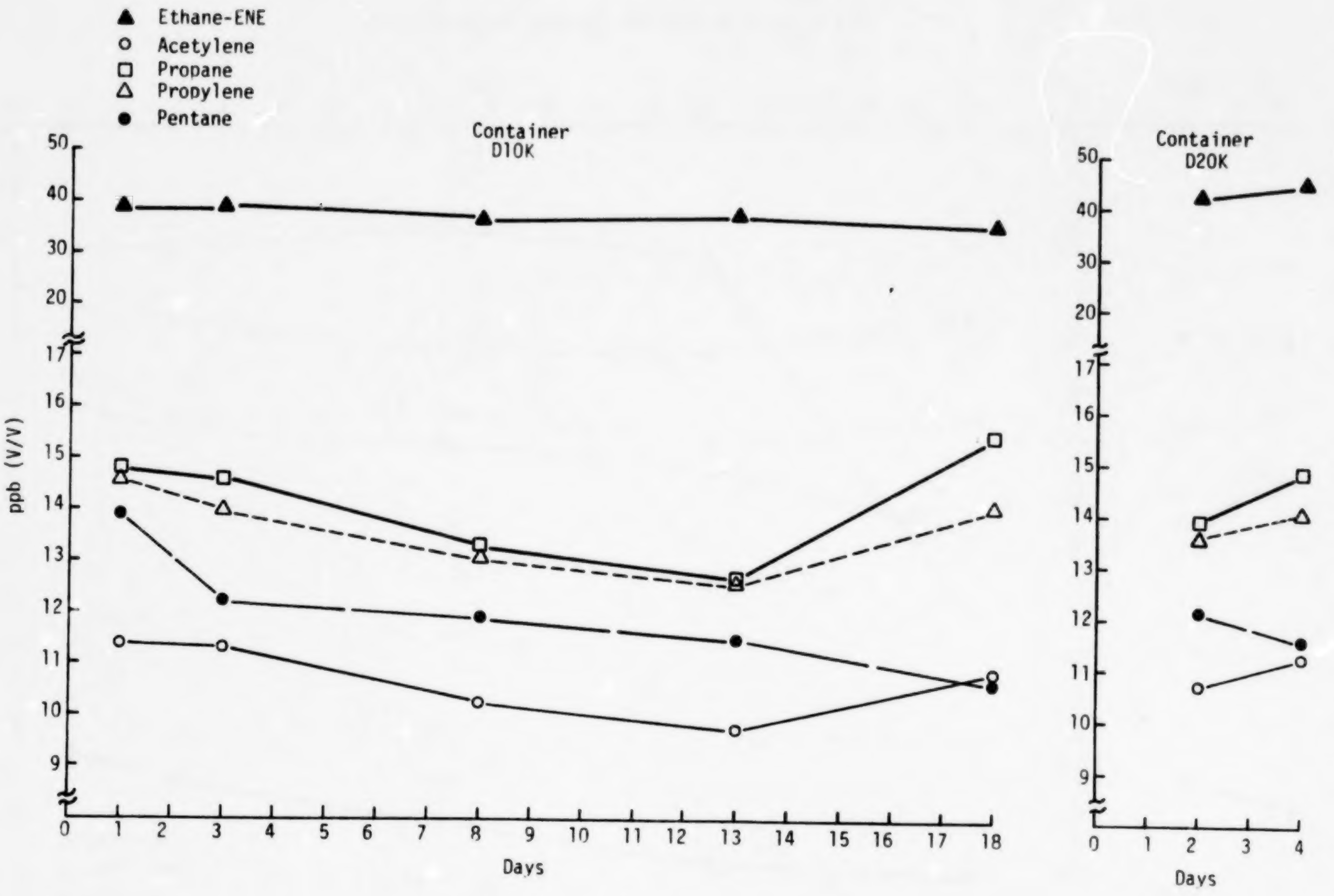

Figure A-5b. Tedlar® bag evaluation (HC + O_3).

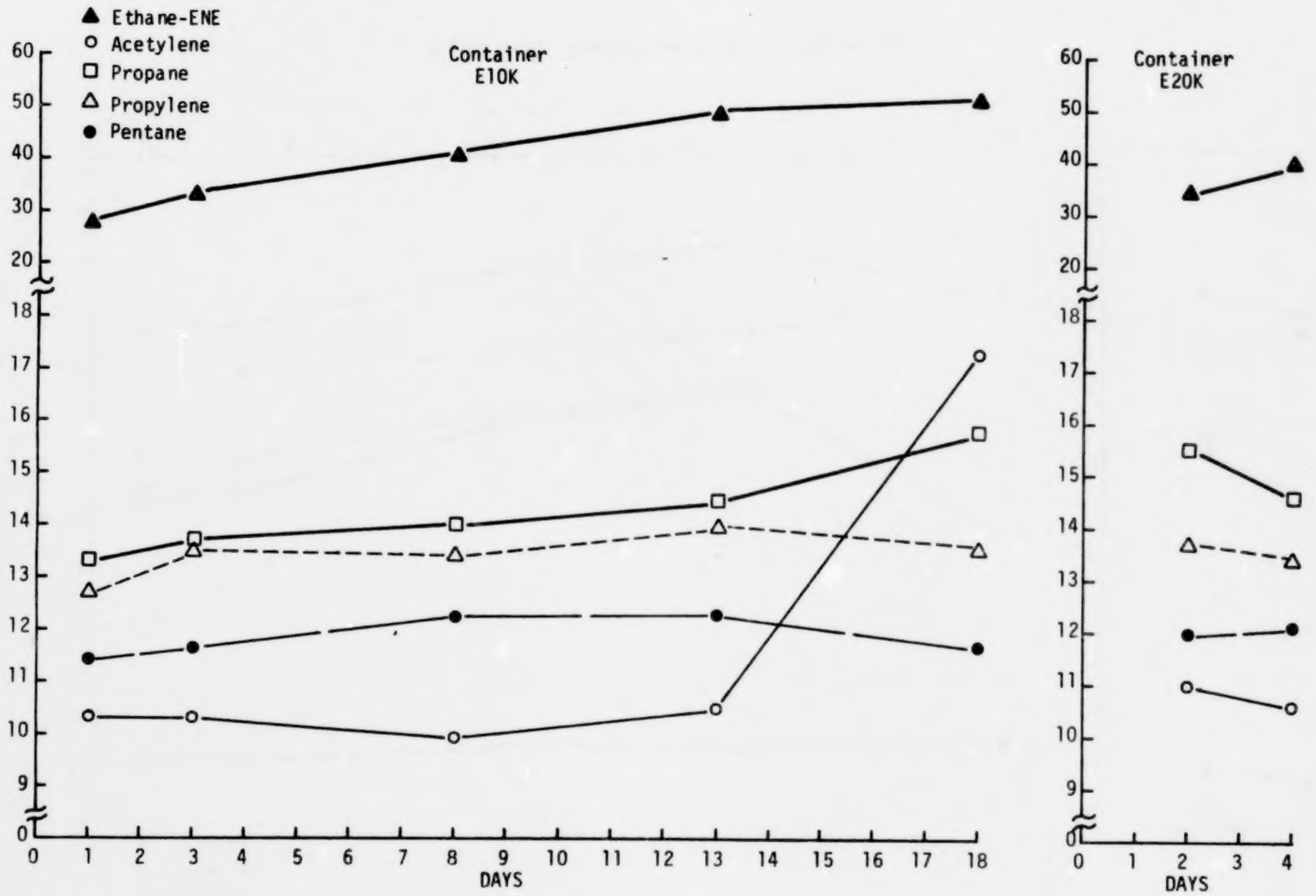

Figure A-5c. Teflon® bag evaluation (HC + O_3).

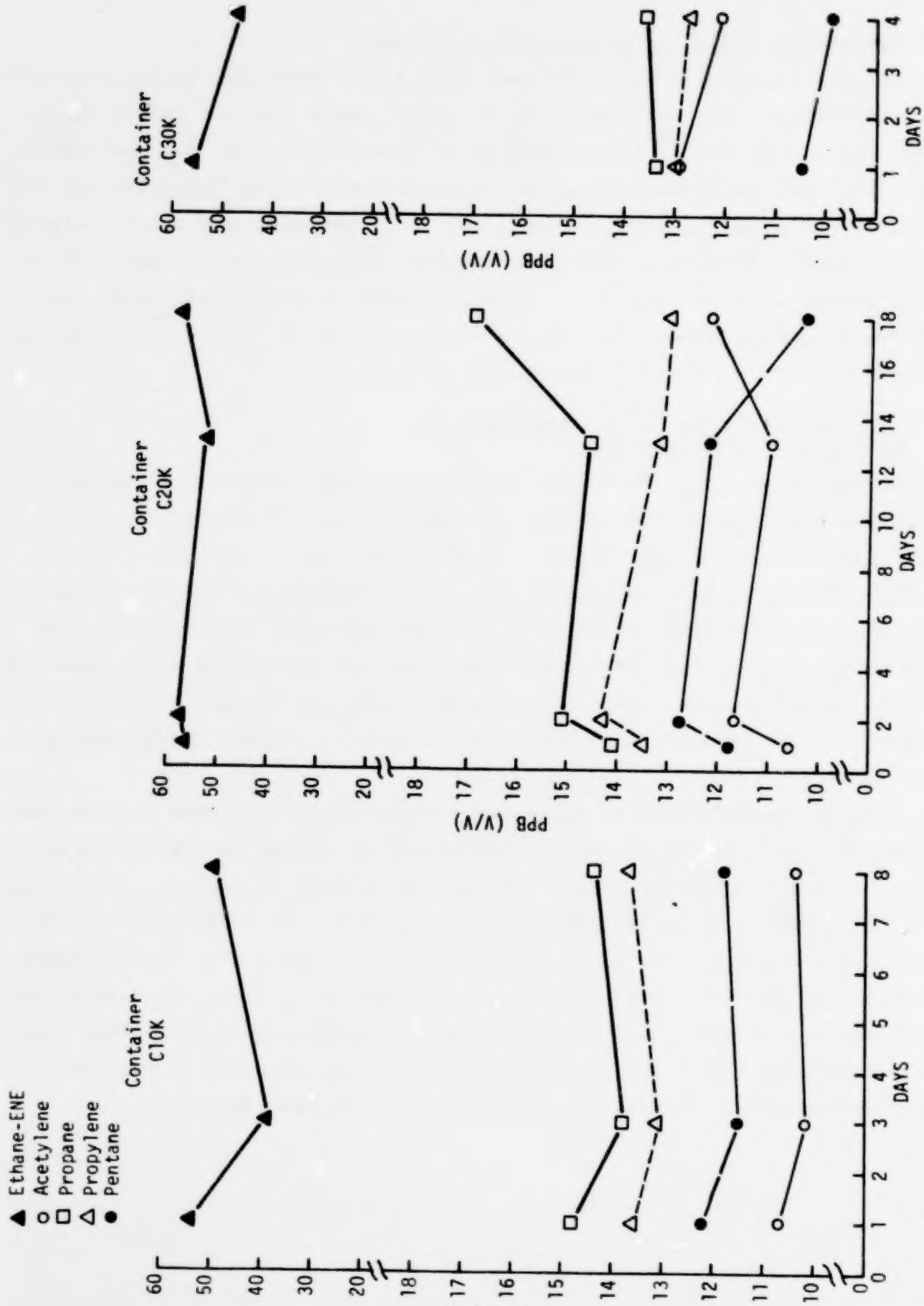

Figure A-5d. Glass container evaluation (HC + O_3).

A-6 Hydrocarbon Stability Results (C_5-C_{10} Range)

Further evaluations were performed with higher molecular weight compounds that included cyclopentane, n-heptane, toluene, and o-xylene. Due to the background in the Tedlar® and Teflon® bags, these containers were not evaluated. Nor were the glass containers evaluated due to their fragility and the difficulty of rcovering samples from them. Only the stainless steel containers were evaluated. Unfortunately, these samples were evaluated without heating the container. The results (see figure A-6) reflect those conditions. Later experimentation has shown that the containers need to be heated just prior to analysis to 70° C to minimize adsorption effects.

A-7 Evaluation of Effects of Prescrubber to Remove Ozone During Samples

During the Da Vinci II flight, the RTI air sample collection system employed a prescrubber (MnO_2 filter) to remove ozone. The filter consisted of a 1/4" stainless steel tube filled with MnO_2 powder mixed with glass wool. The MnO_2 glass wool plug is held in the 1/4-in. tube with glass wool plugs at each end. The efficiency of the MnO_2 was experimentally determined and was found to be approximately 50 percent effective with 0.1 ppm O_3. The effect of the MnO_2 on the various hydrocarbons was not known and further evaluation was required. Four compounds were tested as follows: n-pentane, propylene, propane, and acetylene.

A known concentration of these compounds was passed through various components that made up the filters. The mixture was passed through an empty Teflon® tubing, a piece of Teflon® tubing with a glass wool plug, a filtering unit with 0.033 gm MnO_2, and another filtering unit with 0.082 gm MnO_2. The results of these tests are shown in figures A-7 through A-10. These figures indicate that the error bars for the analyses are as great as the changes in the concentration that could be attributed to interaction of the filter with the various compounds. The only conclusion that can be drawn is that the effect of the MnO_2 is minimal on these various compounds evaluated.

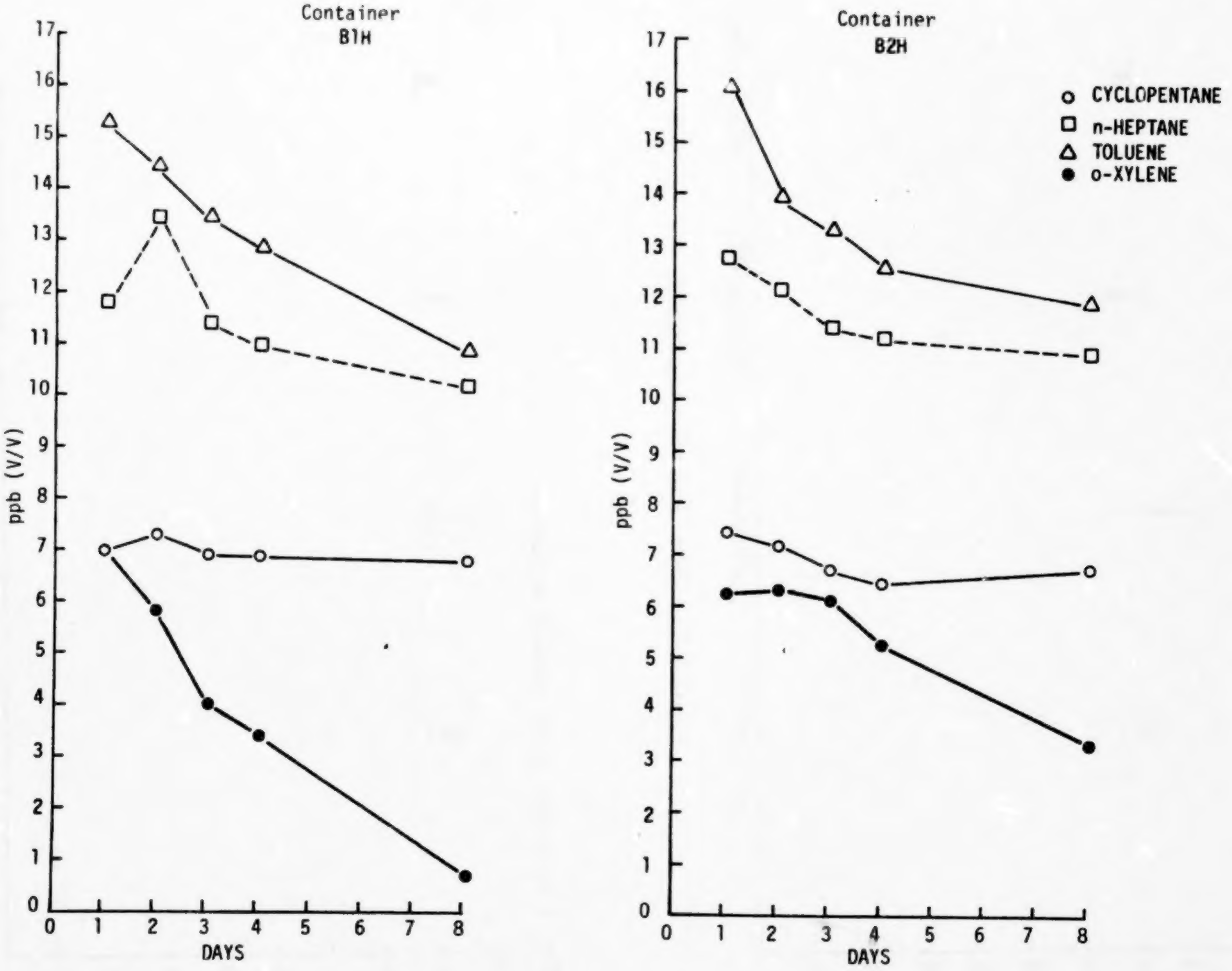

Figure A-6. High molecular weight hydrocarbon stability in stainless steel containers.

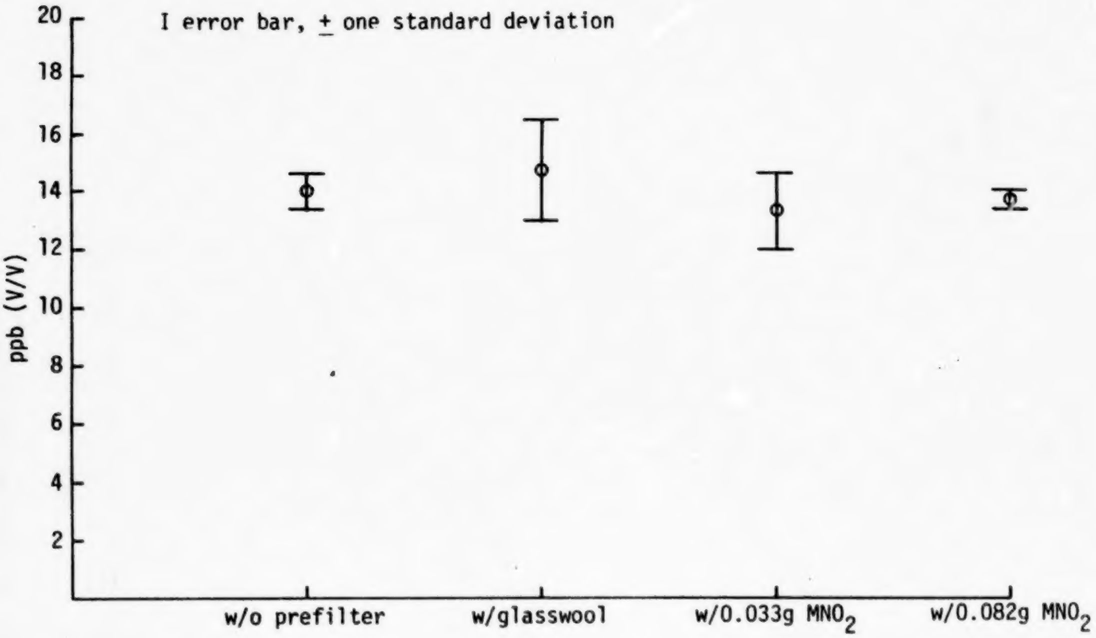

Figure A-7. Prefilter evaluation (n-pentane).

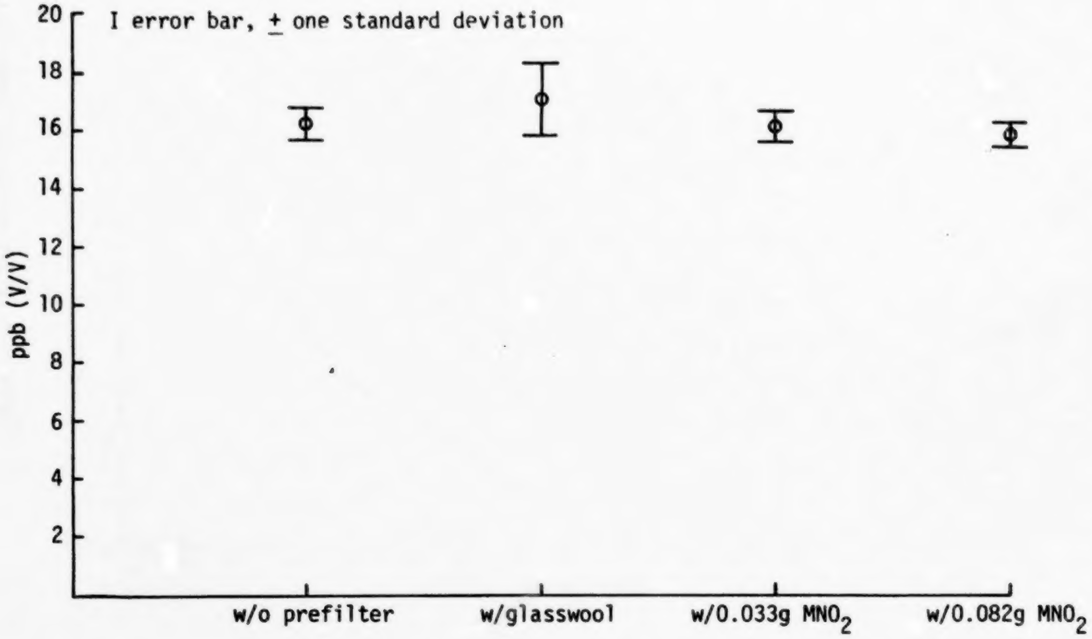

Figure A-8. Prefilter evaluation (propylene).

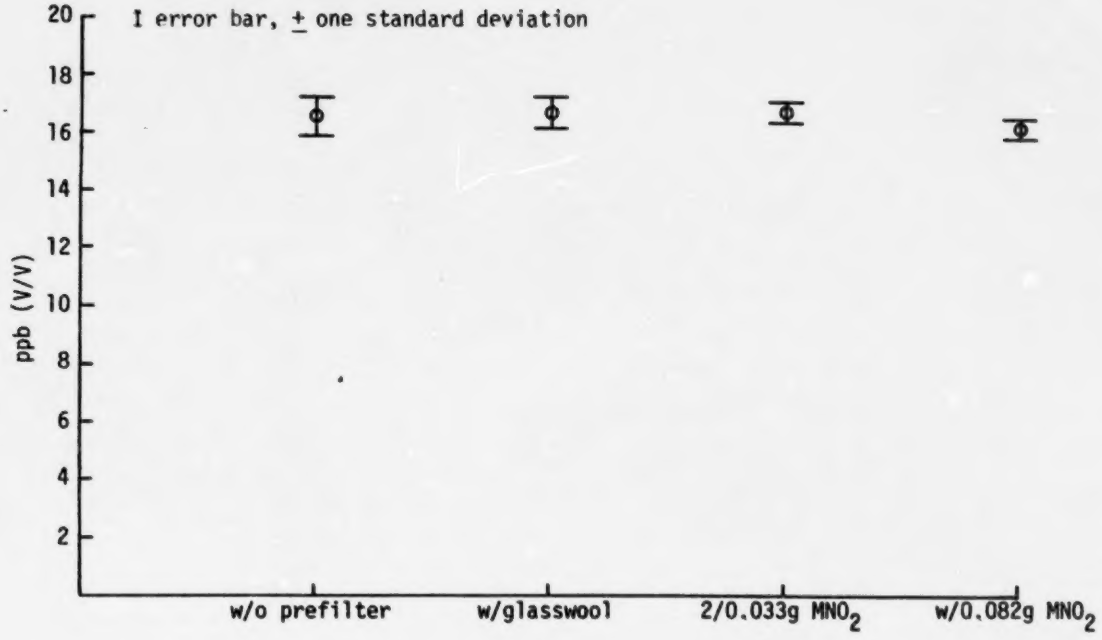

Figure A-9. Prefilter evaluation (propane).

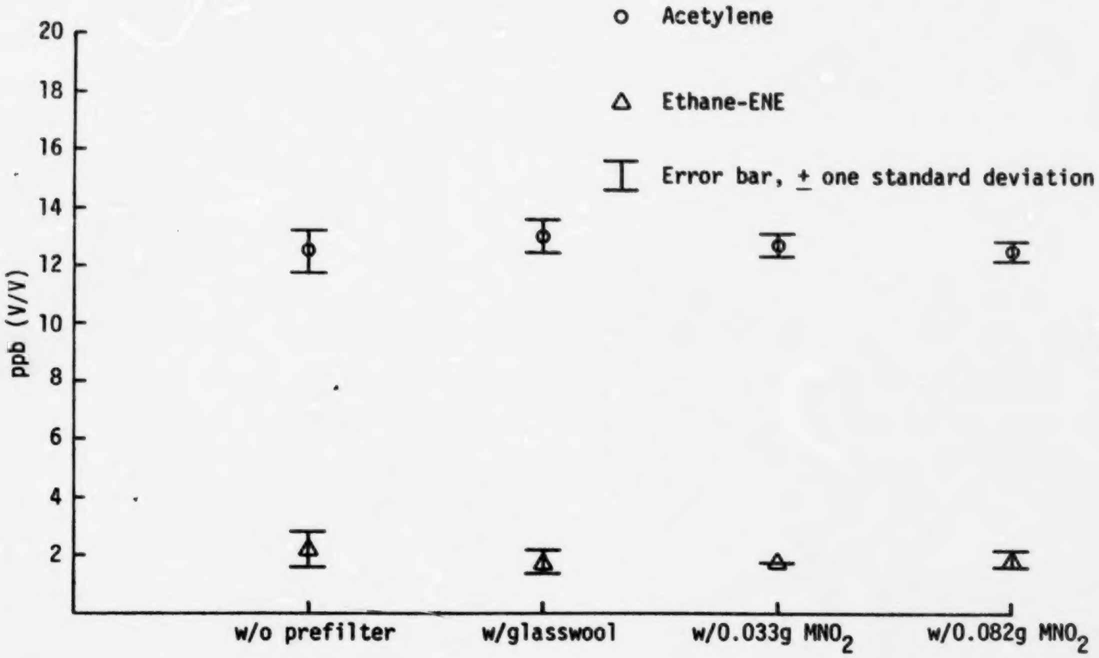

Figure A-10. Prefilter evaluation (acetylene).

APPENDIX B

EVALUATION OF LABORATORY AND QUALITY CONTROL PRACTICES FOR HYDROCARBON SAMPLING AND ANALYSIS (DA VINCI II PARTICIPANTS)

Preceding page blank

APPENDIX B

EVALUATION OF LABORATORY AND QUALITY CONTROL PRACTICES FOR HYDROCARBON SAMPLING AND ANALYSIS (DA VINCI II PARTICIPANTS)

B-1 Introduction

In addition to the experimental work conducted to determine the effects of sample container construction on hydrocarbon stability it was decided that a better understanding of the laboratory and quality control practices for each participant (i.e., WSU, NCAR, and RTI) was warranted. RTI quality control practices and analysis methodology are described in appendix C and section 3.5 of this report, respectively. WSU and NCAR laboratories were visited by RTI investigators and the following areas relative to hydrocarbon sampling and analysis were discussed: (1) analytical methodology, (2) calibration procedure, (3) sampling containers and stability of compounds, (4) preparation of sampling device, (5) time duration between sampling and analysis of Da Vinci II samples, and (6) quality control program and estimated quality of the data.

B-2 Review of Laboratory and Quality Control Practices at National Center for Atmospheric Research (Dr. Leroy E. Heidt)

The first participant laboratory visited was the National Center for Atmospheric Research (NCAR) in Boulder, Colorado. Dr. Heidt was extremely cooperative and freely discussed the work done by NCAR for Da Vinci II samples and conducted a tour of his facilities. Results of these discussions are summarized below and address each of the six areas described above as follows:

1. The analytical methodology used by NCAR was designed to analyze samples that were collected in the stratosphere. Much care is taken to insure that the sample is not contaminated during transfer from the sampling container to the gas chromatograph. The gas chromatograph used was modified extensively to accommodate samples that are at very low pressures (i.e., 0-100 millitorr). Methane and carbon monoxide concentrations are analyzed by flame ionization detection. Carbon monoxide is methanated prior to analysis. Hydrogen analyses are performed on a gas chromatograph with an RF detector. Neon analyses are performed on a high resolution mass spectrometer.

2. Primary calibrations of the various instruments are performed on a monthly basis. Calibration gas mixtures are prepared based on an absolute pressure basis. The pure compound of interest is diluted through transfer from one stainless steel container to another. The accuracy of this method should be as good as the accuracy of pressure measuring devices.

3. Collection devices used by NCAR are constructed from stainless steel. Due to the severe treatment of the containers prior to sampling, Dr. Heidt felt that the stability of some components, such as carbon monoxide, may not be as good as for methane. Hydrogen measurements are considered to be excellent with these containers, but components, such as carbon tetrachloride, are not stable.

4. Stainless steel containers for sampling hydrocarbons are prepared by filling with pure oxygen and heating to 350° C for a period of time. High temperatures are needed to minimize degassing of hydrogen from the stainless steel. Unfortunately, an oxide layer is formed on the interior of the container, due to the oxidizing atmosphere. The oxide layer can act as a catalyst and transform some species, such as carbon monoxide and carbon tetrachloride. After the container has been heated under the oxidizing atmosphere, the containers are evacuated to 10^{-7} torr. The containers are normally used within 4 weeks. The containers used by Sandia Laboratories were cleaned approximately 2-3 weeks before the flight. Dr. Heidt was unaware as to how the samples were collected during Da Vinci II.

5. Dr. Heidt was not certain of the duration of the time between sample collection and analysis, but felt that the samples were analyzed within 1 week after receipt from St. Louis. Information was not readily available as to the date of sample container cleanup, date of shipment and receipt of sample, date of sample analysis, etc.

6. Discussion with Dr. Heidt revealed that NCAR did not have an active quality control program during the time of the Da Vinci II project. NCAR, at that time, relied on previous experience with the analytical methodology to insure the quality of the data. Dr. Heidt felt that the quality of the reported data was good.

B-3 Review of Laboratory and Quality Control Practices at Washington State University (Dr. Rei Rasmussen)

The second participant laboratory visited was Washington State University in Pullman, Washington. Dr. Rasmussen was extremely cooperative and provided RTI valuable information relative to the six areas listed in B-1.

1. The analytical methodology for hydrocarbons utilized flame ionization detection with sample injection from stainless steel containers using a 100-ml syringe. The sample is concentrated at liquid oxygen temperatures. Several 100-ml injections are sometimes required to concentrate enough material for analysis. The sample is then volatized onto the gas chromatographic column using a beaker of hot water. Data are acquired using an HP 3352 data system. Halocarbon measurements are performed by flushing a sample loop and

direct injection onto the column at atmospheric pressure and room temperature. Halocarbon analyses are measured using either peak height of the chromatogram or digital integration of the peak area.

2. Calibration procedures and protocols are not clearly defined as to frequency, etc. Halocarbon calibration concentrations are prepared in large glass carboys by dilution of cylinder gas purchased from Matheson Gas Products with zero nitrogen. WSU also utilizes 6-l air samples collected in remote areas as standards. These "standard" samples are analyzed from time to time to check instrument stability.

3. Dr. Rasmussen's opinion was that the stability of compounds analyzed by WSU was excellent in stainless steel containers. He did not have supportive data to substantiate this, but said that WSU experience indicates that hydrocarbons and halocarbons are stable.

4. Stainless steel containers employed by WSU have brass values and are connected to the container with NPT fittings and sealed with Teflon® tape. Routine cleaning of the containers consist of evacuation to 10×10^{-3} torr, only. According to Dr. Rasmussen, severe treatment of the container activates the surface and makes it more susceptible to wall adsorption.

5. Dr. Rasmussen was not aware of the time frame from sample collection to analysis. Records were not readily available to document this.

6. Discussions with Dr. Rasmussen indicate that at that time no quality control program was in use at WSU with respect to hydrocarbon sampling and analysis. His opinion was that it was not necessary since the sample containers and methodology were reliable. Further discussions with Dr. Heidt of NCAR indicate that NCAR and WSU had exchanged halocarbon samples and that WSU values were running low. Subsequent modifications to the original set of halocarbon data submitted by WSU were made for Da Vinci II samples.

B-4 Review of Laboratory and Quality Control Practices at Research Triangle Institute

The quality control program utilized by RTI during Da Vinci II is described in the final report for EPA Contract No. 68-02-2391 and in appendix C to this report. Further comments relative to the six areas described for hydrocarbon sampling and analysis for NCAR and WSU are presented below.

1. The analytical methodology employed by RTI consists of concentration of sample by liquid oxygen trapping followed by detection of compounds by gas chromatographic separation and flame ionization detection. A modified Perkin Elmer Model 900 gas chromatograph and Hewlett Packard 3352 data system are

used in the analysis. Halocarbons are analyzed using the same chromatograph with electron capture detector. The technique has been described extensively in the literature and utilized by RTI and EPA in several previous programs.

2. Calibration procedures and protocols are clearly defined and documented. Calibration frequency is at least once per month for primary standardization and weekly for retention time verification. Primary standards are prepared by dilution of pure compounds with zero air in stainless steel containers (≈100 l in volume). Mixtures are also purchased from Scott Research Laboratories for use in a double dilution system capable of generating mixtures in the low ppb range. Comparisons are always run against primary standards prepared from pure compounds. Interlaboratory comparisons are also run between RTI and ERSL-EPA on a periodic basis.

3. RTI utilized Tedlar® bags covered by Scotchpak to prevent light absorption as sampling containers. The stability of various hydrocarbons in the C_2-C_5 range was documented in appendix A.

4. Tedlar® bags were purged with zero air and evacuated at least three times immediately before the flight of Da Vinci II. After the flight of Da Vinci II, the samples were returned to RTI for immediate analyses.

5. Documentation was maintained to show a chain of custody from the time the Tedlar® bags left RTI until sample analysis was complete. Individual records are kept for all samples such that the time is known to the nearest hour from sample collection to analysis.

6. RTI has maintained a quality control program for all measurements for the last 5 years. Quality control/quality assurance has been an integral part of all RTI programs since 1973.

The results of this qualitative evaluation of laboratory and quality control practices cannot by themselves be used to make judgments on the quality of the data generated by various participants with respect to hydrocarbon sampling and analysis; however, they do point up certain deficiencies in the respective measurement programs. Although the existence or use of a quality control program does not guarantee the collection and generation of quality data, it does place more confidence in the measurements.

APPENDIX C

RTI QUALITY CONTROL PROGRAM RELATIVE TO DA VINCI II FOR HYDROCARBON SAMPLING

Preceding page blank

APPENDIX C

RTI QUALITY CONTROL PROGRAM RELATIVE TO DA VINCI II FOR HYDROCARBON SAMPLING

A quality control program was implemented to determine whether (if) air samples collected in Tedlar® bags for subsequent C_2-C_5 hydrocarbon analysis would experience significant contamination from the bag material or constituent loss (by wall permeation or sorption). The sampling protocol for the program was as follows:

1. All Tedlar® bags were purged with hydrocarbon-free air prior to installation on Da Vinci II;
2. Tedlar® bags were protected from sunlight by an aluminized material (Scotchpack);
3. Samples were stored after collection in air-tight aluminum suitcases and transported to RTI in the RTI-EML;
4. The mean time between sample collection and analysis was 8 days; and
5. Samples were analyzed in random order as they came from the shipping containers.

The quality control program consisted of sets of experiments to determine the potential for contamination of zero air by the Tedlar® film and concentration losses due to sorption or permeation for hydrocarbon mixtures stored in Tedlar® bags. These tests and results are described in the following paragraphs.

Zero air was analyzed directly from a cylinder purchased from Scott Environmental and then introduced into a Tedlar® bag (Q.C.1). Q.C.1 was analyzed immediately and then shipped to St. Louis in the RTI-EML. Q.C.2 and Q.C.3 were filled using the same zero air cylinder at the field site on May 20 and June 7. Q.C. bags were returned to RTI and analyzed gas chromatographically. Results of this study, includng the dates of preparation and analysis, are presented in table C-1.

The results in table C-1 indicate that contamination of zero air from hydrocarbon permeation from the outside and from the Tedlar® film itself was insignificant and suggest that hydrocarbon contamination of ambient air samples should also be similar. Contamination due to halocarbons such as Freon® 11 and 12 was also considered minimal; however, the data show serious problems

Table C-1. Contamination study of zero air stored in Tedlar® bags

Condition	Concentration				
	Cylinder Analysis	Q.C. 1	Q.C. 2	Q.C. 3	Q.C. 1*
Date Filled	5-13-76	5-13-76	6-7-76	5-20-76	5-13-76
Date Analyzed	5-13-76	5-13-76	6-11-76	6-14-76	6-17-76
Elapsed Time (days)	0	0	4	25	37
Ethane/ethylene†	0.5	0.6	2.2	7.8	7.0
Propane	N.D.	0.1	0.5	1.8	0.2
Propylene	0.6	0.3	0.7	0.7	N.D.
Acetylene	N.D.	N.D.	N.D.	1.2	0.9
Butane	N.D.	0.2	1.5	0.4	0.4
1-Butene	N.D.	N.D.	0.6	N.D.	N.D.
Trans-2-Butene	N.D.	N.D.	N.D.	N.D.	N.D.
Isopentane	N.D.	N.D.	N.D.	0.2	N.D.
Freon 11‡	N.D.	N.D.	9.9	9.5	15.0
Freon 12	N.D.	N.D.	N.D.	N.D.	N.D.
Tricholoroethane	42.8	41.3	43.4	35.7	29.8
Carbon Tetrachloride	N.D.	N.D.	5.0	6.3	5.3
Tetrachloroethylene	N.D.	N.D.	417.0	44.3	205.0

*Q.C.1 was reanalyzed 37 days after filling.
†Concentration = ppbV.
‡Concentration = pptV.
N.D. = nondetectable, <0.1 ppbV.

with the other halogenated compounds analyzed. Therefore, the only halogens analyzed and reported in this study are Freon® 11 and 12.

To examine the storage capability of the Tedlar® bags, a blend of three hydrocarbon mixtures (acetylene, 1-butene, and trans-2-butene) was used to fill Q.C. bags in the field. The concentration for each hydrocarbon blended into the bag by dilution of a standard cylinder containing these hydrocarbons was approximately 71 ppbV. Q.C.4 was blended at RTI, analyzed, and transported to the field. Six additional Q.C. bags were blended using the same gases and procedure at the St. Louis field site immediately prior to the launch of Da Vinci II. It is estimated that the blending accuracy for these bags under field conditions was ±10 percent. These bags were then returned to RTI for analysis with elapsed times of 10 to 36 days between filling and analysis. Results of this study are presented in table C-2.

The data in table C-2 show that the stability of acetylene, 1-butene, and trans-2-butene was quite good in Tedlar® bags for up to 23 days. The deviation of the analysis results is within the estimated accuracy for blending of the mixtures in most cases. It should be noted that the matrix in which these compounds were blended was zero air that was free of hydrocarbons and other reactive pollutants. Changes in the matrix, i.e., ambient air for field samples, may have some effect on stability of collected field samples.

Table C-2. Stability of acetylene, 1-butene, and trans-2-butene in Tedlar® quality control bags

Condition/ Constituent	Concentration*						
	QC-4	QC-5	QC-6	QC-7	QC-8	QC-9	QC-4**
Date Blended	5-13-76	6-07-76	6-07-76	6-07-76	6-07-76	6-07-76	5-13-76
Date Analyzed	5-13-76	6-17-76	6-17-76	6-18-76	6-30-76	6-30-76	6-18-76
Elapsed time in days	0	10	10	11	23	23	36
Ethane/ethylene	1.7	2.9	2.2	9.6	6.8	1.9	116.6
Propane	N.D.	0.8	0.2	0.4	0.4	0.4	8.5
Propylene	0.5	0.5	N.D.	0.6	0.8	0.3	2.4
Acetylene	55.3	65.3	65.8	66.8	58.3	55.2	61.4
Butane	0.3	0.5	0.7	1.6	0.9	0.4	10.5
1-Butene	74.5	76.4	72.3	74.1	67.2	66.9	69.9
Trans-2-Butene	68.6	72.5	69.8	70.3	64.0	61.7	63.9
Isopentane	N.D.	N.D.	N.D.	N.D.	1.0	0.4	6.9

*Concentration = ppbV.
†Sampling bag leaked.
N.D. = nondetectable.

The data obtained in this study substantiate previously reported work regarding sampling of hydrocarbons using Tedlar® bags in the C_2-C_5 range.[C.1] In summation, results of the quality control program indicate that Tedlar® bags were satisfactory for collection of hydrocarbons in the C_2-C_5 range and Freon® 11 and 12, when samples were protected from the sunlight and analyzed within 2 weeks. Sampling bags fabricated from Tedlar® were not satisfactory for the collection of other halogenated compounds.

REFERENCE

C.1 R. B. Denyszyn, L. T. Hackworth, P. M. Grohse, and D. E. Wagoner, "Hydrocarbon and Halocarbon Measurements: Sampling and Analysis Procedure," presented at the International Conference on Photochemical Oxidant Pollution and Its Control, Raleigh, North Carolina, September 12-17, 1976.

APPENDIX D

OBJECTIVE ANALYSIS TECHNIQUE

Preceding page blank

APPENDIX D

OBJECTIVE ANALYSIS TECHNIQUE

The objectives of this research require horizontal, vertical, and temporal analyses of the air chemistry and meteorological data. Those data were taken at fixed and mobile platforms, continuously and sporadically. A systematic objective to collate and interpolate the observation to a given time and space scale is needed.

Barnes$\underline{\text{D-1}}/$ used a weighted space-time interpolative procedure to ascertain winds, temperature, and moisture in the vicinity of a moving thunderstorm. The procedure is fairly simple and straightforward. If $\hat{\phi}_o = \phi(x_o,y_o,t_o)$ is the scalar variable to be interpolated from a set of observations $\hat{\phi}_{i,n} = \phi(x_i,y_i,t_n)$, then a weighted interpolation analysis technique is written:

$$\hat{\phi}_o = \frac{\sum_i \sum_n w(r_i,r_o,t_n,t_o) \cdot \phi_{i,n}}{\sum_i \sum_n w(r_i,r_o,t_n,t_o)}$$

where $r^2 = x^2 + y^2$.

Barnes chooses the w, the weight function, as

$$w(r_i,r_o,t_A,t_o) = \alpha \exp \{ - R^2/4k*^2 - T^2/4\nu^2\}/8\Pi^{3/2}k*\nu$$

where

$R^2 = (x_i-x_o)^2 + (y_i-y_o)^2$

$T = t_n-t_o$

$4k*^2 = 4k* (1+ \beta \cos^2 \psi)$

$\beta = V_i/V*$ for $V* > 0$, $= 0$ otherwise,

ψ = the angle between the position vector from r_o to r_i and the wind velocity vector $\vec{V}_i$

$V_i = |\vec{V}_i|$

and $V^* =$ a characteristic speed of the system moving past the observing locations.

The parameters k and ν are chosen according to the data density and the scale of motions represented by the analyses.[D.1/] The term α represents the confidence in the data. If the data is suspect, then α is small (<1); whereas with total confidence in the data, $\alpha = 1.0$.

Weighted interpolation analyses fall short by smoothing the analysis in a highly variable scalar and by underestimating large values and overestimating small ones. Maxima and minima occur only near maxima and minima in the input field. Barnes improves the initial analysis by interpolating the differences of the observed and interpolated values $\delta_{i,n} = \hat{\phi}_{i,n} - \phi_{i,n}$ over a small area near the observation. By adding the two fields, the new estimate of $\hat{\phi}$ at the observation time and place should be improved. For the second interpolation, Barnes shows that using W^{γ} as the weight function for the $\delta_{i,n}$ analysis is equivalent to using an iterative error reduction. In practice, γ, exceeds 2 but is usually less than 5.

Computer programs were developed to interpolate (a) two variables, e.g., u and v, to a single point in space and time for the cross section analyses and streak line computations, and (b) one variable to an array of grid points (x,y) for the analysis of RAMS pollutant data. Those programs proceed by first computing the error of the interpolation at the observing point, interpolating for both the first estimate and its error at each desired location, and finally forming the final analysis by the sum of the two. In these applications, $R^2/4K^2 + T^2/4\nu^2$ was restricted to <5 for the cross section analyses, and <8 for the RAMS pollutant data. Thus, data, remote in time or space, are not incorporated in the analyses. In some cases, data-sparce areas are not included in the analysis, although they are within the domain of the figure (e.g., some RAMS pollutant data analyses).

REFERENCE

D-1 S. L. Barnes, "Mesoscale Objective Map Analysis Using Weighted Time-Series Observations," NOAA TM ERL NSSL-62, Norman, Oklahoma, 1973.

APPENDIX E

PLANETARY BOUNDARY LAYER MODEL

Preceding page blank

APPENDIX E
PLANETARY BOUNDARY LAYER MODEL

E-1 The Model

The PBL model is a one-dimensional, time-dependent model that incorporates surface heat flux and a time-independent geostrophic wind through the planetary boundary layer to drive the motions. The model divides the atmosphere into two regimes--a surface layer from the ground to 10 m, which is characterized as a constant flux layer, and a free atmosphere above. The equations of motion and thermodynamics are:

$$\frac{\partial u}{\partial t} = f\ (v - v_g) - \frac{1}{\rho}\frac{\partial}{\partial z}\ \overline{\rho u'w'} \tag{1}$$

$$\frac{\partial v}{\partial t} = f\ (u_g - u) - \frac{1}{\rho}\frac{\partial}{\partial z}\ \overline{\rho v'w'} \tag{2}$$

$$\frac{\partial T}{\partial t} = - \frac{1}{\rho}\frac{\partial}{\partial z}\ \overline{\rho w'T'} \tag{3}$$

where the symbols have their usual meteorological meaning. Fluctuations in density have been neglected.

E.1.1 Surface Layer

In the lowest 10 m of the model, the nondimensional gradients of wind speed and potential temperature are obtained from similarity theory:

$$\frac{u}{u_{*o}} = \frac{1}{k}\ \{\ell n\ (z/z_o) - \Psi_m\ (z/L)\} \tag{4}$$

$$\frac{\Theta - \Theta_o}{\Theta_{*o}} = 0.74\ \{\ell n(z/z_o) - \Psi_h\ (z/L)\} \tag{5}$$

where z_o is the surface roughness length and L is a Monin-Obukov length, defined by

$$L = \frac{Cp\ \rho\ To\ u_{*o}^2}{K\ g\ H_o} \tag{6}$$

with H_o, u_{*o}^2 being the surface fluxes of heat and momentum respectively. The functions Ψ_m and Ψ_h are integrals of universal functions ϕ_m, ϕ_h as given by Businger[E-1]. The fluxes of momentum and heat in the surface layer can be derived from

$$-\overline{u'w'} = U_{*o}^2 \left|\frac{\partial u}{\partial z}\right| \bigg/ \left|\frac{\partial \vec{v}}{\partial z}\right| \tag{7}$$

$$-\overline{v'w'} = u_{*o}^2 \left|\frac{\partial v}{\partial z}\right| \bigg/ \left|\frac{\partial \vec{v}}{\partial z}\right| \tag{8}$$

$$-\overline{w'T'} = u_{*o}\,\Theta_{*o} = -\,H_o/(\rho\,C_p) \tag{9}$$

The solution for the surface layer properties begins with an initial guess of L, from the previous step, and the values of u, v, and Θ at 10 m. The value of L is used in equations 4 and 5 to estimate new values of u_{*o} and Θ_{*o} which, through equation (9), gives a new value of L. The iterative procedure continues until L changes by less than 5 percent and $10/L \leq 5$.

E.1.2 Boundary Layer

In the atmosphere above the surface, vertical flux terms are related to the eddy momentum and heat transfer coefficients K_m and K_h by

$$-\overline{u'w'} = K_m \frac{\partial u}{\partial z} \tag{10}$$

$$-\overline{v'w'} = K_m \frac{\partial v}{\partial z} \tag{11}$$

$$-\overline{w'T'} = K_h \frac{\partial \Theta}{\partial z} - \delta_c \tag{12}$$

where δ_c ($= 0.7 \times 10^{-3}$ K m^{-1}) represents a counter gradient heat flux. The eddy heat transfer coefficient is given by

$$u_*^2 \equiv \lambda^2 \frac{\partial \vec{v}}{\partial z}^{\,2} \equiv K_m \frac{\partial \vec{v}}{\partial z} \tag{13}$$

where u_*^2 is the local friction velocity, and λ is the mixing length, which is a function of the local friction velocity, the convective scale velocity, w_*, the height, H, of the planetary boundary layer, and the local value of ϕ_m. The value for K_h is obtained from

$$\frac{K_h}{K_m} = \frac{\phi_m}{\phi_h} \quad . \tag{14}$$

The height, H, of the planetary boundary layer was chosen as the first altitude at which the local Richardson number exceeds 0.25.

E.1.3 Initial Conditions

The initial conditions for the PBL are given by specifying the vertical profile of potential temperature. The geostrophic wind components u_g and v_g are assigned at the upper and lower boundaries, and a linear shear is presumed to exist. The initial vertical wind profiles of u and v were obtained by either of two methods. The equations of motion were integrated for a period of 4 h without permitting sensible heat flux from below while keeping the height of the inversion fixed. This procedure produces a quasi-steady-state wind profile. A second technique used Schaefer's[E-2] solution for an Ekman spiral for a given profile of K and geostrophic wind. From the solution profile a new set of K's were computed. This procedure continued iteratively until a quasi-steady-state was achieved. There appears to be no substantial difference in the results of the two approaches, although Schaefer's technique is faster.

The equations of motion and thermodynamics were integrated in time using an implicit technique[E-3] to integrate the diffusion equation with the ageostrophic wind component as a forcing function. With the implicit formulation, the time step was not constrained by the vertical spacing of grid points. Tests of the model with a 50-m vertical increment and a 10-min time step gave substantially the same results as those obtained with a time step of 30 s.

Computations for U, v, and Θ at the surface were derived from equations 4 and 5. Fluxes of momentum and heat in the surface layer were included in the computation of the variables at the 10-m level.

The heat flux at the ground could be described in two different ways in the model. Initially, the approach of Busch, Chang, and Anthes[E-4] was followed by specifying the function

$$-\overline{w'T'} = \text{MAX} \begin{cases} 0.25 \sin\left[2\pi (t-to)/24\right] \\ -0.06 \end{cases} \text{Kms}^{-1} \tag{15}$$

in testing the model. For simulations of the Da Vinci II flight, however, $\overline{w'T'}$ is an unknown quantity. Consequently the temperature at 10 m was specified by the linear interpolation between hourly temperatures. Equation (3) was solved diagnostically for the surface heat flux required to give that observed change in temperature.

E.2 Verification Results

The equations of motion were integrated in time. Initially, a constant geostrophic wind (u_g = 10 m/s, v_g = o) throughout a layer 1.2 km thick was used with the heat flux formulation given in equation (15). Integrations were done using 0.5-, 1.0-, 2.5-, 5.0-, and 10.0-min time steps without substantial differences in the resulting profiles, surface fluxes, U_{*o}, or θ_{*o}.

An unexpected problem arises in the iterative solution for the surface layer terms when the surface heat flux is negative and L is positive. In that situation, L can be obtained from the solution to

$$(L + a)^3 - bL^2 = 0 \qquad (16)$$

when a and b are parameters of the existing conditions. There may be three real roots to the equation, but each root may not be physically consistent with the atmosphere. One root to which the solution tended was very small, making ϕ_h much too large. Businger's flux profile relationship of ϕ_h as a function of z/L was developed for $-2.5 < z/L < 2.0$. The value of L was chosen such that $z/L \le 5$, (when z = 10 m) thereby prohibiting the extremely small values of L from occurring.

A second problem occurred in using a prognostic equation to determine the mixing length λ. The equation used by Busch, Chang, and Anthes[E-4] is

$$\frac{\partial\lambda}{\partial t} = \frac{\lambda_s - \lambda}{\lambda}\left(u_*^2 + w_*^2\right)^{1/2} \qquad (17)$$

where λ_s is a steady-state value of λ and u_* and w_* are the local friction and convection velocities. Using the large time step taken to integrate the diffusion equation, this equation became unstable. Solutions were attained for λ by iteratively solving the transcendental equation

$$(\lambda_s - \lambda) - \lambda_s \log\,(\lambda_s - \lambda)\Big|_{t=o}^{t=\Delta t} = \left(u_*^2 + w_*^2\right)^{1/2} \Delta t \qquad (18)$$

resulting from time integration of equation (17), with a constant λ_s for a time Δt. The vertical profiles of λ were very similar to profiles of λ_s, unlike the original modeler's results.

After solving those two problems, the meteorological variables were integrated for 36 h, simulating the PBL from dawn on one day to dusk on the following day. The results were very encouraging. The lower portion of the boundary layer became unstable, the mixing height increased during the first day, and the wind speed increased in the mixed layer. A stable atmosphere developed from the ground upward during the night, and surface wind speeds decreased markedly. Above the inversion, supergeostrophic winds developed in the marginally stable remains of the afternoon mixed layer aloft. The v component of the wind became negative (from the north) as an oscillatory response to the loss of surface friction at those levels. A low level jet (~12 m/s) developed in, rather than above, the stable layer as a result of the relatively thin afternoon mixed layer (~700 m) and the large amount of momentum (u_g = 10 m/s at all altitudes) available to the PBL.

With the onset of heating on the next day, the inversion layer was lifted by heating from below, increasing the mixing depth, and gradually approached the θ of the previous day's boundary layer. The wind distribution showed the effects of the presence and absence of surface friction across the thin stable layer separating the older from the newer boundary layer. When that layer was destroyed, the mixing height increased rapidly to the previous day's value and increased slowly thereafter.

The model was modified to incorporate up to five trace substances of concentration, c, each having an equation of mass continuity of

$$\frac{\partial c}{\partial t} = \frac{\partial}{\partial c} - \overline{w'c'} - \Gamma c \tag{19}$$

for constant destruction or depletion rate, Γ, and for

$$\begin{aligned} -\overline{w'c'} &= K_c \frac{\partial c}{\partial z} \qquad z > 10 \text{ m} \\ &= \text{constant} \qquad z \leq 10 \text{ m} \end{aligned} \tag{20}$$

The implicit formulation was used to integrate these equations with $K_c = K_h$, coupling the equation of continuity with the meteorological portion of the model. The equation of continuity for one unspecified material was integrated for 24 h, beginning in the afternoon with a constant value throughout the PBL (above and below the upper stable layer); with $\underline{\Gamma} = 0$; and $\overline{w'c'} = 0.05$ m/s. The results showed a buildup of material during the night in the surface inversion layer and only minimal vertical diffusions. Vertical mixing on the following morning gave a decrease in concentrations at and below 10 m and an increase within the surface mixed layer as a result of increasing the volume containing the surface emission. The concentration profile followed the vertical mixing trend as the day progressed, until a deep well-mixed layer developed by the following afternoon.

REFERENCES

E-1 J. A. Businger, "Turbulent Transfer in the Atmosphere Surface Layer," Workshop on Micrometeorology, D. A. Haugen, Ed., American Meteorology Society, pp. 67-98, 1973.

E-2 J. T. Schaefer, "On the Solution of the Generalized Ekman Equation," Mon. Wea. Rev., 101:535-537, 1973.

E-3 D. W. Peaceman and H. H. Rachford, Jr., "The Numerical Solution of Parabolic and Elliptic Differential Equations," J. Soc. Indust. Appl. Math., 3:28-41, 1955.

E-4 N. E. Busch, S. W. Chang, and R. A. Anthes, "A Multi-Level Model of the Planetary Boundary Layer Suitable for Use With Mesoscale Dynamic Models," J. Appl. Meteor., 15:909-919, 1976.